ISSN 1913-1844

MODERN APPLIED SCIENCE

Vol. 2, No. 5
September 2008

CCSE
Canadian Center of Science and Education

Modern Applied Science

www.ccsenet.org/journal.html

Vol. 2, No. 5

September 2008

Contents

Modern Applied Science

www.ccsenet.org/journal.html

Vol. 2, No. 5

September 2008

Contents

Modern Applied Science

www.ccsenet.org/journal.html

Vol. 2, No. 5

September 2008

Decolorization of Cibacron Yellow S-3R Using *Coriolus Versicolor* (MTCC 138)

Sivakumar Venkatachalam (Corresponding author)

Department of Chemical Engineering, Kongu Engineering College

Perundurai, Erode - 638052, TN, India

Tel: 91-4294-226-602 E-mail: drvsivakumar@yahoo.com

Chitradevi Venkatachalam

Department of Chemical Engineering, Kongu Engineering College

Perundurai, Erode - 638052, TN, India

Tel: 91-4294-226-602 E-mail: erchitrasuresh@yahoo.com

Abstract

The aim of the present study is to analyze the ability of the white rot fungi *Coriolus Versicolor* (MTCC 138) in the decolorization of Cibacron Yellow S-3R, a recalcitrant azo reactive textile dye. The influencing parameters that affect the percentage of decolorization rates are optimized in batch mode. The optimal values of the parameters such as mycelia age, temperature, pH, initial dye concentration and carbon source concentration are found to be 7 days, 30°C, 5.4, 100 mg/l and 2 mg/l respectively. The maximum percentage of decolorization at the optimized conditions is found to be 90%. It is also conferred that there is substrate inhibition to fungal decolorization when initial dye concentration is greater than 100 mg/l.

Keywords: Decolorization, Textile dye, White rot fungi, Percentage decolorization

1. Introduction

Textile dyeing industries is one of the fast growing, major export oriented industrial sectors in India. Dyeing, the fundamental unit operation during textile fiber processing, is gifted with large amounts of structurally diverse dyestuffs which are classified as azo dyes, anthraquinone dyes, phthalocyanine dyes etc., based on the chemical structure of the chromophoric group. Amongst them utilization of azo reactive dyes has been consistently increasing, as they provide ease of application, high wet fastness profiles, brilliant color shades and less energy consumption. These dyeing operations result in the production of more or less colored wastewaters (Rodrigues et al., 1999), depending on the degree of fixation of the dyestuffs on the substrates, which varies with the nature of the fabrics, the desired intensity of coloration, and the application method (Pearce et al., 2003). The presence of unfixed dyes in such waste waters is much higher than the allowable limits and extremely harmful to aquatic flora, fauna and human beings through food chains (Pierce, 1994). The textile dyeing process consumes large quantities of water and due to increasing global water scarcity, total or partially reuse of effluent after the necessary treatments becomes mandatory. Therefore, color removal criteria are more and more demanding attention. The conventional physical and chemical effluent treatment methods such as adsorption, chemical precipitation and flocculation are inefficient as they result either in large volumes of sludge or in the release of toxic substances (Spadaro et al., 1992). All the methods possess significant differences in color removal results, volume capability, operating time and capital costs. White rot fungi have been studied for their ability to degrade recalcitrant organo-pollutants such as polycyclic aromatic hydrocarbons (Bogan & Lamar, 1996), chlorinated phenols (Ruckenstein & Wang, 1994), PCBs (Sasek et al., 1993, Beaudette et al., 1998), dioxins (Takada et al., 1996), pesticides (Kullman & Matsumura, 1996), explosives (Gorontzy et al., 1994), dichloroaniline (Arjmand & Sandermann, 1985) and dyes (Kirby et al., 1995, Shin et al., 1997, Rodriguez et al., 1999). From the analysis of literature it is found that many authors used white rot fungi for decolorization of textile effluents (Chagas & Durrant, 2001, Swamy & Ramsay 1999, Yesilada et al., 2002, Kirby et al., 1995, Shin et al., 1997, Rodriguez et al., 1999, Wesenberg et al., 2003).

Though the number of studies on the biodegradation of dyestuffs have been steadily increasing in recent years, very few researches are reported for biodegradation of azo dyes, such as Cibacron Yellow S-3R using white rot fungi (Yesilada et al., 1998) and hence in this present research an attempt has been made to investigate the biological decolorization of the azo dye Cibacron Yellow S-3R using *Coriolus Versicolor* (MTCC 138).

2. Material and Methods

The organism used for decolorization *Coriolus Versicolor* (MTCC 138) is purchased from the Microbial Type Culture Collection and Gene Bank, Institute of Microbial Technology, Chandigarh, India. The fungus is cultured at 30°C on slant Sabouraud's Dextrose Agar and after a week a conidial suspension is prepared and utilized for the cultivation of the inoculums. 5 ml of the suspension is transferred to 250 ml flask containing 100 ml Sabouraud's Dextrose Broth. It is incubated at 30°C for 5 days in a shaking incubator at 130 rpm.

Batch experiments are performed in 250 flasks containing fresh SDB (2 ml homogenate / 100 ml SDB) along with desired concentration of dye (Yesilada et al., 2002). The contents of the flasks are sterilized for 20 min (1.5 atm, 121°C) and incubated in shaking incubator at 130 rpm. Samples are collected for every time interval and they are centrifuged at 1200 rpm, 20 min and supernatant is used for analysis. Absorbance measurements are done at maximum absorbance (λ_{max} = 472nm) of dye using UV-Visible Spectrophotometer 119. Percentage decolorization efficiency is calculated according to the following formulation:

$$\text{Percentage of Decolorization} = \frac{A_b - A_a}{A_b}$$

Where A_b is the absorbance at the maximum absorption wavelength of dye before decolorization and A_a is the absorbance at the maximum absorption wavelength of dye after decolorization

3. Results and Discussion

3.1 Effect of mycelia age

The effect of mycelia age on percentage of decolorization is studied using different days of culture growth, namely 5 days, 7 days 8 days and 9 days. From the results shown in Figure 1, it is found that 5 days of growth culture requires 48 hours to achieve maximum decolorization, whereas 7 days of growth culture takes only 24 hours for decolorization. Further increasing days of culture growth doesn't make any appreciable change in the percentage of decolorization and hence 7 days of culture growth is found to be optimum for further studies. The same trend is also observed by Duygu et al., (2005) for bio decolorization of Brilliant Blue using *Funalia trogii*

3.2 Effect of carbon source concentration

Addition of a carbon source such as glucose at different concentrations has an effect on the percentage of decolorization and it is shown in Figure 2. The concentration of glucose is varied from 0.5mg/l to 5mg/l. From the analysis of Figure 2 it is found that the percentage of decolorization increases with the increase in concentration of glucose upto maximum glucose concentration of 2 mg/l and after which there is not much appreciable increase in percentage of decolorization (Swamy et al., 1999).

3.3 Effect of temperature

The operating temperature of the incubation process is varied between 20°C and 60°C, to study the effect of temperature on the decolorization process that is shown in Figure 3. It clearly shows that at temperatures below 30°C, the growth of the fungi was too slow, that it took more days for decolorization and at temperatures above 30°C the activity of *Coriolus Versicolor* (MTCC 138) is reduced and hence percentage of decolorization decreases. From the analysis of the results it is found that optimal temperature for decolorization occurs at 30°C.

3.4 Effect of pH

The effect of pH is studied by incubating the reaction mixtures with the pH varying from 3.5 – 7. The fungus is able to decolorize the dye during the pH range of 4.5 – 7 which is shown in Figure 4**.** The optimum pH is found to be 5.5 at which the maximum decolorization has occurred. For pH values below 5.5 there is no appreciable growth of fungi and hence percentage of decolorization decreases. Increase in pH greater than 5.5 resulted in the fragmentation of mycelia pellets and hence percentage of decolorization decreases.

3.5 Effect of initial dye concentration

The effect of initial concentration of the dye is studied by varying the concentration from 50mg/l to 300mg/l with the optimal values of temperature, pH and glucose concentration at 30°C, 5.5 and 2mg/l respectively. The results show that in all initial dye concentrations, *Coriolus Versicolor* (MTCC 138) could effectively decolorize Cibacron Yellow dye. From the plot (Figure 5), it can be seen that though the percentage of decolorization increases with the initial dye concentrations and it reaches the maximum of 90 percentage of decolorization at 100 mg/l of initial concentration. There is a decrease in the percentage of decolorization for initial dye concentrations above 100mg/l, and it is mainly due

to substrate inhibition.. (Al-Sabti, 2000, Chen, 2002, Gottlieb et al., 2003, Marlasca et al., 1998, Rosa et al., 2001, Walthall & Stark, 1999, Yesilada et al., 2003, Yun & Qi-xing, 2002).

4. Conclusion

From the study of decolorization of Cibacron Yellow S3-R by *Coriolus Versicolor* (MTCC 138), it is found that the optimal mycelia age is 7 days and optimal initial dye concentration is 100 mg/l and also the optimum temperature, pH and glucose concentration are found to be 30°C, 5.5 and 2 mg/l respectively. The potential ability of fungi shows that it can be used for the biodegradation of textile effluents. This study has to be further improved for continuous treatment of textile effluents.

5. References

Al-Sabti, K. (2000). Chlorotriazine reactive azo Red 120 textile dye induces micronuclei in fish. *Exotoxicol. Environ. Saf*, 47, 149-155.

Arjmand, M., & Sandermann, H. (1985). Mineralization of chloraniline/ lignin conjugates and of free chloranilines by white rot fungus *Phanerochaete chrysosporium*. *J. Agric. Food Chem.*, 33, 1055-1060.

Beaudette, L. A., Davies, S., Fedorak, P. M., Ward, O. P., & Pickard, M. A. (1998). Comparison of biodegradation and mineralization as methods for measuring loss of selected polychlorinated biphenyl congeners in cultures of four white rot fungi. *Appl. Env. Microbiol*, 64, 2020-2025.

Bogan, B. W., & Lamar, R. T. (1996). Polycyclic aromatic hydrocarbon degradation capabilities of *Phanerochaete leavis* HHB-1625 and its extracellular ligninolytic enzymes. *Appl. Env. Microbiol, 62, 1597-1603.*

Chagas, E. P., & Durrant, L. R. (2001). Decolorization of azo dyes by *Phanerochaete chrysosporium* and *Pleurotus sajorcaju*. *Enzyme Microbial Technol*, 29,473-477.

Chen, B. Y. (2002). Understanding decolorization characteristics of reactive azo dyes by *Pseudomonas luteola* toxicity and kinetics. *Process Biochem*, 38, 437-446.

Duygu, H., zsoy, O¨., Ali, U¨ nyayar., & Ali Mazmanc, M. (2005). Decolourisation of reactive textile dyes Drimarene Blue X3LR and Remazol Brilliant Blue R by *Funalia trogii* ATCC 200800. *Biodegradation,* 16, 195-204.

Gorontzy, T., Drzyga, O., Kahl, M. W., Bruns-Nagel, D., Breitung, J., von Loew, E., & Blotevogel, K. H. (1994). Microbial degradation of explosives and related compounds. *Crit. Rev. Microbiol,* 20, 265-284.

Gottlieb, A., Shaw, C., Smith, A., Wheatley, A., & Forsythe, S. (2003). The toxicity of textile reactive azo dyes after hydrolysis and decolourisation. *J. Biotechnol*, 101, 49-56.

Kirby, N., McMullan, G., & Marchant, R. (1995). Decolourisation of an artificial textile effuent by *Phanerochaete chrysosporium*. *Biotechnol. Lett*, 178, 761-764.

Kullman, S. W., & Matsumura, F. (1996). Metabolic pathways utilized by *Phanerochaete chrysosporium* for degradation of cyclodiene pesticide Endosulfan. *Appl. Environ. Microbiol*, 62, 593-600

Marlasca, M. J., Sanpera, C., Riva, M. C., Sala, & R., Crespo, S. (1998). Hepatic alterations and induction of micronuclei in rainbow trout (Oncorhynchus mykiss) exposed to a textile industry effluent. *Histol. Histopathol*, 13,703-712.

Pearce, C. I., Lloyd, J. R. & Guthrie, J. T. (2003). The removal of colour from textile wastewater using whole bacterial cells: a review. *Dyes and Pigments*, 58, 179-196.

Pierce, J. (1994). Color in textile effluents: the origins of the problem. *J. Soc. Dyers Colorists,* 110, 131-134.

Rodrigues, E., Pickard, M. A., & Vazquez-Duhalt, R. (1999). Industrial dye decolourisation by laccases from ligninolytic fungi. *Curr. Microbiol*, 38, 27-32.

Rosa, E. V. C., Simionatto, E. L., Sierra, M. M. D. S., Bertoli, S. L., & Radetski, C. M. (2001). Toxicity-based criteria for the evaluation of textile wastewater treatment efficiency. *Environ. Toxicol. Chem*, 20, 839-845.

Ruckenstein, E., & Wang, X. B. (1994). Production of lignin peroxidase by *Phanerochaete chrysosporium* immobilized on porous poly(styrene-divinylbenzene) carrier and its application to the degrading of 2-chlorophenol. *Biotechnol Bioeng,* 44, 79-86.

Spadaro, J. T., Gold, M. H., & Renganathan, V. (1992), Degradation of azo dyes by the lignin-degrading fungus. *Phanerochaete chrysosporium*. *Appl. Environ. Microbiol*, 58, 2397-2410.

Swamy, J., & Ramsay, J., (1999). The evaluation of white rot fungi in the decoloration of textile dyes. *Enzyme Microb. Technol,* 24, 130-137.

Sasek, V., Volfova, O., Erbanova, P., Vyas, B. R. M., & Matucha, M. (1993). Degradation of PCBs by white rot fungi, methylotrophic and hydrocarbon utilizing yeasts and bacteria. *Biotechnol. Lett*, 15, 521-526.

Shin, K. S., Oh, I. K., & Kim, C. J. (1997). Production and purification of Remazol Brilliant Blue R decolorization peroxidase from the culture filtrate of *Pleurotus ostreatus*. *Appl. Env. Microbiol,* 63, 1744-1748.

Takada, S., Naksamura, M., Matsueda, T., Kondo, R., & Sakai, K. (1996). Degradation of polychlorinated dibenzo-p-dioxins and polychlorinated dibenzofurans by the white rot fungus *Phanerochaete sordida* YK-624. *Appl. Env. Microbiol*, 62, 4323-4328.

Walthall, W. K., & Strak, J. D. (1999). The acute and chronic toxicity in two xanthene dyes fluorescein sodium salt and phloxine B to *Daphnia pulex*. *Environ. Pollut*, 104, 207-215.

Wesenberg D, Kyriakides I, & Agathos S. N. (2003). White-rot fungi and their enzymes for the treatment of industrial dye effluents. *Biotechnol. Adv*, 22, 161-187.

Yesilada O, & Ozcan B (1998). Decolourisation of orange II with the crude culture filtrate of white rot fungus, *Coriolus Versicolor*. *Tr.J.Biol*, 22, 463-476.

Yesilada, O., Cing, S., & Asma, D. (2002). Decolourisation of the textile dye Astrazon Red FBL by Funalia Trogii Pellets. *Bioresource technology,* 81, 155-157.

Yesilada, O., Asma, D., & Cing, S. (2003). Decolorisation of textile dyes by fungal pellets. *Process Biochem*. 38, 933-938.

Yun, C., & Qi-xing, Z. (2002). Ecological toxicity of Reactive X-3B Red dye and cadmium acting on wheat (*Triticum aestivum*). *J. Environ. Sci*, 14, 136-140.

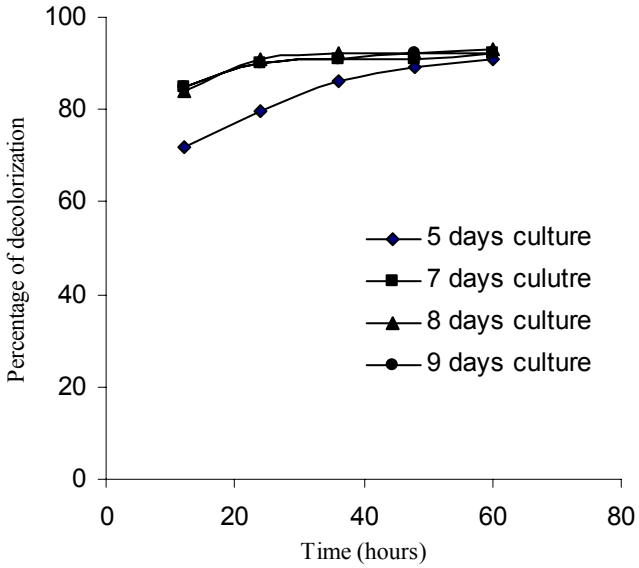

Figure 1. Effect of mycelia age on percentage of decolorization

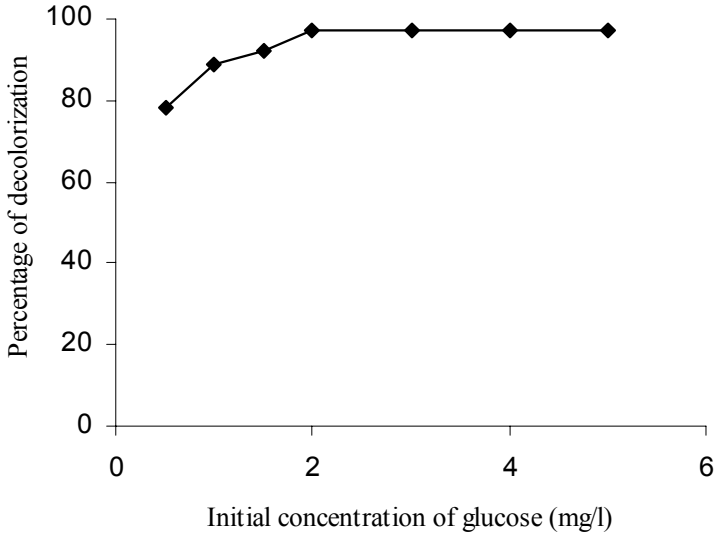

Figure 2. Effect of initial concentration of glucose on percentage of decolorization

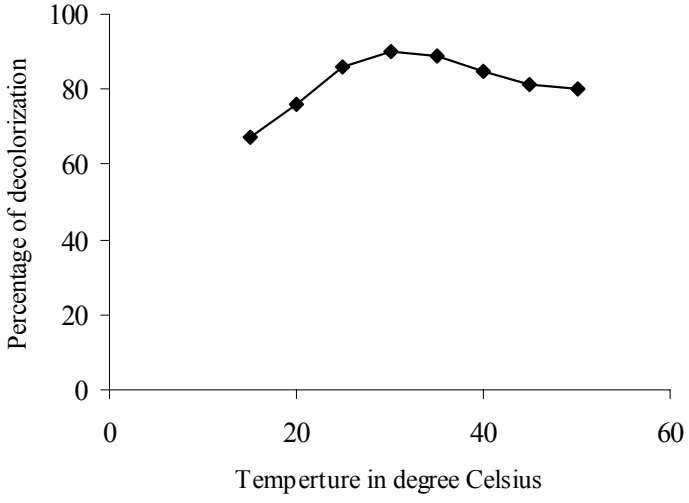

Figure 3. Effect of temperature on percentage of decolorization

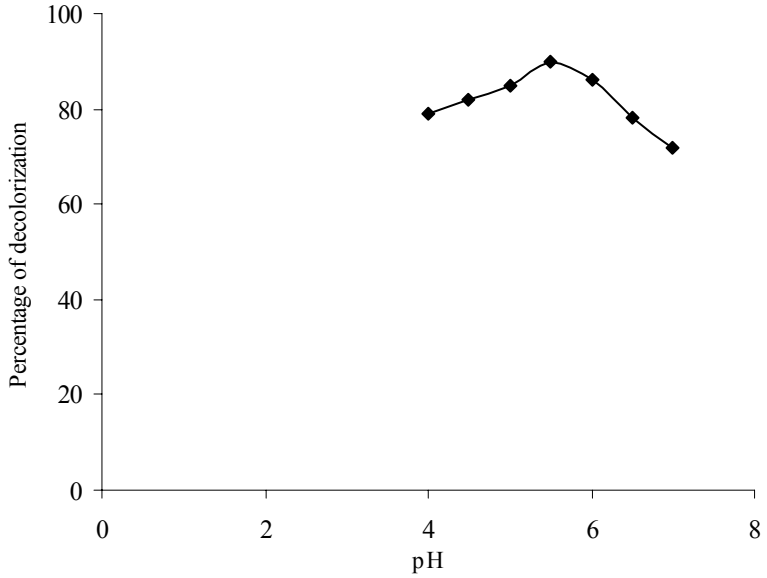

Figure 4. Effect of pH on percentage of decolorization

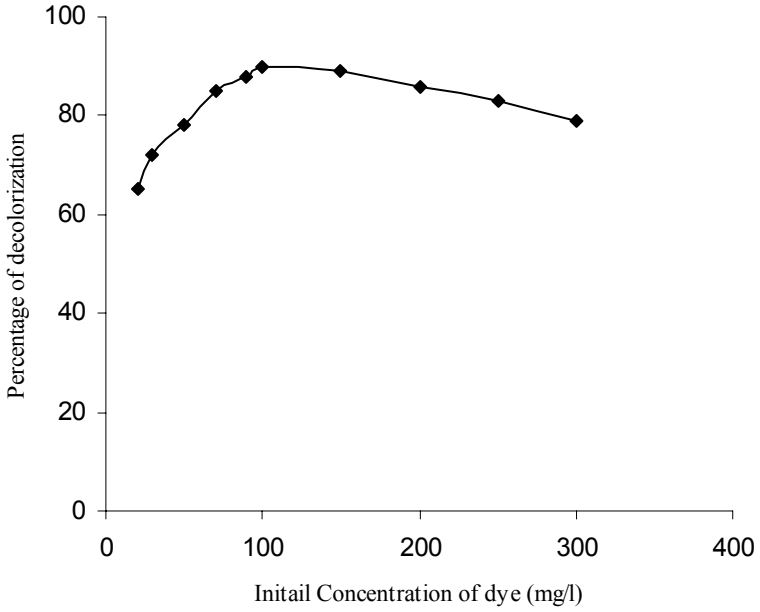

Figure 5. Effect of initial concentration of dye on percentage of decolorization

Modern Applied Science

www.ccsenet.org/journal.html

Vol. 2, No. 5

September 2008

Redevelopment of ANSYS in Mechanics Analysis of Railway-highway Combined Bridge

Yiping Yin

College of Civil Engineering and Mechanics

Hua Zhong University of Science and Technology

Wuhan 430074, China

Tel: 86-027-8755-2231 E-mail: yinjw@yahoo.cn

Weishi Liu

Chaling Construction Bureau

Hunan 412400, China

Abstract

The length of railway-highway combined bridge is large and it's calculating model having many elements makes it need a great of manpower and time in the Finite Element Analysis (FEA). With redevelopment of ANSYS, a FEA program is empoldered so that complex load calculation and loads combination is worked out automatically in ANSYS. It reduces manpower, shortens time and improves work efficiency. the FEA program was used successfully in analysis of Zhengzhou Yellow River railway-highway combined bridge, and all the work of calculation and results processing can be finished in sixteen days, which saves much time in researching and designing bridge and obtains good social benefits and economic benefits. It also provides convenience for other analysis of railway-highway combined bridges and demonstrates idea for other similar questions of development of ANSYS.

Keywords: ANSYS, Redevelopment, Railway-highway combined bridge, FEA

1. Introduction

The integral spatial mechanics analysis of bridge structure needs a variety of load calculation, including the dead load, vehicles and crowd load, bearing sedimentation load, site wind load and extreme wind load, temperature load and seismic load, and so on. The analysis also should consider the loads combination, including the dead loads combination, the main loads combination and the additional loads combination, and identify the most disadvantaged loads combination. Given importance and complexity of the bridge analysis, the Finite Element Method is often used instead of the manual calculation.

Some bridge analysis software, such as Bridge Doctor, 3D3S, 3D-BRIDGE, are widely used in China now, but the MIDAS, a Korea bridge analysis software, has the largest number of users. These software are major to bridge with great convenience, it is limited only to the general scale of the bridge structure analysis. ANSYS (SAS IP,1998) is a good general-purpose finite element analysis software can solve large-scale problems. However, it is difficult to solve the professional structure problem of bridge directly, which costs much manpower to carry out loads combination and results processing. So sometimes the redevelopment of ANSYS for concrete problem of bridge structure is needed (CHEN Jin,2003; YE Meixin,2005).

In 2005 the authors of this article used ANSYS to calculate integral spatial stress of cable-stayed bridge in Ningbo City Airport Road, which has degrees of freedom less than 80,000. It took more than 50 days to finish the calculation and get the detailed researching report.

That the large length of railway-highway bridge with lots of components makes the researchers spend a long time in doing the FEA work, however, the researching and designing time is now very urgent, so the FEA can not be worked by using conventional bridge professional software or artificial results collation of the analysis of ANSYS software.

The investigation commissioned by the China Zhongtie Major Bridge Reconnaissance & Design Institute Co., Ltd., we developed a FEA program by redevelopment of ANSYS to calculate the integral spatial mechanics of railway-highway

combined bridge, making tedious analysis of the structure, combination of loads and collation of results in ANSYS completed automatically. The use of the program in the FEA of Zhengzhou Yellow River railway-highway combined bridge (China Zhongtie Major Bridge Reconnaissance & Design Institute Co., Ltd.,2007) (about 14,600,000 degrees of freedom) costs only 16 days to finish the calculation and get a satisfactory report. Development of the program has greatly shortened the researching and designing time of the bridge, rapidly improved the efficiency, provided a convenient analysis to other railway-highway combined bridge, and took a example for similar problems in redevelopment of ANSYS.

2. Redevelopment of ANSYS

Developed by ANSYS company, ANSYS software was the first design analysis software that passed through the ISO9001 quality certification. The finite element analysis software uses advanced technology, and at the same time it has a good pre-processing and post-processing functions. ANSYS is a powerful and practical tool for the calculation of very complex regulatory structure.

2.1 User Interface Design Language

ANSYS software provides a dedicated language, UIDL (User Interface Design Language), for user interface design. UIDL is a procedural language, which allows users to change ANSYS graphical user interface (GUI) and some of the groups. UIDL provides a powerful tool, which allows users to use flexibly, to organize GUI according to personal preferences. It plays a role that can not be underestimated in reorganizing commands, erecting bridges between ANSYS and other software.

2.2 ANSYS Parametric Design Language

APDL stands for ANSYS Parametric Design Language, a scripting language that you can use to automate common tasks or even build your model in terms of parameters (variables). APDL also encompasses a wide range of other features such as repeating a command, macros, if-then-else branching, do-loops, and scalar, vector and matrix operations, particularly worth mentioning of which is macro. You can record a frequently used sequence of ANSYS commands in a macro file (these are sometimes called command files). Creating a macro enables he to, in effect, create your own custom ANSYS command. In addition to executing a series of ANSYS commands, a macro can call GUI functions or pass values into arguments.

While APDL is the foundation for sophisticated features such as design optimization and adaptive meshing, it also offers many conveniences that you can use in your day-to-day analyses. As you become more adept at the language, you will see that the applications for APDL are limited only by your imagination.

2.3 User-Programmable Features

User-Programmable Features (UPFs) are ANSYS capabilities for which you can write your own FORTRAN routines. UPFs allow you to customize the ANSYS program to your needs, which may be a user-defined material-behavior option, element, failure criterion (for composites), and so on. You can even write your own design-optimization algorithm that calls the entire ANSYS program as a subroutine. In fact, some standard ANSYS features began as user-programmed features. Typically, you can obtain good results with the ANSYS program when you exercise documented features using standard, recommended procedures. In some cases, however, you may need to employ nonstandard procedures.

3. Redevelopment of ANSYS in railway-highway combined bridge

ANSYS used in mechanics analysis of railway-highway combined bridges has some difficulties: load calculation, loads combination and results collation. Here we will use the redevelopment technology of ANSYS to address these difficulties one by one.

3.1 Load calculation

3.1.1 Dead load

Calculating the material density according to the first period dead load, and defined the material density of the bridge deck based on second period dead load:

```
mp,dens,1,125350        ! material density of the railway bridge deck
mp,dens,5,3397          ! highway bridge deck
mp,dens,2,9800          ! other material
```

3.1.2 Vehicle load

Acting a moving point load and considering the reduction factors. The value of the moving point is calculated by the total vehicles load on railway bridge and highway bridge respectively:

```
*do,i,0,1488,1                    ! load moving by loop
fdele,all,all                     ! delete the original loads
nsel,s,loc,x,i*0.5                ! select location for acting load
f,all,fy,-1.0*Fcor*1e4            ! acting unit point load
*enddo                            ! Fcor is the reduction factor
```

3.1.3 Bearing sedimentation load

The value of settlement at intermediate piers is 0.015m and 0.010m at side piers:

```
d,n1,uy,-0.015                    ! intermediate pier
d,n2,uy,-0.010                    ! side pier
```

3.1.4 Temperature load

Increasing and decreasing temperature in bridge is 20℃, in components is 10℃:

```
      Allsel                      ! select all elements in bridge
bfe,all,temp,,-20                 ! decreasing temperature
esel,s,elem,, 1,140000            ! select elements in highway bridge deck
bfe,all,temp,,-10
```

3.1.5 Site wind load

Includes positive longitudinal wind and negative longitudinal wind, left transverse wind and right transverse wind:

```
f,n1,fz,-1180                     ! right transverse wind
f,n2,fx,-1180                     ! negative longitudinal wind
```

3.1.6 Vehicle braking load

Calculated based on you lane load acted on railway bridge and highway bridge respectively and considering the coefficient to brake:

```
nsel,s,loc,z,4.5
nsel,r,loc,y,0
f,all,fx,-4.8e3                   ! braking load in railway bridge
nsel,s,loc,z,4.5
nsel,r,loc,y,14
f,all,fx,-2.1e3                   ! braking load in highway bridge
```

3.1.7 Extreme wind load

Direction can be referred from the part 5): site wind load. This item must not combine with vehicle load:

```
f,n1,fz, -3072                    ! right transverse wind
f,n2,fx, -3072                    ! negative longitudinal wind
```

3.2 Loads combination

There are eight groups of loads combination:

1) Dead load combination:dead load

2) Main loads combination:dead load+ vehicles and crowd load + bearing sedimentation load

3) Additional loads combination 1:main loads combination +increasing temperature combination + transverse wind load + vehicle braking load

4) Additional loads combination 2:main loads combination +decreasing temperature combination + transverse wind load + vehicle braking load

5) Additional loads combination 3:main loads combination +increasing temperature combination + longitudinal wind load + vehicle braking load

6) Additional loads combination 4:main loads combination +decreasing temperature combination + longitudinal wind load + vehicle braking load

7) Additional loads combination 5: dead load+ bearing sedimentation load + extreme wind load

8) Seismic loads combination: dead load+ bearing sedimentation load + seismic load

Procedures for vehicle loads combination in highway are as follows:

```
*do,i,0,1488,1
    Lcdef, i+1, i                                    ! time i represents load (i+1)
*enddo
max=0                                                ! compare the results to get the
min=0                                                ! maximum value and minimum value
*do,i,0,1488,1
          *if, Lcdef(i+1),gt,0,then
              max =max + Lcdef(i+1)*1.6785           ! vehicle load coefficient is 1.6785
          *else
              min =min + Lcdef(i+1)*1.6785
          *endif
      *enddo
```

3.3 Results collation

The results include displacement (ux, uy, uz), reaction force, member forces (axial force, in-plane shear, in-plane bending moment, out-plane shear, out-plane bending moment), stress of bridge decks (normal stress and shear stress), cable force and cable stress amplitude. As the number of the bridge components is very large, it is very cumbersome to collate the results by manpower.

Here APDL is used to collate the results. Attaching statement heading to the calculating data can get reporting results, then output the reporting results to EXCEL software to form researching report.

Procedures to get calculating data of reaction force:

```
*dim,Reaction_fy, , 6                                ! dimension Reaction_fy
*do,i,1,6,1
*get, Reaction_fy(i), node, I, rf, fy                ! save reaction force to dimension
*enddo
```

Reporting data of member forces:

```
*do,i,1,3960,1                                       ! F_beam_C(i) is calculating result
  F_beam_R(k)= F_beam_C(i)                           ! F_beam_R(i) is reporting result
*if,mod(i,5),eq,0,then                               ! Each table consists of 5 rows data
k=k+6                                                ! 5 rows interval between two tables:
*else                                                ! 2 rows space and 3 rows heading
  k=k+1
*endif
*enddo
```

4. Calculation example

The proposed Zhengzhou Yellow River railway-highway combined bridge will become the world's longest railway-highway combined bridge. The main bridge is designed with six consecutive cable-stayed steel truss bridges with 168m. In FEA, the mid three span can be combined into only you span for easy calculation, so the calculating model has five spans, however the bridge is seven spans in fact. That manual calculating load, combining loads and collating results in usual practice not only encounters inevitable human errors, but also it will costs too much time to get a detailed researching report. Here the redevelopment of ANSYS is used to the analysis, so that complex load calculation and loads combination is worked out automatically in ANSYS. It reduces manpower, shortens time, improves work efficiency and avoids man-made errors.

The FEA models of Zhengzhou Yellow River railway-highway combined bridge are in figure 1, and some calculating results are in Figure 2.

5. Conclusions

With redevelopment of ANSYS, a FEA program is empoldered so that complex calculation of internal force analysis and cases combination is worked out automatically in ANSYS. It reduces manpower, shortens time, improves work efficiency and avoids man-made errors, as well as demonstrates idea for other similar questions of development of ANSYS.

References

ANSYS APDL Programmer' s Guide[S]. USA: SAS IP,1998.

CHEN Jin, XIAO Rucheng, JIANG Jianjing. Probabilistic determination for initial cable forces of cable-stayed bridges under dead loads [J]. China Civil Engineering Journal, 2003,36 (12):58 - 63.

The Third Survey and Design Institute of China Railway, China Zhongtie Major Bridge Reconnaissance & Design Institute Co., Ltd.. Design files for Zhengzhou Yellow River railway-highway combined bridge [R], 2007.

YE Meixin, HAN Yanqun, ZHANG Min. Development and application of ANSYS in long - span cable - stayed bridge[J]. Journal of railway science and engineering, 2005, 2(5):56-59.

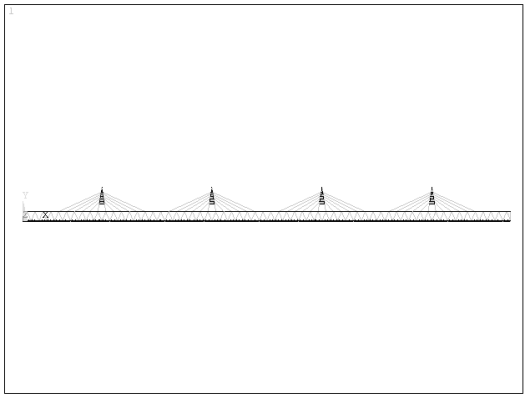

Figure 1.a bridge model (front view)

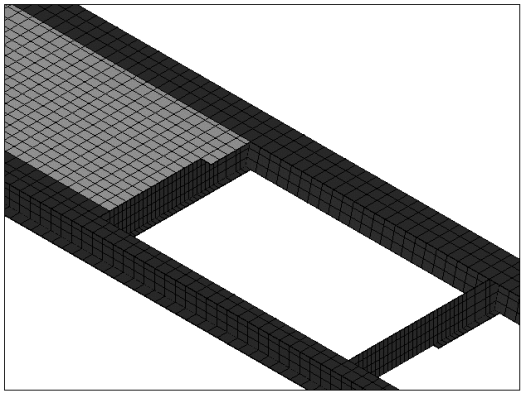

Figure 1.b elements of railway bridge deck

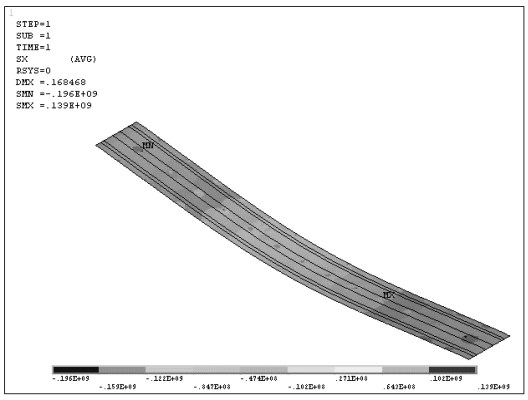

Figure 2.a stress of railway bridge deck(:Pa)

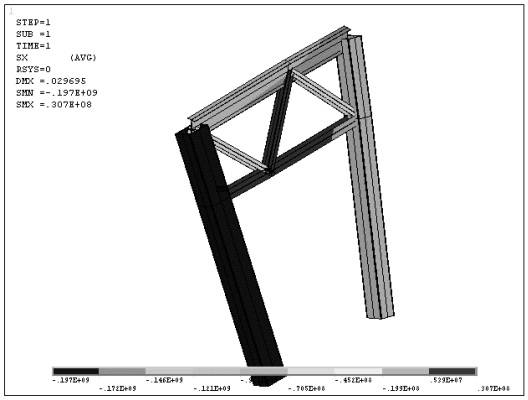

Figure 2.b stress of frame cushion of bridge(:Pa)

Modern Applied Science

www.ccsenet.org/journal.html

Vol. 2, No. 5

September 2008

An Experimental Investigation of Heat Transfer Coefficients for Spiral Plate Heat Exchanger

Kaliannan Saravanan

Department of Chemical Engineering

Kongu Engineering College, Anna University

Erode Tamilnadu, India-638 052

E-mail:rumisivaesh@yahoo.com

Rangasamy Rajavel (Corresponding author)

Department of Mechanical Engineering

Kongu Engineering College, Anna University

Erode, Tamilnadu, India -638 052

E-mail:rajavel_7@yahoo.com

Abstract

Spiral plate heat exchangers play a vital role in cooling high density and high viscous fluids. This paper presents an experimental investigation of convective heat transfer co-efficient for electrolytes using spiral plate heat exchanger. The test section consists of a Plate of width 0.3150 m, thickness 0.001 m and mean hydraulic diameter of 0.01 m. The mass flow rate of hot fluid is varying from 0.4 kg sec^{-1} to 0.8 kg sec^{-1} and the mass flow rate of cold fluid varies from 0.3 kg sec^{-1} to 0.8 kg sec^{-1}. Experiments have been conducted by varying the mass flow rate, temperature and pressure of cold fluid, keeping the mass flow rate of hot fluid constant. The effects of relevant parameters on spiral plate heat exchanger are investigated. The data obtained from the experimental study are compared with the theoretical data. Besides, a new correlation for the nusselt number that can be used for practical applications is proposed.

Keywords: Spiral plate heat exchanger, Reynolds number, Nusselt number, Heat transfer coefficient, Mass flow rate

1. Introduction

Heat exchanger is a device in which energy is transferred from one fluid to another across a solid surface. Spiral plate heat exchangers are good heat transfer devices in process industries that handle slurries and viscous fluids. A great number of applications are there for the spiral plate heat exchanger due to its compactness, high heat transfer coefficients, resistance to fouling and economy in operation. It is more satisfying to chemical, flush, and reversing fluid cleaning techniques because of the single passage. No insulation is used outside the exchanger because of the cold fluid flowing in the outermost passage, resulting in negligible heat loss, if any, due to its temperature closer to atmospheric temperature. It is used in the cellulose industry for cleaning relief vapors in sulfate and sulfite mills. Considerable research is being pursued in spiral heat exchanger in heat transfer and flow areas.

Seban and McLaughlin (Seban, R. A. and E. F. McLaughlin., 1963) calculated heat transfer in coiled tubes for both laminar and turbulent flows. Plot of Nusselt versus Graetz numbers were presented for coils with curvature ratios of 17 and 104 with Reynolds numbers ranging from 12 to 5600 for the laminar flow region. Prandtl numbers ranged from 100 to 657. Heat transfer and pressure loss in steam heated helically coiled tubes were studied by Rogers and Mayhew (Rogers, G. F. C. and Y. R. Mayhew., 1964). They observed that even for a steam heated apparatus, uniform wall temperature was not obtained, mainly due to the distribution of the steam condensate over the coil surface. Mori and Nakayama (Mori, Y. and W. Nakayama., 1965) studied the fully developed flow in a curved pipe with a uniform heat flux for large Dean Numbers. Flow and temperature fields were studied both theoretically and experimentally. They assumed that the flow was divided into two sections, a small boundary layer near the pipe wall, and a large core region making up the remaining flow. Pressure drop and heat transfer for laminar flow of glycerol was presented by Kubair and Kuloor (Berg, R. R. and C. F. Bonilla., 1950) for different types of coiled pipes, including helical and spiral

configurations. Reynolds numbers were in the range of 80 to 6000 with curvature ratios in the range of 10.3 to 27. The number of turns varies from 7 to 12. The results of Kubair and Kuloor (Berg, R. R. and C. F. Bonilla., 1950) match with those of Seban and McLaughlin (Seban, R. A. and E. F. McLaughlin. ,1963) at low Graetz numbers, but deviated at higher Graetz numbers.

Outside-film and inside-film heat transfer coefficients in an agitated vessel were studied by Jha and Rao (Jha, R. K. and M. R. Rao., 1967). Five different coils were studied, along with different speeds and locations of the agitator. They derived an equation to predict the Nusselt number based on the geometry of the helical coil and the location of the agitator. Numerical studies for uniform wall heat flux with peripherally uniform wall temperature for Dean numbers in the range of 1-1200, Prandtl numbers of 0.005-1600, and curvature ratios of 10 to 100 for fully developed velocity and temperature fields were performed by Kalb and Seader (Kalb, C. E. and J. D. Seader., 1972). They found that the curvature ratio parameter had insignificant effect on the average Nusselt number for any given Prandtl number. Kalb and Seader (Kalb, C. E. and J. D. Seader. ,1974) furthered this work by applying the method to the case of a uniform wall-temperature boundary condition with Dean numbers up to 1200, Prandtl numbers and curvature ratios in the ranges of 0.05 to 1600 and 10 to 100, respectively. Their results illustrate that there is a slight effect of curvature on the peripheral variation of the Nusselt number. However, it did not affect the average Nusselt number. The effects of buoyancy forces on fully developed laminar flow with constant heat flux were studied analytically by Yao and Berger (Yao, L.-S., and S. A. Berger.,1978). Their studies were based on the Boussinesq approximation for the buoyancy forces and analyzed for both horizontally and vertically orientated curved pipes. Nusselt number relationships based on the Reynolds number, Raleigh number and Dean Number were presented for both orientations.

Laminar flow and heat transfer were studied numerically by Zapryanov et al (Zapryanov, Z., Christov, C. and E. Toshev. ,1980) using a method of fractional steps for a wide range of Dean numbers from 10 to 7000 and Prandtl numbers from 0.005 to 2000. Their work focused on the case of constant wall temperature and showed that the Nusselt number increased with increasing Prandtl numbers, even for cases at the same Dean number. They also presented a series of isotherms and streamlines for different Dean and Prandtl numbers. The effect of buoyancy on the flow field and heat transfer was studied numerically by Lee et al (Lee, J. B., H. A. Simon, and J. C. F. Chow., 1985) for the case of fully developed laminar flow and axially steady heat flux with a peripherally constant wall temperature. They found that buoyancy effects resulted in an increase in the average Nusselt number, as well as modifying of the local Nusselt number allocation. It was also found that the buoyancy forces result in a rotation of the orientation of the secondary flow patterns. The heat transfer to a helical coil in an agitated vessel was studied by Havas et al. (Havas, G., A. Deak, and J. Sawinsky.,1987). Correlation was developed for the outer Nusselt number based on a modified Reynolds number, Prandtl number, viscosity ratio, and the ratio of the diameter of the tube to the diameter of the vessel. Heat transfer enhancements due to chaotic particle paths were studied by Acharya et al. (Acharya, N., Sen, M., and H. C. Chang., 1992, Acharya, N., Sen, M., and H. C. Chang., 2001) for coiled tubes and alternating axis coils. They developed two correlations of the Nusselt number, for Prandtl numbers less than and greater than one, respectively. Lemenand and Peerhossaini (Lemenand, T. and H. Peerhossaini., 2002) developed a Nusselt number correlation based on the Reynolds number, Prandtl number and the number of bends in the pipe. For the same Reynolds and Prandtl numbers, their work showed that the Nusselt number slightly drops off with increasing number of bends.

Heat transfer for pulsating flow in a curved pipe was numerically studied by Guo et al (Guo, L., Chen, X., Feng, Z., and B. Bai., 1998) for fully developed turbulent flow in a helical coiled tube. In their work they examined both the pulsating flow and the steady state flow. They developed the following correlation (1) for steady turbulent flow for the Reynolds number range of 6000 to 1 80 000

$$Nu = 0.328\,\mathrm{Re}^{0.58}\,\mathrm{Pr}^{0.4} \tag{1}$$

They found that the Reynolds number was increased to very large values [>1 40 000], the heat transfer coefficient for coils began to match the heat transfer coefficient for straight tubes. They also presented correlations of the peripheral local heat transfer coefficients as a function of the average heat transfer coefficients, Reynolds number, Prandtl number, and the location on the tube wall. Inagaki et al. (Inagaki, Y., Koiso, H., Takumi, H., Ioka, I., and Y. Miyamoto ,1998) studied the outside heat transfer coefficient for helically coiled bundles for Reynolds numbers in the range of 6000 to 22 000 and determined that the outside Nusselt number described by the following relationship (2) for their particular setup.

$$Nu = 0.78\,\mathrm{Re}^{0.51}\,\mathrm{Pr}^{0.3} \tag{2}$$

Heat transfer and flow characteristics in the spiral and helical coils have been studied by a number of researchers. Although some information is currently available to calculate the performance of the spiral plate heat exchanger, the study of heat transfer and flow characteristics in spiral plate heat exchanger has received relatively less attention. This is because the heat transfer and flow characteristics of spiral plate heat exchanger have been studied. In the present study, the heat transfer and flow characteristics of mixture of water and Mgso4, Feso4 and Nacl for spiral plate heat exchanger have been experimentally studied, in addition to the development of a new correlation for Nusselt number.

2. Experimental Setup

The experimental setup consists of spiral plate heat exchanger, thermocouple, pumps and tanks as shown in Figure 2.1. The parameters of heat exchanger are shown in the Table 2.1. The hot fluid inlet pipe is connected at the center core of the spiral heat exchanger and the outlet pipe is taken from periphery of the heat exchanger. The hot fluid is heated by pumping the steam from the boiler to a temperature of about 60-70° C and connected to hot fluid tank having a capacity of 1000 liters then the hot solution is pumped to heat exchanger using a pump. Thus the counter flow of the fluid is achieved. The cold fluid inlet pipe is connected to the periphery of the exchanger and the outlet is taken from the centre of the heat exchanger. The cold fluid is supplied at room temperature from cold solution tank and is pumped to the heat exchanger using a pump.

3. Experimental Procedure

The heat transfer and flow characteristic of mixture of water and Mgso4, Feso4 and Nacl is tested using an Alfa Laval; Model P5-VRB, Spiral plate heat exchanger as shown in Figure. 2.1. The inlet hot fluid flow rate is kept constant and the inlet cold fluid flow rate is varied using a control valve. The flow of hot and cold fluid is varied using control valves, C2 and C1 respectively. Thermocouple T1 and T2 are used to measure inlet temperature of cold and hot fluids respectively; T3 and T4 are used to measure the outlet temperatures of cold and hot fluids respectively. For different cold fluid flow rate the temperatures at the inlet and outlet of hot and cold fluids are recorded, after achieving the steady state. The same procedure is repeated for different hot fluid flow rates and the data related to temperatures, the corresponding temperatures and mass flow rates are recorded. The mass flow rate is noted by using the Rotometer R1 and R2, fitted at the outlet of the corresponding fluids. Experimental conditions are shown in Table 3.1.

4. Results and Discussion

4.1 Reynolds Number Vs Heat Transfer Coefficient

In this study electrolytes such as Feso4, Nacl and Mgso4 have been used. The concentration of electrolytes has been varied from 5% to 15 %(volume %). The effect of heat transfer rate on Reynolds number for different electrolytes is shown in Figure 4.1. It is observed that the heat transfer rate increases with increasing Reynolds number of mixture of water and electrolytes. Solvation of ion with water is the reason enough to account for maximum heat transfer rate.

4.2 Reynolds Number Vs Nusselt Number

Figure 4.2 shows the variation of the Nusselt number with Reynolds number of electrolytes for different inlet temperatures. From the experimental results, it is shown that the Nusselt number increases with increasing of Reynolds number of mixture of water and electrolytes.

4.3 Nusselt number (Experimental) Vs (Predicted)

Figure 4.3 shows the comparisons of the Nusselt numbers obtained from the experiment conducted with those calculated theoretically. It can be noted that the experimental and predicted Nusselt numbers fall within ±20%. The major discrepancy between the measured data and calculated results may be due to the difference in the configuration of test sections and uncertainty of the correlation.

The Nusselt number correlation (3) for spiral plate heat exchanger is expressed as follows.

The correlation is obtained by fitting a total of 153 experimental data. (R^2 =0.97)

$$N_u = 0.0476 R_e^{0.832} P_r^{-0.149} \quad (3)$$

$3800>R_e<8500$

4.4 Comparison of Experimental number with Holger Mortin Correlation

Holger martin correlation (4)

$$Nu = 0.04 \, Re^{0.74} \, Pr^{0.4} \quad (4)$$

$4.10^2<Re<3.10^4$

Comparisons of the Nusselt numbers obtained from the present experiment with those calculated from the existing correlation are shown in Figure 4.4.It can be noted that the values obtained from the correlation are slightly consistent with the experimental data and lie within ±21%for the Holger martin correlation.

5. Conclusion

This paper presents new experimental data from the measurement of the heat transfer coefficient of mixture of water and electrolyte flows in a spiral plate heat exchanger. The effects of relevant parameters are investigated. The data obtained from the present study are compared with the theoretical data. In addition, a new correlation based on the experimental data is given for practical applications.

6. Acknowdgement

The authors are grateful to the Management and the Principal of Kongu Engineering College, Erode, Tamilnadu, India, for granting permission to carry out the research work.

7. Nomenclature

Nu- Nusselt number

Re-Reynolds number

Pr-Prandtl number

h- Heat transfer coefficient [wm^{-2} k^{-1}]

References

Acharya, N., Sen, M., and H. C. Chang. (1992). Heat transfer enhancement in coiled tubes by chaotic mixing. *International Journal of Heat and Mass Transfer*, Vol.35 (10):2475-2489.

Acharya, N., Sen, M., and H. C. Chang. (2001). Analysis of heat transfer enhancement in coiled-tube heat exchangers. *International Journal of Heat and Mass Transfer*, Vol.44: 3189-3199.

Berg, R. R. and C. F. Bonilla. (1950). *Trans. N. Y. Acad. Sci*. Vol. 13:12 (as cited in Kubair and Kuloor, 1966).

Guo, L., Chen, X., Feng, Z., and B. Bai. (1998). Transient convective heat transfer in a helical coiled tube with pulsating fully developed turbulent flow. *International Journal of Heat and Mass Transfer*, Vol. 41:2867-2875.

Havas, G., A. Deak, and J. Sawinsky. (1987). Heat transfer to helical coils in agitated vessels. *The Chemical Engineering Journal*, Vol. 35:61-64.

Holger Martin., Heat exchangers. (1992). *Hemisphere publishing corporation*., London.

Inagaki, Y., Koiso, H., Takumi, H., Ioka, I., and Y. Miyamoto.(1998). Thermal hydraulic study on a high-temperature gas-gas heat exchanger with helically coiled tube bundles. *Nuclear Engineering and Design*, Vol. 185:141-151.

Jha, R. K. and M. R. Rao. (1967). Heat transfer through coiled tubes in agitated vessels. *International Journal of Heat and Mass Transfer*, Vol. 10:395-397.

Kalb, C. E. and J. D. Seader. (1972). Heat and mass transfer phenomena for viscous flow in curved circular tubes. *International Journal of Heat and Mass Transfer*, Vol. 15:801-817.

Kalb, C. E. and J. D. Seader. (1974). Fully developed viscous-flow heat transfer in curved circular tubes with uniform wall temperature. *AIChE Journal*, Vol. 20(2):340-346.

Lee, J. B., H. A. Simon, and J. C. F. Chow. (1985). Buoyancy in developed laminar curved tube flows. *International Journal of Heat and Mass Transfer*, Vol. 28(2):631- 640.

Lemenand, T. and H. Peerhossaini. (2002). A thermal model for prediction of the Nusselt number in a pipe with chaotic flow. *Applied Thermal Engineering*, Vol. 22:1717-1730.

Mori, Y. and W. Nakayama. (1965). Study on forced convective heat transfer in curved pipes (1st report, laminar region). *International Journal of Heat and Mass Transfer*, Vol. 8:67-82.

Rogers, G. F. C. and Y. R. Mayhew. (1964). Heat transfer and pressure loss in helically coiled tubes with turbulent flow. *International Journal of Heat and Mass Transfer*, Vol. 7:1207-1216.

Seban, R. A. and E. F. McLaughlin. (1963). Heat transfer in tube coils with laminar and turbulent flow. *International Journal of Heat and Mass Transfer*, Vol. 6:387-395.

Yao, L.-S., and S. A. Berger. (1978). Flow in heated curved pipes. *Journal of Fluid Mechanics*, Vol. 88(2):339-354.

Zapryanov, Z., Christov, C. and E. Toshev. (1980). Fully developed laminar flow and heat transfer in curved tubes. *International Journal of Heat and Mass Transfer*, Vol. 23:873-880.

Table 2.1 Dimensions of the Spiral plate Heat Exchanger

Parameters	Dimensions (P5-VRB plate)
Plate width, m	0.3150
Plate thickness, m	0.0010
Mean channel spacing, m	0.0050
Mean hydraulic diameter, m	0.0100
Heat transfer area, m^2	2.2400

The above table gives the dimensions and the parameters of the Spiral Plate Heat Exchanger.

Table 3.1 Experimental Conditions

Sl.No	Variables	Range
1	Hot water temperature	65-50 °C
2	Cold Water temperature	30-50 °C
3	Mass flow rate of hot water	0.4-0.8 kg sec^{-1}
4	Mass flow rate of cold Water	0.3-0.8 kg sec^{-1}

The table above provides the experimental conditions of the hot and cold water temperature, mass flow rate of hot and cold water.

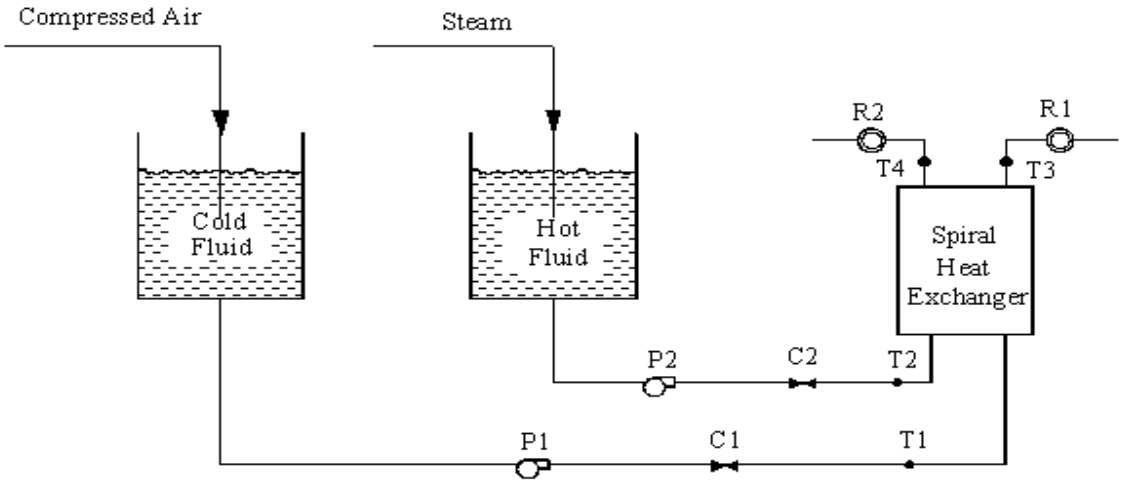

Figure 2.1 Schematic diagram of experimental apparatus

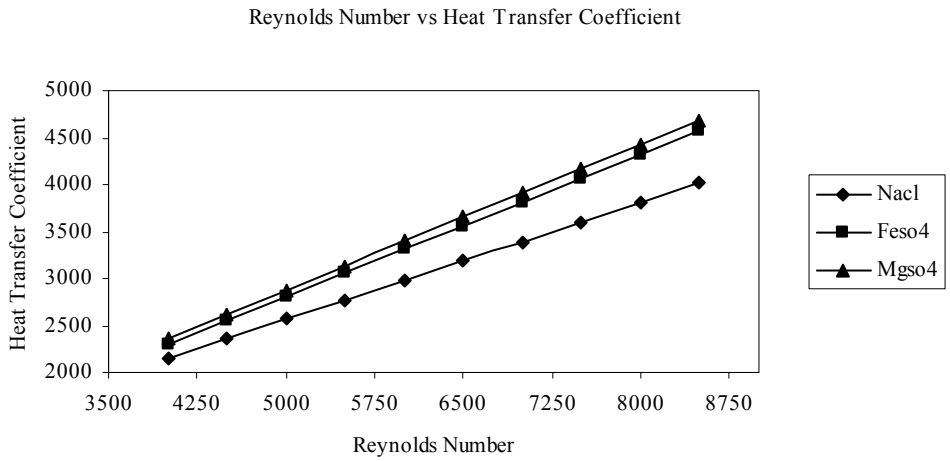

Figure 4.1 Variation of Reynolds number with Heat transfer rate

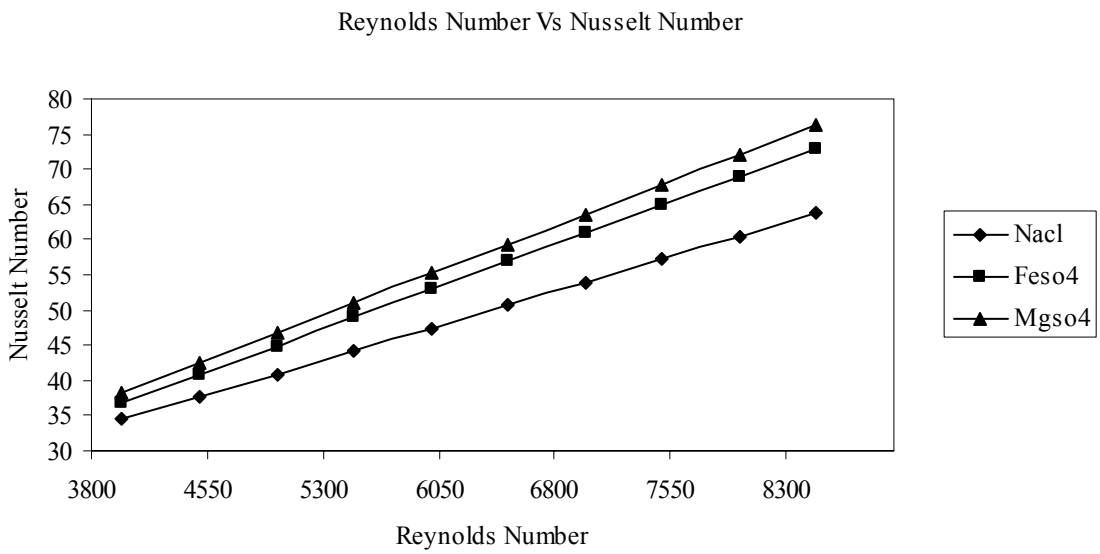

Figure 4.2 Variation of Reynolds number with Nusselt number

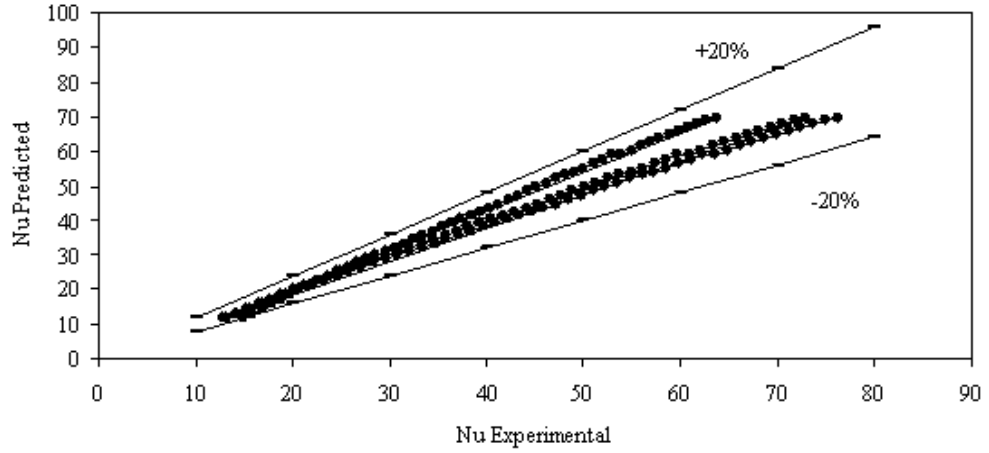

Figure 4.3 Variation of Nusselt number (Experimental) with Nusselt number (Predicted)

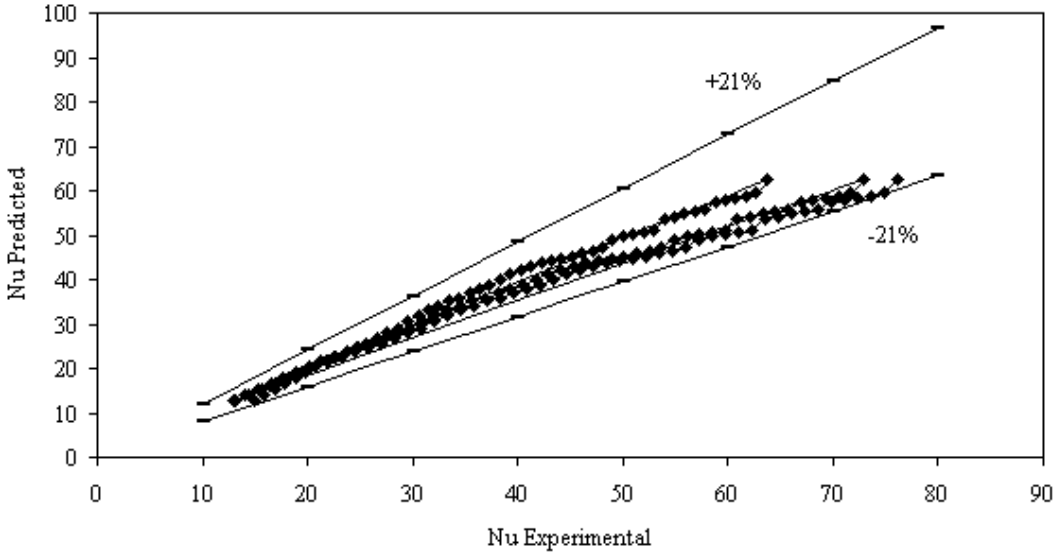

Figure 4.4 Comparison of Experimental data with Holger Martin correlation

Modern Applied Science

www.ccsenet.org/journal.html

Vol. 2, No. 5

September 2008

Several Theorems for the Trace of Self-conjugate Quaternion Matrix

Qinglong Hu

Department of Engineering Technology

Xichang College

Xichang, Sichuan, 615013, China

E-mail: shjecho@126.com

Limin Zou(Corresponding author)

College of Mathematics and Physics

Chongqing University

Chongqing, 400044, China

E-mail: zlmlohr@163.com

The research is Supported by Chongqing University postgraduates' Science and Innovation Fund (200801A 1 A0070266).

Abstract

The purpose of this paper is to discuss the inequalities for the trace of self-conjugate quaternion matrix. We present the inequality for eigenvalues and trace of self-conjugate quaternion matrices. Based on the inequality above, we obtain several inequalities for the trace of quaternion positive definite matrix.

Keywords: Quaternion matrix, Trace, Inequalities, Eigenvalues

1. Introduction

Quaternion was introduced by the Irish mathematician Hamilton (1805-1865) in 1843. The literature on quaternion matrices, though dating back to 1936 [1], is fragmentary. Quaternion is mostly used in computer vision because of their ability to represent rotations in 4D spaces. It is also used in programming video games and controlling spacecrafts [2, 3] and so forth. The research on mathematical objects associated with quaternion has been dynamic for years. There are many research papers published in a variety of journals each year and different approaches have been taken for different purposes, and the study of quaternion matrices is still in development. As is expected, the main obstacle in the study of quaternion matrices is the non-commutative multiplication of quaternion. The theory on eigenvalues, determinant, singular values and trace of real and complex matrices has been well established. On the contrary, little is known for the trace of quaternion matrices.

As usual, R and C are the set of the real and complex numbers. We denote by H (in honor of the inventor, Hamilton) the set of real quaternion:

$$H=\{a=a_0+a_1i+a_2j+a_3k, a_0,a_1,a_2,a_3\in R\}.$$

For $a=a_0+a_1i+a_2j+a_3k\in H$, the conjugate of a is $\bar{a}=a^*=a_0-a_1i-a_2j-a_3k$ and the norm of a is $N(a)=\sqrt{a\bar{a}}=\sqrt{\bar{a}a}=(a_0^2+a_1^2+a_2^2+a_3^2)^{1/2}$. Let $H^{n\times n}$ and $H^{n\times 1}$ be respectively the collections of all $n\times n$ matrices with entries in H and n-column vectors. Let I_n be the collections of all $n\times n$ unit matrices with entries in H. For $X\in H^{n\times 1}, X^T$ is the transpose of X. If $X=(X_1,X_2\ldots X_n)^T$, then $\bar{X}=(\bar{X}_1,\bar{X}_2,\ldots,\bar{X}_n)^T$ is the conjugate of X and $X^*=(\bar{X}_1,\bar{X}_2,\ldots,\bar{X}_n)$ is the conjugate transpose of X. The norm of X is defined to be $N(X)=\sqrt{X^*X}$. For an

$n \times n$ matrix $A = (a_{ij})_{n\times n}$ $(a_{ij} \in H)$, the conjugate transpose of A is the $n \times n$ matrix $A^* = \bar{A}^T = (a_{ij}^*)_{n\times n}$.

The research of matrices is continuously an important aspect of algebra problems over quaternion division algebra, the subject, such as eigenvalues, singular values, congruent and positive definite of self- conjugate matrices as well as sub-determinant of self- conjugate matrices and so on, has been extensively explored [4-15], while little is known for the trace of quaternion matrices. For linear algebraists and matrix theories, some basic questions on the trace of quaternion matrix are different from real or complex matrix. For instance, if A and B are the $n \times n$ matrices, then $Tr(AB) = Tr(BA)$ and $Tr(A) = \sum_{i}^{n} \lambda_i$ are not always right. In this section, we introduce the notation and terminology. In section 2, we define some definitions and recall several lemmas. In section 3, we discuss the inequality about eigenvalues and trace of self-conjugate quaternion matrices. In section 4, we conclude the paper with several inequalities for the trace of quaternion positive definite matrix obtained by the result in section 3 and the Holder's inequality over quaternion division algebra.

2. Definitions and Lemmas

We begin this section with some basic definitions and lemmas.

Definition 2.1 Let $A \in H^{n\times n}$. A is said to be the self-conjugate quaternion matrix if $A^* = A$.

$H(n,*)$ is the set of self-conjugate quaternion matrices, $H(n,>)$ is the set of quaternion positive definite matrices.

Definition 2.2 Let $A \in H^{n\times n}$. A is said to be the quaternion unitary matrix if $A^*A = AA^* = I_n$. $H(n,u)$ is the set of quaternion unitary matrices.

Definition 2.3 Let $A \in H^{n\times n}$. $\sum_{i=1}^{n} a_{ii}$ is said to be the trace of matrix A, remarked by $Tr(A)$. That is $Tr(A) = \sum_{i=1}^{n} a_{ii}$.

Lemma 1. [4] Let $A \in H(n,*)$. Then, A is unitary similar to a real diagonal matrix, that is, there exists a unitary matrix $U \in H(n,u)$, such that

$$U^*AU = diag(\lambda_1, \lambda_2, \cdots, \lambda_n),$$

where, $\lambda_1, \lambda_2, \cdots \lambda_n \in R$ are the eigenvalues of A.

Lemma 2. Let $A \in H(n,*)$ and $B \in H(n,*)$. If there exists $U \in H(n,u)$, such that $B = UAU^*$, then, $TrA = TrB$.

Proof. Since $A \in H(n,*)$, by Lemma 1, there exists $V \in H(n,u)$, such that

$$V^*AV = diag(\lambda_1, \lambda_2, \cdots, \lambda_n),$$

where, $\lambda_1, \lambda_2, \cdots \lambda_n \in R$ are the eigenvalues of A. For any $U \in H(n,u)$, we have

$$\sum_{i=1}^{n} u_{ij}u_{ij}^* = \sum_{i=1}^{n} N^2(u_{ij}) = 1, (j = 1,2,\cdots,n) \tag{2.2}$$

$$\sum_{j=1}^{n} u_{ij}u_{ij}^* = \sum_{j=1}^{n} N^2(u_{ij}) = 1, (i = 1,2,\cdots,n) \ . \tag{2.3}$$

So

$$TrA = \sum_{i=1}^{n} a_{ii} = \sum_{i=1}^{n} \left\{ \sum_{k=1}^{n} v_{ik} \left(\sum_{l=1}^{n} \lambda_k \delta_{kl} \right) v_{il}^* \right\} = \sum_{i=1}^{n} \left\{ \sum_{k=1}^{n} \sum_{l=1}^{n} \lambda_k v_{ik} \delta_{kl} v_{il}^* \right\}$$

$$= \sum_{i=1}^{n} \left\{ \sum_{l=1}^{n} \lambda_l v_{ll} v_{ll}^* \right\} = \sum_{i=1}^{n} \lambda_l \left\{ \sum_{l=1}^{n} v_{ll} v_{ll}^* \right\} = \sum_{i=1}^{n} \lambda_l$$

Meanwhile, we have $B = UAU^*$, then

$B = UVdiag(\lambda_1, \lambda_2, \cdots, \lambda_n)V^*U^*$.

Since $UV \in H(n,u)$, therefore

$TrA = TrB = \sum_{i=1}^{n} \lambda_l$.

Thus

$$TrA = TrB \tag{2.4}$$

3. The inequality for the trace of self-conjugate quaternion matrices

It is well known that the eigenvalues and trace of any self-conjugated quaternion matrix are all real numbers. In this section, we shall discuss the inequality about eigenvalues and trace of self-conjugate quaternion matrices.

Theorem 1. Let $A \in H(n,>), B \in H(n,*)$, their eigenvalues are $\alpha_1 \geq \alpha_2 \geq \cdots \geq \alpha_n$, $\beta_1 \geq \beta_2 \geq \cdots \geq \beta$ respectively, if A, B are commutative, then $Tr(AB) \leq \sum_{i=1}^{n} \alpha_i \beta_i$.

Proof. Since $A \in H(n,*), B \in H(n,*)$, by lemma 1, there exists unitary matrices $U_1, U_2 \in H(n,u)$, such that

$$U_1^{*} A U_1 = diag(\alpha_1, \alpha_2, \cdots, \alpha_n) \tag{3.1}$$

$$U_2^{*} B U_2 = diag(\beta_1, \beta_2, \cdots, \beta_n) \tag{3.2}$$

where $\alpha_i > 0 (i = 1,2,\cdots n)$.Therefore

$$Tr(AB) = Tr\left[U_1 diag(\alpha_1, \alpha_2, \cdots, \alpha_n) U_1^{*} U_2 diag(\beta_1, \beta_2, \cdots, \beta_n) U_2^{*}\right].$$

By (3.1) and (3.2), we have

$$U_1^{*} AB U_1 = diag(\alpha_1, \alpha_2, \cdots, \alpha_n) U_1^{*} U_2 diag(\beta_1, \beta_2, \cdots, \beta_n) U_2^{*} U_1.$$

Let $U_1^{*} U_2 = U = (u_{ij})_{n \times n}$, it is easy to know $U \in H(n,u)$, then

$$\sum_{i=1}^{n} u_{ij} u_{ij}^{*} = \sum_{i=1}^{n} N^2(u_{ij}) = 1, (j = 1,2,\cdots,n)$$

$$\sum_{j=1}^{n} u_{ij} u_{ij}^{*} = \sum_{i=1}^{n} N^2(u_{ij}) = 1, (i = 1,2,\cdots,n).$$

Since $(AB)^{*} = B^{*} A^{*} = BA$, and A, B are commutative, then $(AB)^{*} = AB$, so $AB \in H(n,*)$. Hence, by Lemma 2, $Tr(AB) = Tr(U_1^{*} AB U_1)$, then

$$Tr(AB) = Tr\left[diag(\alpha_1, \alpha_2, \cdots, \alpha_n) U diag(\beta_1, \beta_2, \cdots, \beta_n) U^{*}\right]$$

$$= (\alpha_1, \alpha_2, \cdots, \alpha_n) \begin{pmatrix} N^2(u_{11}) & N^2(u_{12}) & \cdots & N^2(u_{1n}) \\ N^2(u_{21}) & N^2(u_{22}) & \cdots & N^2(u_{2n}) \\ \cdots & \cdots & \cdots & \cdots \\ N^2(u_{n1}) & N^2(u_{n2}) & \cdots & N^2(u_{nn}) \end{pmatrix} \begin{pmatrix} \beta_1 \\ \beta_2 \\ \vdots \\ \beta_n \end{pmatrix}.$$

Let

$$\begin{pmatrix} \xi_1 \\ \xi_2 \\ \vdots \\ \xi_n \end{pmatrix} = \begin{pmatrix} N^2(u_{11}) & N^2(u_{12}) & \cdots & N^2(u_{1n}) \\ N^2(u_{21}) & N^2(u_{22}) & \cdots & N^2(u_{2n}) \\ \cdots & \cdots & \cdots & \cdots \\ N^2(u_{n1}) & N^2(u_{n2}) & \cdots & N^2(u_{nn}) \end{pmatrix} \begin{pmatrix} \beta_1 \\ \beta_2 \\ \vdots \\ \beta_n \end{pmatrix}$$

then

$$\sum_{i=1}^{n} \xi_i = \sum_{i=1}^{n} \beta_i. \tag{3.3}$$

For any $k (1 \leq k < n)$, we have

$$\sum_{i=1}^{k} \xi_i = \sum_{i=1}^{k} \sum_{j=1}^{n} N^2(u_{ij}) \beta_j = \sum_{i=1}^{k} \beta_i - \sum_{i=1}^{k} \left(1 - \sum_{j=1}^{k} N(u_{ij})\right) \beta_i + \sum_{i=1}^{k} \sum_{j=k+1}^{n} N^2(u_{ij}) \beta_j$$

$$\leq \sum_{i=1}^{k} \beta_i - \beta_k \sum_{i=1}^{k} \left(1 - \sum_{j=1}^{k} N^2(u_{ij})\right) + \beta_k \sum_{i=1}^{k} \sum_{j=k+1}^{n} N^2(u_{ij})$$

$$= \sum_{i=1}^{k} \beta_i - \beta_k \sum_{i=1}^{k} \left(1 - \sum_{j=1}^{k} N^2(u_{ij})\right) + \beta_k \left(1 - \sum_{j=1}^{k} N^2(u_{ij})\right)$$

$$= \sum_{i=1}^{k} \beta_i \quad . \tag{3.4}$$

By (3.3), (3.4) ,and $\alpha_i > 0 (i = 1,2,\cdots n)$, then

$$Tr(AB) = \sum_{i=1}^{n} \alpha_i \xi_i \le \sum_{i=1}^{n} \alpha_i \beta_i \cdot$$

4. The inequality for the trace of quaternion positive definite matrix

In this section, we first obtain an inequality for the trace of two quaternion positive definite matrices based on Theorem 1.Then by Theorem 1 and the Holder's inequality over quaternion division algebra, the inequality for trace of the sum and multiplication of quaternion positive definite matrices is obtained.

Theorem 2. Let $A \in H(n,>), B \in H(n,>)$, their eigenvalues are $\alpha_1 \ge \alpha_2 \ge \cdots \ge \alpha_n$, $\beta_1 \ge \beta_2 \ge \cdots \ge \beta$ respectively, if A, B are commutative, then

$$\sqrt{Tr(AB)} \le \sqrt{Tr(A)Tr(B)} \le \frac{Tr(A)+Tr(B)}{2} \le \sqrt{\frac{Tr^2(A)+Tr^2(B)}{2}} \cdot$$

Proof. Since $Tr(A) = \sum_{i=1}^{n} a_{ii} = \sum_{i=1}^{n} \alpha_i > 0$ and $Tr(B) = \sum_{i=1}^{n} b_{ii} = \sum_{i=1}^{n} \beta_i > 0$, by Theorem 1,we have

$$Tr(AB) \le \sum_{i=1}^{n} \alpha_i \beta_i \cdot$$

Because of $A \in H(n,>)$, then there exists $U \in H(n,u)$, such that

$$U^* AU = diag(\alpha_1, \alpha_2, \cdots, \alpha_n)$$

where $\alpha_i > 0 (i = 1,2,\cdots n)$.So,

$$U^* ABU = U^* AUU^* BU = diag(\alpha_1, \alpha_2, \cdots, \alpha_n) U^* BU \cdot \tag{4.1}$$

Since $B \in H(n,>)$, then B and I_n are self-congruent, hence $U^* BU$ and I_n are self-congruent, that is , $U^* BU$ is quaternion positive definite matrix. For any main sub-matrix L of $U^* ABU$, by (4.1), we know that L can be obtained by the main sub-matrix G of $U^* BU$ .Then

$\| L \| = | L |^{\text{row}} = \alpha_i \alpha_j \cdots | G |^{\text{row}} = \alpha_i \alpha_j \cdots \| G \| > 0$,

where $\| \cdot \|$ is the determinant of quaternion matrix defined by Chen L X [10]. So, $U^* ABU$ is quaternion positive definite matrix, hence $Tr(AB) > 0$ .Since

$$Tr(A)Tr(B) - Tr(AB) \ge \sum_{i=1}^{n} \alpha_i \sum_{i=1}^{n} \beta_i - \sum_{i=1}^{n} \alpha_i \beta_i \ge 0$$

so

$$\sqrt{Tr(AB)} \le \sqrt{Tr(A)Tr(B)} \cdot \tag{4.2}$$

Because of

$$Tr^2(A) + Tr^2(B) \ge 2Tr(A)Tr(B)$$

then

$$2Tr^2(A) + 2Tr^2(B) \ge Tr^2(A) + 2Tr(A)Tr(B) + Tr^2(B)$$

namely

$$\frac{Tr^2(A)+Tr^2(B)}{2} \ge \left(\frac{Tr(A)+Tr(B)}{2} \right)^2$$

so

$$\frac{Tr(A)+Tr(B)}{2} \le \sqrt{\frac{Tr^2(A)+Tr^2(B)}{2}} \cdot \tag{4.3}$$

By (4.2) and (4.3), the conclusion holds.

Theorem 3. Let $A \in H(n,>), B \in H(n,>)$. Their eigenvalues are $\alpha_1 \geq \alpha_2 \geq \cdots \geq \alpha_n$, $\beta_1 \geq \beta_2 \geq \cdots \geq \beta$ respectively, if $p>1, \frac{1}{p}+\frac{1}{q}=1$,and A, B are commutative, then

$$Tr(AB) \leq \left(Tr\left(A^p\right)\right)^{\frac{1}{p}} \left(Tr\left(B^q\right)\right)^{\frac{1}{q}}.$$

Proof. By Theorem 1 and the Holder's inequality, we have

$$Tr(AB) \leq \sum_{i=1}^{n} \alpha_i \beta_i \leq \left(\sum_{i=1}^{n} \alpha_i^p\right)^{\frac{1}{p}} \left(\sum_{i=1}^{n} \beta_i^q\right)^{\frac{1}{q}} = \left(Tr(A^p)\right)^{\frac{1}{p}} \left(Tr(B^q)\right)^{\frac{1}{q}}.$$

Specially, when $p=q=2$, we have

$$Tr(AB) \leq \sqrt{\left(Tr(A^2)\right)} \sqrt{\left(Tr(B^2)\right)}.$$

Theorem 4. Let $A \in H(n,>), B \in H(n,>)$. Their eigenvalues are $\alpha_1 \geq \alpha_2 \geq \cdots \geq \alpha_n$, $\beta_1 \geq \beta_2 \geq \cdots \geq \beta$ respectively, if $p>1$,and A, B are commutative, then

$$\left(Tr\left((A+B)^p\right)\right)^{\frac{1}{p}} \leq \left(Tr\left(A^p\right)\right)^{\frac{1}{p}} + \left(Tr\left(B^p\right)\right)^{\frac{1}{p}}.$$

Proof. Let $q=\frac{p}{p-1}$, then $p>1, q>0, \frac{1}{p}+\frac{1}{q}=1$ .Since

$$(A+B)^p = A(A+B)^{p-1} + B(A+B)^{p-1}$$

then, by Theorem 3 and the Holder's inequality, we have

$$Tr\left[(A+B)^p\right] = Tr\left[A(A+B)^{p-1} + B(A+B)^{p-1}\right]$$

$$\leq \left(TrA^p\right)^{\frac{1}{p}} \left[Tr\left(\left((A+B)^{p-1}\right)^q\right)\right]^{\frac{1}{q}} + \left(TrB^p\right)^{\frac{1}{p}} \left[Tr\left(\left((A+B)^{p-1}\right)^q\right)\right]^{\frac{1}{q}}$$

$$= \left[Tr\left(\left((A+B)^{p-1}\right)^q\right)\right]^{\frac{1}{q}} \left[\left(TrA^p\right)^{\frac{1}{p}} + \left(TrB^p\right)^{\frac{1}{p}}\right]$$

$$= \left[Tr\left(\left((A+B)^{p-1}\right)^{\frac{p}{p-1}}\right)\right]^{\frac{p-1}{p}} \left[\left(TrA^p\right)^{\frac{1}{p}} + \left(TrB^p\right)^{\frac{1}{p}}\right]$$

$$= \left[Tr\left((A+B)^p\right)\right]^{\frac{p-1}{p}} \left[\left(TrA^p\right)^{\frac{1}{p}} + \left(TrB^p\right)^{\frac{1}{p}}\right].$$

That is

$$Tr\left[(A+B)^p\right] \leq \left[Tr\left((A+B)^p\right)\right]^{\frac{p-1}{p}} \left[\left(TrA^p\right)^{\frac{1}{p}} + \left(TrB^p\right)^{\frac{1}{p}}\right].$$

So

$$\left(Tr\left((A+B)^p\right)\right)^{\frac{1}{p}} \leq \left(Tr\left(A^p\right)\right)^{\frac{1}{p}} + \left(Tr\left(B^p\right)\right)^{\frac{1}{p}}.$$

References

Chen Longxuan. Definition of determinant and Cramer solutions over the quaternion Acta Math Sinica, New ser.1991 (07)171-180.

Huang Liping, Wan Zhexian. Geometry of skew-Hermitian matrices [J]. Linear .Algebra. Appl. 396(2005) 127-157.

Huang Liping. On two questions about quaternion matrices [J] Lin Alg Appl .323(2003)105-116.

L.A. Wolf, Similarity of matrices in which elements is real quaternion [J]. Bull. Amer. Math. Soc. 42 (1936) 737–743.

Ran Ruisheng, Huang Tingzhu. The recognition of color Images based on the singular value decompositions of quaternion matrices [J] (in Chinese). Computer Science. 2006(07)227-229.

Tu Boxuen. Weak kronecker product and weak Hadamard product of Quaternion matrix [J] (in Chinese). Journal of Fu dan univ. 1991 (03)331-339.

Tu Boxun. The centralized basic theorem of a real quaternion self-conjugate matrix and its application [J]. (in Chinese). Journal of Mathematics, 1988(8), 143-150.

Wang Qinggui. Quaternion transformation and its application on the display-cement analysis of spatial mechanisms [J] (in Chinese). Acta Mechanica Sinica.1983(01), 54-61.

Wang Qingwen, Song Guangjing, Lin Chunyan. Extreme ranks of the solution to a consistent system of linear quaternion matrix equations with an application [J]. Appl. Math. Com.189 (2007) 1517 - 15 32.

Wang Qingwen. A system of matrix equation and a linear matrix equation over arbitrary regular rings with identity[J]. Linear Algebra. Appl. 384 (2004) 43-54.

Wang Qingwen. The General Solution to a system of real quaternion matrix equation [J]. Computer and Mathematics with Applications 49 (2005) 665-675.

Wu Junliang. Distribution and Estimation for Eigenvalues of Real Quaternion Matrices [J]. Computers and Mathematics with Applications. 55 (2008) 1998–2004.

Zhang Fuzhen. Quaternions and matrices of quaternions [J]. Linear Algebra Appl. 251 (1997) 21–57.

Zhang Fuzhen. Gersgorin type theorems for quaternionic matrices [J]. Linear .Algebra. Appl. 424 (2007). 139-153.

Zhuang Wajin. The guide of quaternion algebra theory [M] (in Chinese). Science press, Beijing, 2006.

Modern Applied Science

www.ccsenet.org/journal.html

Vol. 2, No. 5

September 2008

The Malaysian Construction Industry's Risk Management in Design and Build

Hamimah Adnan

Department of Quantity Surveying

Faculty of Architecture Planning and Surveying

University Teknologi MARA, Malaysia

Tel: 60-3-5544-4935 E-mail: hamimah689@salam.uitm.edu.my

Kamaruzaman Jusoff (Corresponding author)

Yale University, Tropical Resources Institute

210 Prospect St, New Haven, CT 06511, USA

Tel: 60- 203-676-7761 E-mail: jusoff.kamaruzaman@yale.edu

Mohd Khairi Salim

Department of Quantity Surveying

Faculty of Architecture Planning and Surveying

Universiti Teknologi MARA, UiTM Shah Alam, Selangor, Malaysia

The research is financed by Universiti Teknologi MARA (UiTM), Shah Alam, Selangor,Malaysia (Sponsoring information)

Abstract

Over the past twenty years, there have been large-scale and expensive public works tenders that adopted design and build procurement (D&B) contracts which consist of construction and civil engineering. Experts from the academic and construction circles have been studying the effective implementation of these tenders, the difficulties they encountered and the solutions for them. However, design and build (D&B) projects have additional stages such as the pre-planning and design and post-operative stages compared to traditional construction projects. As a result, contractors are faced with a higher chance of project risk probability and impacts. The risks that were to be assumed by the original employer may be transferred to the design and build contractors by means of a written agreement. Risk Management involves appropriate handling of risks after evaluation and analysis to minimize the negative impacts risks have on the finance with the lowest costs. Risk management is applied to establish necessary guidelines and to obtain key indices for successful design and build projects for contractor to follow. The method incorporated in this research included literature review, questionnaire surveys and interviews. The encountered risk factors were compiled and placed in the right sequence. The possible ways of minimizing risks that design and build members have on the project according to the definition and implementation of risk management been also looked into. From the findings, it is recommended that contractors should have clear employer briefing, clear specifications and statement of needs, good quality of workmanship, implementing code of practice, key elements effective management, effective communication with all components of the project team and decisive action in the event of deviation from plans for a successful (D&B) projects

Keywords: Risk Management, Design and build, Malaysian construction Industry

1. Introduction

The construction industry is a vehicle through which a nation's physical developments are activated by initiating projects from the blue print stage to the implementation. The implementation and materialization of such projects inevitably can bring about benefits to the people and the nation, thus satisfying the aspiration of national progress and

growth and in up-lifting the status of the nation economically. At the implementation stages of developing a project the client has to make decisions on technical choices such as size, location and standard. By then the client should decide on a contract strategy regarding the best method to employ contractors for construction and other services. This would depend on his priorities on the cost of the project, construction time, quality or any secondary objective. Lack of a contract strategy in reference to risk allocation can produce very unpleasant surprises that will lead to future disputes. It is possible to find that contract duration and the processes involved are beyond the clients' initial expectations. Therefore, careful analysis for a contract strategy should lead to the selection of the right allocation of responsibilities, type of contract and tendering procedure for a project and eventually for the contract itself.

The increasingly complex and varying demands placed upon the construction industry by the clients do not only stem from the need to provide more sophisticated commercial and industrial working environments at minimum cost and maximum speed, but also from the fact that the organizations of the clients' are also complex in nature with different categories of consumers requiring discrete solutions to their procurement needs. The choice of a procurement method route for construction work is one of the many important decisions that construction clients have to make. An early decision on the preferred method of contract procurement is essential, as it will have an impact on the amount of the pre-contract work, the employers' financial and human resources, outlay for the completion of the project as well as issues such as risk transfer and allocation of responsibilities under the contract. Therefore, modern owners of constructed facilities are increasingly investigating a variety of alternative procurement methods. These methods include design-build, turnkey and construction management. To effectively service this market driven expansion of project delivery strategies in the construction community a fundamental understanding of owner's attitudes is required.

Design and build is an arrangement where contracting organization takes sole responsibility, normally on a lump sum fixed price basis, for the bespoke design and construction of a client's project (Masterman, 1992). Design and build is a procurement method where one entity or consortium is contractually responsible for both the design and construction of a project (Murdoch & Hughes, 2000). In contract to the lump sum method, design and build has two concurrent phases. The clients enter into one contract with a design and build company that is responsible for project development and construction. The contractual arrangement is the simplest of the other contractual arrangement like management contracting (MC) and construction management (CM). There is one contract and one line of communication for the client. The designer-builder may be a single company that employs both the design and construction staff (known as D&B) or the design-builder may be a partnership of two or more design and construction companies (known as joint venture D&B). The objectives of this paper are two-folds: to identify common risks associated with design and build method and to make recommendation in order to mitigate the risks.

Construction is a dynamic and complex industry requiring enormous amounts of capital and resources to function efficiently. The factor of the size and diversity of the construction industry, the major industry player-owners, designers and contractors appear to be in conflict. These conflicts can be brought on by any number of situations, but the results from a lack of consideration about the real risks involved with a construction project. Risk Management involves appropriate handling of risks after evaluation and analysis to minimize the negative impacts risks have on the finance with the lowest costs. It is important for contractor to identify and analyze the risks that occur in design and build to ensure that it does not impede the success of the design and build project. In ideal risk management, a prioritization process is followed whereby the risks with the greatest loss and the greatest probability of occurring are handled first, and risk with lower probability of occurrence and lower loss are handled later. The process can be very difficult, and balancing between risks with a high probability of occurrence but lower loss versus a risk with high loss but lower probability of occurrence can often be mishandled. Risk management also faces a difficulty in allocating resources properly. Ideal risk management spends the least amount of resources in the process while reducing the negative effects of risk as much as possible. Proactive risk management doesn't necessarily mean avoiding projects that could incur a high level of risk. Formal risk management makes sure we go into such projects with our eyes open, so that we know what kinds of things that could go wrong, and we've done our best to make sure those factors won't prevent the ultimate success of the project. Risk management is a scientific approach to the problem of dealing with the pure risks faced by individuals and business aiming at systematically reducing the costs of risks and other inconvenience.

The main objective of risk management is to protect the continuity of operations also in case some threatening risk becomes a reality. Generally, risk management is a system to identify and quantify all risks to which the business or project is exposed so that a conscious decision can be taken on how to manage the risks. It must be practical, realistic and must be cost effective. Risk management also is a discipline for living with the possibility that future events may cause adverse effect.

Its principal aim is to ensure that risks associated with a construction project are managed in the most effective manner. According to Smith (1999), the process of risk management may be defined as identification of risk, analysis of the implications, response to minimize risk and allocation to appropriate contingencies

2. Methods and materials

Questionnaire surveys were distributed to (60) respondents who are contractors under Grade G7 and who are registered under the Malaysian Construction Industry Board. A response rate of fifty-percent (50%) was obtained. The purpose of the questionnaire survey was intended for a better feedback on the extent of the use of D&B arrangement and the risk encountered during their projects.

The 2nd part of the research involved an in-depth interview which involved (10) participants from various public and private companies. It was carried out with the senior managers to provide detail information on the background, knowledge and experience of D&B project and the risks that occurred in design and build projects and ways to overcome them.

3. Results

A Likert-Type Scale of (5) which range from 1 to 5 where 5 are very important and 1 is not important was given to the respondent. Data obtained from the questionnaire survey were collected and analysed. Frequency counts and percentages of the data were computed. The average index used in order to analyse the data. In this research, average index was used. Results from the questionnaire surveys found that a majority of the respondents had prior experience on 1-5 projects. The others had undertaken 6-10 projects and only 7 respondents had embarked on the 10 projects. Fifteen (15) or 46% had experience in handling D&B projects below 5 years. 27% had experience of more than 6 years and nine (9) with experience of more than 10 years which includes projects such as hospital, school and commercial, residential and offices. Most of the projects included hospitals, schools, commercial buildings, residential buildings and others. Sixty-seven respondents (67%) were involved in government projects while twenty-five (25%) had experiences in private projects and eight (8%) respondents were involved in both governments and project projects. Sixteen (16) respondents or forty-eight percent (48%) of respondents had at least 5 projects in D&B. Eight (8) or 24% had embarked on 6-10 projects, 6 respondents or 18 % were involved in 10-15 projects and only 3 respondents had more than fifteen (15) D & B projects.

From the analysis, it was found that time overrun and cost overrun, employer's/government delay, lack of information from the employer, difficulty of following instructions, conflict of interest and variation to changes were ranked as the highest risks in design and build procurement.

3.1 Time overrun

In D&B projects, every contractor wants to avoid time overrun. Time overrun caused by contractors will not only effect the contractor financially but will also place the contractor's reputation at stake in handling D&B projects. According to Contractor A, any kind of delay whether in the change of design and construction method, technical, environmental or government caused delays are main reason for time overrun. Most of the factors like risk changes that contribute to time overrun can be avoided even at early stage. The Employer plays an important role as well in ensuring that the project is completed within a stipulated time and cost.

3.2 Cost overrun

The client usually has a rough idea on what he wants in a D&B project. Therefore, the D&B contractors who bid for the tender will prepare a tender consisting of a brief design and also the cost to construct the project based on the requirements of the client. The tendered sum submitted by the contractor is usually fixed. Therefore, if the design-build contractor incurred extra cost because of his mistakes in the design or construction, he cannot claim from the excess from the client. When the client changes his mind on the design or the specifications, the contractor can claim the excess from the client causing the client to incur extra costs. This is because the client has agreed to the tender sum submitted by the D&B contractor. The price submitted by the contractor covers all aspects of work from inception to completion; based on the brief and specifications required by the client. When the client finds a need to hire a consultant to work on his behalf, the professional fees paid to them will result in a cost overrun for selecting the D&B contract. When there is any delay on time overrun, cost overrun will occur.

3.3 Delay caused by the owner or the government

When there is any delay in a project, time and cost overrun will occur. According to Contractor B, critical factors that are controllable during the design-construction process have been identified as insufficient owner-info, ill-conceived scheme of client requirement, changes of employer requirement, and significant changes to the original design, delay in approval and client initiated changes during construction. It shows that the clients themselves cause most of the factors that contribute to risk in time and cost. The clients have a precise understanding of the scope of projects before it is submitted to the D&B team but once it is submitted, the clients always change the project scope or even the design. The government through its department such as the Environmental Department, Land Office, Electrical National Board, Water and Irrigation Department may also cause delays in D&B projects. These various departments have their own laws and regulations that adhered to by the contractor to execute their work. Most of the time, the regulations change

accordingly to current situations making such a way that the contractors have to deal with them. This will consume time. Problems like squatters which have to be dealt by the local authority were also time consuming thus causing further delay to the projects.

3.4 Overlapping of roles

In D&B projects, the clients usually find that they still have to engage their own consultants, usually Project Monitoring Committee (PMC), for technical guidance and preparation of material setting out for their requirements. The difficulty with the preparation of the clients' requirement does not end at the preparation stage but many clients do not realize that their requirement will only amount to a schematic design of the end product. The concept behind the design-build contracts assumes that the contractor takes care of the detailed design and this is conferred a relatively wide mandate when interpreting the clients' requirements. According to Edwards, J and Bowen, A (2005), clients whom are new to the D&B concept seem to find this mandate difficult to accept when they realize that they do not have the exclusive say or a free hand in deciding the implementation or outcome of the end product. Unfortunately, there is a tendency for clients who are new to the D&B concept to issue numerous instructions through their representatives without realizing the full implications of such instructions. Prudent D&B contractors will often ensure that their contractual rights are protected by notification of claims for delay, time related damages and actual costs for having to implement such instructions that are equivalent to variations orders.

Some clients when providing too many details may realize that they are doing what their contractor is being paid to do. Some other clients may not realize that they may be prejudice their contractual position by assuming responsibilities for parts of the design, particularly so if a detailed design is imposed on the contractor. Some consultants also provide full time supervision which is already covered by the in-house supervision. It is true that during the design phase and construction phase the contractor has complete control of matters but there are always interruption from the client's consultants regarding design correction, method and specifications. The contractors have always done their best in fulfilling the requirements. Many problems arise in the clients' consultant has differing opinions in particular types of construction or materials. What the contractor always does to solve this problem is to have a genuine discussion between both parties to agree on a solution. In most situations, the discussions will solve the problem. When this problem can lead to time overrun, extension of time (E.O.T) will be given. Another way to overcome the problem besides discussion is to ensure that the main-contractor can perform the job himself and not sublet the work to too many parties because this can place huge pressure on the sub-con who is actually executing out the work. All parties involved in the project must also be experienced and must establish their duties and responsibilities. These people should also understand the exact method of implementing the D&B contract.

3.5 Difficulty in adhering/following instructions

The major difference for a contractor in D&B contract is that it assumes liability for design. It is incumbent on the contractor to engage a design team to come up with a design that complies with the client's requirement. But for the inexperienced D&B contractors, the selection of designers for the design team is vital. Not only should the contractor select team members that know how to integrate their portion of works into the overall design intended by the contractor but it is also imperative that each team members know how to receive instructions from the contractor. According to Contractor C, a great number of consultants in our country are not accustomed to receive instruction from a contractor. Irrespective of the terms and conditions of the contract at hand where some consultants either consciously or sub-consciously attach more weight to the requirement of the clients rather than the contractor. These consultants appear to be entrenched in the traditional form of arrangements and are inflexible. As it is the role of the contractor to form the design team, the selection process for design consultants must be exercised with great care to ensure that they are able and willing to receive instruction from a contractor. To overcome this problem, the contractor must discuss the matter and remind the consultants whom they are working for and the design team should accept the orders from the contractors.

3.6 Lack in employer brief

The problem that normally arises in D&B project is the bidding of the proposal. Most of the respondents think that lack of information in employer brief will create problem in the future. Normally, it happens in the local construction industry where the employer brief is not really complete. The client then will ask for changes during the construction. This will increase the cost and delay the project duration. According to Contractor D, a brief which is not detailed enough can be subjected to a lot of interpretations and understandings which could make the whole exercise futile and certainly not to the best interest of the client.

3.7 Conflict of interest

In D&B contracts, the contractor provides the design and is usually perceived to have a conflict of interest because he also executes construction work. If the project is a direct negotiation with the contractor that means only one contractor will go for the tender. The clients may have their own idea or need in terms of design. However, because of e

experience by the selected contractor, the employer's may be dissent. This is because the client still wants his idea and his needs to be catered to and the contractor suggestion. This will result in the late commencement of the work. The appointment of an independent professional to evaluate the design proposal may be a solution, but it involves additional cost.

3.8 Variation to changes in design criteria

Most of the details are not finalized for D&B projects during the contract stage, and this increases the area of disputes, since changes are inevitable, particularly in large scale projects. Deviation from the original design will create higher risks for the contractor, for he has to pay for his own mistakes or decisions. This causes a variation. According to Contractors D, if the variations come from the client, the extent to which the contractor can lodge a claim for abortive work and additional expense will depend upon the extent to which the original brief, specification and construction has been detailed and defined.

4. Discussions

Out of ten (10) interviews conducted, it was found that only seven (7) contractor who were that handling D&B projects had experience in formal risk management, the other three (3) contractors used risk management in an informal approach. According to respondents, they must make sure that their application of risk management is efficient to the project. The right application can effectively reduce the probability of loss and increase the company's profitability.

4.1 Risk identification

From the interviews it was found that under risk identification method, the contractor used checklists methods, physical inspections, analysis of available records and brainstorming sessions. Eight (8) contractors informed that these methods are commonly used because they are reasonable and inexpensive, and their applications are simple and quick. For risk identification in a D&B project, the respondents stated that they identified risk every month while other respondents identified risk in a particular project quarterly basis. According to them, the risks are controllable during the third quarter of the project duration, so these contractors felt it is best to identify risk on such a time frame. Risk identification depends on the overall condition of the project including its location, resources and work task. Therefore, different projects may require different modes of identification due to different factors.

4.2 Risk analysis

According to Contractor No.8, sensitivity analysis is commonly used because it is a simple technique. She also adds that although Monte Carlo testing is an efficient risk analysis system, it is seldom used by the contractor due to its complicated method. The testing has to be repeated hundreds or thousands time to obtain an accurate outcome. Besides, its implementation requires experienced personnel, suitable risk analysis training, applicable with computer software and specialist advice. These incurred cost for the contractor. The duration taken by the contractor to analyze the identified risk were mostly around 8 – 14 days or around 2 weeks, and other contractor took only 7 days or a week to analyze those risks and to find a suitable response.

4.3 Risk response

According to the respondents, most of them favour to investigate the risks in order to reduce the probability of losses. However, only risks that have high probability of occurrence and high impact to the project will be managed.

4.4 Problems encountered

The problem encountered were the difficulties in evaluating tender. In D&B proposal, however, each contractor submits his own design and price, and this makes evaluation very difficult, as the client is faced with different design proposals with differing prices. The situation can be further aggravated if a financing package is included in some of the proposals. The employer however, eventually decides to consider neither the lowest price nor the most aesthetic design but instead to concentrates on selecting the proposal that accorded best with the project brief. The selection problem can be overcome by reviewing all the proposals in totality and choosing the proposal which best meets the client's brief, and that which best offers the best value for money in all aspects. On the other hand, most of the respondents stated that problem also arise with work specification and definition. In D&B contract, detailed design is usually involved only as work proceeds. As such, difference in opinion and interpretation of the specifications and requirements may develop between the contractor and employer. To reduce this, sometimes sophisticated specifications for major parts are needed right from the start. Poor quality of workmanship is also another problem. It was normally due to the sub-contractor selected by the employer and not by the D&B contractor.

5. Conclusion and recommendations

It was found that changes of design scope by employer, over interference by employer consultant, variations with changes in design criteria, conflict in interest in design between employer and contractor, lack in employer's brief, force majored & social disorder and employer's cause delays are critical risk factors in D&B projects.

In order to improve D&B projects, it is recommended that contractors should have clear employer briefing, clear specifications and statement of needs, good quality of workmanship, implementing code of practice, key elements effective management, effective communication with all components of the project team and decisive action in the event of deviation from plans.

The results of the study are expected to provide useful guidelines for forming and operating effective and efficient D&B projects in Malaysia and other countries. It can be concluded that risk management is a tool that must be applied in all D&B projects in order for the construction and employer to achieve a satisfaction in a project.

In order to improve the D&B system for further research, the following are the recommendation that need to be considered:

1) Clear employer briefing

Employer briefing is essential. The employer has to alert when giving the briefing. The briefing given at the initial stages of the pre-contract comprises all the employer's needs and requirement of the building. Another respondent gave the opinion that during the implementation of the D&B project, the employer should be clear on a D&B project. A clear briefing by the employer will avoid misunderstandings.

2) Clear specifications and Statement of Needs

The consultant has the main role in preparing a specification for the project according to requirements specified by the employer. A good specification will provide a clear picture for the contractor to implement the work on site. Besides that, a clear statement needs should be prepared by the employer. Clear specifications and need of statement will result in better execution of the project.

3) Good quality of workmanship

Several respondents thought that the employers and contractors should conduct more supervision work during the construction period. This supervision is essential to ensure that the contractor is regularly informed of the work progress that the employer is not cheated by the contractor. Both parties should work together during these supervisions.

4) Implementing code of practice

One respondent suggested that in improving the D&B system and quality, some code/standard of practice should be enforced by the employer before getting involved in D&B projects. This code/standard of practice is a guide in appointing D&B contractor and consultants to ensure that the parties appointed are well-equipped and have sufficient experience in D&B projects. The result of appointing suitable contractors and consultants is a proper implementation of work, the best of workmanship and better management by the employer and contractor.

5) Proper Identification of the Employer's Requirement and Project Objectives

Many problems on a project arise as a result of the project team designing something which is different from that which the developer needs. This is often a result of an inadequate understanding by the developer of his actual needs in building terms, and a misunderstanding by the D&B team of the developer's objectives. If left unchecked, the confusion and discrepancy between employer's needs and the design proposal can result in unnecessary and abortive work by the D&B team. The ineffective use of the design phase of the project programme can result in a less than ideal solution to the employer's requirement. Time invested by the developer and the D&B team in a series of valuable management meetings during the early stages of the project can help to establish and prioritize the actual needs of the employer. The process of rigorous dialogues between both the employer and D&B team can help to ensure the preparation of an appropriate brief. The process can also provide the D&B team with a firm understanding of the employer's objectives for the project and their relevant priorities. The clear understanding of the employer's requirements can help the D&B team to propose a design that meets the needs of the project, and prevents the abortive use of design time and resources in developing inappropriate design solutions.

6) Key elements of effective management

The successful management of projects undertaken by the D&B method of procurement is found on the same principles as that are appropriate for all construction projects. The key difference is that by the selection of the D&B arrangement, where one team is responsible from the concept to completion, greater potential and opportunity exist to practice effective project management. The key issue here is the opportunity to exercise control over all facets and phases of the project. As a result, no component of the project team is isolated from action taken by management in the event of difficulties. In particular, the project can be planned to aptly address the key requirements of each component of the team including specialist suppliers.

7) Effective Communication with all Components of the Project Team

One of the D&B project manager's key tasks is the implementation and practice of an effective communications policy for the project. An effective communication process incorporates the construction programme into the design process.

This can help to ensure that design information is always available to meet the needs of the construction stage. The communication process can contribute to an effective information management system. It is a coordinated flow of related information amongst all parties with regard to changes in design and requirement by authorities. The clear definition and co-ordination of communication between the different disciplines in the design team can help to reduce design problems.

8) Decisive Action in the Event of Deviation from Plans

Effective and decisive actions in the event of deviation from plans to recover the situation are vital to prevent the project from being disrupted. Should there be a situation where there are changes to the scope by the employer, the impact of the change on the project in terms of time, costs and quality must be communicated and understood by the employer.

References

Banks, E & Dunn, R., (2003). Practical Risk Management, John Wiley & Sons Ltd.

Beard, L.J., (2001). Design and Build: The Project Delivery Administration and Construction, McGraw Hill.

Carmicheal, D.G., (2000). Contracts and International Project Management, A.A. Balkema Publishers.

Chong, S.N., (2001). Mutation of Design and Build, Seti Putrajaya Sdn. Bhd., The Surveyor Vol.26, No.3 (3rd Quarter) 2001.

Dennis, F.T., (1995), Design and Build Contract Practice (2nd edition), Longman Scientific and Technical.

Dulaimi, M.F, Morris, G.K & Baxendale, T., (1998). Design and Build: The Need for Effective Design Management, The Surveyor Vol.33 No.1. (1st Quarter).

Edwards, L., (1995). Practical Risk Management in the Construction Industry, Thomas Telford Publications.

Edward, R. Fisk., (2003). Construction Project Administration (7th edition), Prentice Hall.

Flanagan, R & Norman, G., (1993). Risk Management and Construction, Blackwell Scientific Publications.

Franks, J (1984). Building Procurement Systems, CIOB.

Knowles, R., (2000). 100 Contractual Problems and Their Solutions, Blackwell Science.

Masterman, J.W.E., (1992). An Introduction to Building Procurement System, E&FN Spon.

Murcutt, A.G., (1998). Design and Build, CIOB.

Murdoch, J& Hughes, W., (2000). Construction Contracts Law and Management (3rd edition), E&FN Spon.

Nael, G.B., (2003). Risk and Insurance in Construction (2nd edition), Spon Press.

Standard Form of Design and Build/Turnkey Contract 2000 Edition, Public Work Department (PWD).

Smith, N.J., (1999), Managing Risk in Construction Projects, Blackwell Science Ltd.

The Aqua Group (1982), Tenders and Building Contract, Granada.

Wong, J, Inherent Problems in Design and Build and its Solutions, The Surveyor.

Standard Form of Design and Build/Turnkey Contract 2000 Edition, Public Work Department (PWD).

Modern Applied Science

www.ccsenet.org/journal.html

Vol. 2, No. 5

September 2008

Exact Solutions for a Class of Variable Coefficients Nonlinear Evolution Equations

Haiming Fu

Mathematics Department

Yunnan University

No. 2 Cuihu Road, Kunming 650091, China

E-mail:haimingfu@163.com

Abstract

A class of Variable Coefficients nonlinear evolution equations $u_t+[\alpha(t)+\beta(t)u^2]u^2u_x+\gamma(t)u_{xxx}=0$ With $\alpha(t)>0,\beta(t)<0$. By using the general process of working out the exact solution of the nonlinear evolution equations in the homogeneous balance method, and the exact solutions of the equations are obtained.

Keywords: Nonlinear equation, Homogeneous balance method, Solitary wave solution

1. Introduction

Nonlinear science is the nucleus of modern science, in natural science, some descriptions concern soliton equation, at soliton theory, the solve method of soliton equation is the importance of question research. Because of new methods' appearing, not only the equations hard to solve before have been solved, but also discover the soliton equation have important physics significance. Recently, homogeneous balance method successful solves some of soliton equations.

2. Exact Solutions of Solitary Wave Solution

We consider a class of Variable Coefficients nonlinear evolution equations as following:

$$u_t+[\alpha(t)+\beta(t)u^2]u^2u_x+\gamma(t)u_{xxx}=0 \tag{1}$$

With $\alpha(t)>0,\beta(t)<0$. Suppose (1) has the solution

$$u(x,t)=f^{'}\varphi_x^m\varphi_t^n \tag{2}$$

with $f=f(\varphi)$ and $\varphi=\varphi(x,t)$. Then

$$u^2u^2u_x=f^{',2}\varphi_x^{2m}\varphi_t^{2n}f^{',2}\varphi_x^{2m}\varphi_t^{2n}(f^{''}\varphi_x^{m+1}\varphi_t^n+mf^{'}\varphi_x^{m-1}\varphi_t^n\varphi_{xx}+nf^{'}\varphi_x^m\varphi_t^{n-1}\varphi_{tx}) \tag{3}$$

$$u_{xxx}=f^{(4)}\varphi_x^{m+3}\varphi_t^n \tag{4}$$

Using homogeneous balance method, we get

$$\begin{cases} m+3=2m+2m+m+1 \\ 2n+2n+n=n \end{cases}, \text{ further } \begin{cases} m=\dfrac{1}{2} \\ n=0 \end{cases}$$

Let

$$u(x,t)=a(t)\varphi_x^{\frac{1}{2}}\varphi^{-\frac{1}{2}} \quad (a(t)\neq 0) \tag{5}$$

Thus

$$u_t=a^{'}(t)\varphi_x^{\frac{1}{2}}\varphi^{-\frac{1}{2}}+\frac{1}{2}a(t)\varphi_x^{-\frac{1}{2}}\varphi_{xt}\varphi^{-\frac{1}{2}}-\frac{1}{2}a(t)\varphi_x^{\frac{1}{2}}\varphi^{-\frac{3}{2}}\varphi_t \tag{6}$$

$$u^2=a^2(t)\varphi_x\varphi^{-1} \tag{7}$$

$$u_x=\frac{1}{2}a(t)\varphi_x^{-\frac{1}{2}}\varphi_{xx}\varphi^{-\frac{1}{2}}-\frac{1}{2}a(t)\varphi_x^{\frac{1}{2}}\varphi^{-\frac{3}{2}}\varphi_x \tag{8}$$

$$u_{xx}=\frac{3}{4}a(t)\varphi_x^{\frac{5}{2}}\varphi^{-\frac{5}{2}}-\frac{3}{4}a(t)\varphi_x^{\frac{1}{2}}\varphi^{-\frac{3}{2}}\varphi_{xx}-\frac{1}{4}a(t)\varphi_x^{\frac{1}{2}}\varphi_x^{-\frac{3}{2}}\varphi_{xx}+\frac{1}{2}a(t)\varphi_x^{-\frac{1}{2}}\varphi^{-\frac{1}{2}}\varphi_{xxx}-\frac{1}{4}a(t)\varphi_x^{-\frac{3}{2}}\varphi^{-\frac{1}{2}}\varphi_{xx}^2$$

$$=\frac{3}{4}a(t)\varphi_x^{\frac{5}{2}}\varphi^{-\frac{1}{2}}-a(t)\varphi_x^{\frac{1}{2}}\varphi^{-\frac{3}{2}}\varphi_{xx}+\frac{1}{2}a(t)\varphi_x^{-\frac{1}{2}}\varphi^{-\frac{1}{2}}\varphi_{xxx}-\frac{1}{4}a(t)\varphi_x^{-\frac{3}{2}}\varphi^{-\frac{1}{2}}\varphi_{xx}^2 \tag{9}$$

$$u_{xxx}=\frac{15}{8}a(t)\varphi_x^{\frac{3}{2}}\varphi_{xx}\varphi^{-\frac{5}{2}}-\frac{15}{8}a(t)\varphi_x^{\frac{7}{2}}\varphi^{-\frac{7}{2}}-\frac{3}{8}a(t)\varphi_x^{-\frac{1}{2}}\varphi_{xx}^2\varphi^{-\frac{3}{2}}-\frac{3}{4}a(t)\varphi_x^{\frac{1}{2}}\varphi_{xxx}\varphi^{-\frac{3}{2}}+$$

$$\frac{9}{8}a(t)\varphi_x^{\frac{3}{2}}\varphi_{xx}\varphi^{-\frac{5}{2}}-\frac{1}{8}a(t)\varphi_x^{-\frac{1}{2}}\varphi_{xx}^2\varphi^{-\frac{3}{2}}-\frac{1}{4}a(t)\varphi_x^{\frac{1}{2}}\varphi_{xxx}\varphi^{-\frac{3}{2}}-\frac{3}{8}a(t)\varphi_x^{\frac{3}{2}}\varphi_{xx}\varphi^{-\frac{5}{2}}-$$

$$\frac{1}{4}a(t)\varphi_x^{-\frac{3}{2}}\varphi_{xx}\varphi_{xxx}\varphi^{-\frac{1}{2}}+\frac{1}{2}a(t)\varphi_x^{-\frac{1}{2}}\varphi_{xxxx}\varphi^{-\frac{1}{2}}-\frac{1}{4}a(t)\varphi_x^{\frac{1}{2}}\varphi_{xxx}\varphi^{-\frac{3}{2}}+\frac{3}{8}a(t)\varphi_x^{-\frac{5}{2}}\varphi_{xx}^3\varphi^{-\frac{1}{2}}-$$

$$\frac{1}{2}a(t)\varphi_x^{\frac{3}{2}}\varphi_{xxx}\varphi^{-\frac{1}{2}}\varphi_{xx}+\frac{1}{8}a(t)\varphi_x^{-\frac{1}{2}}\varphi_x^2\varphi^{-\frac{3}{2}}$$

$$=\frac{21}{8}a(t)\varphi_x^{\frac{3}{2}}\varphi_{xx}\varphi^{-\frac{5}{2}}-\frac{15}{8}a(t)\varphi_x^{\frac{7}{2}}\varphi^{-\frac{7}{2}}-\frac{3}{8}a(t)\varphi_x^{-\frac{1}{2}}\varphi_{xx}^2\varphi^{-\frac{3}{2}}-\frac{5}{4}a(t)\varphi_x^{\frac{1}{2}}\varphi_{xxx}\varphi^{-\frac{3}{2}}-$$

$$\frac{3}{4}a(t)\varphi_x^{-\frac{3}{2}}\varphi_{xx}\varphi_{xxx}\varphi^{-\frac{1}{2}}+\frac{1}{2}a(t)\varphi_x^{-\frac{1}{2}}\varphi_{xxxx}\varphi^{-\frac{1}{2}}+\frac{3}{8}a(t)\varphi_x^{-\frac{5}{2}}\varphi_{xx}^3\varphi^{-\frac{1}{2}} \tag{10}$$

From (6),(7),(8),(10) and (1),we have

$$\frac{1}{2}a(t)\varphi_x^{-\frac{1}{2}}\varphi_{xt}\varphi^{-\frac{1}{2}}-\frac{1}{2}a(t)\varphi_x^{\frac{1}{2}}\varphi^{-\frac{3}{2}}\varphi_t+a'(t)\varphi_x^{\frac{1}{2}}\varphi^{-\frac{1}{2}}+\frac{1}{2}a^3(t)\alpha(t)\varphi_x^{\frac{1}{2}}\varphi_{xx}\varphi^{-\frac{3}{2}}+\frac{1}{2}a^3(t)\alpha(t)\varphi_x^{\frac{5}{2}}\varphi^{-\frac{5}{2}}+$$

$$\frac{1}{2}a^5(t)\beta(t)\varphi_x^{\frac{3}{2}}\varphi_{xx}\varphi^{-\frac{5}{2}}-\frac{1}{2}a^5(t)\beta(t)\varphi_x^{\frac{7}{2}}\varphi^{-\frac{7}{2}}+\frac{15}{8}a(t)\gamma(t)\varphi_x^{\frac{3}{2}}\varphi_{xx}\varphi^{-\frac{5}{2}}-\frac{15}{8}a(t)\gamma(t)\varphi_x^{\frac{7}{2}}\varphi^{-\frac{7}{2}}-$$

$$\frac{3}{8}a(t)\gamma(t)\varphi_x^{-\frac{1}{2}}\varphi_{xx}^2\varphi^{-\frac{3}{2}}-\frac{3}{4}a(t)\gamma(t)\varphi_x^{\frac{1}{2}}\varphi_{xxx}\varphi^{-\frac{3}{2}}+\frac{9}{8}a(t)\gamma(t)\varphi_x^{\frac{3}{2}}\varphi_{xx}\varphi^{-\frac{5}{2}}-\frac{1}{8}a(t)\gamma(t)\varphi_x^{-\frac{1}{2}}\varphi_{xx}^2\varphi^{-\frac{3}{2}}-$$

$$\frac{1}{4}a(t)\gamma(t)\varphi_x^{\frac{1}{2}}\varphi_{xxx}\varphi^{-\frac{3}{2}}-\frac{3}{8}a(t)\gamma(t)\varphi_x^{\frac{3}{2}}\varphi_{xx}\varphi^{-\frac{5}{2}}-\frac{1}{4}a(t)\gamma(t)\varphi_x^{-\frac{3}{2}}\varphi_{xx}\varphi_{xxx}\varphi^{-\frac{1}{2}}+\frac{1}{2}a(t)\gamma(t)\varphi_x^{-\frac{1}{2}}\varphi_{xxxx}\varphi^{-\frac{1}{2}}-$$

$$\frac{1}{4}a(t)\gamma(t)\varphi_x^{\frac{1}{2}}\varphi_{xxx}\varphi^{-\frac{3}{2}}+\frac{3}{8}a(t)\gamma(t)\varphi_x^{-\frac{5}{2}}\varphi_{xx}^3\varphi^{-\frac{1}{2}}-\frac{1}{2}a(t)\gamma(t)\varphi_x^{-\frac{3}{2}}\varphi_{xxx}\varphi^{-\frac{1}{2}}\varphi_{xx}+\frac{1}{8}a(t)\gamma(t)\varphi_x^{-\frac{1}{2}}\varphi_{xx}^2\varphi^{-\frac{3}{2}}=0 \tag{11}$$

Suppose (5) and (11) have the solutions as a type of follows

$$\varphi(x,t)=1+e^{k(t)x+w(t)} \tag{12}$$

Thus $\varphi_x=k(t)e^{k(t)x+w(t)}$, $\varphi_{xx}=k^2(t)e^{k(t)x+w(t)}$, $\varphi_{xxx}=k^3(t)e^{k(t)x+w(t)}$, $\varphi_{xxxx}=k^4(t)e^{k(t)x+w(t)}$,

$\varphi_t=[k'(t)x+w'(t)]e^{k(t)x+w(t)}$, $\varphi_{xt}=[k'(t)x+k(t)k'(t)+w'(t)k(t)]e^{k(t)x+w(t)}$,

From (12) and (11), we have

$$(\frac{k(t)e^{k(t)x+w(t)}}{1+e^{k(t)x+w(t)}})^{\frac{7}{2}}[-\frac{1}{2}a^5(t)\beta(t)-\frac{15}{8}a(t)\gamma(t)]+$$

$$(\frac{k(t)e^{k(t)x+w(t)}}{1+e^{k(t)x+w(t)}})^{\frac{5}{2}}[-\frac{1}{2}a^3(t)\alpha(t)+\frac{1}{2}a^5(t)\beta(t)k(t)+\frac{21}{8}a(t)\alpha(t)k(t)]+$$

$$(\frac{k(t)e^{k(t)x+w(t)}}{1+e^{k(t)x+w(t)}})^{\frac{3}{2}}[-\frac{1}{2}a(t)\frac{k'(t)+w'(t)}{k(t)}+\frac{1}{2}a^3(t)k(t)-\frac{3}{8}a(t)k^2(t)-\frac{5}{4}a(t)\gamma(t)k^2(t)]+$$

$$(\frac{k(t)e^{k(t)x+w(t)}}{1+e^{k(t)x+w(t)}})^{\frac{1}{2}}[\frac{1}{2}a(t)(k'(t)+k(t)k'(t)+k(t)w'(t))-\frac{3}{4}a(t)k^3(t)\gamma(t)+$$

$$\frac{1}{2}a(t)\gamma(t)k^2(t)+a'(t)+\frac{3}{8}a(t)\gamma(t)k^3(t)]=0 \tag{13}$$

Let the coefficient of $(\frac{k(t)e^{k(t)x+w(t)}}{1+e^{k(t)x+w(t)}})^{\frac{7}{2}}$, $(\frac{k(t)e^{k(t)x+w(t)}}{1+e^{k(t)x+w(t)}})^{\frac{5}{2}}$, $(\frac{k(t)e^{k(t)x+w(t)}}{1+e^{k(t)x+w(t)}})^{\frac{3}{2}}$, $(\frac{k(t)e^{k(t)x+w(t)}}{1+e^{k(t)x+w(t)}})^{\frac{1}{2}}$ are zero in (13), we obtain:

$$-\frac{1}{2}a^5(t)\beta(t)-\frac{15}{8}a(t)\gamma(t)=0 \tag{14}$$

$$-\frac{1}{2}a^3(t)\alpha(t)+\frac{1}{2}a^5(t)k(t)\beta(t)+\frac{21}{8}a(t)k(t)\gamma(t)=0 \tag{15}$$

$$-\frac{1}{2}a(t)[w'(t)+k'(t)]+\frac{1}{2}a^3(t)k^2(t)\alpha(t)-\frac{3}{8}a(t)k^3(t)\gamma(t)-\frac{5}{4}a(t)k^3(t)\gamma(t)=0 \tag{16}$$

$$\frac{1}{2}a(t)[k'(t)+k(t)k'(t)+k(t)w'(t)]+a'(t)-\frac{3}{4}a(t)k^3(t)\gamma(t)+\frac{1}{2}a(t)k^2(t)\gamma(t)+\frac{3}{8}a(t)k^3(t)\gamma(t)=0 \tag{17}$$

We get the solution of equations as following:

$$a(t)=\pm\sqrt[4]{-\frac{15\gamma(t)}{4\beta(t)}} \tag{18}$$

$$k(t)=-\frac{\alpha(t)}{3\beta(t)\gamma(t)}\sqrt{-15\beta(t)\gamma(t)} \tag{19}$$

$$w(t)=\int[\frac{35}{36}\alpha^3(t)\gamma(t)-\frac{1}{3}\alpha'(t)\beta(t)\gamma(t)-\frac{1}{6}\alpha(t)\beta'(t)\gamma(t)-\frac{1}{6}\alpha(t)\beta(t)\gamma'(t)]\frac{\sqrt{-15\beta(t)\gamma(t)}}{\beta^2(t)\gamma^2(t)}dt \tag{20}$$

From (19), (20) and (12),we have

$$\varphi(x,t)=1+\exp\{-\frac{\alpha(t)x}{3\beta(t)\gamma(t)}\sqrt{-15\beta(t)\gamma(t)}+\int[\frac{35}{36}\alpha^3(t)\gamma(t)-\frac{1}{3}\alpha'(t)\beta(t)\gamma(t)-\frac{1}{6}\alpha(t)\beta'(t)\gamma(t)-\frac{1}{6}\alpha(t)\beta(t)\gamma'(t)]\frac{\sqrt{-15\beta(t)\gamma(t)}}{\beta^2(t)\gamma^2(t)}dt\} \tag{21}$$

From (18),(21) and (5), we have the solutions of (1):

$$u(x,t)=\pm\sqrt{-\frac{5\alpha}{2\beta}}\bullet\sqrt{\frac{\exp\{-\frac{\alpha\sqrt{-15\beta\gamma}}{3\beta\gamma}x+\int[\frac{35}{36}\alpha^3\gamma-\frac{1}{3}\alpha'\beta\gamma-\frac{1}{6}\alpha(\beta'\gamma+\beta\gamma')]\frac{\sqrt{-15\beta\gamma}}{\beta^2\gamma^2}dt\}}{1+\exp\{-\frac{\alpha\sqrt{-15\beta\gamma}}{3\beta\gamma}x+\int[\frac{35}{36}\alpha^3\gamma-\frac{1}{3}\alpha'\beta\gamma-\frac{1}{6}\alpha(\beta'\gamma+\beta\gamma')]\frac{\sqrt{-15\beta\gamma}}{\beta^2\gamma^2}dt\}}}$$ with

$\alpha=\alpha(t),\beta=\beta(t),\gamma=\gamma(t).$

References

Bai Chenglin, Liu Xiqiang and Bai Chengjie. (1999). Multiple soliton solutions of the (2+1)-dimensional Broer-Kaup equations. Acta photonica sinica, 28, 1029-1030.

M. J. Ablowitz, P. A. Carkson, Solitons. (1991). *Nonlinear Evolution and Inverse Scattering* . Cambridge University Press, New York. pp.47-350.

M. R. Miura. (1978). *Backlund Transformtion*. Springer Verlag, Berlin. pp. 4-156.

Senthilvelan M. (2001). on the extended applications of homogeneous balance method. Applied Mathematics and Computation, 123, 381-388.

Wang M L, Zhou Y B. (1996). Application of a homogeneous balance method to exact solutions of nonlinear equations in mathematical physics. Phys Lett A, 216, 67-75.

Modern Applied Science

www.ccsenet.org/journal.html

Vol. 2, No. 5

September 2008

Removal of Adsorbable Organic Halides (AOX) from Recycled Pulp and Paper (P&P) Mill Effluent Using Granular Activated Carbon–Sequencing Batch Biofilm Reactor (GAC-SBBR)

Abu Bakar Mohamad

Department of Chemical & Process Engineering, Faculty of Engineering

Universiti Kebangsaan Malaysia (UKM), 43600 Bangi, Selangor, Malaysia

Tel: 6-038-921-6406 E-mail: drab@vlsi.eng.ukm.my

Rakmi Abd Rahman

Department of Chemical & Process Engineering, Faculty of Engineering

Universiti Kebangsaan Malaysia (UKM), 43600 Bangi, Selangor, Malaysia

E-mail: rakmi@vlsi.eng.ukm.my

Abdul Amir Hassan Kadhum

Department of Chemical & Process Engineering, Faculty of Engineering

Universiti Kebangsaan Malaysia (UKM), 43600 Bangi, Selangor, Malaysia

E-mail: amir@vlsi.eng.ukm.my

Siti Rozaimah Sheikh Abdullah

Department of Chemical & Process Engineering, Faculty of Engineering

Universiti Kebangsaan Malaysia (UKM), 43600 Bangi, Selangor, Malaysia

Zakiah Wan Sudin

Department of Chemical & Process Engineering, Faculty of Engineering

Universiti Kebangsaan Malaysia (UKM), 43600 Bangi, Selangor, Malaysia

Tel: 6-038-921-6428 E-mail: zakiah_sudin@yahoo.com

Safura Shaari

Department of Chemical & Process Engineering, Faculty of Engineering

Universiti Kebangsaan Malaysia (UKM), 43600 Bangi, Selangor, Malaysia

The research was financed by Swedish International Development Agency under the Asian Regional Research on Environment and Technology Programme (SIDA-ARRPET) Phase II.

Abstract

Paper mills generate varieties of pollutants depending upon the type of the pulping process. The wastewaters discharged from these mills have high chemical oxygen demand (COD) and colour, in which indicating high concentrations of recalcitrant organics. This study was conducted using a Granular Activated Carbon – Sequencing Batch Biofilm Reactor (GAC-SBBR) of 3.0 L working volume, operated in an aerobic condition and packed with 200 gL^{-1} of 2-3 mm granular

activated carbon (coconut shells) as a medium for the biofilm growth. For the six of months, the hydraulic retention time (HRT) was set at 36 hours and later it was adjusted to 24 hours in order to evaluate the performance of the system. The treated wastewater samples for these studies were taken from a recycled pulp and paper mill factory in Pahang, Malaysia with 4 different batch characteristics. The adsorbable organic halides (AOX) that had been determined and treated were pentachlorophenol (PCP), 2,3,4,5-tetrachlorophenol (2,3,4,5-TeCP), 2,4,6-trichlorophenol (2,4,6-TCP), 2,4-dichlorophenol (2,4-DCP), 2-chlorophenol (CP) and phenol at various concentration ranges. The Monod growth kinetic parameters for the process specific growth rate coefficient (μ_h), half saturation coefficient (K_s), endogenous decay coefficient (D_H) and Yield coefficient (Y_H) obtained were 0.0037 hr^{-1}, 65.23 mgL^{-1}, $4x10^{-5}$ hr^{-1} and 0.36 mg/mg, respectively. Analysis of the growth kinetic parameters in GAC-SBBR had deduced that the system was suitable to operate on long biomass retention time (BRT) under anoxic condition. The results also indicated that the biofilm attached onto granular activated carbon (GAC) can substantially remove these recalcitrant organics in the wastewater, within the range of 10 – 100% AOX removal depending on the selected HRTs.

Keywords: Adsorbable organohalides, Recalcitrant organics, Paper mill effluent, Biofilm, Sequencing batch reactor

1. Introduction

Chloroorganic compounds such as phenol and chlorophenol have become a major concern to public health due to their toxicological and recalcitrant characteristics. In order to remove these recalcitrant organics from industrial wastewater, the high costs activated carbon (AC) adsorption, as final treatment step is indispensable. This normal conventional adsorption technique has the disadvantages of inadequate exploitation of the adsorptive capacity, high cost of conventional thermal or chemical regeneration process for spent AC as well as decreasing adsorptive capacity of the AC, ultimate disposal problem, and toxic products such as chlorodibezodioxins might be generated in the thermal oxidation process (Kolb and Wilderer, 1997; Jaar and Wilderer, 1992). To solve most of these problems, the idea of using combined biofilm and granular activated carbon (GAC) adsorption were undertaken.

Granular Activated Carbon Sequencing Batch Biofilm Reactor (GAC-SBBR) was a technology system that was earlier developed by Wilderer (1992). It is a discontinuous technology where the sequencing batch reactor (SBR) was packed with GAC and the microorganisms were allowed to grow in the reactor by clinging onto suspended plastic media which later form the biofilm layer. Jaar and Wilderer (1992) had conducted the GAC-SBBR to study the removal of problematic wastewater containing 3-chlorobenzoate and thioglycolic acid. They had found that by adding the GAC inside the SBR, the system indicated high substrate removal efficiency with high process stability under various shock loading conditions. Furthermore, the study also found that the activated carbon had maintained approximately 90% of its adsorption capacity over a continuous operation period of 14 months. In addition, by introducing GAC inside the SBR, the GAC adsorption process was able to reduce the toxic effects of the pollutants and also increase the stability of the pollutant removing system (Xiaojian et al., 1991; Caldeira et al., 1999; Jaar and Wilderer, 1992).

Therefore the aim of this research is to investigate the performance and the effectiveness of the GAC-SBBR process in the removal of adsorbable organohalides (AOXs) and COD found to contain in the recycled paper mill effluent.

2. Approach and Methods

2.1 Effluents

The bleached effluent samples were collected from a recycled pulp and paper mill effluent in Pahang, Malaysia and it was taken after the second clarifier of the wastewater treatment plant. Samples were stored in 20-L plastic containers, kept at 4 $^{\circ}$C and transported back to our laboratory. The left over collected effluent was kept in the cold room for later use.

2.2 Inoculums

The original inoculums were a mixture obtained from a sewage oxidation pond in Kuala Lumpur and from the garden soils. The inoculums used in this experiment were procured from a batch anaerobic reactor located in the laboratory which has been maintained at ambient temperature condition.

2.3 GAC – SBBR

A reactor with 3 L working volume was used in this study. It was operated at room temperature and packed with 200 g/L of 2-3 mm granular activated carbon (coconut shells) as a medium for the biofilm growth as presented in Figure 1. The reactor was earlier operated at hydraulic retention time (HRT) of 36 hours for the six months and later was adjusted to HRT of 24 hours in order to make the performance comparison of the biofilm between both the HRTs. The samples were analyzed for COD, AOXs and the amount of biomass washout before being fed into the reactor.

2.4 Experimental Method

The overall methodology of this study is as illustrated in Figure 2. The GAC-SBBR system was initiated with the characterization of the influent and effluent samples and these were followed by the kinetic studies of the

microorganism growth and the optimization of reactor operating parameters. The COD and biomass parameters were analyzed using the standard methods with the respective instruments as listed in Table 1. The AOXs were extracted using the solid phase extraction (SPE) technique and later analyzed using the HPLC instrument.

3. Results and Discussion

The characteristics of four batches of samples from recycled paper mill factory were determined and the results were as indicated in Table 2. Figure 3 showed that the maximum influent concentrations obtained for COD on all four samples were below 250 mgL^{-1} while the COD values on the effluent were below 100 mgL^{-1}. The removal ranges for COD at HRTs of 36 hours and 24 hours were 50–80% and 50–66%, respectively. As was previously observed by the study of Barr et al. (1996), the removal of COD was found to decrease with the decreasing of the HRT. It was also observed that at the initial stage of the study (approximately within the first 20 days), the COD removal was higher even though the biomass concentration was below 2000 mgL^{-1}. This was most probably due to the adsorption of the COD onto the freshly introduced GAC.

The concentrations of the compounds as identified in the paper mill effluent with their percentage removals were as shown in Figures 4 – 9. In Figure 4, the concentrations of phenol were found to be very low and could hardly be detected. However, in the third and fourth samples the concentrations of phenol started to appear as these samples have undergone almost 100% phenol removal after its treatment in the GAC-SBBR process.

The concentrations of chlorophenol (Figure 5) only exist in the first sample batch and 40-70% was removed after treatment at HRT of 36 hours. For dichlorophenol, 2,4-DCP, as shown in Figure 6, only in the first and third batch samples were detected with 60–100% and 30-80% dichlorophenol removal at HRTs of 36 hours and 24 hours, respectively, after treatment with GAC-SBBR. The percentages removal for trichlorophenol, 2,3,4-TCP, as depicted in Figure 7 at HRT of 36 hours were in range of 20–80% while at HRT of 24 hours its percentage removal was found to decrease in the range of 10–40%. Tetrachlorophenol, 2,4,5,6-TeCP, as shown in Figure 8 have the percentage removal in the range of 30–50% at HRT of 36 hours, and dropped below 20% at HRT of 24 hours. The concentration of pentachlorophenol, PCP, was found to be very low (Figure 9) and only exists in the first batch of samples with removal after treatment of 60–80% in the GAC-SBBR system.

Based on these results, it was observed that the removal of PCP was much higher than the removal of 2,4,5,6-TeCP but was comparable to 2,3,4-TCP and 2,4-DCP under the two selected HRTs. Based on earlier study by Annachhatre and Gheewala (1996), for the anaerobic environment, PCP degradation rate was slower than that of phenol or 2-CP but comparable to 2,4,6-TCP and 2,4-DCP, suggesting that increased chlorination of the aromatic ring does not necessarily have direct correlation with resistance to biodegrade. However, the chlorine positions in the phenolic ring also had significant effects on the biodegradability of the compound as have been indicated by earlier studies (Boyd & Shelton, 1984; Knoll & Winter, 1987).

The percentage removal of chlorophenols for this GAC-SBBR process was also dependent on the selected HRT. Longer HRT has indicated improved biodegradation process while at the reduced expense of GAC adsorption. The longer HRT would mean a much longer period for the microbe to react with chlorophenol in the reactor thus giving rise to more biomass in order to continue with the biodegradation process. Barr et al. (1996) had also confirmed the earlier presumption that an increased HRT could improve AOXs removal and decreasing HRTs would result in a decrease in the toxicity removal. It is thus indicated that as the HRT decreases, a greater proportion of the more recalcitrant compounds will resist to biodegradation.

The efficiency of a system is also very dependent on the characteristics of the microbe population in the reactor. The Monod growth kinetic parameters, namely, μ_h, K_s, D_H and Y_H, obtained for this process were 0.0037 hr^{-1}, 65.23 mgL^{-1}, $4x10^{-5}$ hr^{-1} and 0.36 mg/mg, respectively. Comparisons of these kinetic values from other similar studies for AOX and other persistent organic removals were as indicated in Table 3. Analysis of the growth kinetic parameters in GAC-SBBR had deduced that the system is capable to operate a long biomass retention time under anoxic condition (or less oxygen). Anderson et al. (1996) have reported that the consumption of non-biodegradable substrate would lower the specific growth rate, μ_h.

4. Conclusions

This study has shown that selection of a suitable HRT plays an important role in the COD as well as in the AOXs removal. For long HRT of 36 hours, the percentage removals of COD and AOX were much higher as compared to shorter HRT (24 hours) where their percentage removals were slightly lower. The individual AOX removable varies in ranges according to the specific HRTs being applied with no obvious trend patterns. The results of this initial study thus reaffirm the fact that GAC – SBBR system treatment of recycled pulp and paper mill effluents could be considered as an alternative option not only for energy cogeneration but also as a means of significantly reducing some of the more important, albeit organic recalcitrant, objectionable parameters.

References

Anderson, G.K., Kasapgil, B. & Ince, O. (1996). Microbial Kinetics of A Membrane Anaerobic Reactor System. *Environmental Technology*. 17: 449-464.

Annachhatre, A. P. & Gheewala, S. H. (1996) Biodegradation of Chlorinated Phenolic Compunds. *Biotechnology Advances*. 14(1): 35-56.

Barr, T. A., Taylor., J. M. & Duff., S. J. B. (1996). Effect of HRT, BRT and Temperature on The Performance of Activated Sludge Reactors Treating Bleached Kraft Mill Effluent. *Water Research*. 30: 799-810.

Boyd, S. A & Shelton, D. R. (1984). Anaerobic biodegradation of chlorophenols in fresh and acclimated sludge. *Application Environmental Microbiology.* 47: 272-277.

Caldeira, M., Heald, S.C., Carvalho, M.F., Vasconcelos, L., Bull, A.T., Castro, P.M.L. (1999). 4-Chlorophenol degradation by a bacterial consortium: development of a granular activated carbon biofilm reactor. *Application Microbial Biotechnology*. 52: 722-729.

Hess, T.F. (1990). Supplemental substrate enhancement of 2,4-Dinitrophenol mineralization by a bacterial consortium. *Applied and Environmental Microbiology*. 56:1551-1558.

Jaar, M.A.A. and Wilderer, P.A. (1992). Granular activated carbon sequencing batch biofilm reactor to treat problematic wastewaters. *Water Science and technology*. 26 (5-6): 1195-1203

Jacobsen, B.N. & Arvin, E. (1996). Biodegradation kinetics and fate modeling of pentachlorophenol in bioaugmented activated sludge reactors. *Water Research*. 30 (5): 1184-1194.

Klecka, G.M. & Maier, W.J. (1985). Kinetics of microbial Growth on Pentachlorophenol. *Applied and Environmental Microbiology*. 49: 46-53.

Knoll, G. & Winter, J. (1987). Anaerobic degradation of phenol in sewage sludge. *Application Microbiology Biotechnology.* 25: 384-391

Kolb, F.R. and Wilderer, P.A. (1997). Activated carbon sequencing batch biofilm reactor to treat industrial wastewater. *Water Science Technology*. 35 (1): 169-176.

Wilderer, P.A. (1992). Sequencing batch biofilm reactor technology . Harnessing biotechnology for the 21st century, Ladisch, MR. And Bose (Eds), American Cehnical Socity: 475-479.

Xiaojian, Z. et al. (1991). Simple combination of biodegradation and carbon adsorption – the mechanism of the biological activated carbon process. *Water Research*. 25(2): 165-172.

Table 1. Methods and instruments used to analyze stated parameters

Parameter	Instruments	Method	References
Chemical oxygen demand (COD)	HACH DR/2010 Spectrophotometer	Digestion Method	EPA
Adsorbable organohalides (AOX)	(HPLC) with UV detector (Agilent Series 1100)	Zorbax SB-C18 column (150 mm x 4.6 mm, 5µm) Mobile Phase: 20% Aceton Nitril (ACN)/80% 0.01M H_3PO_4 to 45% CAN in 7.5 min with gradient of 80% ACN in 2.0 min and UV detection at 254 nm	This study Agilent Technologies (2002)
Biomass	Filtration Unit	Mass Liquid Suspended Solids	APHA (1992)
Kinetics Growth	-	Monod Equation	Monod (1949)

Table 2. Characteristics of the four batches of samples taken from recycled pulp and paper mill factory effluents in Pahang

Parameter (unit)	P&P Mill Effluent			
	Batch 1	Batch 2	Batch 3	Batch 4
COD, (mgL^{-1})	184	93	118	177
OLR, (g COD $[Lday]^{-1}$)	0.123	0.062	0.079	0.177
Colour (Pt-Co)	66	59	60	63
pH	7.16	7.3	7.25	7.21
Suspended Solids, SS, (mgL^{-1})	10.5	10	10	10.5
Phenol, (ugL^{-1})	ND	ND	ND	74
Chlorophenol, (ugL^{-1})	13	ND	ND	ND
Dichlorophenol, (ugL^{-1})	35	ND	ND	151
Trichlorophenol, (ugL^{-1})	332	197	176	372
Tetrachlorophenol, (ugL^{-1})	ND	26	30	ND
Pentachlorophenol, (ugL^{-1})	15	ND	ND	ND

ND = Not Detected.

Table 3. Growth kinetic parameters in this study and by other previous researches

Reference	System	Subtract	HRT (hrs)	Growth kinetic parameters			
				Y_H (mg/mg)	D_H ($hour^{-1}$)	μ_h ($hour^{-1}$)	K_s (mgL^{-1})
This study	GAC-SBBR	AOX	24	0.36	$4x10^{-5}$	0.0037	65.23
Jaar & Wilderer (1992)	GAC-SBBR	3-Chlorobenzoat	-	0.45	-	0.40	13
Hess et al. (1993)	SBR	2,4-DNP	79-230	0.41±0.15	-	-	1.12±0.5
Jacobsen & Arvin (1996)	SBR	PCP	4.3-13.9	0.4	-	0.05	-
Klecka & Maier (1985)	Batch	PCP	312-348	0.136	-	0.074	$60x10^{-3}$

*AOX: Adsorbable organic halides; PCP: Pentachlorophenol; DNP: 2,4-Dinitrophenylhydrazine

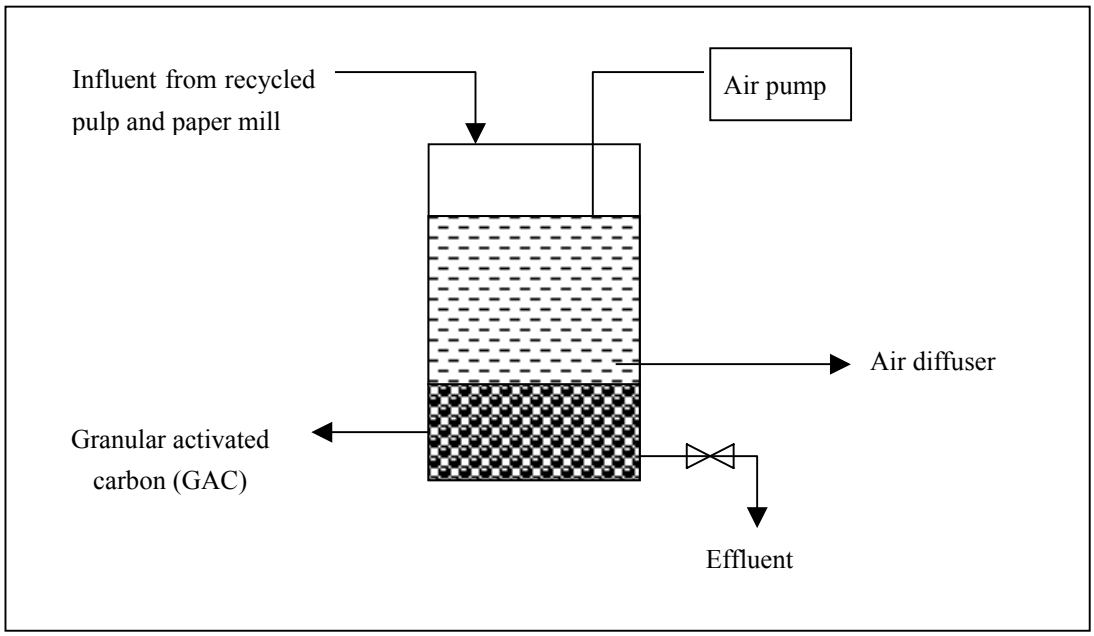

Figure 1. Schematic Diagram of the Granular Activated Carbon-Sequencing Batch Biofilm reactor (GAC-SBBR)

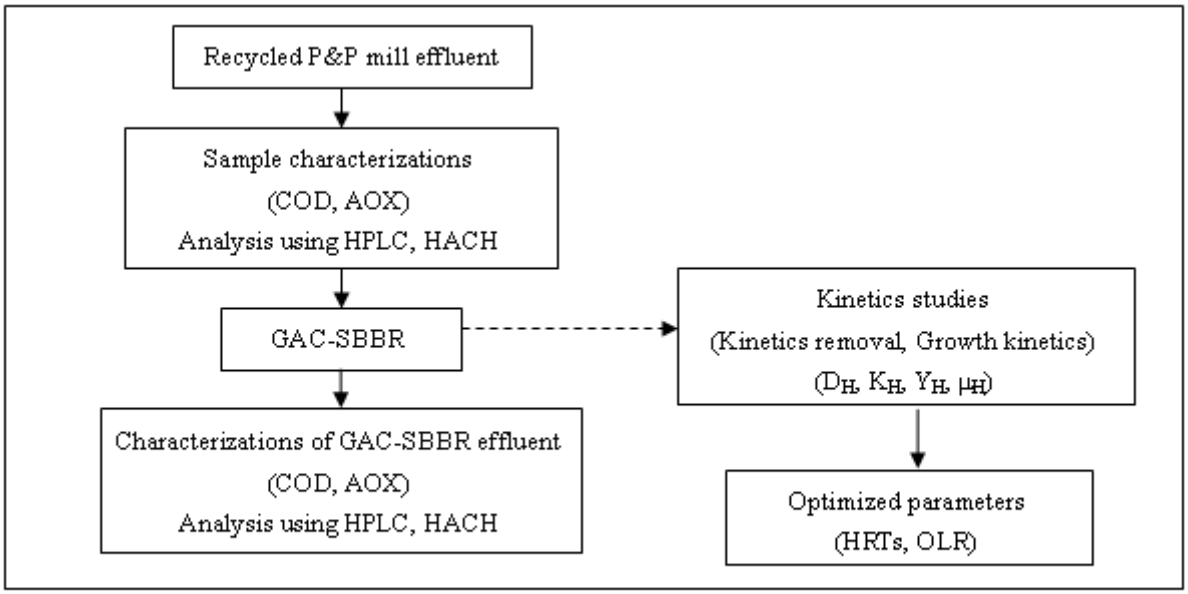

Figure 2. Overall methodology summary

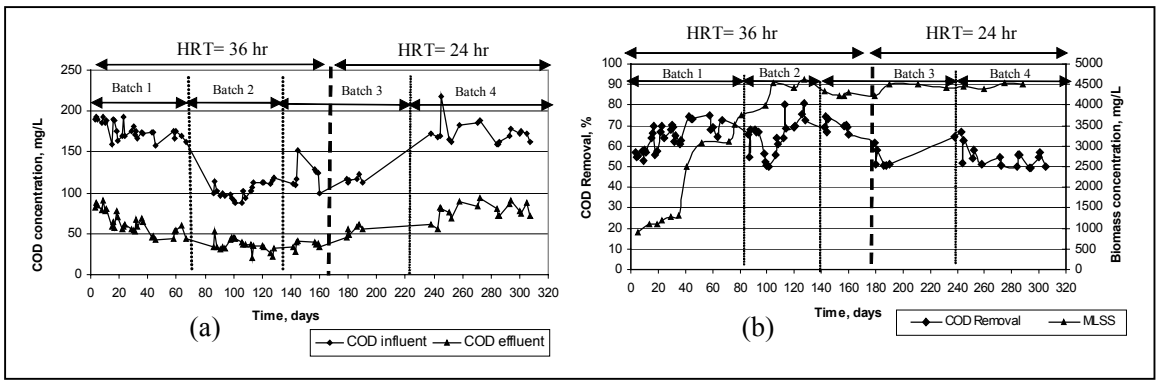

Figure 3. (a) Influent and effluent concentrations of COD and (b) Relation between COD percentage removal with biomass concentrations with both taken at HRTs of 36 hours and 24 hours

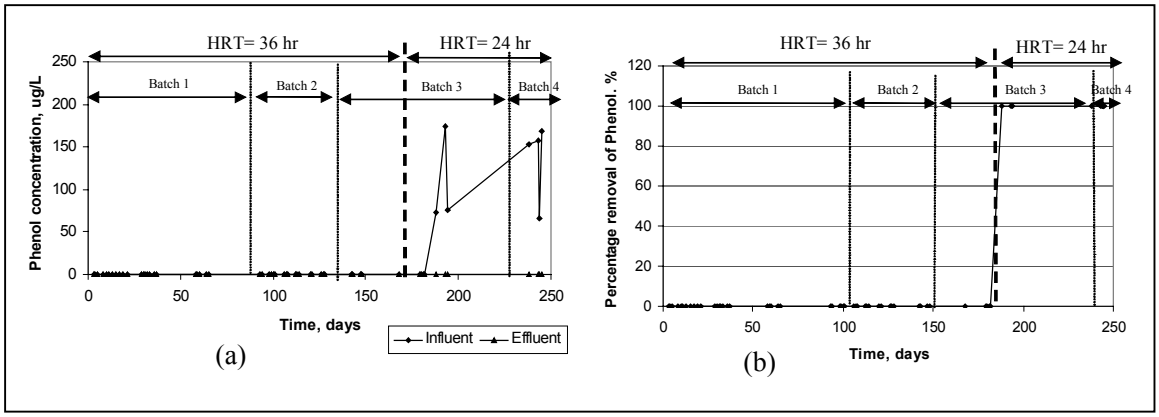

Figure 4. Phenol: (a) Influent and effluent concentrations and (b) percentage removal with both taken at HRTs of 36 hours and 24 hours

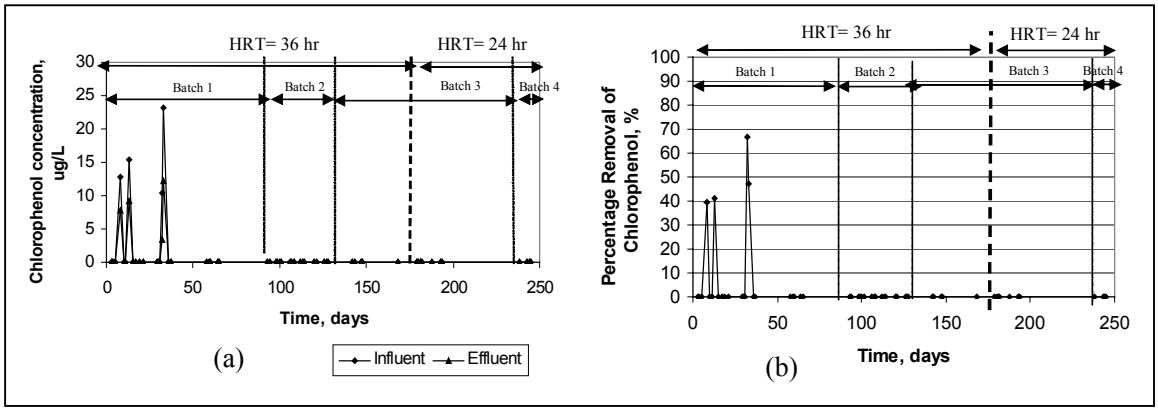

Figure 5. Chlorophenol: (a) Influent and effluent concentrations and (b) percentage removal with both taken at HRTs of 36 hours and 24 hours

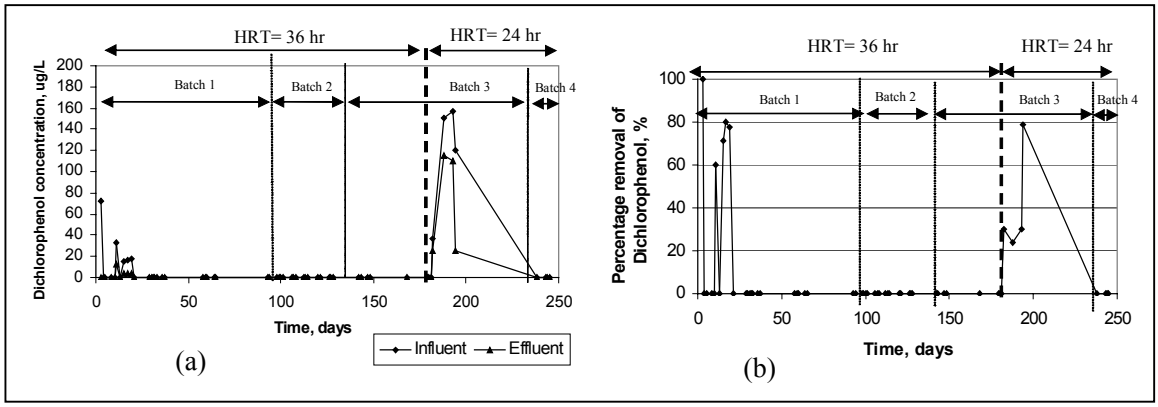

Figure 6. Dichlorophenol: (a) Influent and effluent concentrations and (b) percentage removal with both taken at HRTs of 36 hours and 24 hours

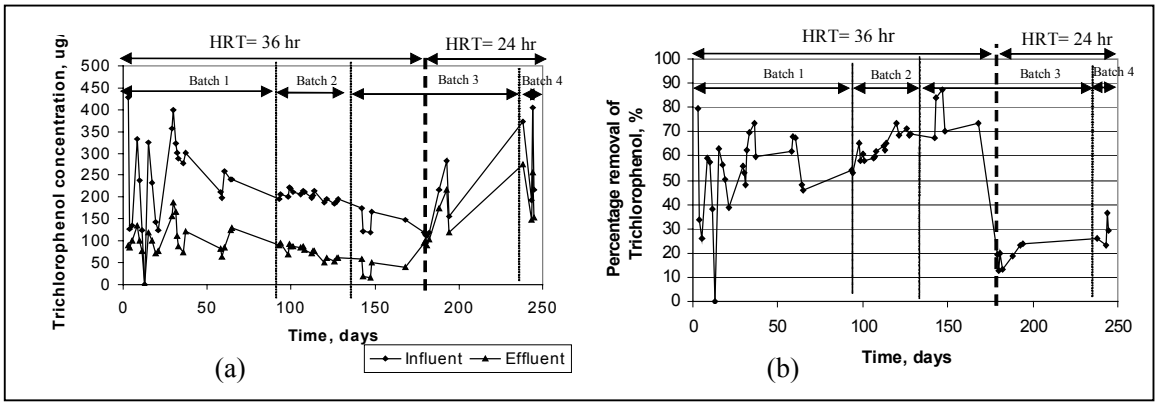

Figure 7. Trichlorophenol: (a) Influent and effluent concentrations and (b) percentage removal with both taken at HRTs of 36 hours and 24 hours

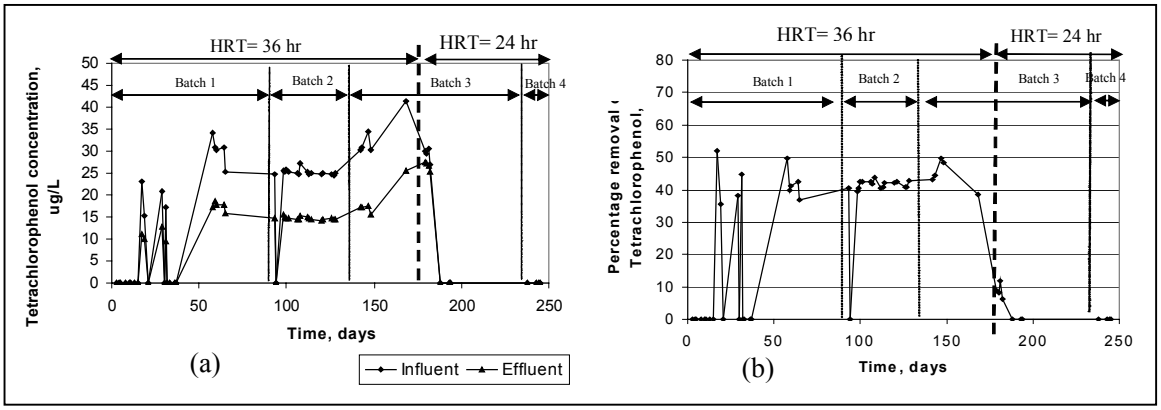

Figure 8. Tetrachlorophenol: (a) Influent and effluent concentrations and (b) percentage removal with both taken at HRTs of 36 hours and 24 hours

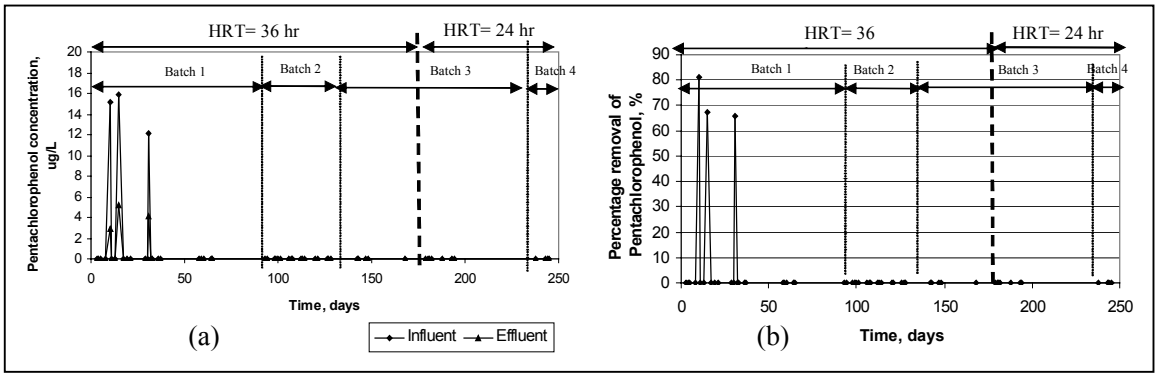

Figure 9. Pentachlorophenol: (a) Influent and effluent concentrations and (b) percentage removal with both taken at HRTs of 36 hours and 24 hours

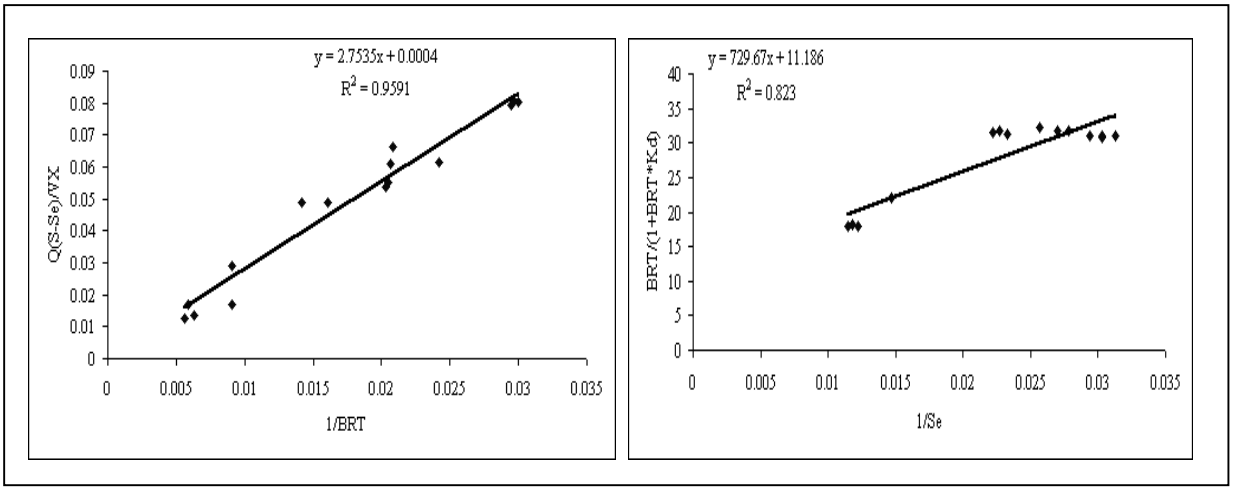

Figure 10. Growth kinetic parameters plot for recycled pulp and paper mill effluent samples

Modern Applied Science

www.ccsenet.org/journal.html

Vol. 2, No. 5

September 2008

A Wide Passband SAW Notch Filter

Zhiqun Lin

College of Science

Hunan Agricultural University

Changsha, 410128, China

Jiuling Liu

Institute of Acoustics

the Chinese Academy of Sciences

Beijing, 100080, China

E-mail: lzqphy@163.com

Wenhui Ren

College of Science

Hunan Agricultural University

Changsha, 410128, China

Shitang He

Institute of Acoustics

the Chinese Academy of Sciences

Beijing, 100080, China

Abstract

Wide passband notch filter is fulfilled by combining LC-all-pass filter with one-port-SAW resonator by means of its impedance characteristics. It possesses good frequency selectivity and low insertion loss due to good frequency selectivity of resonance-frequency resonator and low insertion loss of LC filter. Higher attenuation of specified frequency can be achieved by cascade. Compared with LC notch filter, it posses sharp cutoff frequency and narrower notch width. This paper first discusses the principle of this filter, and then proceeds with theoretical simulation and experimental demonstration.

Keywords: SAW, Resonator, Notch filter

1. Introduction

SAW notch filter is usually applied to coding and decoding system of TV(Wu Yili,1983, pp.204-207). Wide passband notch filter is fulfilled by combining LC-all-pass filter with one-port-SAW resonator by means of its impedance characteristics(O.Ikata,1992, PP.111-115). It inherited good qualities of both SAW filter and LC-circuit and thus it possesses good frequency selectivity, large working frequency and low passband insertion loss(Gopani,1990,pp.1-5). The cascade of SAW notch filter could obtain high attenuation in particular frequency band. Compared with LC notch filter, it has remarkable frequency selectivity for its sharp-cutoff frequency characteristics. Anenna duplexer used in mobile terminals, commonly takes the ladder structure as the transmitting end filter (Hikita M,1993,pp.15-23),but this kind of structure cannot meet the request for anenna duplexer of the high demand of isolation. By coupling this notch filter with a ladder-type SAW filter, low-insertion loss in passband and high attenuation in specified frequency can be achieved(Lin Zhiqun,2006,pp.376-379). With the longitudinally coupled resonator(Moriata T,1999,pp.95-104) coupled with the SAW notch filter,its frequency response can be improved(Lin Zhiqun,2007,pp.247-249).

In this paper the theory and approaches of achieving the notch filter by combining LC-all-pass filter with one-port-SAW resonator is discussed at first, then theoretical simulation is proceeded, and ultimately experimental results are accomplished. This notch filter is characterized by small size, low insertion loss, wide passband and narrow notch frequency band.

2. Structure and theoretical analyses of SAW notch filter

Above-mentioned SAW notch filter is achieved by substituting capacitance in LC-all-pass network (figure 2) for

one-port-SAW resonator (SAWR) (figure 1), and it is illustrated in figure 3.

As figure 1, the structure of one-port-SAW resonator (SAWR) shows, the middle part is interdigital. On the left and right are two metal gratings. And its impedance characteristics are illustrated in figure 4, the solid line represents the resistance, and the broken line represents the reactance. Impedance characteristics of one-port-SAW resonator (SAWR) shows that when frequency f is less than the resonance frequency of the resonator Fr (f<Fr), the impedance characteristics of the resonator appears capacitive; when f=Fr, the reactance of the resonator is equal to zero while the resistance tends to zero; when frequency f is near the anti-resonance frequency of the resonator Fa, the impedance characteristics of the resonator tends to the maximum. The needed notch filter is achieved by utilizing its impedance characteristics and combining it with LC-all-pass network.

The above notch filter has narrow stop band at the frequency of the anti-resonance frequency of the SAW resonator; meanwhile it has the same frequency response characteristics as the original LC circuit at other frequencies. The notch frequency is mainly determined by the anti-resonance frequency of the SAW resonator, which leads to good frequency selectivity. The notch frequency band could be controlled by adjusting the difference of resonance-frequency between the two resonators. With the increase of difference, the notch frequency band broadens while the attenuation in notch frequency decreases. So the difference should be adjusted in accordance with our needs.

3. Theoretical simulations of frequency response characteristics of notch filter

In figure 3, Z_{s1}, Z_{s2} represent the impedance of two one-port-SAW resonators, theoretical frequency response of one-stage SAW notch filter is:

$$S_{21} = \frac{R_D}{1 + R_{in}\left(\frac{1}{R_A j\omega L_2} + \frac{1}{R_A Z_{s2}} + R_D R_F + \frac{1}{j\omega L_1}\right)} \tag{1}$$

in which

$$R_A = 1 + \frac{Z_{s1}}{j\omega L_2} + \frac{Z_{s1}}{Z_{s2}} \qquad R_B = 1 + \frac{R_0}{j\omega L_1} + \frac{R_0}{Z_{s2}}$$

$$R_C = 1 - \frac{Z_{s1} R_0}{R_A R_B Z_{s2}^2} \qquad R_D = \frac{R_0}{R_C R_B j\omega L_1} + \frac{R_0}{R_A R_B R_C Z_{s2}}$$

$$R_F = \frac{Z_{s1}}{Z_{s2} R_A j\omega L_2} + \frac{Z_{s1}}{R_A Z_{s2}^2} - \frac{1}{j\omega L_1} - \frac{1}{Z_{s2}}$$

R_0 is loaded impedance, R_{in} is source impedance.

In accordance with formula (1), theoretical simulation of frequency response of one-stage structure is conducted (as illustrated in figured 3). ST quartz is applied in SAW resonator. Its central frequency is 217MHz and its periphery inductance is L1=145nH, L2=40nH respectively.

Simulation results are shown in figure 5 (power impedance and loaded impedance are both 50 ohm); figure A demonstrates the frequency response characteristics of narrow frequency domain and figure B demonstrates the frequency response characteristics of wide frequency domain (0~900MHz). As shown in simulation results: attenuation in notch frequency band amounts to more than 30dB, passband insertion loss less than 1.5dB and the ripple less than 2dB in the whole passband (from 0Hz to 900MHz). Deeper attenuation is obtained by multiple-stage structure when needed.

4. Experimental results

The experimental devices are fabricated on the piezoelectric crystal ST-X quartz in accordance with the two-stage of the structure shown in figure 3. The experimental characteristics curves are shown in figure 6.

As shown in the experimental result: attenuation in notch frequency f0 in two-stage structure amounts to more than 50dB, while at the frequency of f0±1.5MHz the insertion loss is less than 1.5dB. Compared with LC notch filter, it has much sharper cutoff frequency characteristics. The experimental results are approximately coincident with the theoretical simulation except that the loss in high frequency of the experimental results is more than that of simulation results (about 1 dB). This is somehow caused by the characteristics of inductance in high frequency.

5. Conclusion

Accomplishing wide passband notch filter by one-port-SAW resonator is elaborated, and theoretical simulation and experimental result are simultaneously provided in this paper. The accomplished filter inherits good qualities of both SAW resonator and LC-circuit and thus it is characterized by small size, low insertion loss, wide passband and narrow

notch frequency band. High attenuation to particular frequency is obtained by multiple-stage structure.

References

Gopani S, & Horine B A. (1990). 'SAW waveguide-coupled resonator notch filter'. IEEE Ultrasonics Symposium., pp. 1-5

Hikita M, Shibagakin, &Akagi T, et al, (1993). IEEE Ultrasonics Symposium. pp. 15-24.

Lin Zhiqun, Ren , Liu Jiuling, &He Shitang (2007). PIEZOELECTECYRICS & ACOUSTOOPTICS. *SAW Notch Filter Coupled with Longitudinally Coupled Resonator,* 29, 247-249.

Lin Zhiqun, Ren Wenhui, Liu Jiuling, &He Shitang (2006). Applied Acoustics. *SAW Notch Filter Coupled with Ladder-type Filter*, 25, 376-379.

Morita T, Watanabe Y, &Tanaka M, et al (1992). *Wideband low loss double mode SAW filters.*Arizona: IEEE Ultras Sym Proc Tucson. pp. 95-104.

O.Ikata, T.Miyashita, & T.Matsuda, et al, (1992). 'DEVELOPMENT OF LOW-LOSS BAND-PASS FILTERS USING SAW RESONATORS FOR PORTABLE TELEPHONES', IEEE Ultrasonics Symposium. PP. 111-115.

Wu Yili, Liu Shenggang, & Wang Yongde. (1983). *Theory of SAW and Its Application in Electronics Technology*. BeiJing: pp. 204-207.

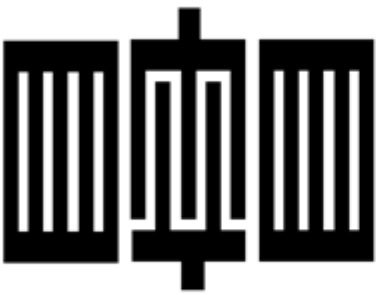

Figure 1. one-port-SAW resonator

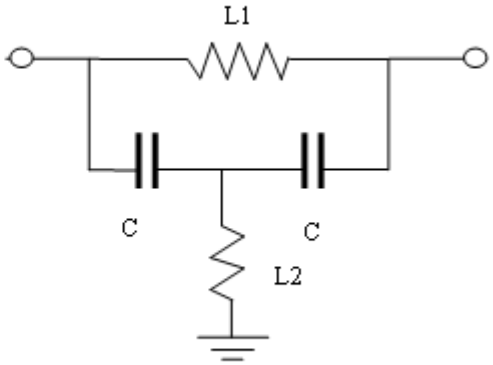

Figure 2. LC-all-pass network

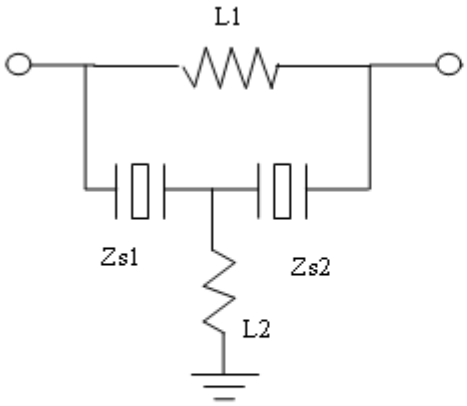

Figure 3. structure of SAW notch filter

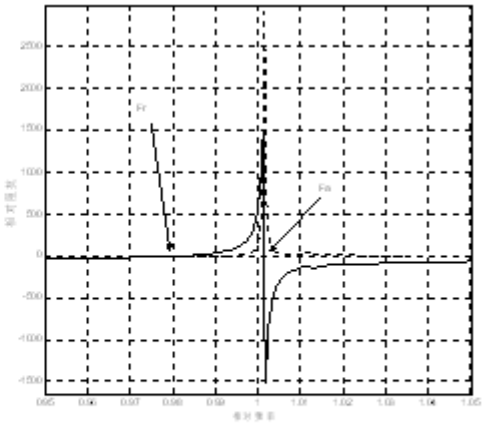

Figure 4. impedance characteristics

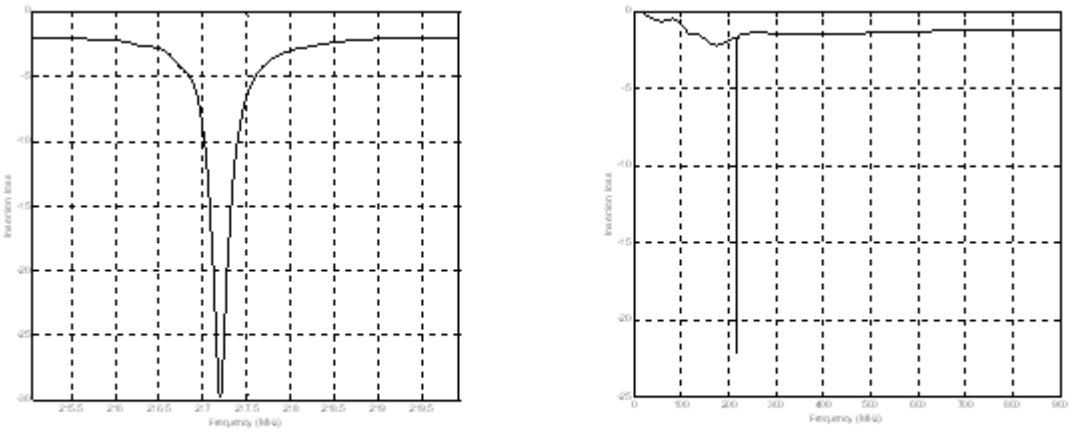

A narrow frequency domain B wide frequency domain

Figure 5. simulation results of one-stage structure

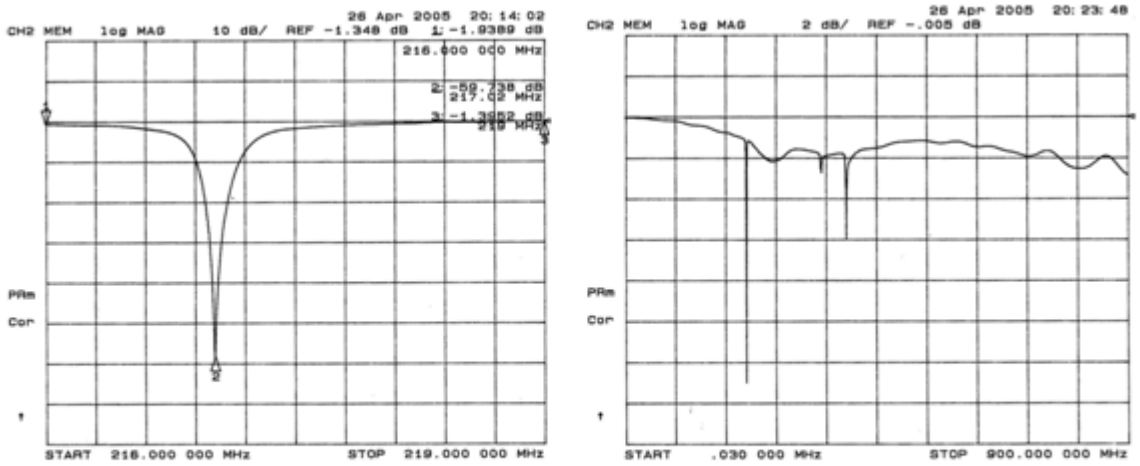

A narrow frequency domain B wide frequency domain

Figure 6. experimental frequency response

Modern Applied Science

www.ccsenet.org/journal.html

Vol. 2, No. 5

September 2008

A Note on Two Theorems of C. Dong and J. Wang Concerning Combinatorial Identities

Arnold R. Kräuter

Department of Mathematics and Information Technology

University of Leoben

Franz-Josef-Strasse 18, A-8700 Leoben, Austria

Tel: 43-3842-402-3803 E-mail: kraeuter@unileoben.ac.at

Abstract

In a recent paper C. Dong and J. Wang rederived three classical combinatorial identities by applying a special Vandermonde determinant. Two of their results, however, turn out to be incorrectly stated. This note presents counterexamples along with revised versions of the results mentioned.

Keywords: Vandermonde determinant, Identities involving binomial coefficients

1. Introduction

C. Dong and J. Wang applied a special Vandermonde determinant in order to establish a couple of well-known combinatorial identities in an elementary way (Dong & Wang, 2007). Unfortunately, two of these are incorrectly stated. In the following we present counterexamples as well as revised versions of the respective theorems in the cited paper.

Let V_n denote the n-square Vandermonde matrix (cf. Lancaster & Tismenetsky, 1985, p. 35, Exercise 6) of the integers 1, 2, …, n,

$$V_n = \begin{bmatrix} 1 & 1 & 1 & \cdots & 1 \\ 1 & 2 & 3 & \cdots & n \\ 1 & 2^2 & 3^2 & \cdots & n^2 \\ \vdots & \vdots & \vdots & \ddots & \vdots \\ 1 & 2^{n-1} & 3^{n-1} & \cdots & n^{n-1} \end{bmatrix},$$

and let $D_n = \det(V_n)$ be the determinant of V_n. Furthermore, let M_j be the minor of the entry in the nth row and jth column of V_n, and let S_j be the minor of the entry in the first row and jth column of V_n.

Lemma 1 (Dong & Wang, 2007, p. 24, Eq. (1)).

$$M_j = \left(\prod_{m=1}^{n-2} m!\right)\binom{n-1}{n-j}, \quad j = 1,2,\ldots,n. \tag{1}$$

Lemma 2 (Dong & Wang, 2007, p. 24, Eq. (2)).

$$S_j = \left(\prod_{m=1}^{n-1} m!\right)\binom{n}{j}, \quad j = 1,2,\ldots,n. \tag{2}$$

Using (1) and (2) Dong and Wang obtained, among others, the following identities for positive integers n (Dong & Wang, 2007, p. 25, Eqs. (3) and (6), resp.):

$$\sum_{j=1}^{n} (-1)^{n+j} j^{n-1} \binom{n}{j} = n!. \tag{3}$$

$$\sum_{j=0}^{n-1}(-1)^j(n-j)^i\binom{n}{j}=0,\quad 1\le i\le n, \tag{4}$$

2. Counterexamples to Eqs. (3) and (4)

In their current form, Eqs. (3) and (4) turn out to be incorrect.

Example 1. Eq. (3) is false. For if, e. g., $n = 4$, (3) would imply

$$\sum_{j=1}^{4}(-1)^{4+j}j^3\binom{4}{j}=-4+48-108+64=0\ne 4!.$$

Example 2. Eq. (4) is false in the case $i = n$. For if, e. g., $i = n = 4$, (4) would imply

$$\sum_{j=0}^{3}(-1)^j(4-j)^4\binom{4}{j}=256-324+96-4=24\ne 0.$$

3. Restatements of Eqs. (3) and (4) with proofs

The original Eqs. (3) and (4) have to be replaced by the following statements.

Theorem 1 (cf. Gould, 1972, p. 2, Eq. (1.13), first part). *For every nonnegative integer* n *we have*

$$\sum_{j=1}^{n}(-1)^{n+j}j^n\binom{n}{j}=n!. \tag{5}$$

Proof. According to the original proof (Dong & Wang, 2007, p. 25, Theorem 1) the following holds:

$$D_n=\sum_{j=1}^{n}(-1)^{n+j}j^{n-1}\left(\prod_{m=1}^{n-2}m!\right)\binom{n-1}{n-j}=\prod_{m=1}^{n-1}m!.$$

This gives

$$\sum_{j=1}^{n}(-1)^{n+j}j^{n-1}\binom{n-1}{n-j}=(n-1)!.$$

Using the identity (cf. Gould, 1972, p. iv)

$$\binom{n-1}{n-j}=\frac{j}{n}\binom{n}{j},\quad 1\le j\le n, \tag{6}$$

we eventually obtain (5). □

Theorem 2 (cf. Gould, 1972, p. 2, Eq. (1.13), second part). *For every nonnegative integer* n *we have*

$$\sum_{j=0}^{n-1}(-1)^j(n-j)^i\binom{n}{j}=0,\quad 1\le i\le n-1. \tag{7}$$

Proof. Let $W_n^{(i)}$ denote the n-square matrix obtained from the Vandermonde matrix V_n by replacing the nth row by the ith row, $1 \le i \le n$ - 1,

$$W_n^{(i)} = \begin{bmatrix} 1 & 1 & 1 & \cdots & 1 \\ 1 & 2 & 3 & \cdots & n \\ \vdots & \vdots & \vdots & \ddots & \vdots \\ 1 & 2^{n-2} & 3^{n-2} & \cdots & n^{n-2} \\ 1 & 2^{i-1} & 3^{i-1} & \cdots & n^{i-1} \end{bmatrix}.$$

Since $W_n^{(i)}$ is singular by construction, expansion of $\det(W_n^{(i)})$ by the nth row gives

$$0 = \det(W_n^{(i)}) = \sum_{j=1}^{n} (-1)^{n+j} j^{i-1} M_j.$$

Using Lemma 1 and Eq. (6) we get

$$0 = \sum_{j=1}^{n} (-1)^{n+j} j^{i-1} \left(\prod_{m=1}^{n-2} m! \right) \binom{n-1}{n-j} =$$
$$= \sum_{j=1}^{n} (-1)^{n+j} j^{i} \left(\prod_{m=1}^{n-2} m! \right) \frac{1}{n} \binom{n}{j}.$$

Replacing j by $n - j$ and by the symmetry of the binomial coefficients we eventually obtain (7). □

Remark. The arguments used in the proof of Theorem 2 still hold when $W_n^{(i)}$ is replaced by the matrix

$$X_n^{(i)} = \begin{bmatrix} 1 & 2^{i-1} & 3^{i-1} & \cdots & n^{i-1} \\ 1 & 2 & 3 & \cdots & n \\ \vdots & \vdots & \vdots & \ddots & \vdots \\ 1 & 2^{n-2} & 3^{n-2} & \cdots & n^{n-2} \\ 1 & 2^{n-1} & 3^{n-1} & \cdots & n^{n-1} \end{bmatrix}, \quad 2 \le i \le n,$$

followed by the expansion of $\det(X_n^{(i)})$ by the first row (which involves the numbers S_j given in Lemma 2).

References

Dong, Changzhou, & Wang, Junqing (2007). Application of Vandermonde determinant in combination mathematics. *Modern Applied Science, 1* (2), 24 – 26.

Gould, Henry W. (1972). *Combinatorial Identities.* Revised Edition. Morgantown, WV: H. W. Gould.

Lancaster, Peter, & Tismenetsky, Miron (1985). *The Theory of Matrices.* Second Edition with Applications. Orlando, FL: Academic Press.

Modern Applied Science

www.ccsenet.org/journal.html

Vol. 2, No. 5

September 2008

A Development of Real-Time-Piecewise Meter for Three-Phase Power

Baida Qu

Communication and Control Engineeringr College

Jiangnan University

Jiangsu 214122, China

Tel: 86-510-8989-0416 E-mail: qbd518@yahoo.com.cn

Abstract

Aiming at realising a whole range precision metering for both ultra-lower load power circumstance and normal one, this paper proposed a device for the piecewise real-time metering in terms of load power. The design, at the measuring entrance, took a piecewise inputting real-time load signal from the entrance according to the ratio of its three-phase power; through controlled switching, the load signal measured under different ratio was processed by ATT7022B-type metering chip, and calculated by AT89S52-type MCU under different range; and then was processed to satisfy the output required for the multi-function electrical power metering device. The result of the experiments has demonstrated that the design has realized an error equilibrium over whole range, precise metering and other functions.

Keywords: Load power, ATT7022B, Error, Piecewise real-time, Switching, Power-metering

1. Introduction

The device of electric kilowaterhour metering is developing into piecewise fee-ratio, multi-function and network at the present. Current three-phase electric kilowaterhour meter has had several functions such as positive and negative direction active power, reactive power metering and frequency, current, power factor measuring etc. some meters has increased complicated data analysis function. Under this development trend, many related scholars are researching in this field and at the same time the research is promoting the trend. J. Chen etc.(Jianguo Chen, Guowei Di and Fuyuan Wang, 2006) proposed a design of broad range electric kilowaterhour meter, based on an ATT7022A-type electric power load metering processing chip (LMP), and gave a realizing plan. T. Chen etc.(Tao Chen, Chunjie Zhang and Wenxu Zhang, 2006,) suggested a design plan of electric power monitoring terminal based on ATT7022A, and developed a hardware system for high-voltage power lines monitoring terminal which can exactly measures electric power parameters in time and has a function of flexible calibration through long-distance software. J. Zhang etc.(Jianxiong Zhang, Hongying Su and Wenzheng Zheng, 2006),applying the active energy and apparent energy measuring function of ADE7763-type LMP, designed a power factor meter which can adapt interfere environment, arrived the precision of the requirement designed. These literatures, from different sides, indicated the developing direction of electric load metering technique. As summarizing up, however, the researches on the combined electric energy metering devices, adopting new materials and having variety of functions, have been found out. The piecewise and combined-type meter, with multi-function include electric-steal against etc., has not been found out. And there have not been the research literatures on both real-time-piecewise measuring and metering at the ratio of load yet. Especially, the problem on high precision equilibrium metering for 10~35kV transmit and distribution electric power grids, has not been researched up to now, and has not involved with piecewise metering. Although there are some piecewise metering as above mentioned, the piecewise, so called peak and valley, is fixed at regulated time, is not essential peak and valley piecewise, the real-time peak and valley piecewise. In the mean time, the roughness of metering in light load range is still not revised. It is just for solving this problem that this paper proposes a design plan of a whole range precision equilibrium metering device for 10~35kV transmit and distribution electric power grid load.

The load signal is educed into the metering part of the device from the second terminals of combined sensor, the measuring part of the device, through the load ratio judging and switching control, high and low load metering channels are automatically switched at real load ratio, for guaranteeing the whole range metering precision balance between high

and low load and reducing metering line loss and error from increased measuring error produced by ultra-high and low load run of sensors.

The general scheme is that: at the measuring part, the current sensor (CT) with high and low ratio are adopted to reflect high and low load ratio, and run in the period of high load power and that of lower, respectively. that is piecewise measuring mode, by which whole range error balance is realized and metering, displaying precision is improved. in the mean time, the device should piecewise and circularly display active, reactive energy, active, reactive power and power factor, according to load power ratio, circularly display records of abnormal records such as high power humorous waves, negative powers, voltage-losses, phase exchanges, power-cuts etc.

2. Foundation and Principle of Load Ratio Piecewise Metering

Many researches (Conai Liu,1991; Yan Huang and Dingbai Li, 2006; Hui Hu, 2005) have indicated that according to the phasic vector graph of the equivalent circuit of CT, $I_1^{'}$, the equivalent primary side load current converted to secondary side, ($I_1^{'}=I_1/n$, I_1 is the primary side load current, $n=I_{1e}/I_{2e}$ is the ratio of CT, I_{1e} and I_{2e} is the rated load current of the primary side and the rated current of the secondary side, respectively)can be approximately expressed as

$$I_1^{'} = I_2 + I_{1M}^{'}\cos\beta ,$$

Where, I_2 is the current of the secondary side of CT, $I_{1M}^{'}$ is the excitation current of CT, β is the leading angle of phasic vector I_2 with respect to phasic vector $I_1^{'}$. And the current' error of CT is expressed as

$$f_i = \frac{I_2 - I_1^{'}}{I_1^{'}} \times 100\% .$$

While CT runs such that primary side load current I_1 goes within a vicinity of rated current I_{1e}, error f_i is minimum. otherwise, the greater the discrepancy that load current departs from the rated value is, the more the error is. An error circumstance of a typical ratio CT, under secondary impedance Z_2=1Ω, leading angle β=0.8, is in Fig.1. If load current is in 120% of the rated, from the Fig., the grater the load is, the smaller the error; while load is light, real load current is lower than 30% of the primary rated current of CT, esp., while load current goes at 20% of the rated and lowers, negative ratio difference f_i goes at allowance $\underline{f_i}$ and rapidly increase along with load current's lowering. The circumstance has been demonstrated by the data of experiment measures.

Fig.2 is the error circumstance of several CTs with different ratios under the same second load. Where, AB is a CT's error curve with ratio n_1 and primary side rated load current I_{1en1}; CD is another CT's error curve with ratio n_2 and rated current I_{1en2}; EF is the curve with ratio n_3 and primary rated load current I_{1en3};……. From the Fig., it is obvious that with ratio n_1, along with primary side load current I_1's lowering, negative ratio difference f_i gradually greatens along curve AB, such as arriving at B (where I_1=20%I_{1en1}, error arrives at allowance limit $f_i=\underline{f_i}$); If I_1 continuously lowers with the ratio, error would be unacceptable. If ratio is changed into n_2 on point B (corresponded rated load current of the primary side is I_{1en2}), such that the CT is switched to run along curve CD, error f_i will greatly lower. By the same reason, once primary load current I_1 lowers and arrives at point D along curve CD under ratio n_2, (where I_1=20%I_{1en2}, error again gradually increase and arrive at allowance limit $f_i=\underline{f_i}$). If ratio is once more changed into n_3 on point D, such that the CT is switched to run along curve EF, error f_i will greatly lower again;……. Like this, corresponding to the varying of load current (*i. e.*, the ratio of load), the ratio of CT is changed to guarantee that the measuring error of CT is always smaller than the given value. The idea, that the ratio of CT is piecewise switched corresponding to load varying to make error small and even, is proposed just based on this principle.

This paper will, by partitioning two sections corresponding to load, design a three-phase power load metering device. Three-phase power load energy, through being transformed by the combination of a voltage transfer (PT) and a double ratio CT, as the form of analog voltage signals, is fetched out from the second side of the combined sensor (CT+PT). The analog signal corresponding to low ratio current and that to high ratio one, together with the voltage analog signal, is delivered to low ratio signal processing channel and high one, respectively. Two channels are switched by channel switch, one of them is chosen to send its signal to metering management module with an LMP as core. LMP transforms the analogs into corresponded digital signals, through energy metering processing such as calculating, managing, etc., gives out many kind of real-time data, including active energy, reactive one, power factor and so on, to calculation and control module with a micro-program control unit shingle chip (MCU) as core. Than, MCU has the corresponded data been output-processed, by means of memory module, liquid crystal display module (LCD), data communication module (COM) etc., and outputted, such as memory renovating, data displaying, data communicating etc. In the mean time, MCU, through the calculating and judging power data inputted from LMP, produces a control level and delivers it to a multi-way simulation switch (SS), to control SS's switching. SS, through its conversion, chooses on low ratio signal processing channel or high one and sends the corresponded load signals to the input terminals of LMP.

3. General Design Requirement for Multi-function Meter

Multi-function compound electric energy meter needs to realize main functions as follows:

1) While no keystroke, displaying for 4 circles with 5 seconds as a circle: (1) the current active and reactive energy under load≤20% of rated power capacity (current) (≤20%: W, V); (2)the current active and reactive energy under load>20% of rated power capacity (current)(>20%: W, V).

2) After keystroke "dispersion" or during its availability, displaying for 4 circles with 5 seconds as a circle: (1) the active and reactive energy at the end of last time (month) under load≤20% of rated power capacity (current) and the dispersions of the current active and reactive energy minus the active and reactive energy at the end of last time (month) under load≤20% of rated power capacity (current) (≤20%: W_0, V_0,W -W_0, V-V_0); (2) the active and reactive energy at the end of last time (month), under load>20% of rated power capacity (current) and the dispersions of the current active and reactive energy minus the active and reactive energy at the end of last time (month), under load>20% of rated power capacity (current)(>20%: W_0, V_0, W -W_0, V-V_0).

3) After keystroke "instant" or during its availability, displaying for 2 circles with 3 seconds as a circle: (1) the active, reactive power and power factor under load≤20% of rated power capacity (current) (≤20%: P, Q, cos); (2) the active, reactive power and power factor under load>20% of rated power capacity (current)(>20%: P,Q,cos).

4) After keystroke "abnormity" or during its availability, displaying for 3 circles with 6 seconds as a circle: (1) the sequence of last four appearances of harmonic power being larger than set value and each begin-end time of them (*k*st H: yy/mm/dd//hh:mm:ss—yy/mm/dd//hh:mm:ss**);** (2) the sequence of last four appearances of inverted power and each begin-end time of them (*k*st F: yy/mm/dd//hh:mm:ss—yy/mm/dd//hh:mm:ss**);** (3) the sequence of last four appearances of voltage-loss phase and each begin-end time of them (*k*st A (B or C): yy/mm/dd//hh:mm:ss—yy/mm/dd// hh:mm:ss**);** (4) the sequence of last four appearances of phase exchange and each begin-end time of them (*k*st A←→: yy/mm/dd//hh:mm:ss— yy/mm/dd//hh:mm:ss**);** (5) the sequence of last four appearances of power-cut and each begin-end time of them (*k*st K: yy/mm/dd//hh: mm:ss—yy/mm/dd//hh:mm:ss**).**

5) Sound and light alarming, once any of the first four abnormities in requirement 4 appearing.

6) While power cut, saving related data.

7) Through communication interface, providing channel for data communication with long-distance terminals.

4. The Circuit Design and Realization of the System

4.1 The overall structure of the combined electric energy metering device

Load power piecewise combined electric energy metering device is composed of measure module, signal processing module, metering and calculation module, data memory, display and output module, power supply unit and so on. Where, measure module, as the measuring part of the device, is mainly combined CT and PT, used to transform load quantity into corresponded current and voltage signals; signal processing, metering and calculation module, data memory, display and output module, power supply unit are combined to meter groupware including a series of software and hardware, they are a system aggregating the functions such as signal processing, switching; data gathering, comparing, processing, analyzing, calculating, saving, renovating, displaying and data communication, etc.

The hardware structure shows in Fig. 3. The CT+PT in the measure module is a dry-type outdoor exact device made from new materials and by new technologies, two current ratios are 150/5A and 30/5A (CT: 150, 30/5A), double level voltage ratio is 10kV/100V/5V (PT: 10kV/100V/5V). The signal processing module is composed of signal compensating, filtering and attenuating resistance-capacitance-networks (F.A.I1 (high ratio current channel), F.A.I2 (low ratio current channel) and F.A.V (voltage channel)) and SS chip CD4053. Such structure order as processing before switching is to consider both that the secondary side of CT does not open and the application of SS and its switch-on-resistances. The metering, calculation and management module includes an electric load metering processing unit which takes ATT7022B-type LMP as core, with the related outer elements, aiming at obtaining several real-data such as active, reactive energy, power factor and so on, and a calculating unit which takes AT89S52-type MCU as core, matched by outer chips such as real-time clock, fail-tolerance circuits etc., aiming at running calculation, control and so on. The memory and renovation module, which takes a FM3116-type ferrous-memory chip (FM) as core, is used to hold current all data and to realize data saving function during power-cut. The display unit, adopting an LCD chip, JHD 204A, is used to display requirement 1 to 4 above mentioned. COM unit, adopting a MAX485 chip and a semiduplex RS485 interface, is to real-time deliver all kinds of related data, programmable parameters, and so on to upper-computer. The power supply unit (PS) adopts double polarity (positive and negative) groups, one of them is a structure that a parallel connection of triple single-phase rectifying bridges links with a voltage regulator, to fit for every run environment.

4.2 A Design Realization of the Signal Processing Circuit and its Work Principle

The feature of the device is mainly embodied in the signal processing module. The signal processing and piecewise switching circuit is given in Fig. 4.

In the Fig., the load current signals of A(B, C) phase come from the corresponded high ratio terminal, AP1 (BP1, CP1),

the corresponded low ratio terminal, AP2 (BP2, CP2), and the conjunct terminal, AN (BN, CN), on the secondary side of CT. On each channel, say A phase high ratio signal channel, RC circuit composed of R_1, R_4, C_1, R_8, C_4 is for shunt, compensation of phase order and low-frequency-pass filtering. Its frequency is set at 4.8kHz. CT would generally produce a 0.1°~1° phase angle error, but it would be corrected in the phase correcting register (PhsregA (PhsregB, PhsregC)) in LMP. Two diodes, reverse parallel connected, become a protecting circuit.

Other channels are similar to the above mentioned. The voltage signal channel of every phase is similar to the current signal channel of the conjunct terminal of corresponded phase.

In three phase voltage signals, each, going though processing channel F.A.V, directly input to corresponded voltage-analog input-terminal pair on LMP, ATT7022B. For example, the signal of A phase inputs to terminals V2P-V2N (B to V4P-V4N, C to V6P-V6N (omitted in Fig.4)). In three phase current conjunct signals, each, going though processing channel F.A.I1 and F.A.I2, directly input to corresponded current-analog input-terminal pair on LMP. For example, the signal of A phase inputs (gong through terminal an) to terminal V1N (B (through bn) to V3N, C (through cn) to V5N (omitted in fig.4)).

High ratio three phase current signals, going though processing channel F.A.I1, and low ratio three phase current signals, going though processing channel F.A.I2, are respectively input (going through terminals ap_1, bp_1, cp_1 and ap_2, bp_2, cp_2) to corresponded input terminals ax, bx, cx and ay, by, cy on SS, CD4053. Controlled by the control level on its control terminals A, B, C, SS switches and sends high ratio three phase current signals or low ratio ones (through its output terminals a, b, c) to corresponded three current analog input terminals V1P (A phase), V3P (B), V5P (C) on LMP.

ATT7022B-type LMP has 7 analog input terminals. The first six of them are partitioned into a current channel and a voltage one. The current channel is for the input of 3 pairs of difference voltages and includes terminals V1P-V1N, V3P-V3N and V5P-V5N, standing for A, B and C phase. The bound of the signal voltages of the 3 channels is ±1.5V. the voltage channel includes 3 pairs of difference voltages terminals V2P-V2N, V4P-V4N, V6P-V6N, for A, B, C phase.

While load is not smaller than 20% of the rated capacity (current) of a power system, MCU, going through calculating and judging, by means of its terminal P1.0, gives off a high level to the control terminals A, B, C of SS, controls SS to switch. Thus, the low ratio signals of three phase load currents are sent to 3 pairs of difference voltages input terminals V1P-V1N, V3P-V3N and V5P-V5N of current channel of LMP, going through the input terminals a, b, c of SS and the conjunct terminals an, bn, cn of F.A.I1, F.A.I2. While load is smaller than 20% of the rated capacity (current) , MCU, through calculating and judging, by its terminal P1.0, gives off a low level to the control terminals A, B, C, controls SS to switch. Thus, the high ratio signals of the load currents are sent to 3 pairs of terminals V1P-V1N, V3P-V3N and V5P-V5N, through terminals a, b, c and terminals an, bn, cn. Besides, the load signals of two ratio conditions are processed, managed and metered by LMP, the load data of two conditions are calculated and control by MCU, and so on. Then the data of the two conditions are saved and renovated by FM, displayed by LCD and prepared for communication by COM.

5. Software Design of the System

The software of the multi-functional metering device is mainly for the calculation of real-time data, inner parameters, dispersion, moment value and so on, the accumulation of energy, the management of every modules, the judging disposal of abnormal circumstances such as harmonious waves with power being larger than given value, inverted power, voltage-loss, phase-exchange and power-cut, the disposal of memory and renovation, display, etc. A block chart of the program function flow is shown in Fig. 5. The software fitting for ATT7022B-type LMP is mainly the control programs of AT89S52-type MCU. They execute the configuration to LMP, the disposal of several related data, and at the same time, make use of the data transmitted by SPI to affect the search of outer data, to calibrate the configuration of data.

The frame of the overall program is follows:

```
#include <reg52.h> ……
sbit     qh=P1^0;       ……
float     h=0;            ……
uchar sr(void);       ……
……
main( )
{……
do{if(P3=0xff) {……}
```

```
if(P3=0xfb) {……}
if(P3=0xf7) {……}
if(P3=0xef) {……}
}while(1);
}
void cw(uchar rw,add,length) {……}
uchar sr( )              {…}
void spiw(uchar var) {…}
void iic(uchar rw, dd, addh, addl, length) {……}
uchar iicr( )            {……}
void iicw(uchar var) {…}
void init(void)          {…}
void cmd(void)           {…}
void wdata(void)         {…}
void cb(void)            {…}
void delay(lint nop)     {…}
void zh(uchar com0,com1,com2){……}
void xs(float g)         {……}
void xsr(float g)        {……}
void sj(uchar g)         {……}
void xz(void)            {……}
```

6. Conclusion

This device has taken a measure that piecewise input real-time load signal according to the ratio of tree-phase power. By controlling and switching the ratio of CT, it, within different range, calculates the different ratio load signal measured, on the basis of the metering proposal from LMP, and more, executes every input function required. The device actualized has, by experiments, been proved to be accurate and feasible. The result of experiments has demonstrated all of functions required. The device has realized error balance and precision metering over whole range. It has passed the technological appraisal held by Science and Technology Department of Anhui Province, China, and has applied an invention patent of nation of China. The other problems and the requirements for expanding functions are easier to solve and have had mature techniques to apply, and do not give unnecessary details in this paper.

References

Jianguo Chen, Guowei Di and Fuyuan Wang. (2006). A Design and Realization of On-line Broad Range Electric Energy Meter Based on ATT7022 , *Modern Electronic Technology*, 9, 94-101.

Tao Chen, Chunjie Zhang and Wenxu Zhang. (2006) . Design of Electric Power Monitoring and Controlling Terminal Based on ATT7022A-type Electric Load Metering Chip. *Information Technology*, 9, 40-43.

Jianxiong Zhang, Hongying Su and Wenzheng Zheng. (2006). A Power Factor Meter Based on Electric Load Metering Chip . *Electricity Applications*, 4, 76-78.

Conai Liu. *Inductance Sensor and Phase Order Filter*. (1991). Beijing: China's Water and Electricity Power Pres.

Yan Huang and Dingbai Li. Reasonable Choice of Current Transformer. (2006). *Jiangxi's Power*, 5, 37-40.

Hui Hu. *Singlechip Principle and Application Design*. (2005). Beijing: China's Water and Electricity Power Pres.

Zhuhai Juli Integrate Circuit Design Co. Ltd. ATT7022B *User Manual*. (2005). www.action.com, 2005.

Zhuhai Juli Integrate Circuit Design Co. Ltd. ATT7022B *Applicaion Note*. (2005). www.action.com, 2005.

Lei Yang and Guangming Huang. A Realization of ATT7022B Automatic Calibrator. (2007). *Electic Measure and Meters*, 5, 44-497.

Zaixin Huang and Daliang Zeng. *Program Design Base—C Language*. (2000). Beijing: People posts and telecom. Pres., (2000.12).

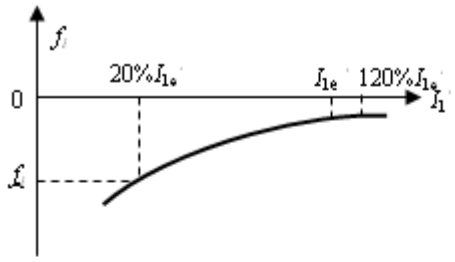

Figure 1. The error of CT' runing

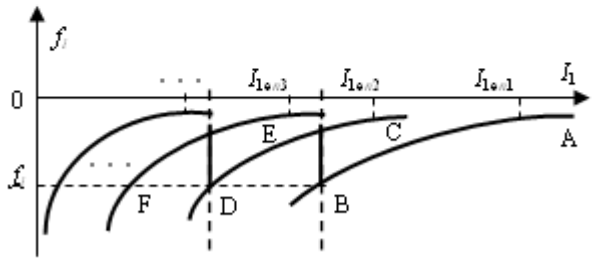

Figure 2. Switching running of multi-ratio

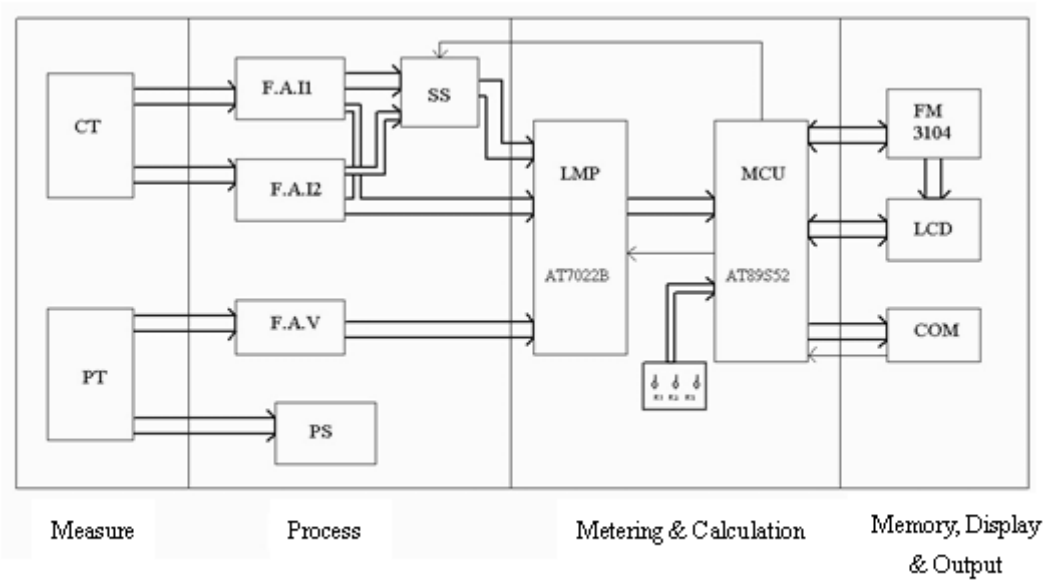

Figure 3. The hardware structure block of the meter

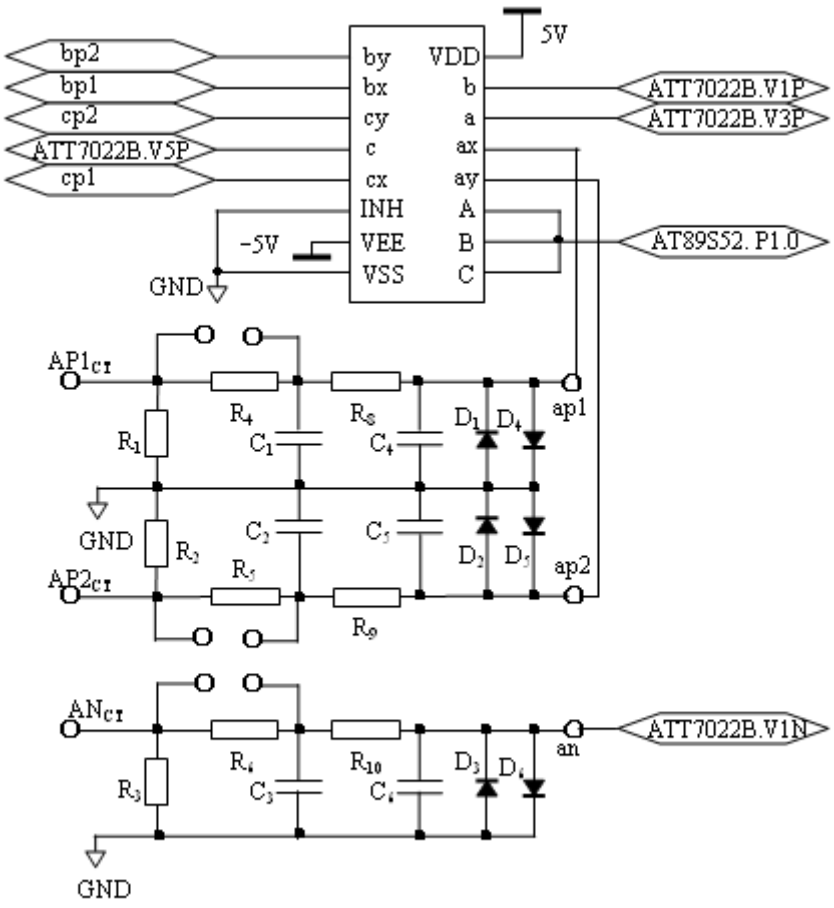

Figure 4. Signal processing and piecewise switching circuit

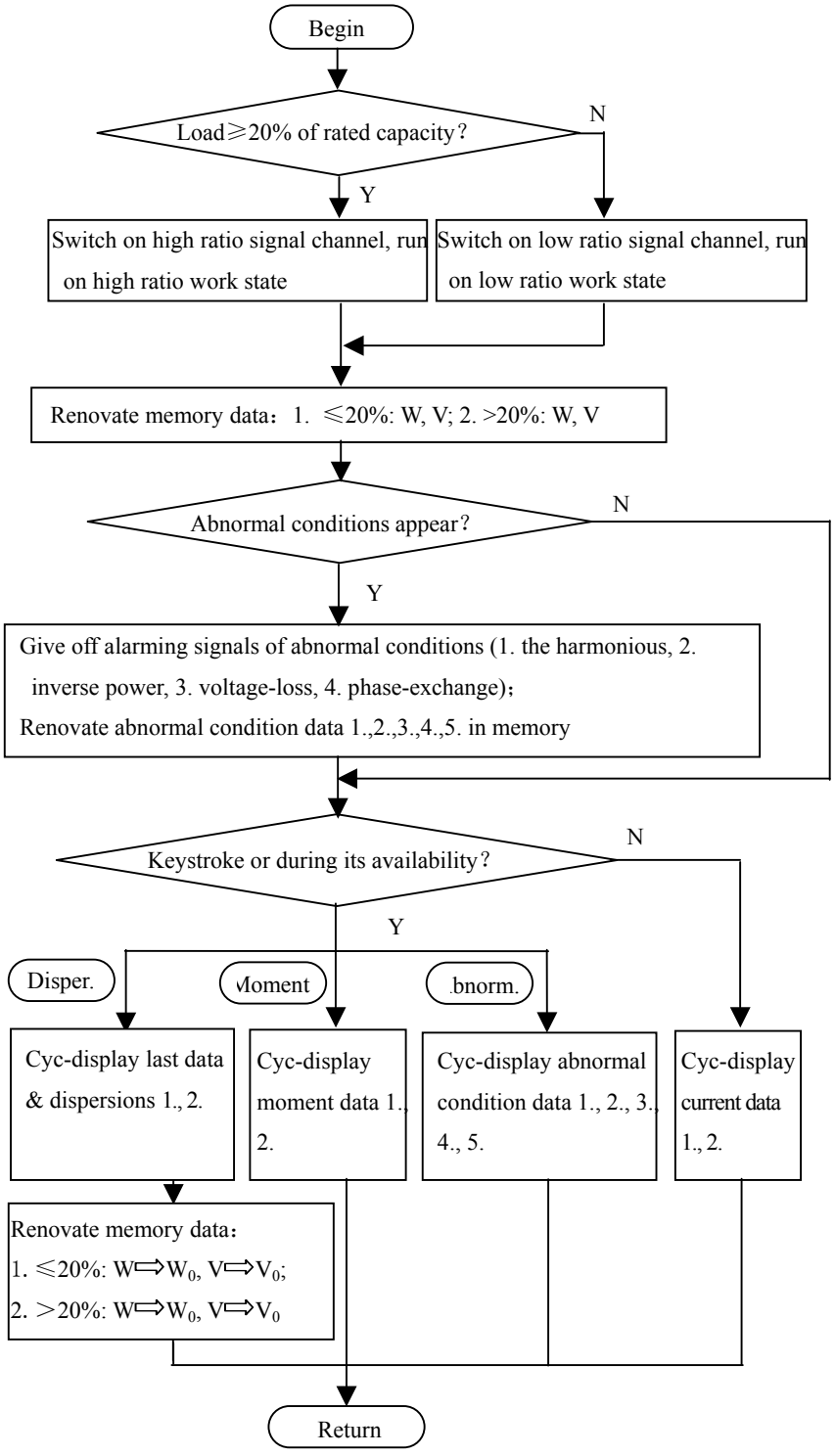

Figure 5. Flow of Program function module

Modern Applied Science

www.ccsenet.org/journal.html

Vol. 2, No. 5

September 2008

Measurement of Relative Efficiency of State Owned Electric Utilities in INDIA Using Data Envelopment Analysis

R.Meenakumari (Corresponding Author)

Department of EEE

Kongu Engineering College

Perundurai, Erode, Tamilnadu,India

Tel: 91-94431-27506 E-mail:oremkay@rediffmail.com

N.Kamaraj

Department of EEE

Thiagarajar College of Engineering

Madurai, Tamilnadu ,India

E-mail: nkeee@tce.edu

Abstract

In this paper two different DEA models were applied to evaluate the relative efficiency of State Owned Electric Utilities (SOEUs) in India. The DEA method was applied to find the overall efficiency, Technical Efficiency and Scale Efficiency. The Most Productive Scale Size (MPSS) is calculated for the scale inefficient utility. The results and discussions of this paper can be used to assist the authorities to pave the way for the improvement in technical and scale efficiency.

Keywords: Benchmarking, Relative Efficiency Measurement, Data Envelopment Analysis, CCR Model, BCC Model, Most Productive Scale Size

1. Introduction

This Paper presents a case study in which Data Envelopment Analysis [1],[2] is applied to evaluate the relative efficiencies of the 29 State Owned Electric Utilities in India. The purpose of this study is to identify the efficient / inefficient SOEU through the development and use of DEA model and to suggest the possible way of improving the overall efficiency, technical efficiency and scale efficiency. Efficiency measurement is an important issue in power delivery. Measure of relative efficiency was motivated by several factors like cost efficiency, operational efficiency, managerial efficiency etc., among which this paper is confined to *operational efficiency measurement* of SOEU's by using DEA.

The Indian power sector commenced an era of reforms and restructuring since the year 1991, with the opening of the sector to Independent power producers. The Indian Government made a vision of "Power to all" by the end of the year 2012 and the projected installed capacity is around 2,12,000 MW which is twice the current value. To achieve such a greater capacity the Indian government has initiated a lot of reforms like APDRP (Accelerated Power Development and Reform Programme), DRUM Distribution Reform, Upgrades and Management) etc,. At this juncture, the knowledge of the operational efficiency of the various SOEU's will help the personnel to refine their ideas for better operation.

The participation of private sector in the distribution sector has been already initiated. There are three private companies already available in Karnataka and two private companies in Maharashtra (Tata Power Company and Reliance Power Company). Lot more initiatives have been taken for the participation of private distribution utilities. In this changing environment there is an urgent need for detailed analysis of various SOEUs performance using standard benchmarking techniques; a process that can reveal finer mechanisms causing inefficiencies. The analysis presented in this paper will help to review the performance of SOEU so that lessons from the failure can be taken note of and effective steps be taken to mitigate the shortcomings. This analysis is also useful because presently the main focus of the reform programme is to make SOEUs efficient and commercialize these entities.

The objective of the present analysis is to develop a benchmark based on the comparison of the operation of similar SOEUs and analyze the inefficiencies of the existing utilities in the policy context of making them efficient. The rest of

this paper is organized as follows. Section 2 reviews the related literature. Section 3 discusses about the Brief Scenario of Indian Electricity Industry. Section 4 discusses about the Data Envelopment Analysis and the mathematical background of the DEA methodology. Section 5 discusses about the selection of inputs/outputs and the factor analysis. Section 6 discusses about the results and analysis. As a conclusion, section 7 follows the results and analysis.

2. Literature Survey

The previous studies that have used DEA to investigate the relative efficiency of the power industry are now described. Fare *et al* [5] used DEA model to assess the relative efficiency of electric utilities in which an output (net generation) and three inputs (fuel, labor and capacity) are considered. Charnes *et al* [6] measured the management efficiency of regulated electric co operatives in which three outputs (net margin, total kWh sales and total revenue received) and eleven inputs (operational expenses, maintenance expenses etc) are considered for anlaysis. Miliotis [7] evaluated the efficiency of 45 EDDs of Greek Public Power Corporation. This research considered eight factors such as served customers, network length etc for analysis.

Golany *et al* [8] assessed the operating efficiency of power plants in Israel Electric Corporation in which four outputs (generated power, operational availability, deviation from operational parameters and SO_2 emissions) and three inputs (installed capacity, fuel consumption and manpower) are considered. Puneet Chitkara [24] used DEA to find the operational efficiency of Indian Power Plants. Kaoru Tone and Miki Tsutsu [25] applied DEA for the decomposition of cost efficiency for Japanese-US electric utility companies where they used three input factors (Capital cost, Number of employees, Fuel consumption) and three cost input data (Total capital cost, Total Labor cost and total fuel cost) and one output (Net electricity power sales). Chyan Yang and Wen-men Lu [22] assessed the managerial performance of Taiwan Power Company where five input factors (Employment expenditure, operating expenditure, total assets, length of distribution network and transformer capacity) and three output factors (number of customers, quantity of energy sold and energy loss rate) were considered for the analysis. Raul Sanhueza *et al* [27] used DEA to determine the distribution added value for the Chilean Electric Utilities where five input factors (Distribution added value, total km line length etc) and three output factors (Total energy sold, coincident power during peak hours and number of customers) are considered. Athanassopoulos *et al* [9] developed data envelopment scenario analysis for setting targets to electricity generating plants in the U.K. This study considered four outputs (electricity produce, plant availability, accidents incurred and generated pollution)and three inputs (fuel, controllable costs and capital expenditure). Sueyoshi [10] explored a marginal cost based pricing system using the DEA approach to examine the tariff structure of nine electric power companies in Japan. This research considered the output of 11 electricity sales and three input prices.

Park *et al* [11] measured the operating efficiency of the 64 conventional fuel plant in South Korea in which he consided an output (net electrical energy output) and three inputs (fuel consumption, installed power and labor). Pahwa *et al* [26] applied DEA to measure the 50 largest electric distribution utilities in the U.S. In this research three outputs (distribution system peak load, retail sales and retail customers) and five inputs (distribution system losses, distribution lines etc) are considered. Tripta Thakur [29] used DEA for the benchmarking study for the Indian Electric Utilities where he used three input factors (Total cost, number of consumers and distribution line length) and an output (Energy sold)

In this paper, the operational efficiency of 29 State Owned Electric Utilities in India are evaluated using DEA where three input factors (Installed Capacity, Circuit km and % T&D losses) and Two output factors (Number of consumers and Quantity of Energy Supplied) are considered for analysis

3. Brief Scenario of Indian Electricity Industry

Electricity is one of the most vital infrastructure inputs for economic development of a country. The demand of electricity in India is enormous and is growing steadily. The vast Indian electricity market, today offers one of the highest growth opportunities for private developers. Since independence, the Indian electricity sector has grown manifold in size and capacity. The generating capacity under utilities has increased from a meagre 1362 MW in 1947 to 112058 MW as on March, 2004. Electricity generation, which was only 4.1 billion KWh in 1947 has risen to a level of over 558.134 billion KWh in 2003-2004. In its quest for increasing availability of electricity, the country has adopted a blend of thermal, hydel and nuclear sources. Out of these, coal based thermal power plants and in some regions, hydro power plants have been the mainstay of electricity generation. Oil, natural gas and nuclear power accounts for a smaller proportion. Thermal plants at present account for 70 percent of the total power generation, hydro electricity plants contribute 26 per cent and the nuclear plants account for the rest. Of late, emphasis is also being laid on development of non-conventional energy sources i.e. solar, wind and biomass.

The structure, ownership pattern and regulatory setup of the Indian power sector have witnessed radical changes especially in the past few years as part of the ongoing reform program with the establishment of independent regulators, corporatisation, unbundling and the advent of privatization in some States

To have an easy access and control, the Indian Power Sector is divided into five regions viz., Northern, Eastern, Western, Southern and North-Eastern Regions. Each state has its own utility previously known as State Electricity Boards. With the introduction of new Electricity Act 2003, Indian power sector is undergoing drastic reformation such as envisaging new National Electricity Policy (NEP), Rationalization of Tariffs, Restructuring of the SOEU's and the provision for new regulatory regime. Each state has the freedom to set up its own regulation and there will be State Electricity Regulatory Commission and each SERC will be centrally coordinated by CERC.

As on March 2005, twenty two states namely, Orissa, Haryana, Andhra Pradesh, Uttar Pradesh, Karnataka, West Bengal, Tamil Nadu, Punjab, Delhi, Gujarat, Madhya Pradesh, Maharashtra, Rajasthan, Himachal Pradesh, Assam, Chatisgarh, Uttaranchal, Goa, Bihar, Jharkhand, Kerala and Tripura have either constituted or notified the constitution of SERC. Eighteen SERCs viz. Orissa, Andhra Pradesh, Uttar Pradesh, Maharashtra, Gujarat, Haryana, Karnataka, Rajasthan, Delhi, Madhya Pradesh, Himachal Pradesh, West Bengal, Punjab, Tamil Nadu, Assam, Uttaranchal, Jharkhand and Kerala have issued tariff orders.

Over the past years, financial performance of SOEU's have deteriorated, resulting in large accumulated losses. There is now a movement towards estimating and monitoring AT&C (Aggregate commercial and technical) losses in the country. The aggregate technical & commercial (AT&C) losses are in the range of 50%. High technical losses in the system are primarily due to inadequate investments over the years for system improvement works, which has resulted in unplanned extensions of the distribution lines, overloading of the system elements like transformers and conductors, and lack of adequate reactive power support. The commercial losses are mainly due to low metering efficiency, theft & pilferages. One must also give due weight to the fact that in the pursuit of the social objective, utilities may not have encouragement to innovate and look for improvements. However the financial and operational performances suggest the necessity for a detailed technical and financial appraisal of the SOEU's in order to reveal the underlying inefficiencies and the extent of scope for improvement in the new reformed regime.

4. Research Methodology

4.1 Introduction

Data Envelopment Analysis is relatively a new data oriented approach for evaluating the performance of set of peer entities called Decision Making Units (DMU) which convert inputs to outputs. It is a popular benchmarking method; a multifactor productivity analysis model for measuring the relative efficiencies of a homogeneous set of DMUs. It is a nonparametric estimation approach for generating the efficiency frontier that is derived from the DMU. These DMU's may be hospitals, universities, schools, Air force wings, business firms etc. As this requires very few assumptions, DEA has also opened up possibilities for use in cases which have been resistant to other approaches because of the complex unknown nature of relations between the multiple inputs and multiple outputs involved in DMU's. DEA is an excellent and easily usable methodology for modeling operational processes for performance evaluations. DEA's empirical orientation and the absence of a need for the numerous priori assumptions that accompany other approaches have resulted in its use in a number of studies involving efficient frontier estimation in the governmental and nonprofit sector, in the regulated sector and in the private sector.

The technique was suggested by Charnes, Cooper and Rhodes [1] and is built on the idea of Farrell. To regulate the electrical power most of the countries have adopted benchmark regulations using model of efficient firm concept. It corresponds to a company whose investments are economically adapted to demand and operates under an optimal operation plan. To design an efficient firm the regulator must specify the production technology with which the service will be delivered, the price of inputs and the cost of assets involved. With all these presumed data, it is possible to define an efficient production frontier used as the comparison benchmark for the group of companies. The efficiency is measured using the ratio of aggregated output to the aggregated input. Following Charnes et al, a DMU is said to be efficient if it is not possible to increase (decrease) the level of output (input) without increasing the use of at least one other input or decreasing the generation of at least one other output. This definition has the same concept as that in the Koopmans Pareto optimality that all the non dominated entities have the highest efficiency score. The DMU's that lie on the efficiency frontier are efficient in the DEA model. In contrast, the entities that do not lie on the efficiency frontier are regarded as inefficient.

DEA is a linear programming method that can deal with multiple inputs and multiple outputs simultaneously, yet DEA does not require the assignment of predetermined weights to the input and output factors. In this study, two DEA models were applied. CCR model developed by Charnes *et al* [1] and the BCC model developed by Banker [2]. In particular CCR model is the basic model which produces Constant Returns to Scale (CRS) efficiency frontier. The relative efficiency evaluated for the CCR model is the overall efficiency score and the efficiency of the DMU's are set to be lie between 0 and 1.

4.2 Mathematical formulation of DEA models:

4.2.1 CCR Model

Let as assume that there are ***n*** DMUs to be evaluated. Each DMU consumes varying amounts of ***m*** different inputs to produce ***s*** different outputs. Specifically, $\boldsymbol{DMU}_j$ consumes x_{ij} amounts of input i and produces y_{rj} amounts of output ***r***. As per the definition of relative efficiency, this is the ratio of weighted sums of outputs to weighted sums of inputs. In mathematical programming parlance, this ratio, which is to be maximized forms the objective function for the particular DMU with a set of normalizing constraints (one for each DMU) reflects that this ratio of every DMU, must be less than or equal to unity.

$$Maxh_0(u,v) = \sum u_r y_{r0} \Big/ \sum v_r x_{io}$$

Subject to $\sum u_r y_{rj} \Big/ \sum v_i x_{ij} \le 1$ for j =1,….n

$u_r, v_i \ge 0 \ \forall$ i and r.

where u_r and v_i are the weights of the input and output, y_{ro} , x_{io} are r^{th} output and i^{th} input of DMU_o

Using Charnes-Cooper transformation, transforming (u,v) to (μ,ν),

$$\text{Max } z = \sum_{r=1}^{s} \mu_r y_{ro}$$

Subject to

$$\sum_{r=1}^{s} \mu_r y_{rj} - \sum_{i=1}^{m} \nu_{ij} x_{ij} \le 0$$

$$\sum_{i=1}^{m} \nu_i x_{io} = 1$$

$$\mu_r, \nu_i \ge 0$$

For which the LP dual problem is

$$\theta^* = \min \theta$$

Subject to $\sum_{j=1}^{n} x_{ij} \lambda_j \le \theta x_{io}$ i = 1,2,….. m

$$\sum_{j=1}^{n} y_{rj} \lambda_j \ge y_{ro}$$ r = 1,2,……s

$\lambda_j \ge 0$ j = 1,2…….n θ unrestricted

4.2.2 BCC Model

The BCC model produces a variable returns to scale (VRS) efficiency frontier and evaluates both technical efficiency and scale efficiency. Thus the overall efficiency can be decomposed into technical efficiency and scale efficiency. Technical efficiency is the efficiency of converting inputs to outputs, while scale efficiency recognizes that economy of scales will not obtained at all scales of production and there is only one Most Productive Scale Size (MPSS) where the scale efficiency is 100%.. Therefore the DMU is said to be efficient if and only if it is both technical and scale efficient..

Thus the dual DEA program for considering the VRS model is as follows

Min θ_m

Subject to $\boldsymbol{Y}\lambda \ge \boldsymbol{Y_m}$

$\boldsymbol{X}\lambda \le \boldsymbol{\theta X_m}$ and

$\sum_{n=1}^{N} \lambda_n = 1$ λ≥0, θ free

In general, DEA programs incorporating the additional convexity constraint to take into account variable returns to scale are called BCC DEA model. The variable λ introduced into the convexity constraint also brings out the value of increasing or decreasing returns to scale.

If $\sum_{n=1}^{N} \lambda_n = 1$, then the reference DMU is expected to exhibit constant returns to scale.

If $\sum_{n=1}^{N} \lambda_n < 1$, then the reference DMU exhibits Increasing returns to scale and

If $\sum_{n=1}^{N} \lambda_n > 1$ then the reference DMU exhibits decreasing returns to scale.

4.2.3 Most Productive Scale Size

The CCR efficiency is the overall efficiency which also takes into account the scale efficiency. For the DMU which are scale inefficient, it is an indirect measure that they are not operating on the Most Productive Scale Size. If the present scale of operation of the DMU does not lead to 100% scale efficiency, then the scale size of every inefficient DMU to be operated will be identified by the calculation of MPSS.

Identifying the Most Productive Scale Size is complex for any DMU when dealing with multiple inputs and multiple outputs. Banker has proved that MPSS for a given inefficient firm can be obtained using the following relationship.

$$\left(X_{i,m}^{MPSS}, Y_{i,m}^{MPSS}\right) = \left[\theta_m^* \frac{X_{im}}{\sum_{n=1}^{N} \lambda_{nm}^*}, \frac{Y_{jm}}{\sum_{n=1}^{N} \lambda_{nm}^*}\right]$$

5. INPUT AND OUTPUT FACTORS

This paper uses samples of 29 SOEUs in India. Each of the SOEU is treated as decision making unit (DMU) under DEA analysis. The data of Inputs and outputs are taken from the TEDDY (TERI Energy Data Directory and Yearbook 2004/05). In selecting the inputs / outputs for evaluating the operational efficiency of DMU, a great care is taken as the success of evaluation depends on the data availability and quality. No universally applicable rational template is available for the selection of variables. However, in general, the inputs must reflect the resources used and the output must reflect the service levels of the utility and the degree to which the utility is meeting its objective of supplying electricity to consumers. In particular, this paper aims in evaluating the performance based on the operational efficiency; the service output is measured by the number of consumers. The product output is measured by the quantity of the energy supplied. The resources to produce the outputs considered are Installed Capacity (in MW), Distribution line length (in km), T & D losses (in %).

Without losing generality, the annual data for the year 2005 was used for this study. The use of annual data can reduce the influence of seasonal problem. For the validation of the data used for the development of DEA model, the assumption of "isotonicity" (ie., an increase in input should not result in a decrease in any output) is examined. Regression analysis on the selected input and output factor is a useful procedure to examine the property of isotonicity. If the correlation between the selected input and output factor is positive, these factors are isotonically related and can be included in the model. It is observed that the selected input and output factors for this study shows positive correlation between them except for the % T& D Losses. As this is the loss attribute, this data has to be considered as negate. An overview about the key characteristics is presented in Table 1. Table 2 indicates the value of correlation between the input and output factors. In addition, according to, Joe Sarkis, the number of DMU's should be at least twice the number of inputs and outputs. In this study the number of DMU is twenty nine, which is twice the number of input and output.

6. OPERATIONAL EFFICIENCY ANALYSIS

In this study, CCR model, with constant returns to scale (CRS) is applied to evaluate the overall efficiency. In addition, the BCC model, with variable returns to scale (VRS), is used to evaluate the technical and scale efficiencies. Both the dual linear programming formulations are run for every DMU. The combined results of the CCR model, BCC model, Peer units for the inefficient DMU and the Slacks in the Inputs are given in Table 3. The analysis of the slack variable shows the way for the improvement for the inefficient DMU. The input slack values represent the needed reductions of the corresponding input factors to become an efficient DMU. For example, Arunachal Pradesh requires decrease of 53.26 MW in its installed capacity, 3683.55 km in circuit length and 0.3289 in percentage T&D losses. Based on the results of the CCR model it is observed that 7 SOEU's are relatively efficient and the overall efficiency score is equal to 1. The average efficiency score of all SOEU's is 0.7739. This implies that the utilization of the resources among the utility is only 77%. Among the inefficient utilities Arunachal Pradesh, Sikkim and Uttranchal shown very low efficiencies with an average efficiency score of 35% which needs improvement in both technical efficiency and scale efficiency.

The BCC model is used to evaluate the technical efficiency and scale efficiency. Some of the DMUs which are inefficient in CCR model now becomes efficient in BCC model. The results of BCC model can show the major sources of inefficiencies among the 22 SOEU's and also provide possible directions of improvement for the overall efficiency for each utility. In the BCC model, four utilities which shown inefficiency in their CCR model became relatively efficient which modifies the frontier line. For example, Maharashtra has the CRS efficiency score of 96.31% and it becomes efficient in the VRS model with an efficiency score of 100%. The Efficiency Score analysis ie. the overall efficiency, technical efficiency and Scale efficiency is given in Table 4. The ten SOEU's viz., Arunachal Pradesh, Goa, Himachal Pradesh, Karnataka, Maharashtra, Meghalaya, Mizoram, Nagaland, Sikkim, Tripura have technical efficiency scores higher than scale efficiency scores. The SOEU that has the scale efficiency less than 1 is called as scale inefficient. This implies that the inefficiency of the SOEU's is primarily due to the scale inefficiency. A scale inefficient DMU that exceeds the Most Productive Scale Size (MPSS) will present decreasing returns to scale. Alternatively, a scale inefficient DMU that is smaller than MPSS will present increasing returns to scale.

For example, in Table 4, Goa and Himachal Pradesh are having technical efficiency higher than the scale efficiency. These two SOEU's can increase their operation scales to improve their overall efficiency because they present IRS. On the other hand, Maharashtra should decrease its operation scale because it presents DRS. The inefficiency in the twelve inefficient (but with high scale efficiency score) SOEU's (Assam, Bihar, Chattisgarh, Haryana, Jammu & Kashmir, Madhya Pradesh, Orissa, Punjab, Rajasthan, Uttar Pradesh, Uttranchal, West Bengal) are mainly due to technical inefficiency. To increase the overall efficiency these SOEU's should improve technical efficiency of resource allocation and utilization in order to improve the overall efficiency. Hence it is for the policy makers and the government to further scrutinize the actual scope for feasibility of increasing the operation scale by taking into account the actual conditions on the field.

The Most Productive Scale Size for the inefficient DMU is tabulated in Table 5. The value of MPSS in the parenthesis showed against the actual value gives the clear idea about its scale of operation. For example, Arunachal Pradesh has installed capacity of 179.4 MW whereas the MPSS calculated for this specific input is 1038.19 MW. Therefore, to become an efficient unit it has to raise the installed capacity to 1038.9 MW. Assam has total circuit length of 78612 whereas the MPSS calculated is 50628.18 km. Therefore it has to reduce its circuit to 50628.18 km to become as efficient unit. Chattisgarh actually has a T& D loss of 42.6 % for a circuit length of 120208 km whereas the MPSS calculated for T & D loss is around 49.81% for a circuit length of 1147435.6km. As this is the loss attribute it is not technically advisable to increase the loss to 49.81%. Moreover when the circuit length decreases then the loss attribute also has to decrease. At this juncture, the Operating Manager has to decide about the technical viability also.

7. Conclusion

This study makes an effort to measure relative efficiency of the SOEU's of the Indian Power Sector using a Frontier tool viz.,Data Envelopment Analysis. From the results of this study it is observed that there is a existence of inefficiency in 22 SOEUs. The findings of the slack variable analysis in CCR model provided the improvement directions for the inefficient districts when compared with other districts. Further more most of the inefficient DMUs suffered from scale inefficiency rather than from technical inefficiency. A majority of the SOEU does not seem to operate on the optimum level of operation. In particular 19 SOEUs presented increasing return to scale which need to increase their scale of operation. Alternatively, Maharashtra exhibited decreasing returns of scale which need to downsize its scale of operation. The knowledge of MPSS helps to know about the scale of operation of the individual DMU with respect to the individual inputs and outputs. To improve the performance, a number of policy measures such as encouraging competition, unbundling and restructuring can be considered.

References

A. Charnes, W. W. Cooper and E.Rhodes, (1978), " Measuring the efficiency of decision making units" *European Journal of Operational Research*, Vol . 2 no 6, pp 429-444

R.D.Banker, A.Charnes and W.W.Cooper, (1984), " Some models for estimating technical efficiency and scale efficiencies in data envelopment analysis" , *Management Science*, Vol 30, no.9, pp 1078 – 1092.

Ministry of Power, Government of India Website (http://powermin.nic.in)

Central Electricity Authority Website (http://cea.nic.in)

R. Fare, S.Grosskopf and J.logan, (1983), " The relative efficiency of Illinois electric utilities" Res.Energy, Vol. 5, pp 349 – 367.

A. Charnes, W. W. Cooper, D.Divine, T.W.Ruefli and D. Thomas, (1989), " Comparision of DEA and existing ratio and regression system for effecting efficiency evaluations of regulated electric cooperatives in Texas", *Res.Govern. Nonprofit account*, Vol. 5, pp187-210.

P. A. Miliotis, (1992), "Data Envelopment analysis applied to electricity distribution districts"' *Journal of Operation*

research Society, vol. 43, no.5, pp549 – 555.

B.Golany, Y.Roll, and D.Rybak, (1994), " Measuring Efficiency of power plants in Israel by data envelopment analysis", *IEEE Transcation on Eng. Manage*, vol. 41, no.3, pp 291 – 301.

A.D.Athanassopoulos, N.Lambroukos and L.M.Seiford, (1999), " Data Envelopment Scenario analysis for setting targets to electricity generating plants", *European Jouranl of Operation Research*, vol. 115, pp 416-3 – 428.

T. Sueyoshi, (1999), "Tariff structure of Japanese electric power companies: An empirical analysis using DEA", *European Jouranl of Operation Research*, vol. 118, pp 350 – 374.

S.U.Park and J.B.Lesourd, (2000), "The efficiency of conventional fuel power plants in South Korea: A comparison of parametric and nonparametric approaches", *International Journal of Production Economics* vol. 63, pp 59 – 67.

T.Jamsab and M.Pollitt, (2001), " Benchmarking and regulation of Electricity distribution and Transmission utilities: Lesson from international experience", *Utilities policy*, vol. 9, pp 107 – 130.

M.J.Farrell, (1957), "The measurement of productive efficiency", *Journal of the Royal Statistical Society*, Vol. 120,no. 3, pp 253-281.

J.E.Blose, W.B.Tankersley and L.R.Flyinh, (2005), " Managing Service Quality using DEA", QMU, Vol. 12, no.2 pp 7-24.

A.D.Athanassopoulos and J.A.Ballantine, (1995), "Ratio and Frontier analysis for assessing corporate performance: Evidence from grocery industry in U.K", *Journal of Operational Research Society*, Vol. 46, no.4, pp 427-440.

T.Sueyoshi, (1991), " Estimation of Stochastic Frontier cost function using DEA: an application to the AT&T Divestiture, *Journal of Operational Research Society*, Vol.42, no.463-471.

M.Meimand, R.Y.Cavana and R.Laking, (2002), "Using DEA and survival analysis for measuring performance of branches in New Zealand's accident compensation corporation", *Journal of Operational Research Society*, Vol. 53, no.3pp 303-313.

Karou Tone and Biresh K.Sahoo, (2005), "Evaluating cost efficiency and returns to scale in the Life Insurance Corporation of India using data envelopment anlaysis", *Elsevier Socio-economic planning sciences*, Vol. 39, pp 261-283.

Quey-Jen Yeh, (1996), "The Application of Data Envelopment Analysis in conjunction with Financial ratios for bank performance evaluation", *Journal of Operational Research Society*, Vol. 47, pp 980-988.

J.E.Beasley, (1995), "Determining Teaching and Research Efficiencies", *Journal of Operational Research Society*, Vol 46, pp 441-452

Chyan Yang and Wen-min Lu, (2006). "Assessing the performance and finding the benchmarks of the electricity distribution districts of Taiwan Power Company", *IEEE transaction on Power Systems*, Vol. 21 no 2, pp 853 – 861.

Pekka J.Korhonen and Mikulas Luptacik, (2004), " Eco - efficiency Analysis of power plants:An extension of data envelopment analysis" , *European Journal of Operational Research*, Vol. 154, pp 437 – 446.

Puneeth Chitkara, (1999), "A Data Envelopment analysis approach to evaluation of operational inefficiencies in Power Generating Units: A Case Study of Indian Power Plants", *IEEE Transactions on Power Systems*, vol. 14,no.2, pp 419 – 425.

Kaoru Tone and Miki Tsutsui,(2005), "Decomposition of cost efficiency and its application to Japanese – US electric utility comparison", *Socio – Economic Planning Sciences.*

Anil pahwa, X.Feng and D.Lubkeman, (2002), "Performance evaluation in electric distribution utilities based on data envelopment analysis", *IEEE transaction on Power System*, vol. 17, no.3, pp 400 – 405.

Raul Sanheuza, Hugh Rudnick and Hector Lagunas, (2004), "DEA efficiency for the determination of the Electric Power distribution added value", *IEEE transactions on Power System*, vol. 19, no.2 pp 919 – 924.

R.Meenakumari and Dr.N.Kamaraj, (2007). " Relative Efficiency measurement of State Owned Electric Utilities in India using Data Envelopment Analysis", Proceedings of National System Conference NSC – 2007, Dec 14 – 15, MIT, Manipal , Karnataka.

Tripta Thakur, (2005). " Benchmarking study for the Indian Electric utilities using Data Envelopment Analysis", *IEEE Transaction on Power System*, pp 545 – 549.

Table 1. Summary Statistics for the Data

Parameter	Mean	Median	Std.Deviation	Max	Min
Installed Capacity(MW)	4099.841379	2077.1	4415.59492	17182.3	102.7
Circuit km	215568.4828	100464	239809.1447	707037	5156
%T & D Losses	38.13448276	39.3	13.08926157	65.2	16.7
Number of Consumers (in Lakhs)	45.16931034	21.49	55.15127967	198.6	0.6
Quantity of Energy Supplied (GWh)	12326.70759	7157.48	14058.17649	51823.9	125.01

Table 2. Input / Output Correlations:

Variable	Installed Capacity (MW)	Circuit km	% T & D Losses	Number of Consumers (in Lakhs)	Quantity of Energy Supplied (GWh)
Installed Capacity(MW)	1	0.926268853	-0.374842659	0.927913676	0.988578193
Circuit km	0.926268853	1	-0.387146885	0.940012764	0.890973283
% T&D Losses	-0.374842659	-0.387146885	1	-0.45796782	-0.365538555
Number of Consumers (in Lakhs)	0.927913676	0.940012764	-0.392683722	1	0.903436179
Quantity of Energy Supplied (GWh)	0.988578193	0.890973283	-0.365538555	0.903436179	1

Table 3. Efficiency Analysis

SL NO	State Owned Electric Utility	CRS efficiency	VRS efficiency	Efficient / Inefficient	PEER units	Slack in Inputs		
						Installed Capacity (MW)	Circuit km	% T&D Losses
1	ANDHRA PRADESH	100	100	EFFICIENT	1	-	-	-
2	ARUNACHAL PRADESH	29.69	90.139	INEFFICIENT	14	53.26	3683.55	0.328926
3	ASSAM	51.458	62.27	INEFFICIENT	1,14,17	548.96	38425.0	19.07
4	BIHAR	74.63	81.37	INEFFICIENT	1,8,17	326.37	80621.5	9.3
5	CHATTISGARH	86.5	89.67	INEFFICIENT	1,8,17	232.44	35328.2	5.75
6	DELHI	100	100	EFFICIENT	6	-	-	-
7	GOA	74.76	97.13	INEFFICIENT	6,14,17	118.78	3601.88	28.18
8	GUJARAT	100	100	EFFICIENT	8	-	-	-
9	HARYANA	93.394	94.88	INEFFICIENT	1,6,8,17	253.63	11722.8	2.12
10	HIMACHAL PRADESH	60.93	80.24	INEFFICIENT	6,14	704.36	29419.4	13.2
11	JAMMU &KASHMIR	60.00	66.43	INEFFICIENT	1,6,8,17	658.42	16709.3	18.199
12	JHARKHAND	100	100	EFFICIENT	12	-	-	-
13	KARNATAKA	98.74	99.64	INEFFICIENT	1,8,17	97.547	142298	0.2919
14	KERALA	100	100	EFFICIENT	14	-	-	-
15	MADHYA PRADESH	70.94	71.43	INEFFICIENT	1,8,17	1942.63	329462	12.03
16	MAHARASHTRA	96.31	100	INEFFICIENT	6,25	2178.20	26053.8	1.256
17	MANIPUR	100	100	EFFICIENT	17	-	-	-
18	MEGHALAYA	57.99	100	INEFFICIENT	1,8,17	167.14	8329.67	9.6845
19	MIZORAM	51.65	95.7	INEFFICIENT	14	56.467	10625.4	55.127
20	NAGALAND	86.283	100	INEFFICIENT	14	14.087	4546.5	54.45
21	ORISSA	67.00	68.64	INEFFICIENT	1,6,8,17	997.562	33148.9	18.84
22	PUNJAB	98.19	79.95	INEFFICIENT	1,9,17	110.937	13922.1	0.47
23	RAJASTHAN	79.47	98.84	INEFFICIENT	1,8,17	114.1	211960.5	8.97
24	SIKKIM	37.19	100	INEFFICIENT	6,14,17	72.915	3238.17	52.148
25	TAMIL NADU	100	100	EFFICIENT	25	-	-	-
26	TRIPURA	51.71	90.69	INEFFICIENT	6,14,17	118.05	6874.8	42.48
27	UTTAR PRADESH	85.94	86.07	INEFFICIENT	1,8,17	1245.57	120543.3	4.94
28	UTTARANCHAL	39.76	39.76	INEFFICIENT	1,6,14,17	1185.94	39503	29.63
29	WEST BENGAL	92.02	92.02	INEFFICIENT	1,6,8,17	443.19	15049.05	2.471

Table 4. Efficiency Score Analysis

Sl.No	State Owned Electric Utility	Overall Efficiency	Technical Efficiency	Scale Efficiency	RTS
1	ANDHRA PRADESH	1.000	1.000	1.00000	CRS
2	ARUNACHAL PRADESH	0.2969	0.9013	0.32938	IRS
3	ASSAM	0.5145	0.6227	0.82637	IRS
4	BIHAR	0.7463	0.8137	0.91717	IRS
5	CHATTISGARH	0.865	0.8967	0.96465	IRS
6	DELHI	1.000	1.000	1.00000	CRS
7	GOA	0.7476	0.9713	0.76969	IRS
8	GUJARAT	1.000	1.000	1.00000	CRS
9	HARYANA	0.9339	0.9488	0.98434	IRS
10	HIMACHAL PRADESH	0.6093	0.8024	0.75935	IRS
11	JAMMU &KASHMIR	0.6000	0.60643	0.90321	IRS
12	JHARKHAND	1.000	1.000	1.00000	CRS
13	KARNATAKA	0.9874	0.9964	0.99097	IRS
14	KERALA	1.000	1.000	1.00000	CRS
15	MADHYA PRADESH	0.7094	0.7143	0.99314	IRS
16	MAHARASHTRA	0.9631	1.000	0.96310	DRS
17	MANIPUR	1.000	1.000	1.00000	CRS
18	MEGHALAYA	0.5799	1.000	0.57990	IRS
19	MIZORAM	0.5165	0.957	0.53971	IRS
20	NAGALAND	0.8628	1.000	0.86283	IRS
21	ORISSA	0.6700	0.6864	0.97611	IRS
22	PUNJAB	0.9819	0.9884	0.99342	IRS
23	RAJASTHAN	0.7947	0.7995	0.99400	IRS
24	SIKKIM	0.3719	1.000	0.37190	IRS
25	TAMIL NADU	1.000	1.000	1.00000	CRS
26	TRIPURA	0.5171	0.9069	0.57018	IRS
27	UTTAR PRADESH	0.8594	0.8607	0.99849	IRS
28	UTTARANCHAL	0.3976	0.3976	1.00000	CRS
29	WEST BENGAL	0.9202	0.9202	1.00000	CRS

Table 5. MPSS for the CRS inefficient DMU's

State Owned Electric Utilities	Installed Capacity (MW)	Circuit km	% T&D Losses	Number of Consumers (in Lakhs)	Quantity of Energy Supplied (GWh)
ARUNACHAL PRADESH	179.4 [1038.19]	14216 [71801.3741]	47.5 [6.412798]	1.13 [74.19]	125.01 [9093.1]
ASSAM	1130.9 [733.135]	78612 [50628.18]	39.3 [25.477]	11.77 [28.815]	1920.38 [4701.55]
BIHAR	1286.8	132126	36.7	12.5	3730.34

	[1524.54]	[81756.18]	[43.48]	[26.58]	[7933.59]
CHATTISGARH	1722 [2013.49]	120208 [114735.6]	42.6 [49.81]	22.13 [34.58]	5420.83 [8471.029]
GOA	470.7 [884.50]	14274 [26822.67]	45.1 [42.51]	3.96 [13.311]	1376.66 [4627.78]
HARYANA	3839.4 [4976.27]	177461 [230008.3]	32.1 [41.605]	39.17 [58.204]	12915.72 [19191.98]
HIMACHAL PRADESH	1803.2 [2177.08]	75315 [90931.08]	22.8 [19.01]	16.46 [53.51]	2736.92 [10315.17]
JAMMU &KASHMIR	1646.1 [1203.12]	41774 [30532.47]	45.5 [33.255]	10 [20.302]	3534.2 [7175.21]
KARNATAKA	7784.3 [10220.57]	597639 [605436]	23.3 [30.59]	128.89 [173.551]	23143.17 [31162.46]
MADHYA PRADESH	6685 [4747.928]	582757 [253591.33]	41.4 [29.403]	64.92 [91.32]	15907.83 [22450.45]
MAHARASHTRA	17182.3 [10077.92]	707037 [457401.49]	34.1 [22.06]	159.05 [110.917]	51823.9 [36140.74]
MEGHALAYA	288.2 [616.54]	15657 [30725.00]	16.7 [35.726]	1.68 [6.196]	797.02 [2939.9]
MIZORAM	116.8 [1806.29]	14798 [124923.4]	55.5 [11.157]	1.28 [74.19]	129.9 [9093.1]
NAGALAND	102.7 [3017.23]	10675 [208671.98]	55 [18.637]	1.88 [74.19]	136.25 [9093.1]
ORISSA	3023.3 [1867.23]	100464 [62047.96]	57.1 [35.26]	21.49 [29.56]	7157.48 [9846.30]
PUNJAB	6135.3 [7846.42]	287520 [356347.34]	26 [33.25]	58.36 [77.41]	22125.3 [29347.742]
RAJASTHAN	5427.6 [4468.79]	441724 [238037.4]	43.7 [35.98]	58.45 [76.19]	14691.24 [19151.58]
SIKKIM	116.1 [327.85]	5156 [14560.12]	55 [21.64]	0.6 [12.24]	182.24 [3719.6]
TRIPURA	244.5 [813.10]	14238 [47349.62]	46.4 [25.16]	2.28 [28.35]	414.26 [5151.2]
UTTAR PRADESH	8864.6 [7250.26]	494417 [355777.8]	35.2 [28.78]	88.06 [97.49]	26659.62 [29516.69]
UTTARANCHAL	1968.9 [815.96]	65583 [27179.37]	49.2 [20.38]	9.61 [25.18]	2662.15 [6976.72]
WEST BENGAL	5559.9 [5941.86]	188789 [201758.86]	31 [33.12]	47.27 [59.64]	17815.87 [22481.07]

The value in the parenthesis is the MPSS for that specific factor

Modern Applied Science

www.ccsenet.org/journal.html

Vol. 2, No. 5

September 2008

The Design of Automatic Temperature Control System for the Dyeing Machine

Jing Dai

Institute of Computer Technology & Automatization

Tianjin Polytechnic University

Tianjin 300160, China

E-mail: mandy_jing@163.com

Abstract

This article analyzed the temperature control system of the dyeing machine in the textile industry, adopted the technology of PLC to automatically control the temperature and realized the automatic temperature adjustment in the work process of the dyeing machine. The spot adjustment proved that this method could fulfill the basic requirement of the dyeing machine to the temperature.

Keywords: PLC, Dyeing machine, Temperature

1. The temperature control principle of the dyeing machine

1.1 The application of automatization technology in the textile industry

The textile machinery manufacturing of China has been quickly developed for almost twenty years and has acquired great achievements, and the technical level and product stability of textile machinery have been fully enhanced. The automatic control of the textile machinery takes the sports control as its core, and is assisted by the textile technical parameters. In recent ten years, the electric power electronic technology, computer control technology and network communication technology have been applied and extended in the control and production management of the textile machinery quickly, which make the mechanical and electronic integration level of China fully enhanced.

1.2 The intention of the control

The parameters of the textile technology are numerous, which generally includes temperature, pressure, flux, liquid position, length, speed and displacement. The dyeing technology of the textile has strict requirement of the temperature, and the temperature ascending process, temperature keeping process, temperature descending process of the dyeing trough must accord with the technical requirements, and the manual control is very difficult. If the used machine is the small sample machine, it may bring trouble for the bulk samples. And the production equipments will make the color replay difficultly and induce serious kettle difference, and finally bring unnecessary losses for the production.

Therefore, the automatic temperature control of the dyeing machine is very important. The control system is required to freely set up the temperature ascending curve, temperature keeping curve, temperature descending curve, and the operation time, actual temperature and process temperature in the work process can be displayed to ensure the right implementation of the technology.

1.3 The Structure of the temperature system

The control objective is the dyeing sample machine, and the structure of its temperature system is seen in Figure 1. The temperature control range of the system is from 20 to 150 centigrade degree, and because the water can not achieve 150 centigrade degree, so the glycerin is adopted. The glycerin can achieve 150 centigrade degree under normal pressure.

When the dyeing machine is working, the temperature of the glycerin in the dyeing trough must be changed according to the technical requirements. If the temperature is lower than the set value, the temperature control system should close the heat switch 7, heat glycerin through the heating wire and stop heating until the temperature achieves the set value. If the temperature of the glycerin is higher than the set value, i.e. the excessive adjustment occurs, or the equipment is working in the quick descending stage of the temperature, the temperature control system will connect the cooling valve 8 to drop the temperature of the glycerin.

Common temperature controller can implement temperature keeping control, which is used in some prior dyeing

machines, and if the automatic degree is further enhanced to make the equipment ascend, keep and descend the temperature according to needed speed until the whole technical process ends, the simple temperature control can not fulfill these requirements, and it is very necessary to design a sort of reliable, convenient temperature complete automatic control system with perfect functions.

2. The design of the temperature control system

2.1 The total structure of the system

In the industry, there are many methods to control the temperature, and here we select PLC to control the temperature. Figure 2 is the sketchy structure of the temperature control system.

The set parameters can be input into PLC through the human-computer interface, and PLC inputs the actual temperature into the A/D convertor through the temperature sensor and a series of automatic computation, and the A/D convertor transforms the temperature and inputs it into the PLC. Through analysis and computation, PLC can exactly decide open the heating switch or the electromagnetic valve.

2.2 The PLC control method

The typical temperature process curve of the dyeing machine is seen in Figure 3 which shows the temperature linearly changed with the subsection. Only the operator sets up the temperature and completed time required by the intersection points of various subsections such as 1, 2, 3…, PLC will automatically compute the corresponding time and temperature value of all points on the curve. After the dyeing machine starts, PLC continually compares the actual temperature in the glycerin trough with the corresponding set temperature on the curve to decide whether the output state is heating, keeping or dropping temperature.

The ideal temperature change in the dyeing process is seen in Figure 4.

When PLC computes the temperature, it divides every temperature sect into many corresponding little interval according to the time, which is called as "step", and PLC computes the corresponding temperature of every step and take it as the set temperature value in this step, so the actual temperature curve provided by PLC is trapeziform, which is seen in Figure 5.

If only the time of every step is enough small, the difference between the computed temperature value and the ideal value in one step can be neglected, and because the heat capacity of the glycerin trough is large, so the system has certain heat inertia. So the temperature ascending curve in the trough will change according to Figure 6, not trapezifrom or approximate exponential curve, which more closes ideal temperature ascending curve with equal speed. The step length is smaller, the control precision is higher, but the performance of the power control circuit should be considered at the same time. The heating wire of the sample machine adopts the contactor to realize connection or breaking, so the frequency is not allowed to be higher, and the step length is confirmed as 6s. If the bidirectional crystal brake-tube or high power transistor is used, the step length can be largely reduced, and we only need considering the limitation of the shortest scanning cycle of PLC.

According to above control principle, we divide the whole work process into many sects, and every sect is divided into many steps, and PLC computes the output state of this step to automatically control the temperature.

3. The selection of hardware

3.1 The selection of PLC

The PLC of new generation was pushed out in the late of 1995 by Germany Siemens Company, which was not only improved in many aspects such as instruction system, operation speed and machine structure comparing with former S5 series, but largely reduced in the price and even achieved higher level than other brands with same functions, and its abundant CPU types and level classes make it possess strong adaptability when solving the problems of users' industrial automatization. Therefore, we select the S7-200 series PLC.

It is a sort of waste to blindly select the machine type with more point number. The input signals of the PLC control system in this project include start switch, pause switch and stop switch for the dyeing machine. The output of PLC mainly includes heating switch, cooling water valve switch, temperature ascending display lamp, temperature keeping display lamp and temperature dropping display lamp. So S7214 can fulfill these requirements. Figure 7 shows the automatic temperature control system of PLC.

3.2 The selection of A/D transformation module

We select EM325 as the A/D conversion module which simulation input/output is 4input/1output × 12bits.

3.3 The selection of human-computer interface

For the human-computer interface, we use TD200 which is professionally designed for S7PLC, and it has liquid crystal display screen which can display two rows or 80 characters or numbers, and TD200 has 9 input keys which can

complete parameter display, data input and modification, the start and stop of data, and can be used as the machine operation panel.

The work program of TD200 is called as parameter module which is stored in the EEPROM of CPU of PLC. The contents that TD200 display are called as information. The programming of parameter module and information and the main program programming of PLC are implemented by the S7 programming software on the computer.

4. The programming of PLC

4.1 The programming figure of PLC

The whole work process confirmed in this article is divided into many sects, and every sect is divided into many steps according to the same time (6s), and PLC computes the output sate of this step to achieve the intention of automatic control. The main program figure of PLC control is seen in Figure 8.

From Figure 8, we can see that the program is mainly divided into two loops. The interior loop program includes the programs to compute the corresponding temperature on the typical temperature process curve of the dyeing machine, read A/D filtering wave, and judge ascending, keeping and dropping temperature. The exterior loop program mainly charges for reading the data of next sect when the present sect ends, and judging whether the total program operation is completed.

4.2 The programming of PLC

First, store the set data into the memorizer V, store the original time 0 into VW0, and store the room temperature into VW2. Store the time from the origin to the point of 1 into VW4, and store the temperature that the point of 1 confirms in advance into VW6. Store the values of points of 2, 3, 4 and 5 into VW8-VW22 in turn. Store the set sect number into VW32. Establish two fingers, AC1 and AC2, and appoint their addresses to the start value and terminal value of every sect, and add 4 to them respectively after every sect completes operation, so they will be appointed to the address of the next sect and the intention of the cycle is achieved.

When every sect starts, the computation is implemented first. Take out the values of the storage units that AC1 and AC2 point and store them into the appointed units (VW24-VW30), and then compute how many steps that the sect can be divided into and how many centigrade degrees of the start and end points in the required time, and store them respectively into fixed storage units.

The number of the step and the temperature difference in this sect can help us to compute the concrete values that every step ascends or descends temperature. Use timers T101 and T102, and in every 6s, they time the time alternately and T102 produces a pulse.

From the first step, when T102 is connected, it will gradually add the changeable temperature value of every step on the start temperature, so the temperature value on the corresponding curve will be obtained, i.e. the required temperature value.

The timer T102 connects once and the corresponding curve value will change once and compare with the actual temperature value of the glycerin. If actual temperature is higher, the cooling water valve will be connected and the temperature dropping display lamp is lightened, and if the corresponding curve temperature is higher, the switch of the heating wire will be connected and the heating wire heats the glycerin and the temperature ascending display lamp is lightened, and if both is same, only the temperature keeping display lamp is lightened. So the control to the glycerin temperature is achieved.

After one sect operation is completed, the value of the finger is automatic increased and the sect number stored in VW32 reduces 1. Then operate next sect, recompute the values, repeat the works of the previous sect, and implement from one sect to another in this way until the value of VW32 is 0, so the control work is completed.

In order to reduce the times to start the cooling valve and drop the temperature only when the actual temperature exceeds the corresponding curve temperature, set up a temperature value, connect the cooling valve only when the actual temperature exceeds the corresponding curve temperature and this temperature value. In the program, subtract the value of the corresponding curve temperature from the actual temperature value, and store the computation result into VW62, and connect the cooling water valve to drop the temperature when VW62 exceeds the set value of the temperature.

To ensure the normal operation of PLC and protect PLC at the same time, compulsively transform to the mode of STOP when I/O error happens.

5. The simulation experiment

5.1 The running of the program

First program by means of the design software of STEP 7-Micro/Win 32, and use LAD as the programming language.

After program, load the program to the Siemens 214PLC under the mode of STOP, and transform it from the mode of STOP to the mode of RUN, and the program can be run. In the experiment, various parameters can be set in advance and input into PLC. According to appointed condition, PLC can automatically decide whether to ascend, keep or drop the temperature.

In order to set up the start temperature in 5 centigrade degree when the experiment runs in the first sect, the temperature of 1 point is appointed as 15 centigrade degree and the time is 1 minute, that is to say, the glycerin temperature in the first sect is required to ascend 10 centigrade degree. The time of the first sect is 60 seconds, and 1 step needs 6 seconds and is divided into 10 steps, so every step needs to ascend 1 centigrade degree. Then set up to drop the temperature when the actual temperature exceeds the curve temperature 1 centigrade degree. After these data are set up, and PLC can automatically and exactly compute various values.

First suppose that the actual temperature of the glycerin is changeless and its value is 8 centigrade degree. After the PLC switch is transformed to the mode of RUN, the parameters will be automatically input into PLC and stored. Then connect I0.0, set up M1.0, and the program formally begins to run. PLC implements one computation in every 6 seconds and judge the first 6 seconds and lightens Q0.3, and it exports nothing. After 6 seconds, if the actual temperature is higher, so lighten Q0.1 and Q0.4. The corresponding curve temperature continually ascends, and when its value achieves 7 centigrade degree, the actual temperature only exceeds 1 second, so only I0.3 is lightened, and in next 6 seconds, the actual temperature and the curve temperature are same and the output is changeless. After that, the curve temperature continually ascends, Q0.0 and Q0.2 are lightened. The program will be run all along until it ends.

5.2 The use of A/D converter

To change the actual temperature, we use EM235.

In actual production, we need to input the temperature of the glycerin into the A/D convertor by the temperature sensor, and input the temperature into the PLC through the A/D convertor. For the temperature sensor, we can select PT100 which is platinum resistance temperature sensor, and it can measure the temperature between -60 centigrade degree to +400 centigrade degree.

In order to measure the temperature by EM235, we can connect PT100 temperature sensor on one input channel of the module. To transform the resistance that reflects the temperature change of PT100 to the voltage, the simulation output is used as the constant current source, i.e. export the constant current of 12.5mA and supply it to the sensor of PT100. In this circuit, the linear input voltage of 5mV/C is produced. EM235 transforms this voltage to the digital quantity, and then the program reads these values periodically and computes the temperature by these values. In the experiment, we can connect a potentiometer in the module EM235, so we can properly adjust the potentiometer to change the actual temperature which is input into PLC and make the experiment achieve the anticipated intention.

5.3 The human-machine interface

In the production, the value of the start point on every sect can be input through the human-computer interface of TD200 which implements programming by the software of STEP 7-Micor/Win and doesn't need other parameter evaluating software. One special area in the CPU of S7-200 series is reserved to change data with TD200. TD200 can interviews the necessary functions of CPU through the data area.

Connect TD200 with PLC, which can conveniently input and modify various parameters, and can also display the operation time and actual temperature in the production process to ensure normal operation of the technology.

6. Conclusions

Through operating the program on Siemens S7-200PLC, the actual temperature will occur in different time sects, so the outputs in PLC will be different, and the PLC can exactly judge whether to ascend the temperature, keep the temperature or drop the temperature and display which display lamp exactly according to the actual temperature and the computed corresponding curve temperature. After EM235 is extended, the adjustment of the value of the potentiometer can realize anticipated objective, which indicates that the PLC can basically realize the automatic control to the temperature system of the dyeing machine in actual production, and this method is feasible. And because Siemens S7 series is improved in many aspects such as instruction system, operation speed and machine structure than former products, and its price is low, so this method is also feasible for the economy.

References

Gao, Xiaogang. (2005). The Application and Development of Textile Machinery Automatization Technology. *Textile Machinery.* No.6. 8(4).

Song, Jianping. (2005). The Technical Innovation and Diversification Strategy of Textile Machinery Manufacturing. *Textile Machinery.* No.6. 2(1).

Yuebin. (2005). The Application of S7-200 to False-twist Texturing Machine. *Textile Machinery.* No.1.

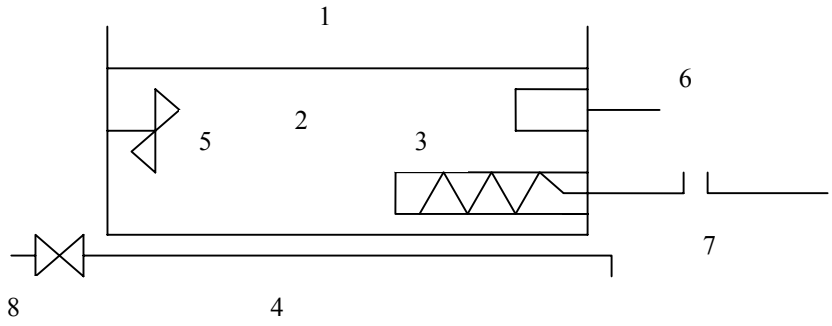

Figure 1. The Temperature System of the Dyeing Sample Machine

Note: 1- dyeing trough, 2- glycerin, 3- heating wire, 4- cooling water pipe, 5- mixer machine, 6- temperature sensor, 7- heating switch, 8- cooling water valve.

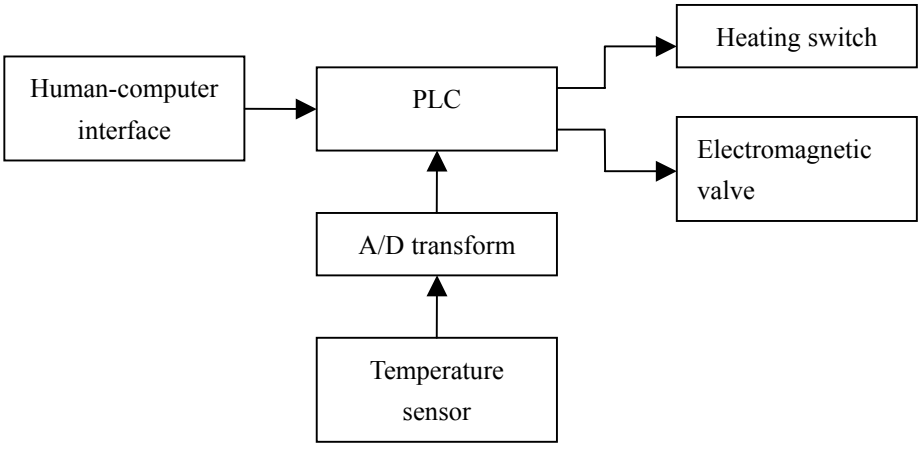

Figure 2. The Sketchy Structure of Control System

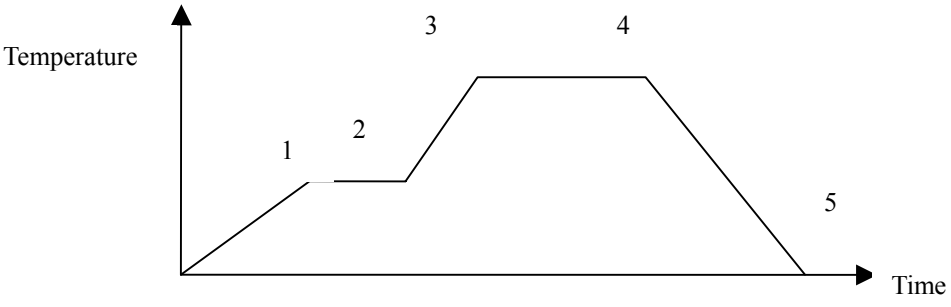

Figure 3. Typical Temperature Process Curve of the Dyeing Machine

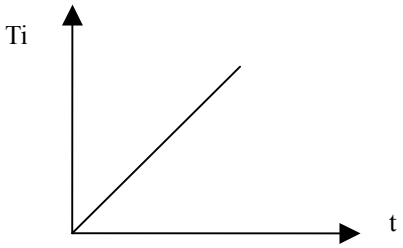

Figure 4. Ideal Temperature Process

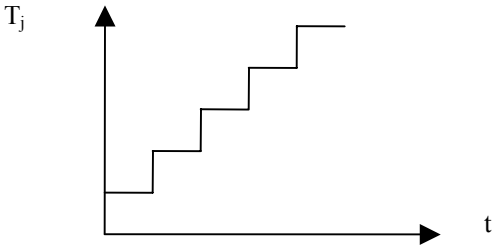

Figure 5. PLC Interpolation Temperature Tj

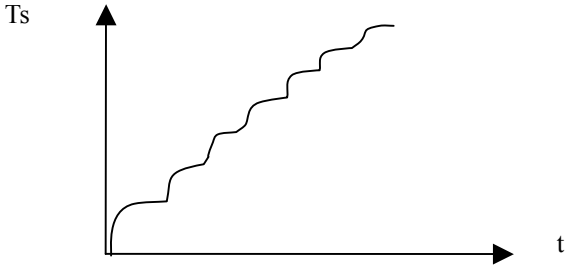

Figure 6. Actual Temperature of the Dyeing Trough Ts

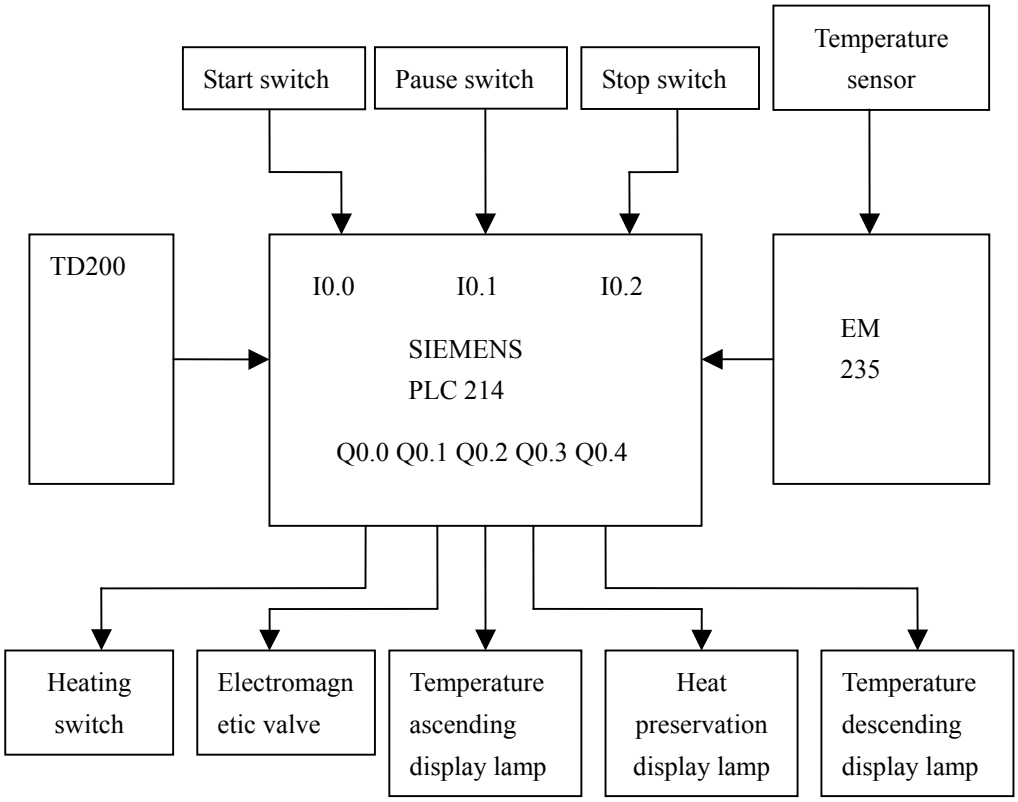

Figure 7. S7 PLC Automatic Temperature Control System

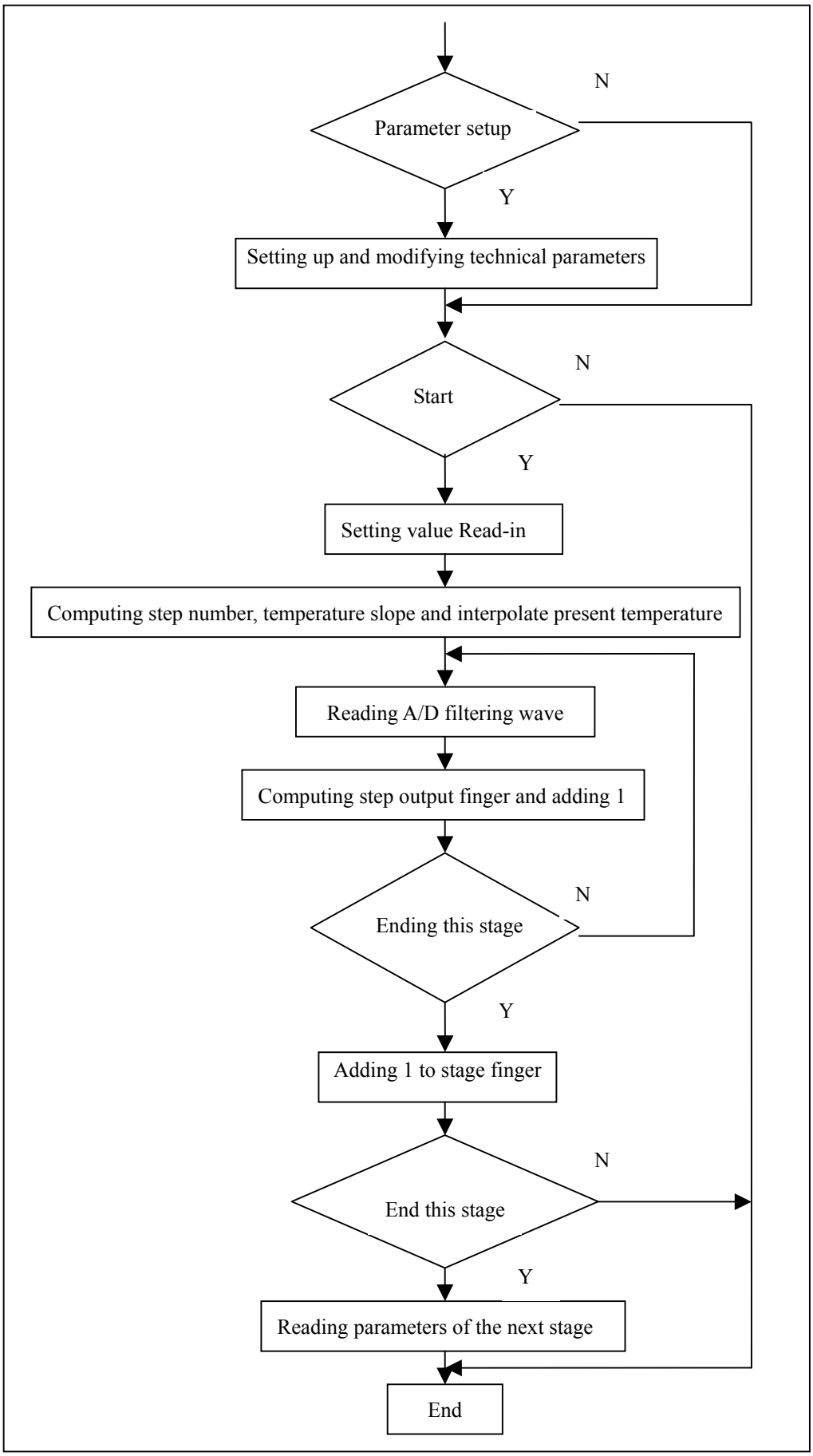

Figure 8. Main Program Layout

Modern Applied Science

www.ccsenet.org/journal.html

Vol. 2, No. 5

September 2008

Experimental Investigation on Relationship between Sedimentation Rate Constants of Solid Materials

K.Senthilkumar (Corresponding author)
Department of Chemical Engineering
Erode Sengunthar Engineering College, Thudupathi
Erode-638057, Tamilnadu, India
Tel: 91-4294-232-701 E-mail: uksen2003@yahoo.co.in

V. Sivakumar
Department of Chemical Engineering
Kongu Engineering College, Perundurai
Erode-638052, Tamilnadu, India
Tel: 91-4294-225-026 E-mail: drvsivakumar@yahoo.com

T. Kannadasan
Director of Research
Anna University- Coimbatore, GCT Campus
Coimbatore-641013, Tamilnadu, India
Tel: 91-422-245-4571 E-mail: tkannadasan56@yahoo.com

Abstract

It has been fount that the sedimentation process is a rate-governed process, which is a combination of a constant rate and falling rate. The various solid materials like Silicate, Calcium Carbonate, and Barium Carbonate were taken and ground in prototype ball mill and sieved to different size fractions and different consistence sedimentation tests were conducted. In this study, an attempt has been made to draw some correlations between sedimentation rate constants (overall sedimentation rate constant (K_o), sedimentation rate constant for constant rate period (K_c) and falling rate constant (K_f)). Variation of K_o on various particle sizes and slurry consistency has also been reported in this work.

Keywords: Sedimentation rate, Sedimentation rate constant, Falling rate, Sedimentation rate correlation

1. Introduction

The separation of dilute slurry by gravity setting into a clear fluid and slurry of higher solids concentration is called sedimentation. Sedimentation is applied in many chemical engineering operations and processes such as filtration, fluidization, two- phase flow and environmental engineering (McCabe et al., 1993). The rate data of sedimentation process is very important for designing equipment used in chemical and metallurgical practices for separating suspended solid particles from liquid or gas stream (Mondal and Majumdar, 2004). Industrial sedimentation operations may be carried out batch- wise or continuously using thickeners. The hydrodynamic analysis of the sedimentation process facilitates the design of thickener (Coulson et al, 1962). Viscosity of the medium is the main physical property, which affects the sedimentation. Density of particles is again an important factor that affects the settling velocity of the particles. When the density of the particles is more, then the settling rate is also more. Batch sedimentation is employed for bio-processing or the process fluids in recycle. Batch sedimentation is mainly used in pharmaceutical industries. Continuous sedimentation is the process in which the solids are settled continuously. This type of sedimentation is found in chemical industries, which reuse the process water or fluid. They are carried out in large diameters and shallow depth diameters, with slowly revolving rakes for removing the sludge. In the binary system, two different sizes of particles are taken and are used for the study of sedimentation process. The mechanism of binary system of sedimentation can be well understood (Brown, 1962). In general, a binary mixture consisting of particles of equal densities will give rise to four zones during the course of sedimentation.

From the literature (Brown, 1962), it is observed that the sedimentation rate is proportional to the difference between the interfacial height at any time (H) and that attained at equilibrium (H_E) [when no further change in the height of sedimented layer occurs]: $(-dH)/dt \alpha (H- H_E)$. In general, the entire sedimentation period is found to be a combination of a constant rate period, which is followed by a falling rate period. The sedimentation rate falls till it vanishes at equilibrium height (H_E). Depending upon the type of period, the proportionality constant is known as constant rate (K_c) or falling rate period constant(K_f) respectively, which are operative between the intervals, $H_c \leq H < H_o$ for $0 < t \leq t_c$ and $H_E \leq H < H_c$ for $t_c < t \leq t_E$. If this condition is applied on overall basis between the initial interfacial height (H_o) and the equilibrium height H_E, the rate constant is called overall sedimentation rate constant (K_o). In this study, an attempt has been made to draw the correlations between these sedimentation rate constants K_c, K_f and K_o. Variation of overall sedimentation rate constant (K_o) on various particle size and slurry consistency has also been described in this work.

2. Materials and Methods

The solids of various materials like Calcium Carbonate ($CaCO_3$), Barium Carbonate ($BaCO_3$) and Silicate were taken and ground in proto type ball mill and sieved to four different size fractions of 52/60,60/72, 72/100 and 100/200 mesh BSS corresponding to particle size of 0.246mm, 0.212mm, 0.147mm and 0.072mm respectively. To make them dust free, the individual size fractions were washed in a gentle stream of water. The required quantities of the solids were put inside a 500 ml-measuring cylinder to make the slurry of a particular consistency. A strip of graph paper was attached to a measuring cylinder to ensure more precise reading. The slurry was stirred and allowed to settle. The height of interface was read from bottom and kept on being continuously recorded with time t, measured by a stopwatch to denote the rate of sedimentation at any time instant. The true density was measured by specific gravity bottle (Perry & Green, 1997).

3. Results and Discussion

In the experimental data, for each of the runs, the initial height of the slurry (H_o) (at t=0), was obtained directly and the equilibrium height (H_E) was determined graphically from the rectangular plot of H against t. It is clear from these plots that the curves tend to be more and more flat with the increase of the solids concentration, which results in a progressive decrease in the value of sedimentation rate. The critical height (H_c) was obtained from a differential plot of the variation of $-\Delta H/\Delta t$ against time t, as the break point between the constant and falling rates.

Though it has been mentioned that the rate of sedimentation is proportional to $(H-H_E)$ and raised to the power 1.0 (Brown, 1962, Perry & Green, 1997), it has been found in the present study that this assumption fails to give good result which is obtained by putting the exponent of $(H-H_E)$ as 0.1 instead of 1.0. The modified exponential term gives a good result in the standard deviation between the calculated and experimental values of H. So, the proportionality is modified as,

$$-dH/dt \alpha (H- H_E)^{0.1} \quad (1)$$

The proportionality constant is known as Sedimentation rate constant K. This equation (1) is integrated between the desired limits to obtain the values of different K.

For constant rate period,

$$-dH/dt = \text{constant} \quad (2)$$

Integrating this equation between the limits $H_c \leq H < H_o$ for $0 < t \leq t_c$

$$(H_o-H_c)/t_c = K_c \quad (3)$$

Where, t_c is the critical time (the value of time t corresponding to the break point between constant and falling rates) and the corresponding height is the critical height (Hc).

For falling rate period,

$$-dH /(H- H_E)^{0.1} \quad \alpha \, dt \quad (4)$$

Integrating this equation between the limits $H_E \leq H < H_c$ for $tc < t \leq t_E$

$$1.1[(H_c- H_E)^{0.9} - (H- H_E)^{0.9}] = K_f t \quad (5)$$

For overall conditions,

$$-dH /(H- H_E)^{0.1} = K_o \, dt \quad (6)$$

Integrating this equation for entire period of the initial interfacial height (Ho) and the equilibrium height H_E,

$$1.1 [(H_o- H_E)^{0.9} - (H- H_E)^{0.9}] = K_o t \quad (7)$$

The values of K_f and K_o can be easily calculated from the rectangular plots of the left hand side of equation (5) and equation (7) against t or $t-t_c$, respectively as the corresponding slopes. The unbiased values have been determined by

using least square technique. The values of K_c can be calculated directly by using the equation (3) for each of the experiments performed. The calculated values of K_o, K_c and K_f are tabulated in the Table 1 and Table 2.

In the process of finding the type of relationship between the rate constants K_c, K_f and K_o, it has been found that the variation of overall sedimentation rate constant (Ko) with the summation of the constant and falling rates (K_c+K_f) as shown in Table 3 and Table 4 and also plotted on a rectangular graph paper which forms a straight line. This relation can be expressed by (in general)

$$| K_o| = m |(K_c+K_f) | + C_1 \quad (8)$$

The values of m and C_1 have been calculated by using least square technique for all the runs and which is given in Table5.

The overall sedimentation rate constant is also found to be dependent on slurry concentration for a constant particle size. Such dependence can be expressed with a fair degree of accuracy by the relation,

$$K_o = A_1(C)^{B_1} \quad (9)$$

The plot plotted between ln (K_o) versus ln (C) satisfies the relation expressed in equation (9). From the results (Table 6) it is observed that the value of B_1 has decreased with increase in particle size in slurry and the value of A_1 has also decreased with increase of particle size of the slurry of the same consistency.

4. Conclusion

The batch sedimentation tests were conducted for the various materials like Silicate, Calcium Carbonate, and Barium Carbonate with various particle sizes and concentrations. Correlation has been made to relate the sedimentation rate constants like K_c, K_f, and K_o.Variation of K_o on various particle sizes and slurry consistency has also been reported in this work. In addition, over all sedimentation rate constant and slurry concentration were related by the equation $Ko= A_1(C)^{B_1}$ .The values of A_1 and B_1 were related with particle size of the solid particles in the slurry.

References

Warren L. McCabe, Julian C. Smith & Peter Harriett (1993). *Unit operation of chemical engineering*, McGraw Hill publications.

Mondal, P., Majumdar C.B (2004). Sedimentation of Hematite Water Slurries, *Journal of the Institution of Engineers (I),* 85, 20-23

Coulson J. M., Richardson J. F., Buckhurst J., Harker J. H. (1962). *Coulson & Richardson Chemical Engineering (volume 2)*, Asian Book Pvt. Ltd., 131

Brown G. G. (1962). *Unit Operation*, Asia publishing house, Calcutta, 117

Robert H.Perry & Don Green (1997). *Perry chemical engineer's hand book* (7th edition), McGraw Hill publications

Nomenclature

A_1 : Coefficient

B_1 : Coefficient

BSS : British standard sieves

C : Percentage slurry consistency, (Kg/m^3)

C_1 : Coefficient

H : Height of interface, m

H_E : Interfacial height at equilibrium, m

H_o : Initial height of the suspension (at t=0), m

K_o : Overall sedimentation rate constant, $(m)^{0.9}(sec)^{-1}$

K_f : Rate constant for falling rate period, $(m)^{0.9}(sec)^{-1}$

K_c : Rate constant for constant rate period, $(m)\ (sec)^{-1}$

|K| : Modulus of K

C_1 : Coefficient

$-r_c$: Rate of sedimentation, cm/s

D_p : Diameter of particle, cm

t : Time, sec

t_c : Critical time, s

t_E : Equilibrium time, s

Table 1. Experimental values of K_o, K_c and K_f for $CaCO_3$ and $BaCO_3$

Materials	Constant rate constant, K_c			Falling rate constant, K_f			Over all rate constant, K_o		
	5%	10%	15%	5%	10%	15%	5%	10%	15%
$CaCO_3$	0.0853	0.0650	0.0317	-0.10794	-0.0356	-0.0535	0.0624	0.0491	0.0294
$BaCO_3$	0.148	0.1378	0.1308	-0.23323	-0.1827	-0.1188	0.1118	0.0977	0.0751

Table 2. Experimental values of K_o, K_c and K_f for Silicate

Materials	Constant sedimentation rate period constant, K_c				
Silicate (BSS)	5%	10%	15%	20%	25%
52/60	0.1203	0.1111	0.1025	0.1006	0.0915
60/72	0.1181	0.0974	0.0946	0.0931	0.0898
72/100	0.1086	0.0914	0.08333	0.0837	0.0754
100/200	0.0892	0.0872	0.0833	0.06926	0.0608
	Falling sedimentation rate period constant, K_f				
Silicate (BSS)	5%	10%	15%	20%	25%
52/60	-0.253	-0.18528	-0.18882	-0.16147	-0.13203
60/72	-0.20459	-0.16349	-0.1514	-0.12318	-0.12299
72/100	-0.19042	-0.16628	-0.13685	-0.10249	-0.12653
100/200	-0.13137	-0.14448	-0.1086	-0.13229	-0.1155
	Overall sedimentation rate constant, Ko				
Silicate (BSS)	5%	10%	15%	20%	25%
52/60	0.110702	0.094218	0.089433	0.086678	0.078563
60/72	0.104175	0.08577	0.078971	0.073904	0.071563
72/100	0.096321	0.080232	0.070811	0.064602	0.062312
100/200	0.064096	0.073587	0.064914	0.063097	0.055385

Table 3. The values of (K_c+K_f) and K_o for $CaCO_3$ and $BaCO_3$

Materials	For 5%		For 10%		For 15%	
	K_c+K_f	K_o	K_c+K_f	K_o	K_c+K_f	K_o
$CaCO_3$	-0.02257	0.062473	0.029412	0.049105	-0.02178	0.029244
$BaCO_3$	-0.08523	0.11187	-0.04493	0.097779	0.011909	0.075109

Table 4. The values of (K_c+K_f) and K_o for Silicate

Silicate (BSS)	5%		10%		15%		20%		25%	
	K_c+K_f	K_o	K_c+K_f	K_o	K_c+K_f	K_o	K_c+K_f	K_o	K_c+K_f	K_o
52/60	-0.1327	0.2348	-0.0742	0.1247	-0.0863	0.0840	-0.0607	0.0707	-0.0405	0.0658
60/72	-0.08649	0.1519	-0.0661	0.1153	-0.0568	0.0793	-0.030	0.06744	-0.0332	0.0634
72/100	-0.08182	0.1393	-0.0748	0.1058	-0.0535	0.0738	-0.0189	0.0634	-0.0511	0.061
100/200	-0.04217	0.1307	-0.0572	0.0999	-0.0253	0.0673	-0.063	0.06085	-0.0547	0.0593

Table 5. Value of constant for the relation among K_o, K_c and K_f

Materials	Constants	
	m	C1
$CaCO_3$	19.4213	-0.442
$BaCO_3$	0.51445	0.0706
For Silicate		
52/60 BSS	2.2346	-0.0603
60/72 BSS	1.6798	-0.0039
72/100 BSS	1.6362	-0.0029
100/200BSS	-14.867	0.8046

Table 6. Value of constants for the relation between K_o and C

Materials	Constants	
	A_1	B_1
$CaCO_3$	0.0093	-0.6539
$BaCO_3$	0.04099	-0.3445
Silicate	A_1	B_1
52/60 BSS	0.06139	-0.1955
60/72 BSS	0.05085	-0.2350
72/100 BSS	0.04186	-0.2787
100/200BSS	0.0382	-0.346

Modern Applied Science

www.ccsenet.org/journal.html

Vol. 2, No. 5

September 2008

A New Algorithm in Maximum Likelihood Estimation for Generalized Linear Models

Yufang Wen(Corresponding author)
Department of Science, Yanshan University
Qinhuangdao 066004, China

Xiangdong Song
Department of Science, Yanshan University
Qinhuangdao 066004, China

Haisen Zhang
Department of Science, Yanshan University
Qinhuangdao 066004, China

Abstract

We intrduce a new algorithm for L_1 regularized generalized linear models. The L_1 regularization procedure is useful,especially because it ,in effect,selects variables according to the amount of penalization on the L_1 norm of the coefficients,in a manner less greedy than forward selection/backward deletion. The algorithm efficiently computes solutions along the entire regularization path using the predictor-corrector method of convex-optimization. Selecting the step length of the regularization parameter is critical in controlling the overall accuracy of the paths; we suggest intuitive and flexible strategies for choosing appropriate values.

Keywords: Generalized Linear Models**,** Predictor-Corrector algorithm

1. Introduction

In this paper we propose a preditor-corrector algorithm for L_1 regularized generalized linear models (GLM). GLM models a random variable Y that follows a distribution in the exponential family using a linear combination of the predictors, $x'\beta$, where x and β denote vectors of the predictors and the coefficients, respectively. The random and the systematic components may be linked through a non-linear function; therefore,we estimate the coefficient β by solving a set of non-linear equations that satisfy the maximum likelihood criterion.

$$\hat{\beta} = \arg\max_{\beta} L(y;\beta) \tag{1}$$

where L denotes the likelihood function with respect to the given data $\{(x_i, y_i): i = 1,\cdots,n\}$.

When the number of predictors p exceeds the number of observations n, or when insignificant predictors are present, we can impose a penalization on the L_1 norm of the coefficients for an automatic variable selection effect. Analogous to Lasso (Tibshirani 1996) that added a penalty term, to the squared error loss criterion, we modify criterion (1) with a regularization:

$$\hat{\beta}(\lambda) = \arg\min_{\beta}\left\{-\log L(y;\beta) + \lambda\|\beta\|_1\right\} \tag{2}$$

where $\lambda > 0$ is the regularization parameter. Logistic regression with L_1 penalization has been introduced and applied by other researchers, for example in Shevade & Keerthi (2003).

2. Problem setup

Let $\{(x_i, y_i): x_i \in \Re^p, y_i \in \Re, i-1,\cdots,n\}$ be n pairs of p factors and a response. Y follows a distribution in the

exponential family with mean $\mu = \mathrm{E}(\mathrm{Y})$ and variance $\mathrm{V} = \mathrm{Var}(\mathrm{Y})$. Depending on its distribution, the domain of y_i could be a subset of $\Re$. GLM models the random component Y by equating its mean μ with the systematic component η through a link function g:

$$\eta = g(\mu) = \beta_0 + x'\beta \tag{3}$$

The likelihood of Y is expressed as follows (McCullagh & Nelder 1989):

$$L(y;\theta,\phi) = \exp\{(y\theta - b(\theta))/a(\phi) + c(y,\phi)\} \tag{4}$$

$a(\cdot), b(\cdot)$, and $c(\cdot)$ are functions that vary according to the distributions. Assuming that the dispersion parameter ϕ is known, we are interested in finding the maximum likelihood solution for the natural parameter θ, and thus $(\beta_0, \beta')'$, with a penalization on the size of the L_1 norm of the coefficients ($\|\beta\|_1$). Therefore, our criterion with a fixed λ is reduced to finding $\beta = (\beta_0, \beta')'$, which minimizes the following:

$$l(\beta,\lambda) = -\sum_{i=1}^{n}\{y_i\theta(\beta)_i - b(\theta(\beta)_i)\} + \lambda\|\beta\|_1 \tag{5}$$

Assuming that none of the components of β is zero and differentiating $l(\beta,\lambda)$ with respect to 4565, we define a function H:

$$H(\beta,\lambda) = \frac{\delta l}{\delta\beta} = -X'W(y-\mu)\frac{\delta\eta}{\delta\mu} + \lambda Sgn\begin{pmatrix}0\\ \beta\end{pmatrix} \tag{6}$$

where X is an n by $p+1$ matrix including the column of $1's$,W is a diagonal matrix with n diagonal elements $V_i^{-1}(\frac{\delta\mu}{\delta\eta})_i^2$, and $(y-\mu)\frac{\delta\eta}{\delta\mu}$ is a vector with n elements $(y_i - \mu_i)(\frac{\delta\eta}{\delta\mu})_i$.

Our goal is to compute the entire solution path for the coefficients β, with λ varying from ∞ to 0. We achieve this by drawing the uniquely determined curve $H(\beta,\lambda) = 0$ in $(p+2)$ dimesional space $(\beta \in \Re^{p+1} and \lambda \in \Re_+)$.Because $l(\beta,\lambda)$ is a convex function of β, there exists a $\beta(\lambda)$ that attains the unique minimum value for each $\lambda \in \Re_+$. In fact, a unique continuous and differentiable function $\beta(\lambda)$, such that $H(\beta(\lambda),\lambda) = 0$ exists within each open range of λ that yields a certain active set of variables; the existence of such mappings $(\lambda \to \beta(\lambda))$ can be shown using the implicit function theorem (Munkres 1991). We find the mapping $\beta(\lambda)$ sequentially with decreasing λ.

3. Predictor-Corrector algorithm

We introduced an algorithm that implements the predictor-corrector method to determine the entire path of the coefficient estimates as λ varies , i.e., to find $\{\hat{\beta}(\lambda): 0 < \lambda < \infty\}$. Starting from $\lambda = \infty$, our algorithm computes a series of solution sets, each time estimating the coefficients with a smaller λ based on the previous estsmate. Each round of optimization consists of three steps: determining the step size in λ; predicting the corresponding change in the coefficients, and correcting the error in the previous prediction.

The following lemma provides the initialization of the coefficient paths:

Lemma 1: *When λ exceeds a certain threshold, the intercept is the only nonzero coefficient: $\hat{\beta}_0 = g(\bar{y})$ and*

$$H((\hat{\beta}_0, 0\cdots, 0), \lambda) = 0 \ \textit{for} \ \lambda > \max_{j\in\{1,\cdots,p\}}\left|x_j'\hat{W}(y-\bar{y}1)g'(\bar{y})\right| \tag{7}$$

Proof. The Karush-Kuhn-Kuhn-Tucker (KKT) optimality conditions for minimizing (5) imply

$$\left|x_i'\hat{W}(y-\hat{\mu})\frac{\delta\eta}{\delta\mu}\right| < \lambda \Rightarrow \hat{\beta}_j = 0 \quad \text{for} \quad j = 1,\cdots,p \tag{8}$$

When $\hat{\beta}_j = 0$ f or all $j = 1,\cdots,p$, the KKT conditions again inply

$$1'\hat{W}(y-\hat{\mu})\frac{\delta\eta}{\delta\mu} = 0 \tag{9}$$

Which, in turn, yields $\hat{\mu} = \bar{y}1 = g^{-1}(\hat{\beta}_0)1$.

As λ is decreased further, other variables join the active set, beginning with the variable $j_0 = \arg\max_j\left|x_j'(y-\bar{y}1)\right|$.

Reducing λ, we alternate between a predictor and a corrector step.

3.1 Predictor step

In the k-th perdictor step, $\beta(\lambda_{k+1})$ is approximated by

$$\hat{\beta}^{k+} = \hat{\beta}^{k} + (\lambda_{k+1} - \lambda_k)\frac{\partial \beta}{\partial \lambda} \tag{10}$$

$$= \hat{\beta}^{k+} - (\lambda_{k+1} - \lambda_k)\left(X_A' W_k X_A\right)^{-1} Sgn(0, \beta^k)' \tag{11}$$

W_k and X_A denote the current weight matrix and the columns of X for the factors in the current active set,respectively. β in the above equations are composed only of current nonzero coefficients.This linearization is equivalent to making a quadratic approximation of the log-likeihood and extending the current solution $\hat{\beta}^k$ by taking a weighted lasso step (as in LARS).

Define $f(\lambda) = H(\beta(\lambda), \lambda)$; in the domain that yields the current active set, $f(\lambda)$ is zero for all λ.By differentiating f with respect to λ,we obtain

$$f'(\lambda) = \frac{\partial H}{\partial \lambda} + \frac{\partial H}{\partial \beta}\frac{\partial \beta}{\partial \lambda} = 0 \tag{12}$$

from which we compute $\delta\beta/\delta\lambda$.

3.2 Corrector step

In the following corrector step,we use $\hat{\beta}^{k+}$ as the initial value to find the β that minimizes $l(\beta, \lambda_{k+1})$,as defined in (5) (i.e.,that solves $H(\beta, \lambda_{k+1}) = 0$ for β).Any (convex) optimization method that applies to the minimization of a differentiable objective function with linear constrains may be implemented. The previous predictor step has provided a warm start;because $\hat{\beta}^{k+}$ is usually close to the exact solution $\hat{\beta}^{k+1}$, the cost of solving for the exact solution is low.The corrector steps not only find the exact solution at a given λ but also yield the directions of β for the subsequent predictor steps.

3.3 Active set

The active set A begins from the intercept as in Lemma 3.1;after each corrector step,we check to see if A should have been augmented.The following procedure for checking is justified and used by Rosset&Zhu(2003) and Rosset(2004):

$$\left| x_j' W (y - \mu)\frac{\delta \eta}{\delta \mu} \right| > \lambda \quad \text{for any} \quad j \in A \Rightarrow A \leftarrow A \cup \{j\} \tag{13}$$

We repeat the corrector step with the modified active set until the active set is not augmented further. We then remove the variables with zero coefficients from the active set. This is,

$$\left|\hat{\beta}_j\right| = 0 \quad \text{for any} \quad j \in A \Rightarrow A \leftarrow A - \{j\} \tag{14}$$

3.4 Step length

Two natural choices for the step length $\Delta_k = \lambda_k - \lambda_{k+1}$ are:

(1) $\Delta_k = \Delta$, fixed for every k,or

(2) a fixed change L in L_1 arc-length,achieved by setting $\Delta_k = L / \left\| \delta\beta/\delta\lambda \right\|_1$.

As we decrease the step size,the exact solutions are computed on a finer grid of λ values,and the coefficient path becomes more accurate.

We propose a more efficient and useful strategy:

(3) select the smallest Δ_k that will change the active set of variables.

We give an intuitive explanation of how we achieve this,by drawing on analogies with the Lars algorithm(Efron et al.2004).At the end of the $k-th$ iteration,the corrector step can be characterized as finding a weighted Lasso solution that satisfies $-X_A' W_k (y - \mu)\frac{\delta \eta}{\delta \mu} + \lambda_k Sgn\begin{pmatrix} 0 \\ \beta \end{pmatrix} = 0$.This weighted Lasso also produces the direction for the next

predictor step.If the weights W_k were fixed,the weight Lars algorithm would be able to compute the exact step length to the next active-set change point.We use this step length,even though in practice the weights change as the path progresses.

Lemma 2: *Let* $\hat{\mu}$ *be the estimates of* y *from a corrector step,and denote the corresponding weighted correlations as*

$$\hat{c} = X'\hat{W}(y-\hat{\mu})\frac{\delta\eta}{\delta\mu}\cdot \tag{15}$$

The absolute correlations of the factors in A *(except for the intercept) are* λ *,while the values are smaller than* λ *for the factors in* A^c.

Proof. The Karush-Kuhn-Tucker(KKT) optimality for minimizing(5)imply

$$\hat{\beta}_j \neq 0 \Rightarrow \left| x_j'\hat{W}(y-\hat{\mu})\frac{\delta\eta}{\delta\mu}\right| = \lambda. \tag{16}$$

This condition,combined with (7) and (8) ,proves the argument.

The next predictor step extends $\hat{\beta}$ as in (11),and,thus,the current correlations change.Denoting the vector of changes in correlation for a unit decrease in λ as a ,

$$c(h) = \hat{c} - ha \tag{17}$$

$$= \hat{c} - hX'\hat{W}X_A\left(X_A'\hat{W}X_A\right)^{-1}Sgn\begin{pmatrix}0\\ \hat{\beta}\end{pmatrix}, \tag{18}$$

Where $h>0$ is a given decrease in λ .For the factors in A ,the values of a are those of $Sgn\begin{pmatrix}0\\ \hat{\beta}\end{pmatrix}$.To find the h with which any factor in A^c yields the same absolute correlation as the ones in A ,we solve the following equations:

$$\left|c_j(h)\right| = \left|\hat{c}_j - ha_j\right| = \lambda - h \quad \text{for any} \quad j \in A^c \tag{19}$$

The equations suggest an estimate of the step length in λ as

$$h = \min_{j\in A^c}{}^{+}\left\{\frac{\lambda-\hat{c}_j}{1-a_j}, \frac{\lambda+\hat{c}_j}{1+a_j}\right\}. \tag{20}$$

In addition,to check if any variable in the active set reaches 0 before λ decreases by h ,we solve the equations

$$\beta_j(\tilde{h}) = \hat{\beta}_j + \tilde{h}\left(X_A'\hat{W}X_A\right)^{-1}Sgn\begin{pmatrix}0\\ \hat{\beta}\end{pmatrix} = 0 \quad \text{for any} \quad j \in A\,. \tag{21}$$

If $0<\tilde{h}<h$ for any $j \in A$,we expect that the corresponding variable will be eliminated from the active set before any other variable joins it;therefore, $\tilde{h}$ rather than h is used as the next step length.

Letting the coefficient paths be piecewise linear with the knots placed where the active set changes is a reasonable simplification of the truth based on our experience(using both simulated and real datasets). If the smallest step length that modifies the active set were to be larger than the value we have estimated,the active set remains the same,even after the corrector step.If the true step length were smaller than expected,and,thus,we missed the entering point of a new active variable by far,we would repeat a corrector step with an increased λ .Therefore,our path algorithm almost precisely detects the values of λ at which the active set changes,in the sense that we compute the exact coefficients at least once before their absolute values grow larger than δ (a small fixed quantity).

We can easily show that in the case of Gaussian distribution with the identity link, the piecewise linear paths are exact. Because $\hat{\mu} = X'\hat{\beta}$ and $V_i = Var(y_i)$ is constant for $i = 1,\cdots,n$, $H(\beta,\lambda)$ implifies to $-X'(y-\mu)+\lambda Sgn(0,\beta)'$. The step lengths are computed with no error; in addition, since the predictor steps yield the exact coefficient values, corrector steps are not deccessary. In fact, the paths are identical to those Lasso.

4. Discussion

We can extend the use of the predictor-corrector scheme by generalizing the loss+penalty function to any convex and almost differentiable functions. For example, we can find the entire regularization path for the Cox proportional hazards models with L_1 penalization,. Just as the solution paths for Gaussian distribution were computed with no error through the predictor-corrector method, so any other piecewise linear solution paths can be computed exactly by

applying the same strategy.

References

R.Tibshirani (1997), The lasso method for variable selection in the cox models, *Statistics in Medicine*, pp: 385-395.

Osborne, M., Presnell, B. & Turlach, B. (2000), On the lasso and its dual, *Journal of Computational and Graphical Statistics* pp. 319-337.

Zou, H & Hastie, T. (2005), Regularization and variable selection via the elastic net, *Journal of the Royal Statistical Society*, Series B, pp:301-320.

M.Osborne,B. Presnell & B.Turlach. (2002), A new approach to variable selection in least squares problems, *IMA Journal of Numerical Analysis*, 20(3): 389-403.

Xiru Chen (2003), Generalized Linear Models(5), *Mathematical Statistics and Management*, 22(3), pp:56-63.

S.Shevade & S.Keerthi (2003). *A simple and efficient algorithm for gene selection using sparse logistic regression*, Bioinformatics, pp:2246-2253.

Modern Applied Science

www.ccsenet.org/journal.html

Vol. 2, No. 5

September 2008

Refractive Indices, Ultrasonic Velocities Surface Tension and Thermo Acoustical Parameters of Anisaldehyde+ Benzene at 323.15K

R. Baskaran

Department of Chemical Engineering

St.Joseph's college of Engineering

old mahabalipuram road, Chennai-119

Tel: 994-128-5866 E-mail: rbaskaran2000@yahoo.com

T.R Kubendran

Department of Chemical Engineering

Alagappa College of Technology

Anna University

Chennai-600025, India

Tel: 944-512-3866 E-mail: trkubendran@yahoo.co.in

Abstract

The studies of ultrasonic velocities, refractive indices and surface tension are being increasingly used as tools for investigation of the properties of pure components and the nature of intermolecular interactions between the liquid mixture constituents. Refractive indices (n_D), ultrasonic velocities (u) and surface tension (σ) have been measured for the binary liquid mixture of Anisaldehyde +benzene over the entire composition range at 323.15 K. This study involves the evaluation of different thermo acoustical parameters along with the excess properties. The Redlich-Kister model was used to correlate the measured properties. It was found that in all cases, the experimental data obtained fitted with the values correlated by the corresponding models very well. The molecular interactions existing between the components were also discussed.

Keywords: Ultrasonic velocities, Thermo Acoustical Parameters, Binary solvents, Deviations, Surface tension, Refractive index

1. Introduction

Binary liquid mixtures due to their unusual behavior have attracted considerable attention (Marsh 1970). Data on some of the properties associated with the liquids and liquid mixtures like refractive index, ultrasonic velocities and surface tension find extensive application in chemical engineering process simulation, solution theory and molecular dynamics (Mchaweh 2004). These properties are important from practical and theoretical point of view to understand liquid theory. The review of literature on acoustical studies of solutions reveals that these measurements are used to estimate the different elastic properties of the molecule from which the type of molecular interactions can be very well understood. Ultrasonic velocity has proved to be useful in understanding the physico- chemical behavior of the particular system. Ultrasonic velocity have been very widely used now a days to study binary liquid mixtures(Pandey 1977) We report refractive index, ultrasonic velocities and surface tension of pure anisaldehyde and benzene as well as for the binary system constituted by these two chemicals at temperatures of 323.15K. From these experimental results acoustical impedence(Z), isentropic compressibility (β_s), intermolecular free length (L_f), degree of intermolecular attraction (α), molar sound velocity (R), molar compressiblity or wada's constant (W), refractive index deviation (δn_D), ultrasonic velocity deviation (δu), intermolecular free length deviation (δL_f), acoustical impedence deviation (δZ), and isentropic compressibility deviation ($\delta \beta_s$) were derived over the entire mole fraction range. The values have been fitted to Redlich-Kister type (Redlich.O.Kister 1948) equation. Literature survey showed that no measurements have been previously reported for the mixture studied in this paper.

2. Experimental

The chemicals used were of analytical grade and obtained from loba chemicals. All the components were dried over anhydrous potassium carbonate and fractionally distilled (Oswal 1995). A thermostatically controlled well-stirred water bath whose temperature was controlled to ±0.01 K accuracy was used for all the measurements. All the measurements were done by using electronic balance Shimadzu Corporation Japan Type BL 2205 accurate to 0.01 g. The possible uncertainty in the mole fraction was estimated to be less than ±0.0001.

2.1 Refractive index

Refractive indices were measured using thermostatically controlled Abbe refractometer with an accuracy less than 0.0001units.Water was circulated in to the prism of the refractometer by a circulation pump connected to an external thermostated water bath. Calibration was performed by measuring the refractive indices of doubly distilled water and propyl alcohol at defined temperatures. The sample mixture was directly injected in to the prism assembly of the instrument using a syringe. The change of refractive index over the composition range was obtained by

$$\delta n_D = n_D - (x_1 n_{D1} + x_2 n_{D2}) \quad (1)$$

Where n_D is the refractive index of the mixture and n_{D1} and n_{D2} are the refractive indices of the pure compounds.

2.1.1 Ultrasonic velocity

Speed of sound was measured by using a variable path, single crystal interferometer. (Mittal Enterprises New Delhi). The interferometer was calibrated using toluene. The interferometer cell was filled with the test liquid, and water was circulated around the measuring cell from a thermostat. The uncertainty was estimated to be $0.1 ms^{-1}$

The change of speed of sound on mixing were calculated by the equation

$$\delta u = u - (x_1 u_1 + x_2 u_2) \quad (2)$$

where u is the speed of sound of the mixture and u_1 and u_2 are the speed of the sound of the pure compounds. The acoustical impedence (Z) was calculated by the equation,

$$Z = \rho u \quad (3)$$

Where ρ is the density of mixture and u is the ultrasonic velocity of the mixture.

The isentropic compressibility (β_s) was calculated by the equation

$$\beta_s = 1/ \rho u^2 \quad (4)$$

Where ρ is the density of mixture and u is the ultrasonic velocity of the mixture.

The molar compressibility or Wada's constant (W), was calculated by the equation

$$W = (M / \rho) \beta_s^{-1/7} \quad (5)$$

where M is the relative molar mass and β_s is the isentropic compressiblity.

The molar sound velocity (R) was calculated by the equation

$$R = (M / \rho) u^{1/3} \quad (6)$$

Where u is the ultrasonic velocity of the mixture.

The intermolecular free length (L_f) was calculated by the equation

$$L_f = K \beta_s^{1/2} \quad (7)$$

where K is the Jacobson constant (Jacobson 1952).

The degree of intermolecular attraction (α) was calculated by the equation

$$\alpha = (u^2 / u^2_{im}) - 1 \quad (8)$$

where $u^2_{im} = 1/ \{ (x_1 M_1 + x_2 M_2)(x_1/M_1 u_1^2 + x_2/M_2 u_2^2)\}$

The δL_f, δZ, and $\delta \beta_s$ were derived over the entire mole fraction range by using the general equation

$$A^E = A - (Xi\ A_1 + (1-Xi)\ A_2) \quad (9)$$

Where A is the corresponding parameters (L_f, Z and β_s)of binary mixture and A_1 and A_2 are the corresponding pure component values. The experimental data for the binary system of this investigation have been correlated using Redlich Kister

$$A^E = x_1 x_2 \Sigma a_i (x_1 - x_2)^I \quad (10)$$

where a's are constant, which are functions of system properties.

2.1.2 Surface tension

Surface tension of pure liquids and binary mixtures over the whole composition range was determined using Interfacial tensiometer (ASTM D.971) with 1No. 4cm platinum ring as per IS 6104. All samples were equilibrated to (303.15, 313.15, and 323.15) K under atmospheric pressure. It was calibrated with distilled water. The accuracy of the surface tension measurement was estimated to be $0.03 mNm^{-1.}$

3. Results and discussion

Table 1 lists the measured, Density (ρ), refractive indices (n_D), ultrasonic velocities (u) and surface tension (σ) for the binary liquid mixture of Anisaldehyde -benzene over the entire composition range at 323.15 K with the corresponding Refractive index deviation (δn_D) and ultrasonic velocity deviation (δu). Table 2 lists Acoustical impedence (Z), isentropic compressibility (β_s), molar compressiblity (W), molar sound velocity (R), intermolecular free length (L_f), degree of intermolecular attraction (α), intermolecular free length deviation (δL_f), acoustical impedence deviation (δZ), and isentropic compressibility deviation ($\delta\beta_s$) of Anisaldehyde – benzene mixture at 323.15 K. Redlich-Kister Constants evaluated from the least square fit for the deviations of refractive index, ultrasonic velocity intermolecular free length, acoustical impedance and isentropic compressibility have been presented in Table 3. The refractive index, ultrasonic velocity and surface tension values increases with the mole fraction. This means that interaction in the mixture is not strong and hence increases. As seen in figure 1, the values of δZ and $\delta\beta_s$ were negative over the entire range of mole fraction and the curves are symmetrical in nature. The values of δL_f, δn_D and δu were positive over the entire range of mole fraction. It can be summarized that excess values may be affected by three factors. The first factor is the specific forces between molecules, such as hydrogen bonds, charge transfer complexes, breaking of hydrogen bonds and complexes bringing negative excess values (Changsheng vang 2006). The second factor is the physical intermolecular forces, including electrostatic forces between charged particles and between a permanent dipole and so on induction forces between a permanent dipole and an induced dipole and forces of attraction and repulsion between non polar molecules. Physical intermolecular forces are weak and the sign of excess value may be positive and negative. Third factor is the structural characteristics of the component arising from geometrical fitting of one component in to other structure due to the differences in shape and size of the components and free volume. The nature of $\delta\beta_s$ and δL_f play vital role in assessing the compactness due to molecular rearrangement .The molecular interactions in liquid mixture may also be due to interstitial accommodation (Kiyohora 1979) leading to more compact structure making δZ and $\delta\beta_s$ negative. The positive deviation of δL_f, δn_D and δu is an indicative of weak interaction involving dispersion forces(Susmita 2005). The α has also been evaluated to study the structural variations and the nature of interaction occurring in the system.

4. Conclusion

Experimental data of the density, refractive index, ultrasonic velocity and surface tension of anisaldehyde and benzene mixture have been measured at 323.15 K. These data have been used to compute the excess properties of the system. Negative deviations were observed for δZ and $\delta\beta_s$. It is clear that redlich kister polynomial equation can represent δn_D, δu, δL_f, δZ, $\delta\beta_s$ very well which is indicated by low standard deviation values.

References

Changsheng, V., Hexilal & peisheng, Ma. (2006). Density and viscosity of diethyl carbonate with alcohols, *J. Chem. Eng. Data,* 51, 1345 – 1358.

Ewing, M.B., Levian, B.J., & Marsh, K.N. (1970). Ultrasonic study on binary liquid mixtures, *J.chem. Thermodynamics,* 2, 689- 691.

Jacobson, B. (1952). Compressibility of binary mixture, *Acta. chem.scand*. 6, 485-487.

Kiyohara, O., Benson, G.C. (1979). Ultrasonic velocity of binary mixtures, *J.Chem.Thermodynamics*, 11, 861-873.

Mchaweh, A., Alsaygh, A., & Moshfeghian, M.A. (2004). *Fluid phase equilibria*, 224, 157-167.

Oswal, S. L., & Patel, N. B. (1995). Viscosity of binary liquid mixtures, *J. Chem.Eng. Data*, 40, 845- 851.

Pandey, J.D., Mishra, R.L. (1977). Ultrasonic measurements, *Ind. J. Pure applied physics*, 15, 505-511.

Redlich, O., Kister, A. T. (1948). Algebraic representation of thermodynamic properties, *Ind.Eng. Chem*, 40, 345-349.

Susmita,K., Satyaban,J., & Bipin,B.S. (2005). Thermo acoustical parameters of binary mixtures, *J.Chem. Thermodyn*. 37, 820-825.

Table 1. Experimental Density (ρ), refractive indices (n_D), ultrasonic velocities (u), surface tension (σ), refractive index deviation (δn_D) and ultrasonic velocity deviation (δu) of Anisaldehyde – benzene mixture at 323.15 K.

X_1	ρ / g/cc	n_D	u / ms^{-1}	σ/m.N.m^{-1}	δu	δn_D
				323.15 K		
0.0000	0.828	1.4691	388	16.21	0	0.0000
0.1198	0.873	1.4762	525	24.09	3	0.0002
0.2141	0.898	1.4835	632	31.13	4	0.0002
0.3951	0.957	1.4960	836	37.38	5	0.0004
0.4081	0.961	1.4965	852	38.51	6	0.0005
0.5214	0.995	1.5045	978	46.71	5	0.0005
0.6605	1.036	1.5138	1134	50.85	5	0.0003
0.7314	1.055	1.5183	1212	56.75	3	0.0002
0.8195	1.079	1.5241	1311	64.64	3	0.0001
0.9316	1.108	1.5316	1472	67.21	2	0.0001
1.0000	1.114	1.5362	1571	78.11	0	0.0000

Table 2. Acoustical impedence (Z), isentropic compressibility (β_s), molar compressiblity (W), molar sound velocity (R), intermolecular free length (L_f), degree of intermolecular attraction (α), intermolecular free length deviation (δL_f), acoustical impedence deviation (δZ), and isentropic compressibility deviation ($\delta\beta_s$) of Anisaldehyde – benzene mixture at 323.15 K.

X_1	Z kgm^2s^{-1}	β_S m^2N^{-1}	W	R	L_f m	α	$\delta L_f \times 10^9$	δZ	$\delta\beta_s \times 10^6$
0.0000	321	8.02	487	674	2.66	0.00	0.00	00.0	0.000
0.1198	426	4.46	546	769	1.98	0.50	2.40	-66.0	-2.640
0.2141	560	2.70	606	841	1.54	1.43	2.21	-66.0	-3.670
0.3951	800	1.49	690	971	1.14	2.72	1.83	-85.0	-3.500
0.4081	818	1.43	697	980	1.12	2.82	1.80	-86.0	-3.450
0.5214	973	1.05	748	1040	0.96	3.42	1.56	-93.0	-2.970
0.6605	1174	0.75	809	1140	0.81	3.62	1.27	-94.0	-2.200
0.7314	1270	0.64	840	1180	0.75	3.42	1.12	-96.0	-1.770
0.8195	1414	0.53	878	1230	0.69	2.83	0.94	-78.0	-1.200
0.9316	1630	0.41	900	1320	0.60	1.46	0.54	-02.0	0.001
1.0000	1750	0.36	974	1380	0.56	0.00	0.00	00.0	0.000

Table 3. Redlich-Kister Constants for the deviations of refractive index, ultrasonic velocity intermolecular free length, acoustical impedence and isentropic compressiblity of Anisaldehyde – benzene at 323.15 K

	Redlich - Kister Constants			
	a_0	a_1	a_2	σ
δn_D	0.001	-0.00	0.00	1.22
δu	23.10	-1.21	-2.41	1.22
δL_f	0.00	-0.00	-0.00	1.84
δZ	-405.9	140.2	-338.9	0.00
$\delta\beta_s$	-13.52	13.23	-31.96	0.99

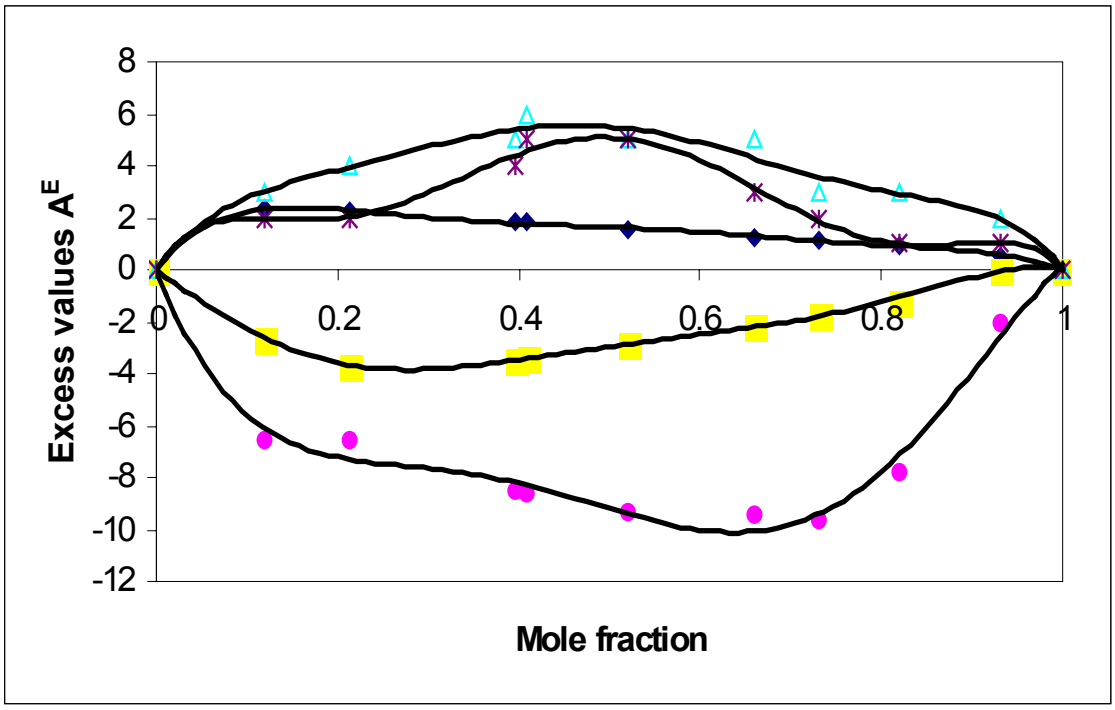

Figure 1. Excess values at 323.15 K. (a)● $\delta Z \times 10^1$ (b)■ $\delta\beta_s \times 10^6$ (c) ♦ $\delta L_f \times 10^9$ (d)* $\delta n_D \times 10^4$ (e) Δ δu

Modern Applied Science

www.ccsenet.org/journal.html

Vol. 2, No. 5

September 2008

A New Way to Determine the Multinomial Divisibility in the Rational Coefficient Field

Xingxiang Liu

College of Mathematics and Computer Science

Yan'an University

Yan'an 716000, China

E-mail: lxx640704@163.com

Abstract

In this article, we utilize the corresponding parallelisms between rational coefficient multinomial and integral coefficient multinomial and between the integral coefficient multinomial and positive rational number to translate the problem of divisibility of the rational coefficient multinomial into the problem of multiplication cross operation among positive rational numbers. This method can determine the divisibility and obtain the quotient.

Keywords: Rational coefficient multinomial, Integral coefficient multinomial, Divisibility, Prime factorization

1. Introduction

As we know, any one positive integer m can be implemented by prime factorization and its formula of prime factorization is

$$m = 2^{a_1}3^{a_2}5^{a_3}\cdots p_n^{a_n} = \prod_{k=1}^{n} p_k^{a_k}.$$

Where, $\alpha_k \in N(k=1,2,\cdots,n)$ and $p_k(k=1,2,\cdots,n)$ are n prime numbers which are different each other and $p_i < p_{i+1}(i=1,2,\cdots,n-1)$.

In the same way, to any positive rational number q, we can obtain same conclusion.

Lemma 1: Any one positive rational number q can be denoted as

$$q = 2^{a_1}3^{a_2}5^{a_3}\cdots p_n^{a_n} = \prod_{k=1}^{n} p_k^{a_k}.$$

Where, $\alpha_k \in Z(k=1,2,\cdots,n)$ and $p_k(k=1,2,\cdots,n)$ are n prime numbers which are different each other and $p_i < p_{i+1}(i=1,2,\cdots,n-1)$.

Lemma 2: Suppose $Z[x]$ is the set of integer coefficient multinomial, $Q[x]$ is the set of rational coefficient multinomial, and to any $f(x) \in Q[x]$, the integer k must exist to make $kf(x) \in Z[x]$, so the sufficient and necessary condition that $f(x)$ is reducible on Q is that $kf(x)$ can be reducible on Z.

2. The multiplication cross operation of positive rational numbers

Definition 1: Suppose the positive rational numbers $q_1 = 2^{\alpha_1}3^{\alpha_2}5^{\alpha_3}\cdots p_n^{\alpha_n} = \prod_{k=1}^{n} p_k^{a_k}$ and

$$q_2 = 2^{\beta_1}3^{\beta_2}5^{\beta_3}\cdots p_n^{\beta_n} = \prod_{k=1}^{n} p_k^{\beta_k}.$$

Where, $\alpha_k, \beta_k \in N(k=1,2,\cdots,n)$ and $p_k(k=1,2,\cdots,n)$ are n prime numbers which are different each other and $p_i < p_{i+1}(i=1,2,\cdots,n-1)$.

So the multiplication cross operation between q_1 and q_2 is

$$q_1 \otimes q_2 = (2^{\alpha_1}3^{\alpha_2}5^{\alpha_3}\cdots p_n^{\alpha_n}) \otimes (2^{\beta_1}3^{\beta_2}5^{\beta_3}\cdots p_n^{\beta_n}) = \prod_{k=1}^{n} p_k^{\sum\limits_{i+j=k}\alpha_i\beta_j}.$$

The summation cross operation between q_1 and q_2 is

$$q_1 \oplus q_2 = (2^{\alpha_1}3^{\alpha_2}5^{\alpha_3}\cdots p_n^{\alpha_n}) \oplus (2^{\beta_1}3^{\beta_2}5^{\beta_3}\cdots p_n^{\beta_n}) = \prod_{k=1}^{n} p_k^{\alpha_k-\beta_k}.$$

3. Main conclusions

To the integer coefficient multinomial $f(x) = a_0 + a_1x + a_2x^2 + \cdots + a_nx^n (a_n \neq 0)$, we can adopt the method $f(x) = a_0 + a_1x + a_2x^2 + \cdots + a_nx^n (a_n \neq 0)$ to correspond with $q = 2^{a_0}3^{a_1}5^{a_2}\cdots p_n^{a_n}$.

Where, $\alpha_k \in Z(k = 0,1,2,\cdots,n)$ and $p_k (k = 0,1,2,\cdots,n)$ are n+1 prime numbers which are different each other and $p_i < p_{i+1} (i = 1,2,\cdots,n-1)$ to make any integer coefficient multinomial $f(x)$ correspond with the positive rational number q, and obviously, this parallelism is the parallelism one by one. So we have:

Theorem 3: Suppose $Z[x]$ is the set of integer coefficient multinomial and Q^+ is the collectivity of positive rational numbers, so $\Phi : Z[x] \to Q^+$ exists to make any $f(x) = a_0 + a_1x + a_2x^2 + \cdots + a_nx^n (a_n \neq 0) \in Z[x]$, and $\Phi(f(x)) \in Q^+$. So Φ is the isomorphic mapping from $< Z[x], +, \times >$ to $< Q^+, \oplus, \otimes >$, i.e. $< Z[x], +, \times > \cong < Q^+, \oplus, \otimes >$.

Deduction 4: Suppose $Z[x]$ is the set of integer coefficient multinomial, Q^+ is the collectivity of positive rational numbers, and Φ is the isomorphic mapping from $< Z[x], +, \times >$ to $< Q^+, \oplus, \otimes >$,

(1) If to any $f(x), g(x)(g(x) \neq 0) \in Z[x]$, $h(x), r(x) \in Z[x]$, exists and makes $f(x) = g(x)h(x) + r(x)$, where, $r(x) = 0$ or $\partial^0(r(x)) \leq \partial^0(g(x))$ (mark $\Phi(f(x)) = q_f, \Phi(g(x)) = q_g, \Phi(h(x)) = q_h, \Phi(r(x)) = q_r,$) so $q_f = (q_g \otimes q_h) \oplus q_r$.

(2) In (1), the sufficient and necessary condition of $g(x) \mid f(x)$ is $q_r = 1$.

(3) In (1), the sufficient and necessary condition of $g(x) \mid f(x)$ is $q_f = q_g \otimes q_h$.

4. Example

Example: Determine whether $g(x) = x^2 - 3x + 2$ can divide $f(x) = x^3 - 4x^2 + 5x - 2$ exactly?

Solution: According to Theorem 3,

The corresponding positive rational number of $f(x) = x^3 - 4x^2 + 5x - 2$ is $2^{-2}3^5 5^{-4}7^1$, and the corresponding positive rational number of $g(x) = x^2 - 3x + 2$ is $2^2 3^{-3} 5^1 7^0$.

Suppose $g(x) \mid f(x)$, so $h(x) \in Z[x]$ exists and makes $f(x) = g(x)h(x)$.

Suppose the corresponding positive rational number of $h(x)$ is $2^{\beta_0}3^{\beta_1}5^{\beta_2}7^{\beta_3}$, so according to Deduction 4, $2^2 3^{-3} 5^1 \otimes 2^{\beta_0}2^{\beta_1}2^{\beta_2}2^{\beta_3} = 2^{-2}3^5 5^{-4}7^1$.

According to the definition of multiplication cross, we can get

$$\begin{cases} \beta_0 = -1 \\ \beta_1 = 1 \\ \beta_2 = 0 \\ \beta_3 = 0 \end{cases} \text{ from } \begin{cases} 2\beta_0 = -2 \\ 2\beta_1 - 3\beta_0 = 5 \\ \beta_0 + 2\beta_2 - 3\beta_1 = -4 \\ 2\beta_3 - 3\beta_2 + \beta_0 = 1 \end{cases},$$

so $h(x) = x - 1$, i.e. $g(x) \mid f(x)$.

About the divisibility of rational coefficient multinomial, we only need translate rational coefficient multinomial into integer coefficient multinomial, i.e. the reducible problem of rational coefficient multinomial in the rational number field is coincident with the reducible problem of integer coefficient multinomial in the integer loop.

5. Conclusions

The method in the article is only a sort of theoretic method, and it is very difficult to use it to determine the divisibility of multinomial in practice, and this new way can also be used to discuss other problems about multinomial.

References

Cao, Xihao, Zhang, Yimin and Huang, Denghang. (1987). *Advanced Algebra.* Beijing: Beijing Normal University Press. p.283-293.

David C. Lay. (2004). *Linear Algebra and Its Applications (Third Edition).* Beijing: Publishing House of Electronics industry.

Goger A. Hom & Charles R. Johnson. (2005). *Matrix Analysis (Volume 1).* Beijing: Posts and Telecom Press. Sep, 2005.

Goger A. Hom & Charles R. Johnson. (2005). *Matrix Analysis(Volume 2).* Beijing: Posts and Telecom Press. Sep, 2005.

Igor R.Shafarevich. (2006). *Algebra Base.* Beijing: Science Press.

I. Martin Isaacs. (2003). *Algebra: A Graduate Course.* Beijing: China Machine Press.

Jiang, Zhongzhang. (2005). A New Way of Factorization of Polynomial for Integral Coefficient Polynomial. *Mathematics in Practice and Theory.* No.35(1). p.219-221.

Kenneth H. Rosen. (1995). *Discrete Mathematics and Its Applications (Third Edition).* New York: American Telephone and Telegraph Company Bell Laboratories Division.

Kurt Bittner & Ian Spenee. (2003). *Use Case Modeling.* Beijing: Tsinghua University Press. March, 2003.

Zhang, Herui & Hao, Bingxin. (1981). *Advanced Algebra.* Beijing: Higher Education Press. p.71-81.

Modern Applied Science

www.ccsenet.org/journal.html

Vol. 2, No. 5

September 2008

Study and Design of Impellers for Multiphase Reactors

D.Devakumar (Corresponding author)

Department of Mechanical Engineering

Excel Engineering College

Komarapalayam-637307, Namakkal Dt, Tamilnadu, India

Tel: 91-944-31-6-1192 E-mail: devakumarand@yahoo.com

K.Saravanan

Department of Chemical Engineering

Kongu Engineering College

Perundurai, Erode – 638052, Tamilnadu, India

Tel: 91-984-270-5656 E-mail: rumisivaesh@yahoo.com

Abstract

The main objective of the project is to design impellers of different dimensions in each of the three types, namely paddle, pitched and turbine, to analyze them under various parameters to find out the best impeller of the best dimension for applications. The parameters to be varied and analyzed are impeller diameter, vessel diameter, clearance between impeller and the vessel, viscosity, liquid height and addition of electrolytes like glycerol, dilatants, etc. These impellers are tested and compared to get maximum gas holdup and minimum power consumption; from the comparison it is found that the pitched is the best among the three. Then it is proceeded to test the pitched impellers of various dimensions under the different parameters as mentioned above. For all comparisons and analysis, graphs are plotted between speed and gas holdup, power and gas holdup. From the results, to find the impeller which has maximum gas holdup and minimum power consumption that is suited for particular application.

Keywords: Multiphase Reactor, Paddle, Pitched, Turbine, Power consumption, Gas hold-up

1. Introduction

Impeller is used to produce centrifugal force to create the mass transfer between the various phases by mixing. Mixing of phases can be accomplished and by which mass and heat transfer can be enhanced between phases or external surfaces. The operation of agitation, which includes mixing as a special case, is now well established as an important and in a wide variety of chemical processes.

Specifically, impellers are applied to three general classes of problems;

(i) To produce static or dynamic uniformity in multicomponent multiphase systems

(ii) To facilitate mass or energy transfer between the parts of a system not in equilibrium

(iii) To promote phase changes in multicomponent system with or without a change in composition

Mixing in tanks is an important area when one considers the number of processes, which are accomplished in tanks. Essentially, any physical or transport process can occur during mixing in tanks. Qualitative and quantitative observations, experimental data, and flow regime identifications are needed and should be emphasized in any experimental pilot studies in mixing. In fact, the geometry is so important that the processes can be considered geometry specific. Solid suspension is very much dependent upon the shape of the tank bottom; liquid-liquid dispersion depend upon the geometry of the impeller; blending, upon the relative size of the tank to the impeller; and power draw, upon the impeller geometry.

Mixing efficiency in a stirred tank is affected by various numbers of parameters such as baffles, impeller speed, impeller type, clearance, tank geometry, solubility of substance, eccentricity of the impeller. Flow patterns can be changed according to the type of impellers, and fall into three categories: axial, radial and tangential. Mixing at high solid concentration is a classical operation in process engineering. Solid-liquid mixing plays an important role in

chemical, biochemical and mining processes dealing for instance with heat and mass transfer, transport and settling, dispersion, homogenization and/or coagulation.

Mechanically agitated three-phase (gas, liquid, and solid) reactors are widely used in industry. The solid phase may act as a catalyst or undergo a chemical reaction. Typical applications include catalytic hydrogenation, oxidation, ammonolysis, fermentation, and wastewater treatment. The reacting solid particles are encountered in hydrometallurgical processes, absorption of CO_2, NO, and SO_2 in lime slurries, oxydesulfurization, etc. For designing mechanically agitated contactors (MAC), knowledge of mixing time, flow pattern, power consumption, and mass-transfer parameters is necessary. Inter-phase mass transfer is often a rate-limiting step that must be reliably predicted in the design of agitated vessels.

Co-axial mixers are used in industry. The co-axial mixers have a specific design for the coating paper industry; it consists of a dispersion impeller (e.g. saw tooth type) and an anchor impeller. The production of sub-micron particles of organic actives has become of paramount importance in the pharmaceutical industry. So the impellers are used in the pharmaceutical industries. The other major applications of impellers are Oil industry, Polymer industry, Waste water treatment, Paint industry and Fermentation process. This project is aimed at the design of different impellers like pitched, paddle and turbine and also the analysis of these impellers by varying the physical properties and fluid properties with different dimensions. Finally to analyze the results of all the impellers to get an impeller with Less power consumption and High gas holdup value.

2. Experimental Setup

The experimental setup consists of mainly 5 components, which are Vessel, D.C.motor, Impeller, Impeller shaft and Revolution meter as shown in Figure.1.

2.1 Vessel

The tank is made up of acrylic material. The acryl material is chosen because it is transparent and hence the reactions can be easily visible.

2.2 D.C.Motor

The principle of motor is to convert the electrical energy to mechanical energy. So this mechanical energy is used to rotate the shaft of the impeller diameter. The specifications of the d.c.motor are Horse power as 1 hp and Speed as 2500rpm.

2.3 Impeller

Impeller is used to produce the centrifugal force. Three types of impeller are used for the analysis, namely Pitched, Paddle and Turbine. The material of impeller used is stainless steel. It is used so that the corrosion can be avoided. By the rotation of the impeller shaft the impeller rotates and there is mass transfer between the liquid phase (water) and the gas phase (compressed air).

2.4 Procedure

The impeller is selected with the low power consumption and high gas holdup fraction. Then the impellers namely pitched, paddle and turbine with two different dimensions are analyzed.

2.4.1 Gas Holdup

Gas holdup is the amount of gas present in the given system. Compressed air is used as the gas for analysis. In this project, air (gas) is allowed to pass through water (liquid) and the mass transfer occurs. The level of water is raised by this procedure. The value of gas holdup is obtained through the graph sheet stuck on the vessel.

2.4.2 Axial Flow

The impellers are also classified according to the flow pattern i.e. axial flow and radial flow.

Axial flow discharge coincides with the axis of impeller shaft, so when the impeller operates in a down pumping mode, the flow impinges on the bottom of the tank and spreads out in all directions toward the wall. The flow rises along the walls up the liquid surface and is pulled back to the impeller. Since axial flow impeller produce only one loop, fluids mix faster and blend time is reduced compared to radial flow impellers. The fluid does not take sharp turns near impellers and because of this, power consumption is less than that of radial flow impellers at the same speed and same the diameter.

2.4.3 Radial Flow

Radial Flow discharge is parallel to the impeller radius toward to the vessel wall. If a radial impeller is not positioned close to the surface or the tank bottom, the flow will split into two streams upon impinging on the tank wall. Each flow loop will continue along the wall and then return to impeller. Impellers based on axial type such as Propeller, Paddle and Curved. Impellers based on radial type such as Paddle, Turbine, Pitched, Helix and Curved.

2.4.4 Viscous and Non-viscous fluid

The variables such as speed, power and the gas holdup are measured for the viscous and non viscous fluids. Viscous fluids for the analysis are Car boxy methyl cellulose and Electrolyte (Polar type e.g. Nacl, MgSO4, Non polar type e.g. amyl alcohol) and water is considered as the non viscous fluid for the analysis and results.

2.4.5 Physical and Fluid properties

The physical properties such **as** Vessel size: The diameter of the acrylic vessel is varied, Impeller type and size: Impeller types of three different diameter of the impeller are considered, Impeller location: The impeller location is then varied which is called the clearance and Liquid level: The height of the liquid is also varied to get accurate results are considered for this analysis. The fluid properties such as Viscosity (Bingham plastic, Pseudo plastic and Dilatants) are considered for this analysis.

3. Design of Pitched Impellers

A pitched blade turbine consists of a hub with an even number of blades bolted and tack-welded on it. It is lighter in weight than a propeller of the same diameter. The blades can be at any angle between 10 degrees and 90 degrees from the horizontal, but the most common blade angle is 45 degrees. The flow discharge from a pitched blade impeller has components of both axial and radial flow velocity in low to medium viscosity liquids, and is considered to be a mixed flow impeller.

The design of the impellers is based on the reference [3-4]. The vessel size is taken as 0.5m based on the reference [3-4]. The impeller diameter is to be taken as one - third of the tank diameter. The width of the impeller is to be taken as one-third of the impeller diameter. The thickness is taken as 0.003m as shown in Figure.2. The material of the impeller can be stainless steel or mild steel depending upon the application. Another one is designed with all similar specifications but with a diameter of half the vessel size as shown in Figure.3.

4. Design of Paddle Impellers

A paddle blade impeller also consists of even number of blades that vary from 2 to 12. Usually 4 or 6 blades are ideally designed. The blades are bolted and tack-welded on a central hub. The angles between the blades in paddle impellers are usually 90 degrees i.e. the blades are perpendicular to each other. Paddle blade impellers can be used to produce both radial and axial flow in fluid.

The design of paddle impeller is similar to that of pitched. The diameter is taken as one third of the vessel diameter. The thickness is taken as 0.003m. The width is taken one third of the impeller diameter. The number of blades can vary from 4 to 6 as shown in the Figure.4. Another one is designed by the varying the diameter to half the diameter of the vessel as shown in the Figure.5. The material of the impeller can be stainless steel or mild steel.

5. Design of Turbine Impellers

There are four types of turbine impellers which are characterized by the flow patterns and level of shear they create axial flow, radial flow, hydrofoil and high shear impellers. They have the widest use in low and medium viscosity liquid applications, solids suspension, liquid-liquid emulsification, and gas dispersion. Turbine impeller can be blades varying from 2 to 12 in number. Two blades are normally unstable mechanically, while it is difficult it install more than six blades in a hub.

The design of turbine is similar to the other two. The impeller diameter is taken as one third of the vessel diameter and the width is to be taken as one third of the impeller diameter. The thickness is to be taken as one fourth of the width. The number of blades can vary from 4 to 6 as shown in the Figure.6. Another one is designed by varying the diameter alone to half the vessel diameter as shown in the Figure.7.

6. Results and Discussion

The tabulations of various properties like physical and fluid properties are noted .The discussion for all the properties are performed and the graph is drawn for the power consumption (P), %fractional gas holdup, and speed (N).

6.1 Comparison of Impellers

The power and gas holdup of the three designed impellers are measured and tabulated in Table.1. From the Figures 5.1 and 5.2, it is found that the pitched blade impeller has lower power consumption and high gas holdup. So the pitched impeller is chosen for further analysis.

6.2 Effect of Impeller Diameter

Three different dimensions of impeller diameter are taken as T/2(0.28 m), T/3(0.19m) and T/4(0.14m) and the readings are tabulated in Table.2. The pitched impeller with the blade angle 45 degrees is used. From the Figures.9 and 10, the impeller with the diameter of T/2 is found to give more gas holdup and consume less power.

6.3 Effect of Clearance

Clearance is defined as the distance between the impeller and the bottom tip of the tank vessel. If the initial height and the final height are noted as H1 and H2 the percentage of the clearance is computed by, (H2-H1/H2) * 100. The readings are measured and tabulated in Table.3. From the Figures 11 and 12, it can be concluded that a clearance of t/3 is ideal.

6.4 Effect of Liquid Height

The liquid height is varied at three different positions corresponding to H=T, H>t and H<T. the readings are taken and are tabulated in Table.4. The ideal liquid height which can give maximum gas holdup and consume minimum power is found to be H<T from the Figures 13 and 14.

6.5 Effect of Electrolyte Addition

The electrolytes are classified as polar, non-polar and water. The gas holdup and power consumed are computed for various densities of polar and non-polar electrolytes and tabulated in Table.5. From the Figures 15 and 16, it can be observed that NaCl is the best among polar and water is better than non-polar in providing gas holdup.

6.6 Effect of Viscosity

6.6.1 Carboxy methyl cellulose

Carboxy methyl cellulose of three different densities are used and the gas holdup and power are measured and tabulated in Table.6. From the Figures 17 and 18, it is found that Carboxy methyl cellulose of viscosity 0.5% weight is the best.

6.6.2 Glycerol

Glycerol of three different densities of weight is used in the vessel and the gas holdup and power readings are measured and tabulated in Table.7. It can be inferred form the Figures 19 and 20, that glycerol with 7.5% weight gives the maximum gas holdup at a low power.

6.6.3 Dilatants

Dilatants of three different viscosities and density of weight are used and the values are measured and tabulated in Table.8. From the Figures 21 and 22, it can be seen that the dilatants with 0.5% weight is the best.

6.7 Effect of Vessel Diameter

The vessel diameter is varied at 0.75m, 0.57m and 0.3m and the values are measured and tabulated in Table.9. The volume is computed and p/v and p/m values are tabulated in Table.10. From the Figures 23, 24, 25 and 26, it can be inferred that the ideal vessel diameter is 0.57m.

7. Conclusion

Impellers are very useful in creating mass transfer between phases by creating centrifugal force in the fluid flow and also very essential in various industrial reactors for mixing. It is mandatory to have an impeller which consumes less power and produces more gas holdup. Thus this work shows the study and design of various impellers to find out the best impeller type and also the one of the dimension that is best suited for specific applications.

8. Future Development

- For tall vessels the holdup generated from impeller does not travel to the bottom of the vessel, so it is suggested to use multistage contactors.
- New impeller can be designed, fabricated and studied for their performances against gas holdup.
- CFD can be developed for various impellers to know the flow pattern.
- Wide range of properties of various fluids can be studied.

References

Chapman, C., M., Nienow, A., W., Cooke, M., Middleton, J., C., (1981). Particle-Gas-Liquid Mixing In Stirred Vessels, Part II: Gas-Liquid Mixing, *Chemical Engineering Research and Design.*

James R. Couper, Roy Penney, W., James R. Fair, and STAN WALAS, Chemical Equipment Design, *Second Edition*, *Butterworth's Publishment.*

Nicholas P. Chopey, Handbook of Chemical Engineering Calculation, *Third Edition*, *McGraw hill*.

Rewatkar, V., B. (1989), Design of Multiphase Reactor, *PhD Thesis submitted to university of Bombay.*

Uhl, V., W., Gray, J., B., (1986). Mixing: theory and practice, *Volume III, Academic Press, Orlando, FL*.

Yatish T. Shah, (1979). Gas-Liquid-Solid Reactor Design, *McGraw hill*.

Table 1. Comparison of Impellers

Speed (N) (rps)	Power (P) (watts)	% Fractional gas holdup		
		Pitched	Turbine	Paddle
2	2.6	0.5	0.25	0.1
3	8.29	2.5	1.5	1
4	19.65	5	3.6	2.6
5	38.38	7.6	5.6	4.2
6	66.32	10.8	7.2	6.4
7	105.31	12.6	8.8	7.1
8	157.20	14	10	8

Table 2. Effect of Impeller Diameter

Speed (N) (rps)	Power (P) (watts)			% Fractional gas holdup		
	T/2	T/3	T/4	T/2	T/3	T/4
2	17.07	2.6	0.53	0.6	0.5	0.3
3	57.6	8.29	1.8	2.6	2.5	1.8
4	136.58	19.65	4.27	5.7	5	4.2
5	266.76	38.38	8.34	7.6	7.6	6.4
6	460.96	66.32	14.41	11.4	10.8	8
7	731.99	105.31	22.87	12.2	12.6	10.2
8	1092.6	157.20	34.15	14	14	12

Table 3. Effect of Clearance

Speed (N) (rps)	Power (P) (watts)	% Fractional gas holdup			
		C=T/2	C=T/3	C=T/4	C=T/6
2	2.6	0.5	0.5	0.4	0.3
3	8.29	2.7	2.5	2	1.8
4	19.65	5.1	5	4.6	3.6
5	38.38	7.4	7	6.8	5.1
6	66.32	11	10.8	9.6	6.8
7	105.31	12.2	12	11.4	10.2
8	157.20	13.8	14	14.5	13

Table 4. Effect of Liquid Height

Speed (N) (rps)	Power (P) (watts)	% Fractional gas holdup		
		H1 = H<T	H2 = H=T	H3 = H>T
2	2.6	0.7	0.5	0.4
3	8.29	2.9	2.5	1.8
4	19.65	5.6	5	3.6
5	38.38	7.8	7	5.9
6	66.32	11.4	10.8	9.4
7	105.31	12.6	12	10.6
8	157.20	15	14	12

Table 5. Effect of Electrolyte Addition

Speed (N) (rps)	Power (P) (watts)						% fractional gas holdup			
	Water	Non polar Amyl alcohol	MgSO4 Den=1.01	Nacl			water	Non polar	Polar	
				Den=1.07	Den=1	Den=1.1		Amyl alcohol	MgSO4	Nacl
2	2.6	0.002	0.00248	0.0026	0.00245	0.0027	0.5	0.4	0.55	0.6
3	8.29	0.009	0.00837	0.00887	0.00828	0.00911	2.5	2.2	3	3.2
4	19.65	0.022	0.019	0.02	0.01	0.021	5	4.6	5.4	6.6
5	38.38	0.044	0.038	0.04	0.03	0.042	7	6.6	7.4	8.2
6	66.32	0.076	0.066	0.07	0.066	0.072	10.8	9.6	11.6	12.1
7	105.31	0.12	0.106	0.11	0.105	0.115	12	11.2	14	15.6
8	157.20	0.18	0.158	0.168	0.157	0.172	14	12	16	18

Table 6. Effect of Viscosity – Carboxy Methyl Cellulose

Speed (N) (rps)	Power (P) (watts)			% Fractional gas holdup		
	Den=1.1	Den=1.25	Den=1.3	0.5 (wt %)	1 (wt %)	2.5 (wt %)
2	0.0027	0.003	0.0031	0.3	0.2	0.1
3	0.00911	0.01	0.01	1.6	1.	0.4
4	0.0216	0.124	0.125	3.4	2.6	1.4
5	0.042	0.047	0.049	5.2	4.6	2.3
6	0.072	0.082	0.086	6.9	5.4	3.6
7	0.115	0.131	0.136	8.1	6.8	4.9
8	0.172	0.196	0.20	10	7.5	6

Table 7. Effect of Viscosity – Glycerol

Speed (N) (rps)	Power (P) (watts)	% Fractional gas holdup		
		1 (wt %)	5 (wt %)	7.5 (wt %)
2	0.0037	0.5	0.3	0.2
3	0.01	1.8	1.4	1.2
4	0.24	3.4	3	2.9
5	0.047	4.7	4.1	3.9
6	0.082	6.5	5.1	4.8
7	0.131	8.6	7.2	7
8	0.196	11	11	13

Table 8. Effect of Viscosity – Dilatants

Speed (N) (rps)	Power (P) (watts)			% Fractional gas holdup		
	Den=1.2	Den=1.3	Den=1.35	0.5 (wt %)	2 (wt %)	3 (wt %)
2	0.0029	0.0031	0.0036	0.2	0.1	0.05
3	0.0099	0.01	0.012	1.1	0.8	0.7
4	0.023	0.025	0.029	2.4	2.1	1.8
5	0.046	0.049	0.057	3.8	3.4	2.6
6	0.079	0.086	0.09	4.9	4.2	3.8
7	0.126	0.136	0.157	7.1	6.8	5.6
8	0.188	0.204	0.235	9	8	7.2

Table 9. Effect of Vessel Diameter - 1

Speed (N) (rps)	Power (P) (watts)			% Fractional gas holdup		
	T1 =0.75 m	T2 = 0.57 m	T3 = 0.3 m	T1 =0.75 m	T2 = 0.57 m	T3 = 0.3 m
2	9.68	2.46	0.09	0.4	0.5	0.51
3	32.69	8.29	0.33	2.4	2.5	2.7
4	77.5	19.65	0.79	4.8	5	5.2
5	151.3	38.38	1.55	7.2	7.6	7.8
6	261.5	66.32	2.67	10.2	10.8	11.4
7	415.3	105.37	4.2	12	12.6	12.8
8	620	157.20	6.35	13	14	14.6

Table 10. Effect of Vessel Diameter – 2

Speed (N) (rps)	P/V (watts/m3)			P/m (watts/kg)			% fractional gas holdup		
	P1/V	P2/V	P3/V	P1/m	P2/m	P3/m	T1=0.75 m	T2=0.57 m	T3=0.3 m
2	66.7	16.9	0.62	0.06	0.01	0.0006	0.4	0.5	0.51
3	225.4	57	2.27	0.22	0.05	0.0022	2.4	2.5	2.7
4	534.4	135.5	5.5	0.53	0.135	0.0054	4.8	5	5.2
5	1043.4	246.6	10.68	1.04	0.26	0.01	7.2	7.6	7.8
6	1803.4	457.3	18.4	1.8	0.45	0.018	10.2	10.8	11.4
7	2864.1	726.6	29.3	2.86	0.72	0.029	12	12.6	12.8
8	4276	1084	43.8	4.27	1.08	0.043	13	14	14.6

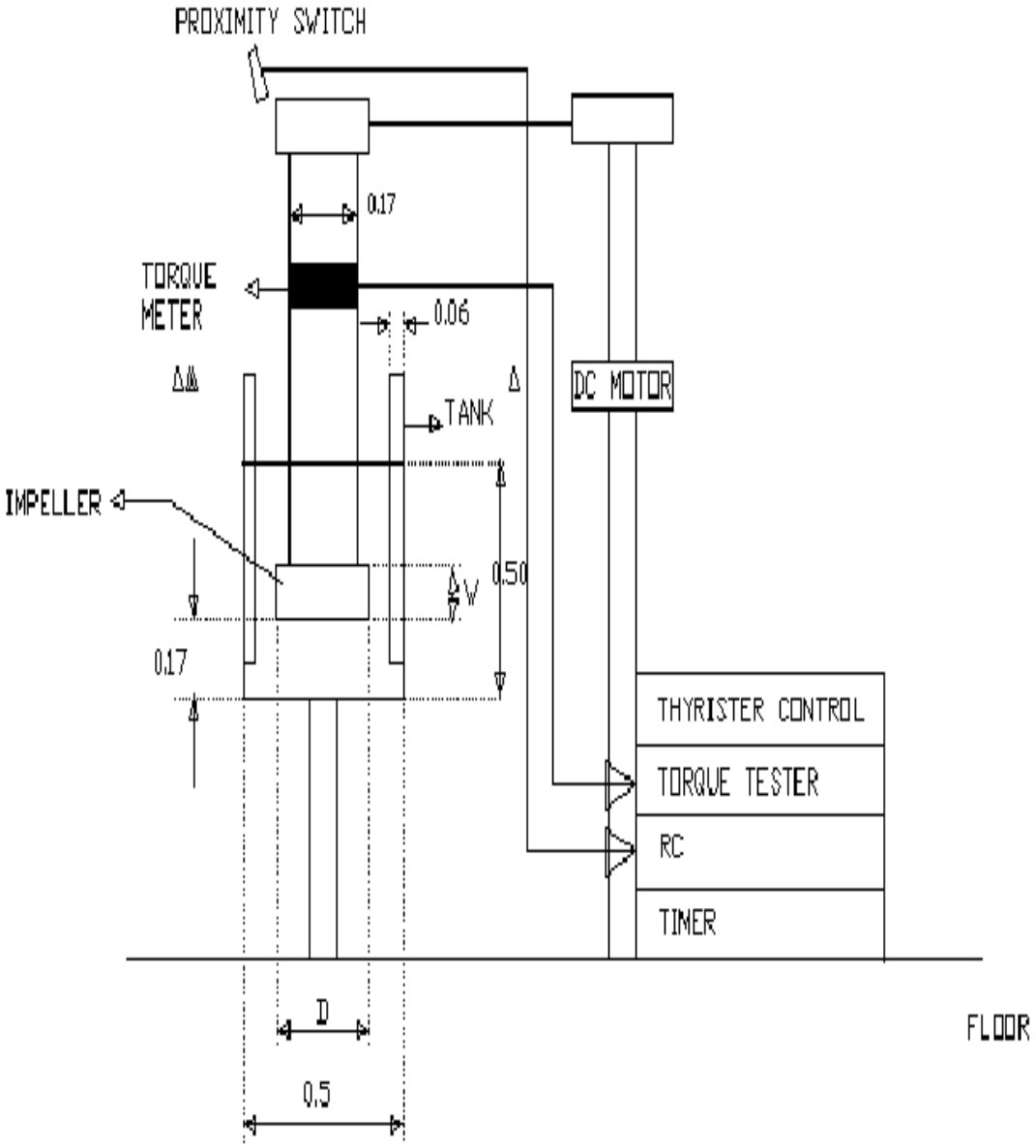

Figure 1. Experimental Setup Design

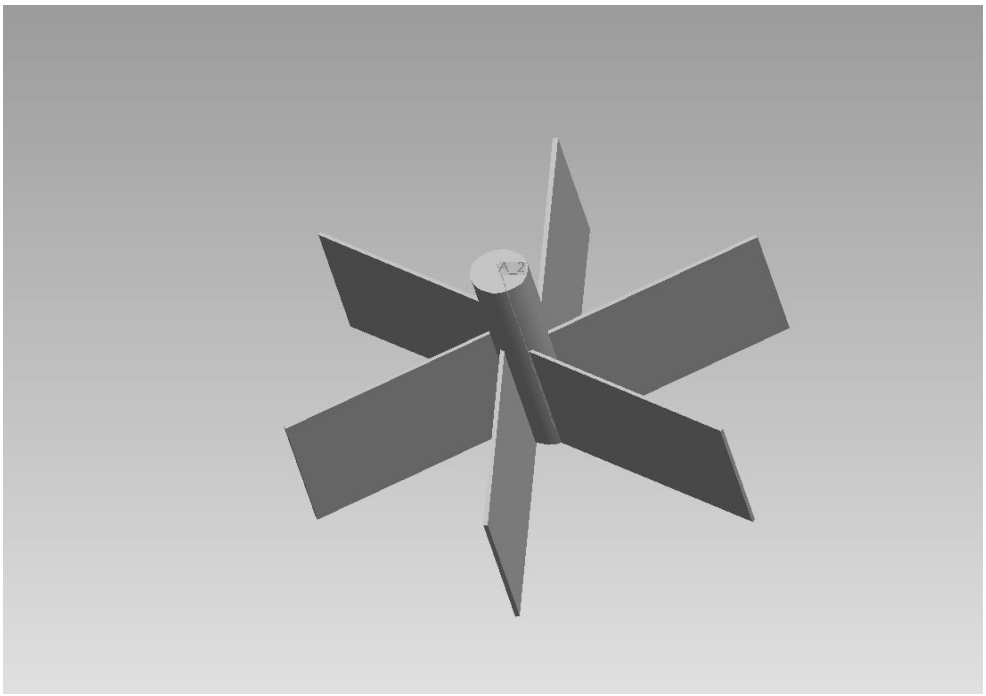

Figure 2. Pitched Impeller – 1

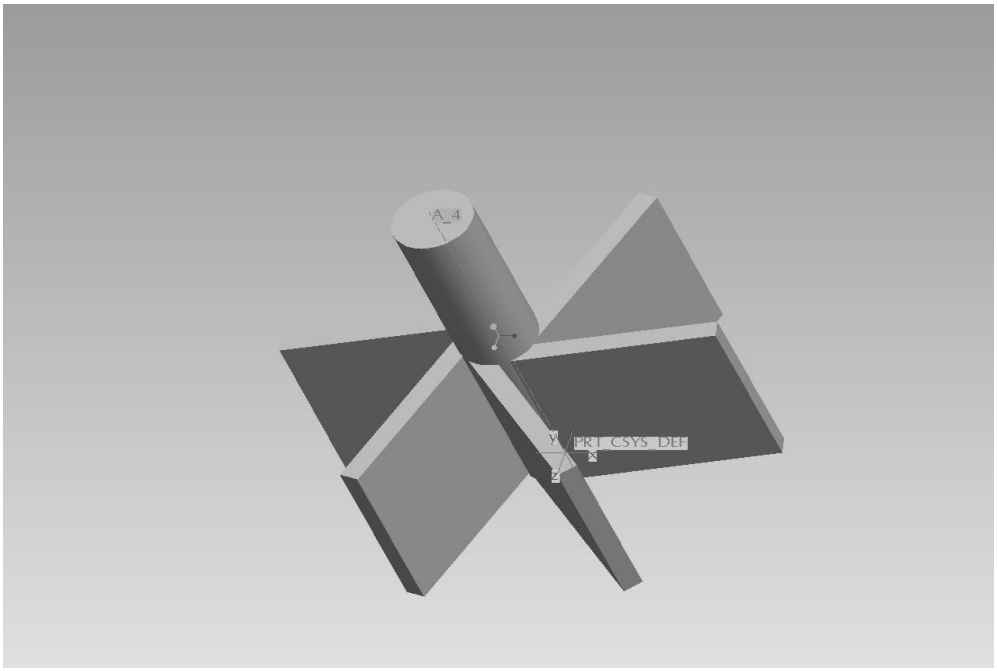

Figure 3. Pitched Impeller - 2

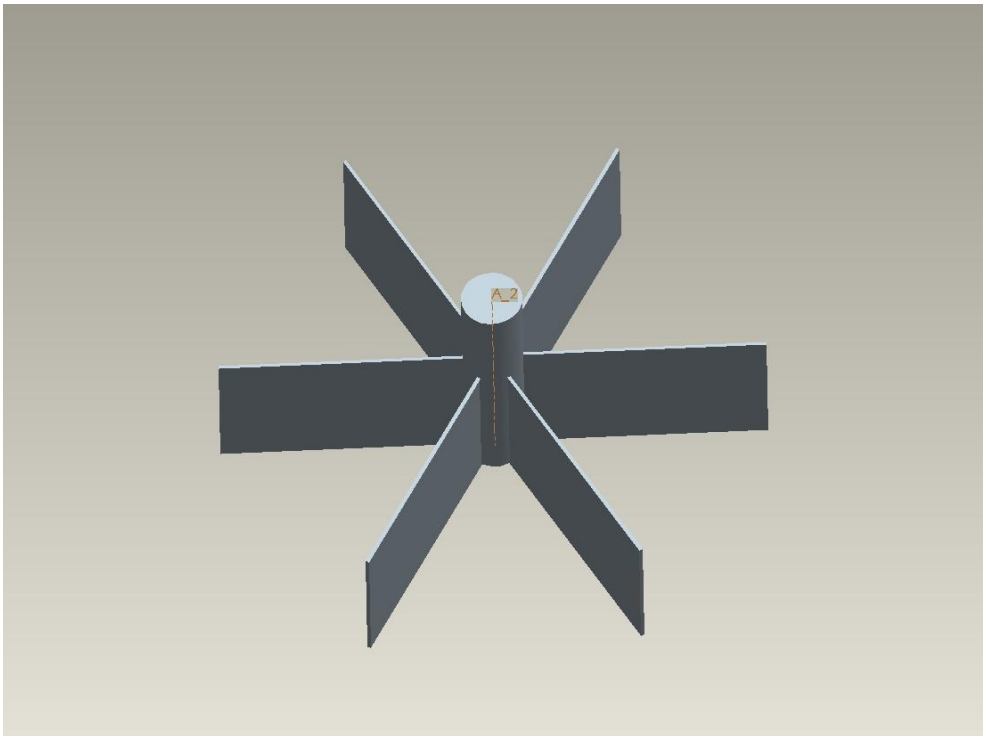

Figure 4. Paddle Impeller – 1

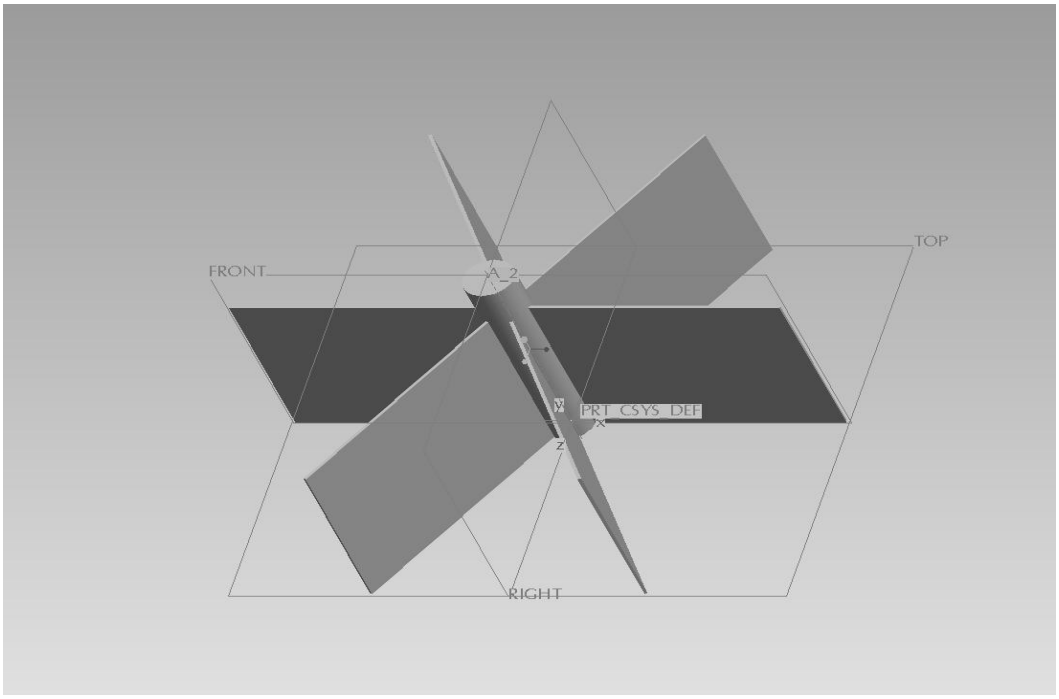

Figure 5. Paddle Impeller - 2

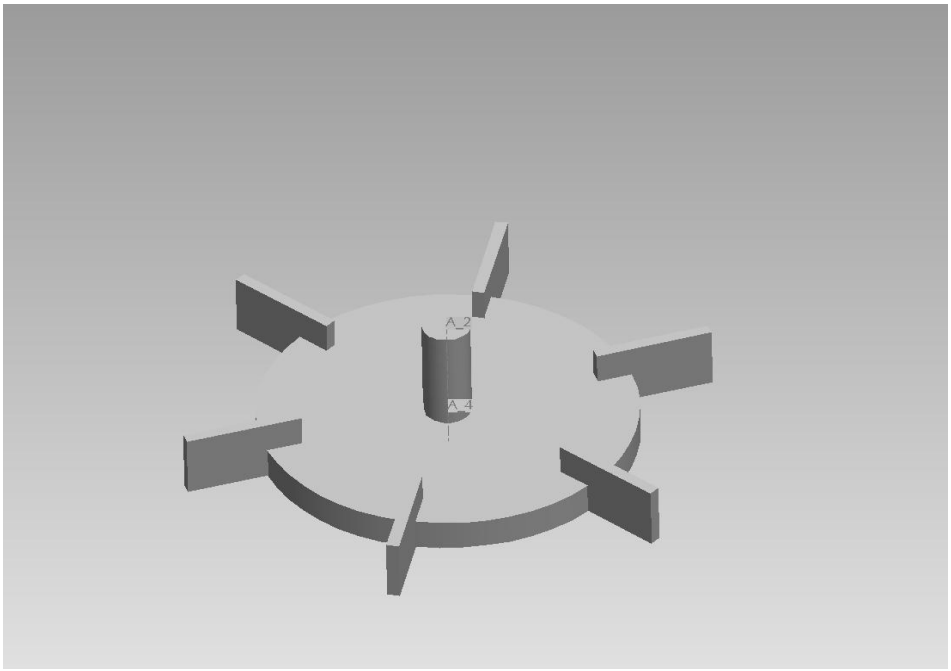

Figure 6. Turbine Impeller – 1

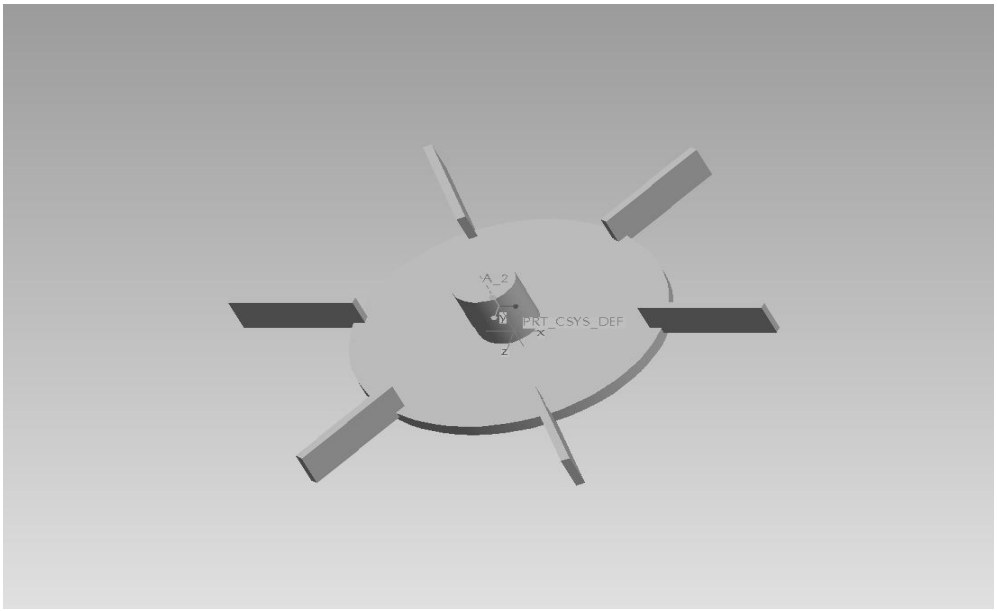

Figure 7. Turbine Impeller – 2

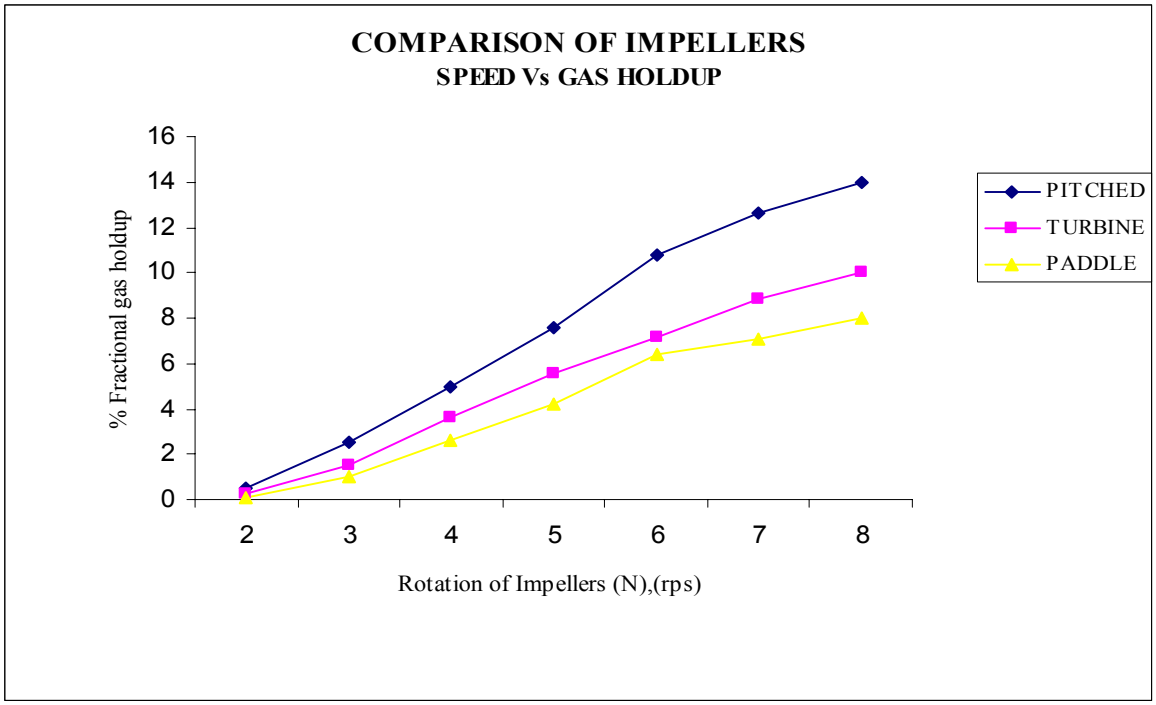

Figure 7. Comparison of Impellers – 1

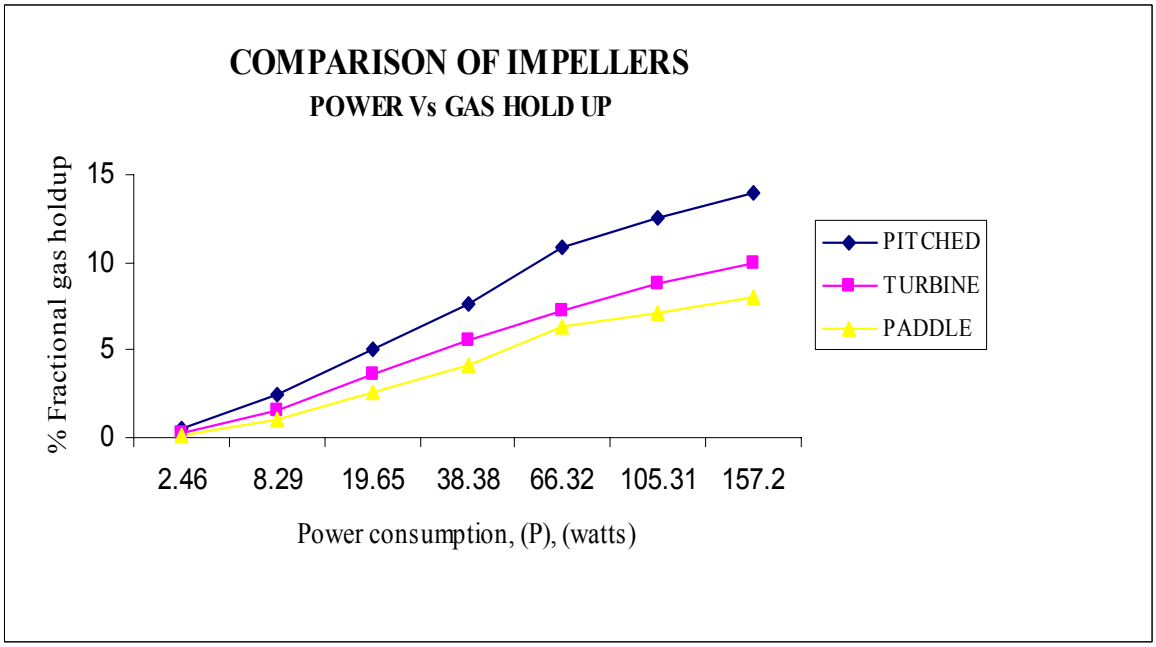

Figure 8. Comparison of Impellers - 2

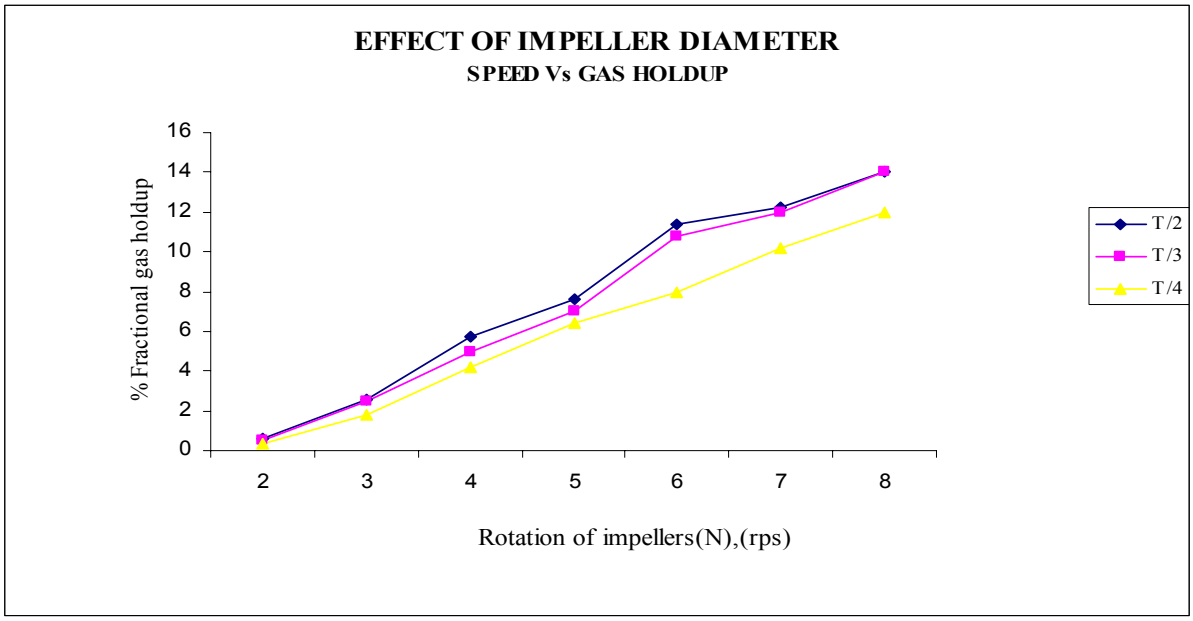

Figure 9. Effect of Impeller Diameter – 1

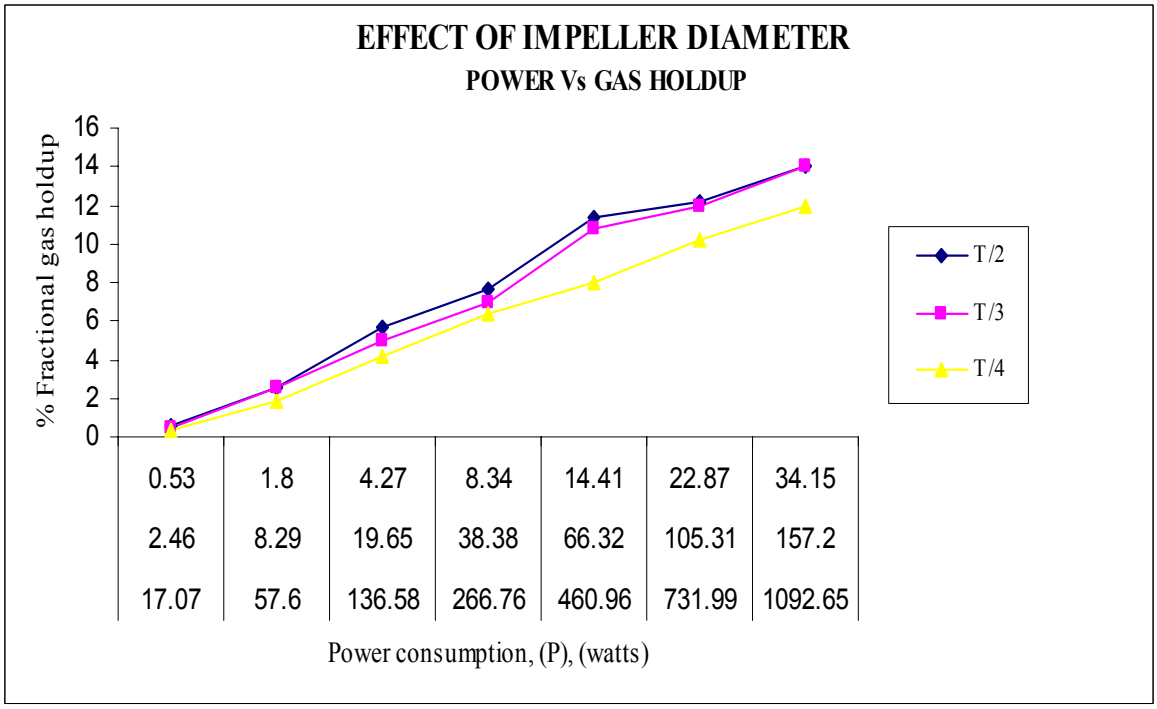

Figure 10. Effect of Impeller Diameter - 2

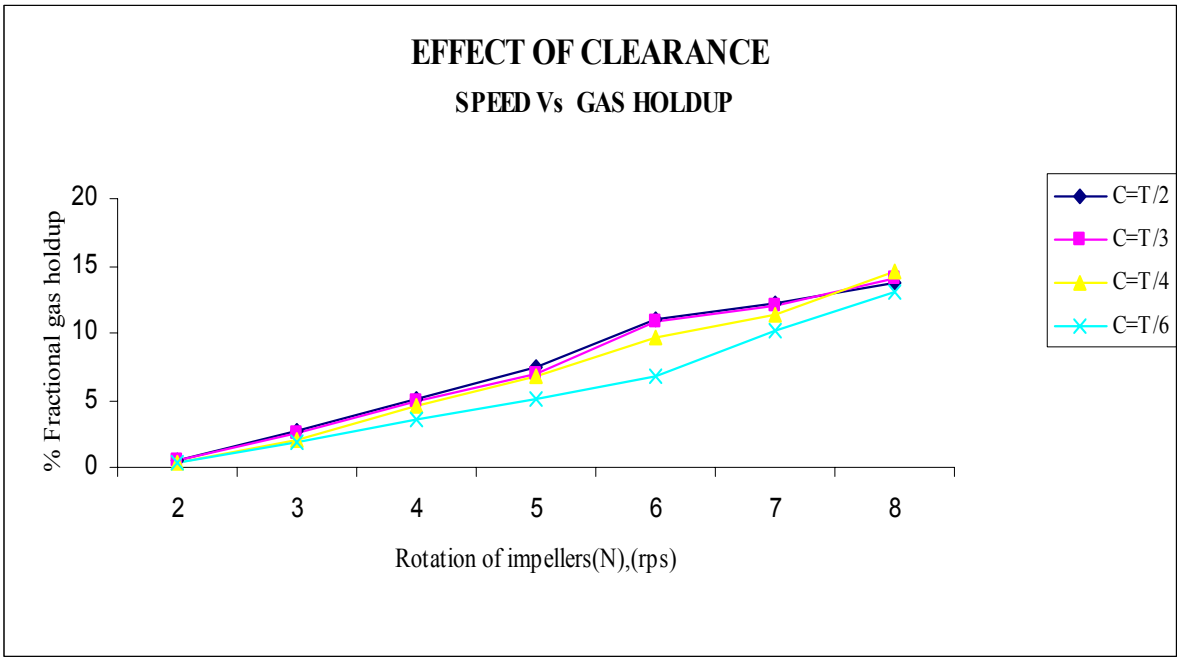

Figure 11. Effect of Clearance - 1

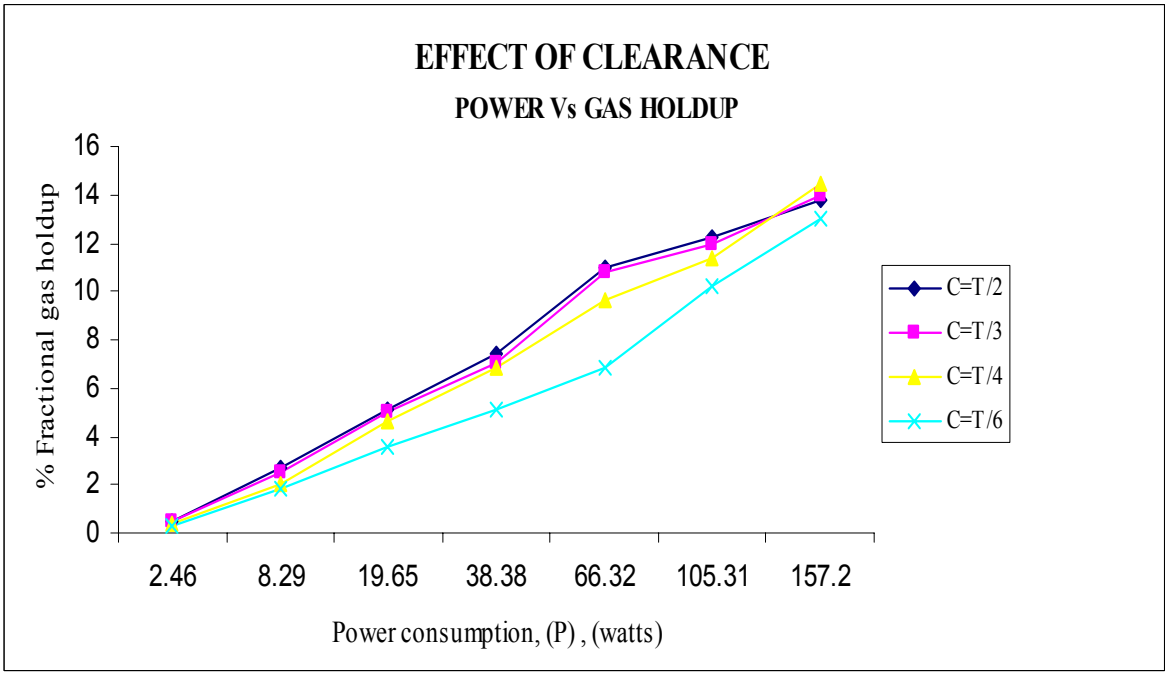

Figure 12. Effect of Clearance - 2

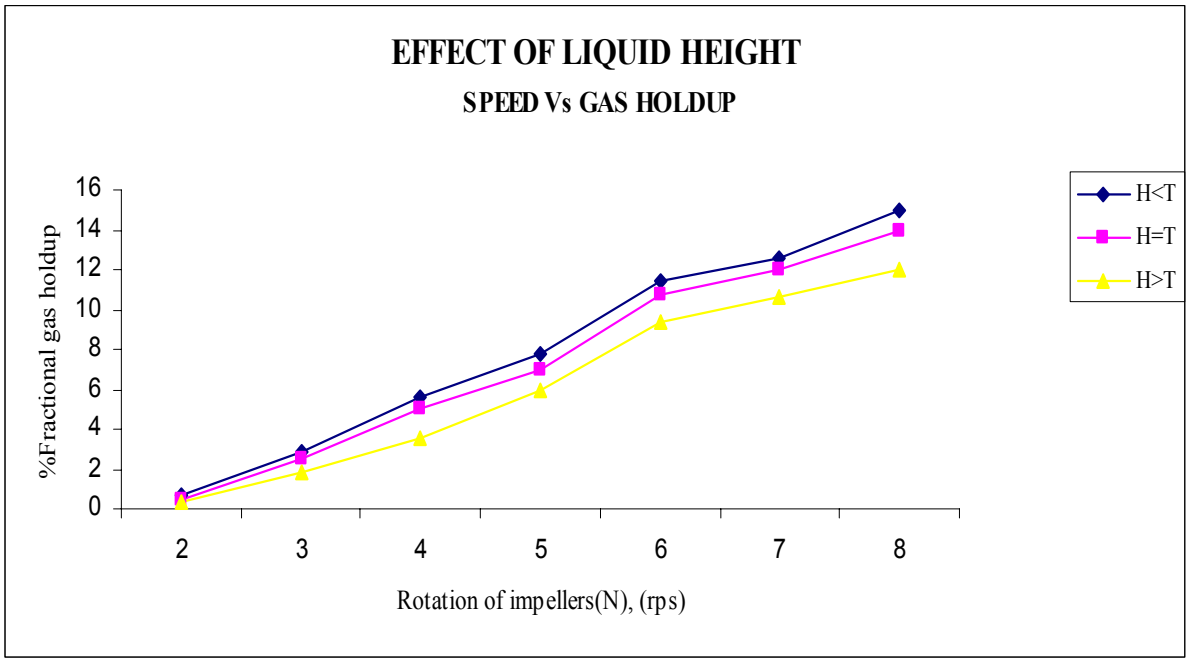

Figure 13. Effect of Liquid Height - 1

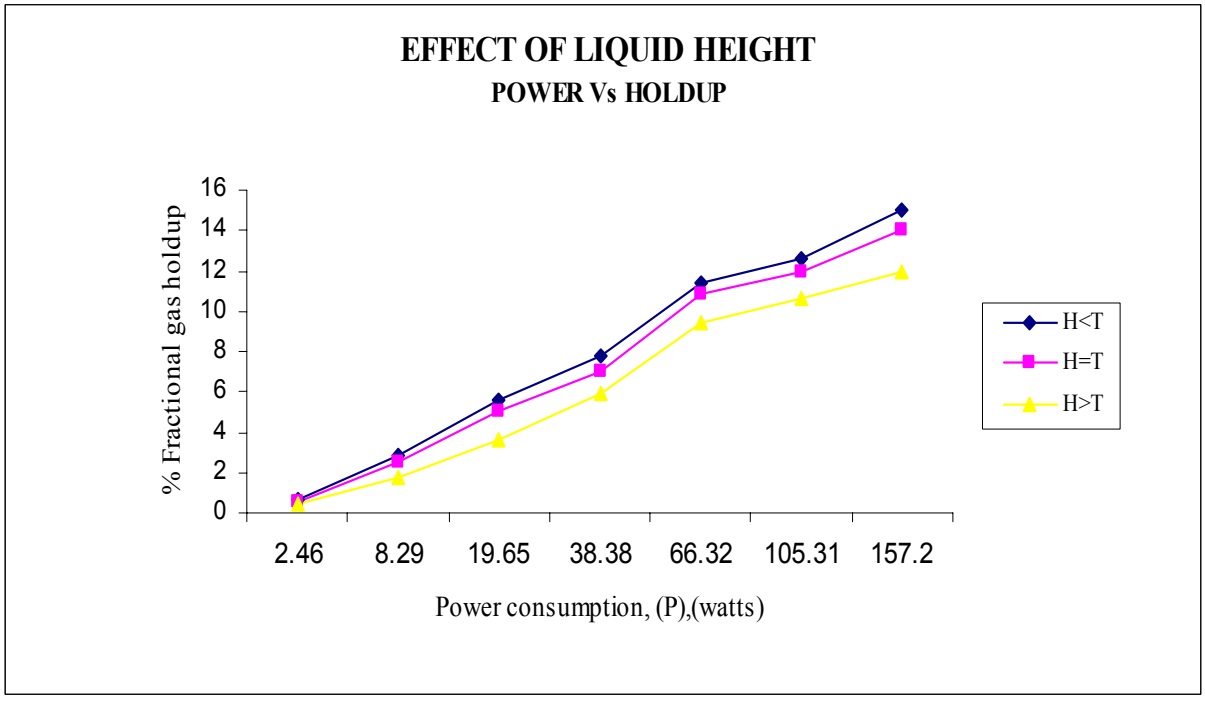

Figure 14. Effect of Liquid Height - 2

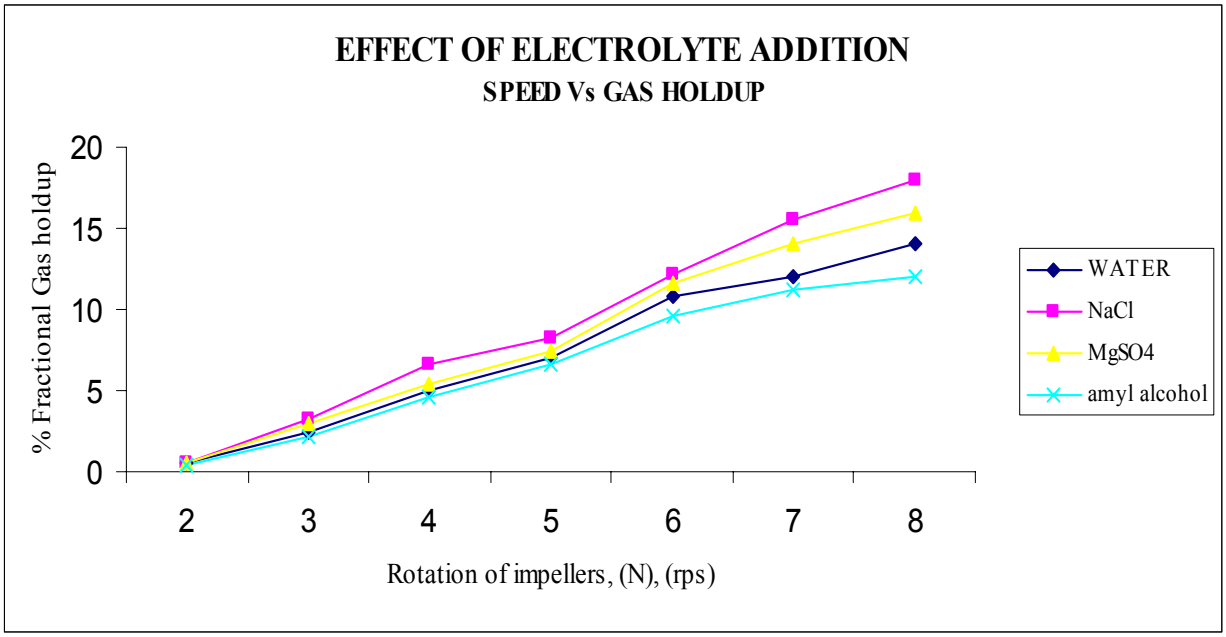

Figure 15. Effect of Electrolyte Addition – 1

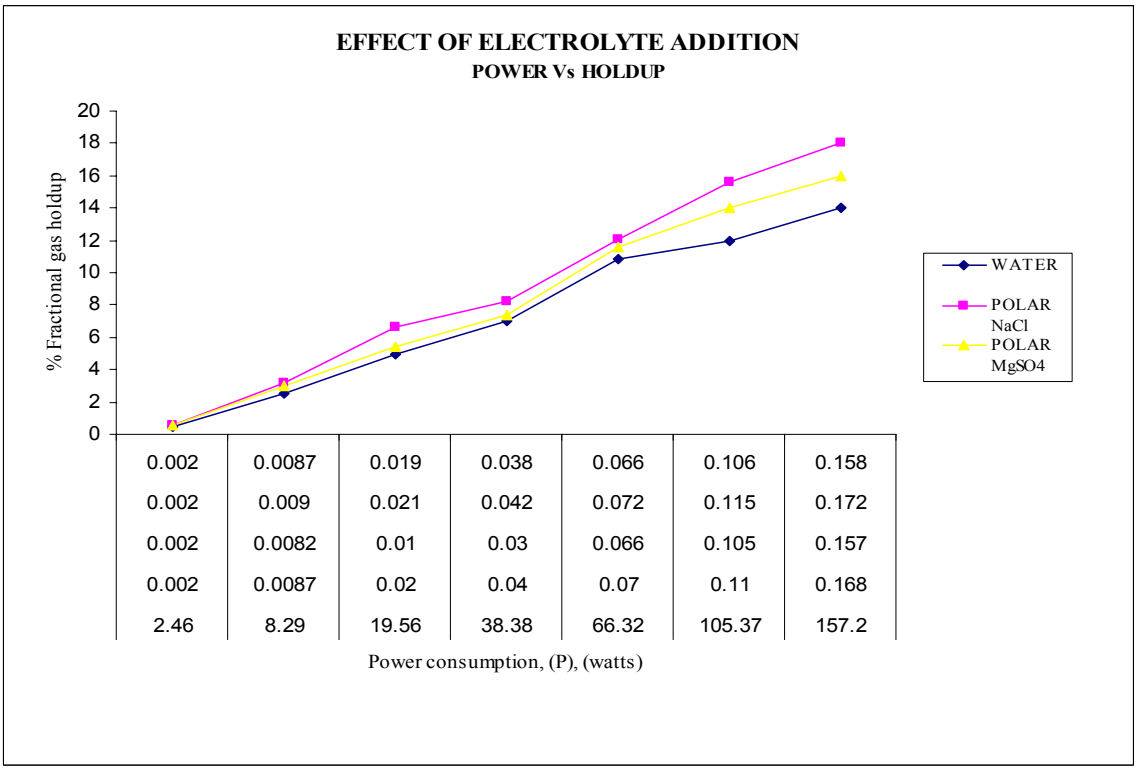

Figure 16. Effect of Electrolyte Addition – 2

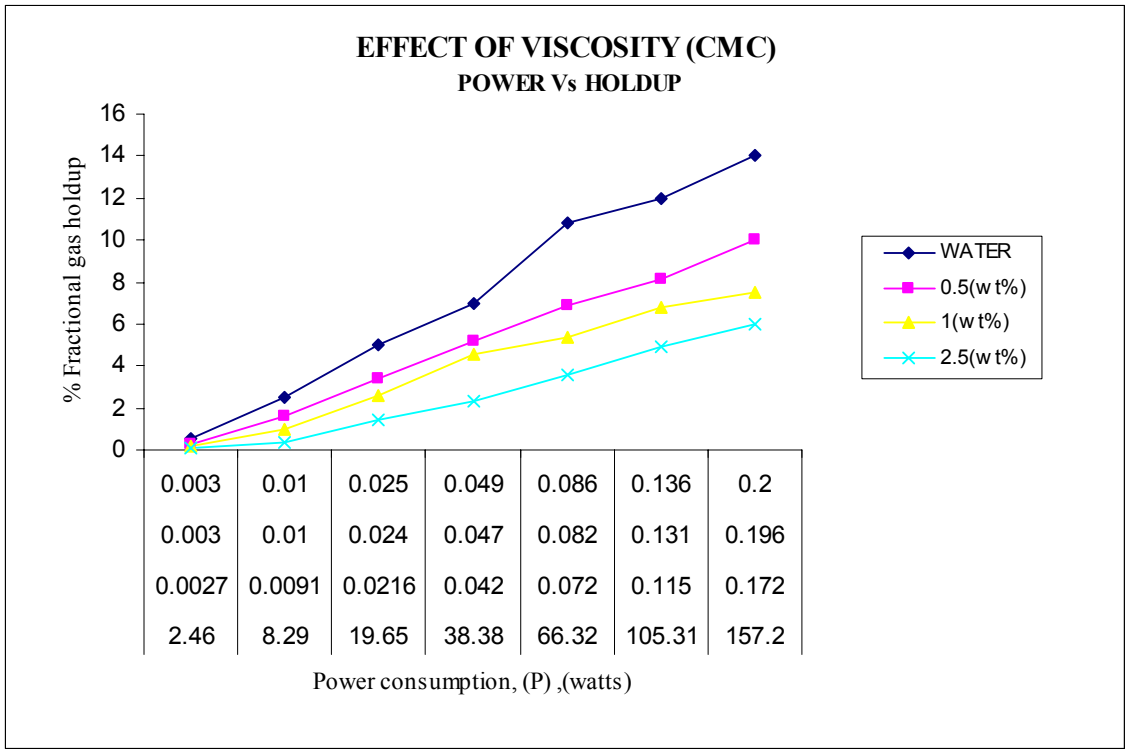

Figure 17. Effect of Viscosity (Carboxy Methyl Cellulose) – 1

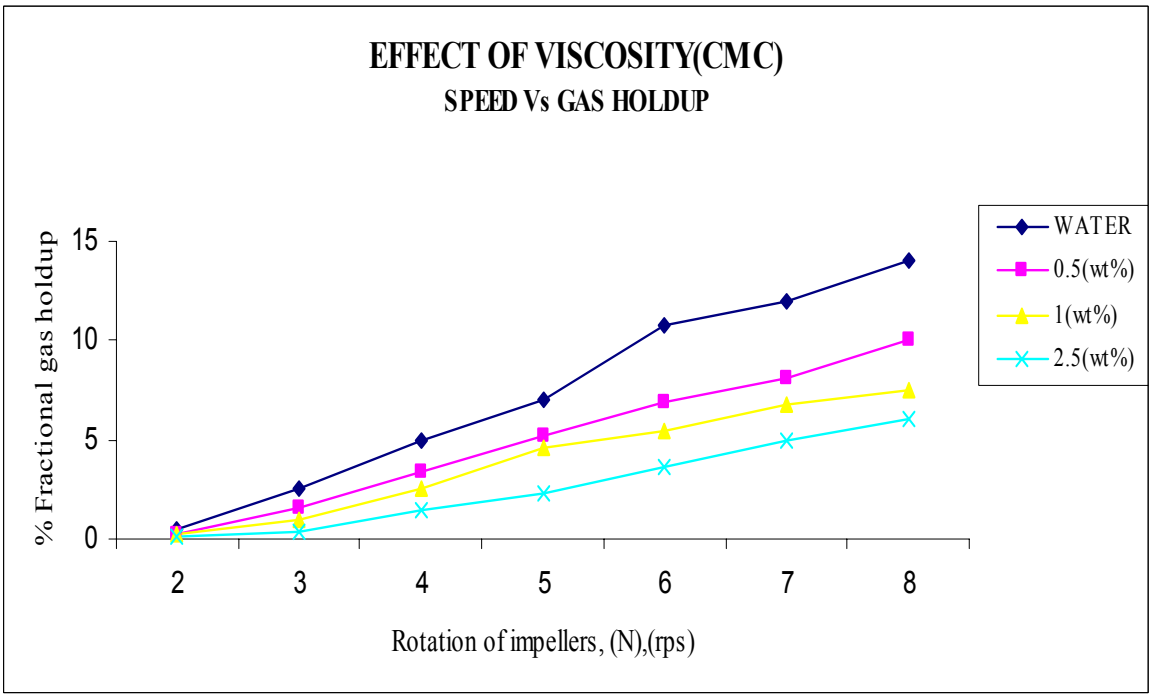

Figure 18. Effect of Viscosity (Carboxy Methyl Cellulose) - 2

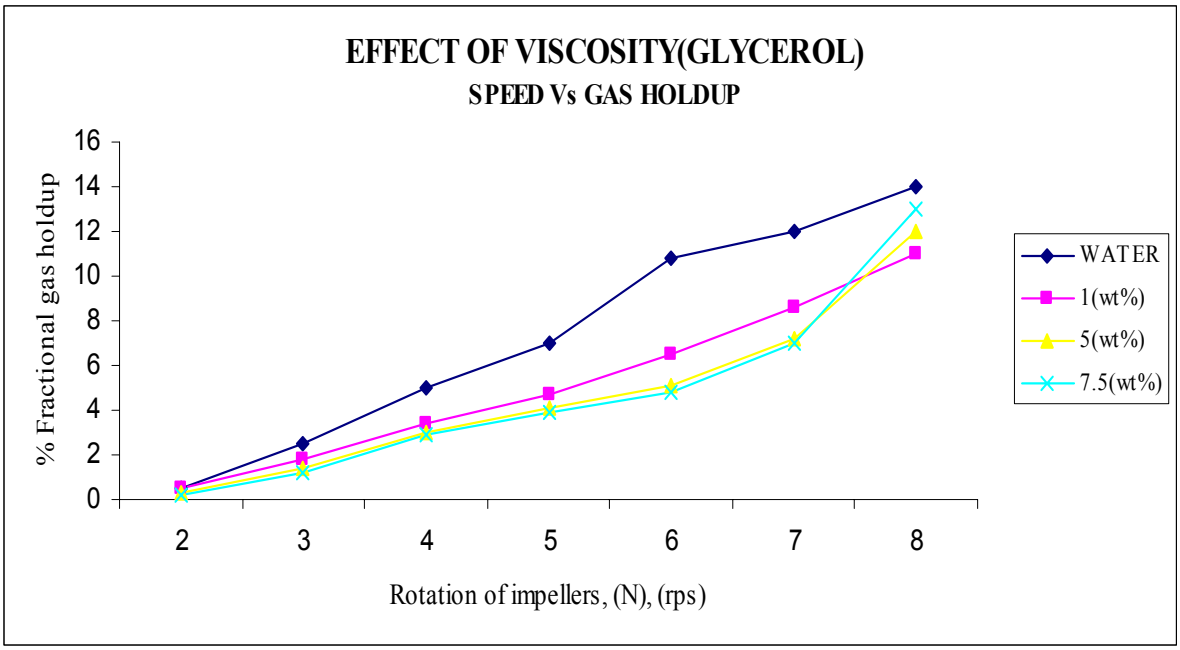

Figure 19. Effect of Viscosity (Glycerol) – 1

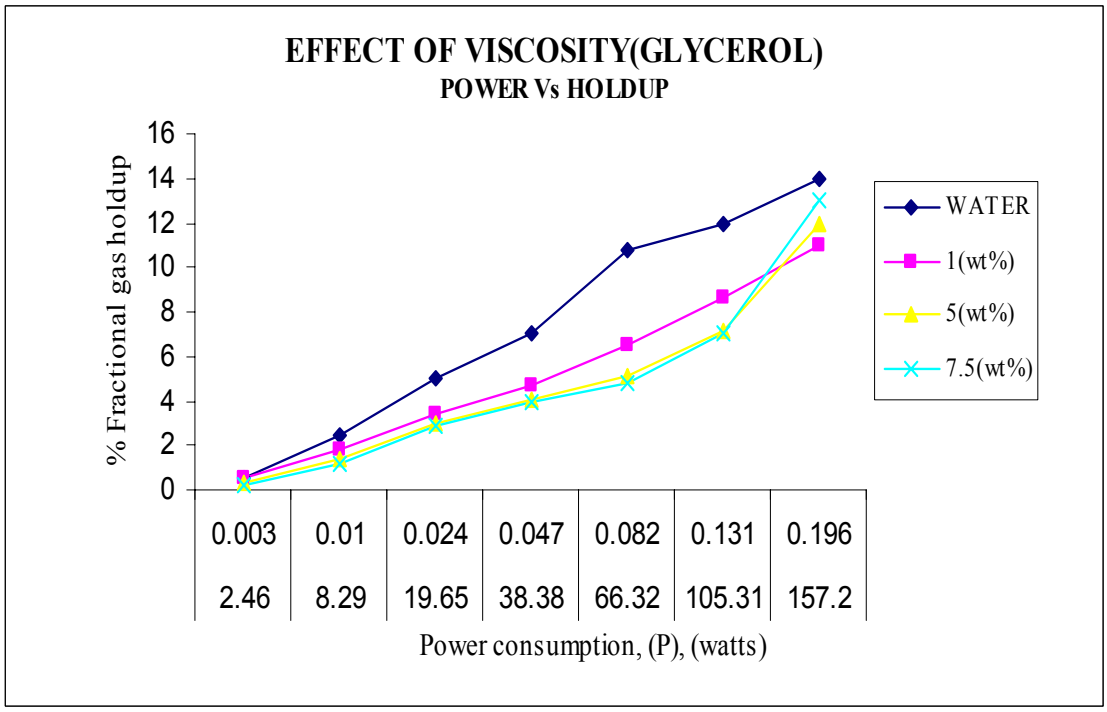

Figure 20. Effect of Viscosity (Glycerol) - 2

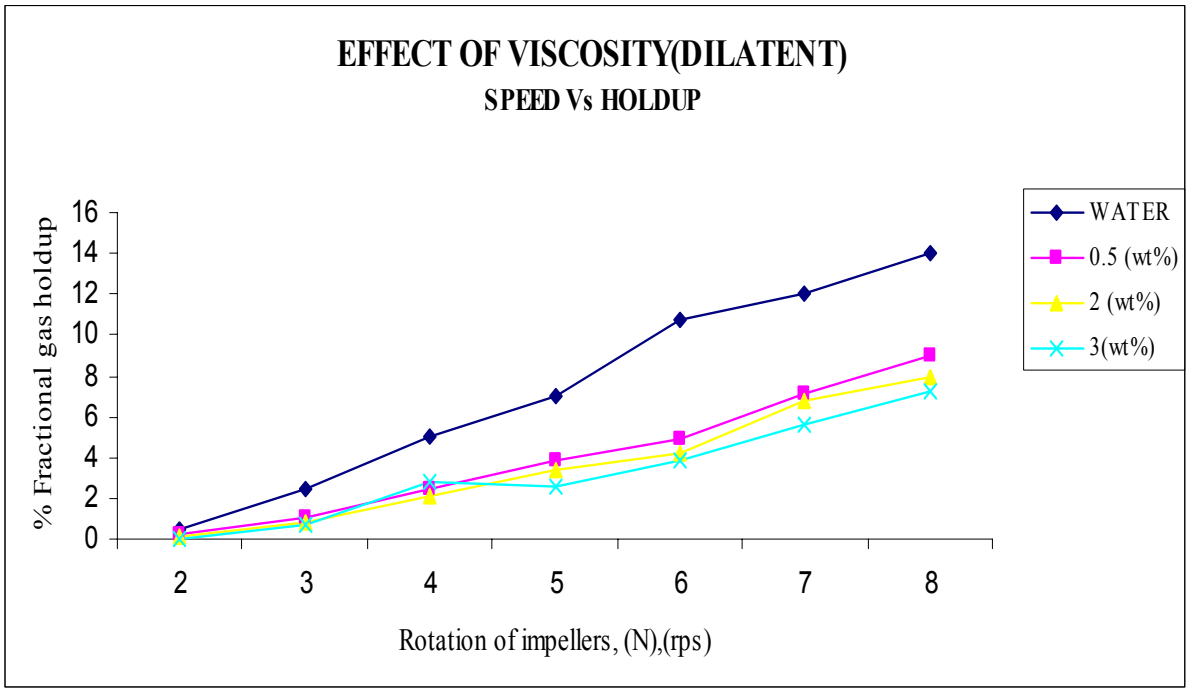

Figure 21. Effect of Viscosity (Dilatants)– 1

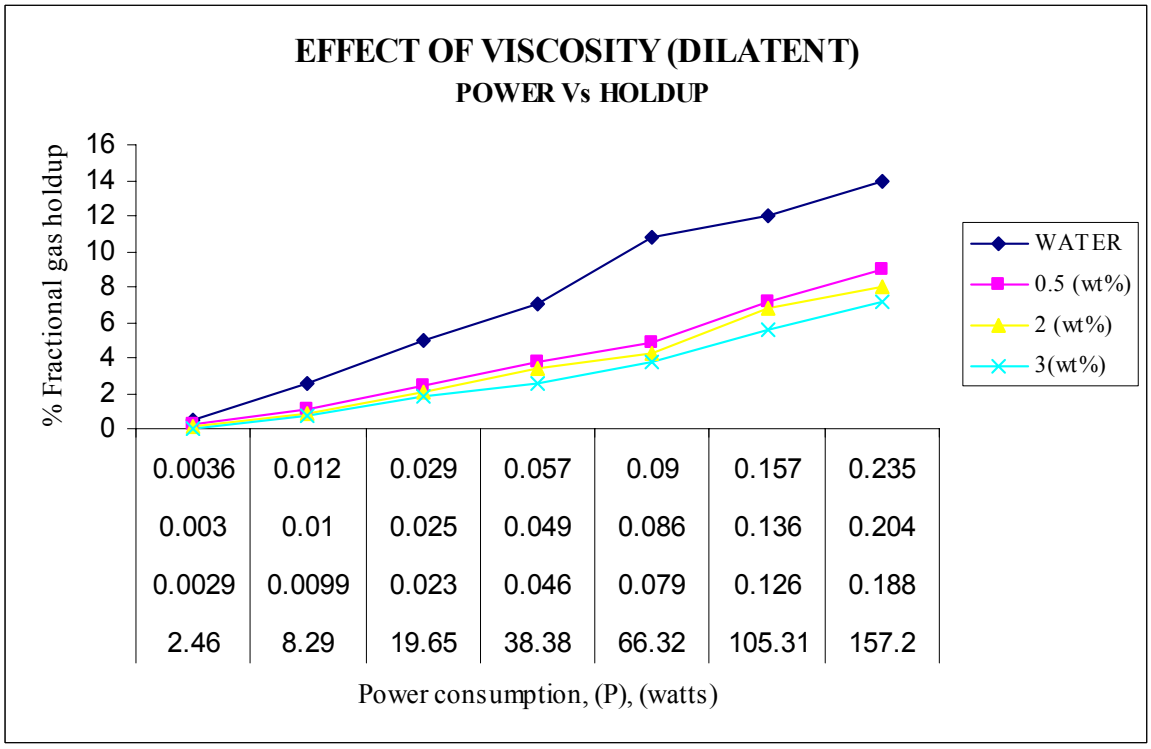

Figure 22. Effect of Viscosity (Dilatants) -2

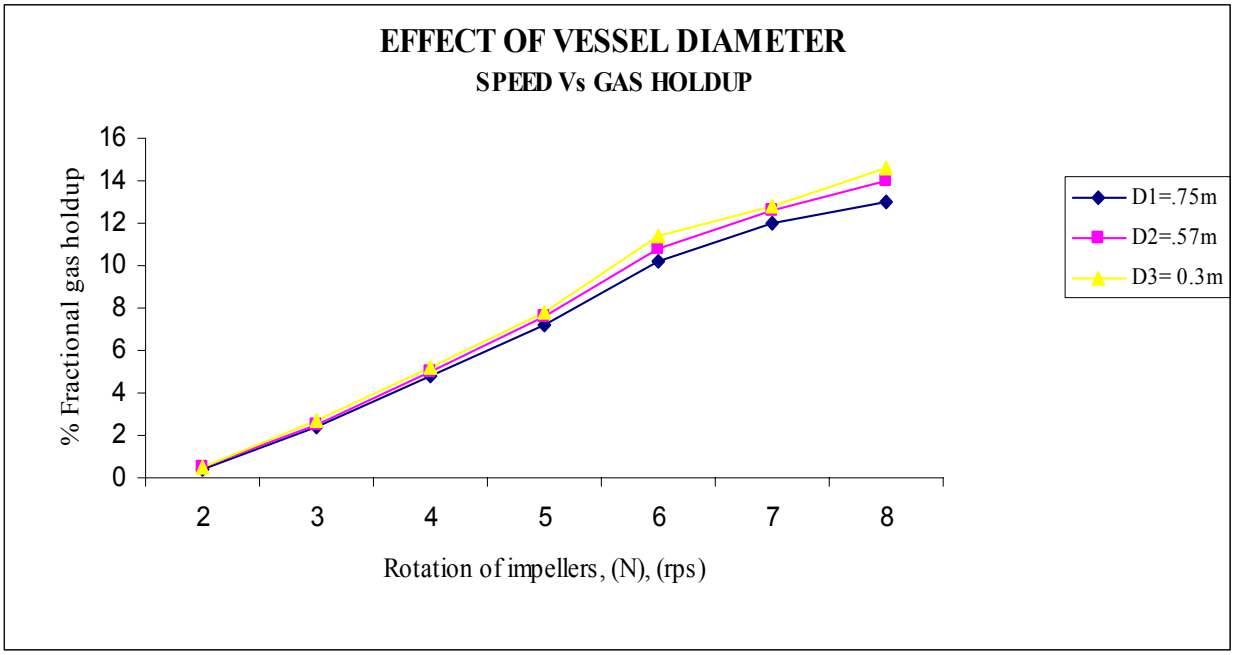

Figure 23. Effect of Vessel Diameter - 1

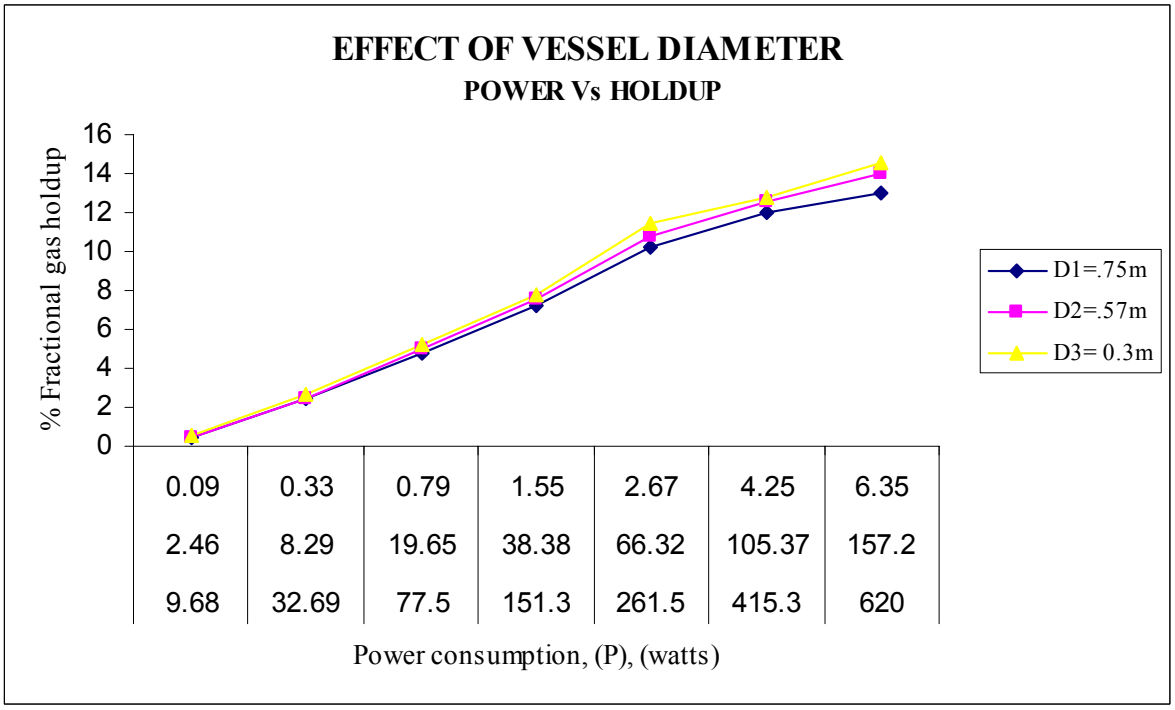

Figure 24. Effect of Vessel Diameter – 2

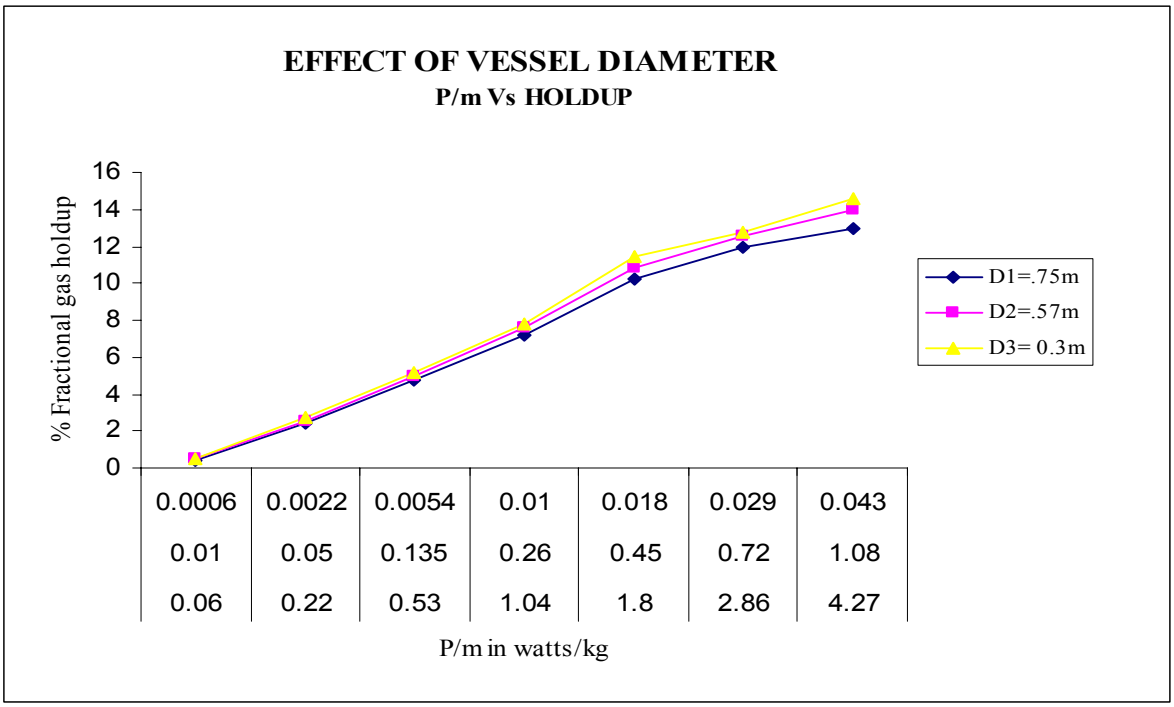

Figure 25. Effect of Vessel Diameter – 3

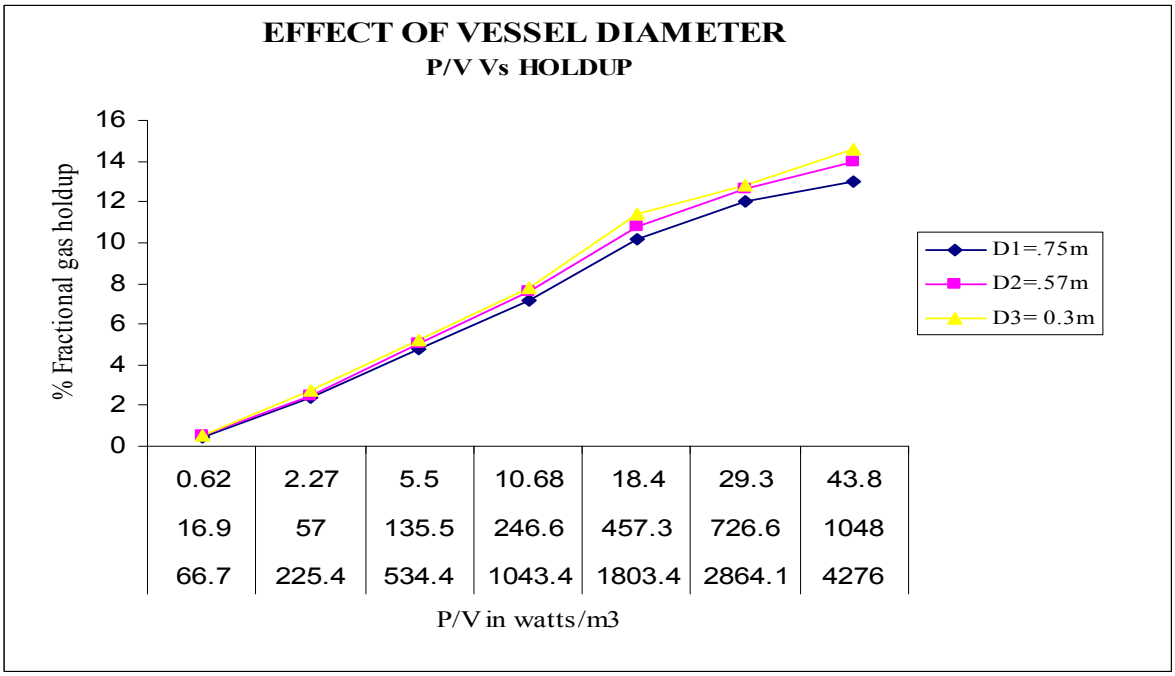

Figure 26. Effect of Vessel Diameter –4

Modern Applied Science

www.ccsenet.org/journal.html

Vol. 2, No. 5

September 2008

Adaptive Multicut Aggregation Method for Solving Two-stage Stochastic Convex Programming with Recourse

Jingsheng Liu(Corresponding author)

College of Information Science and Engineering

Shandong University of Science and Technology

579 Qian Wan Gang Street, Huangdao District, Qingdao 266510, China

E-mail:jingsheng2008@163.com

Changyin Zhou

College of Information Science and Engineering

Shandong University of Science and Technology

579 Qian Wan Gang Street, Huangdao District, Qingdao 266510, China

E-mail: zhoucy@sdust.edu.cn

Xiuping Zhang

College of Information Science and Engineering

Shandong University of Science and Technology

579 Qian Wan Gang Street, Huangdao District, Qingdao 266510, China

E-mail: pingxiu8384@163.com

Abstract

In this paper we extend directly adaptive multicut aggregation method of Svyatoslav Trukhanov, Lewis Ntaimo and Andrew Schaefer to solving two-stage problems of stochastic convex programming. The implement of the algorithm is simple, so less computation work is needed. The algorithm has certain convergence.

Keywords: Multicut aggregation, Adaptive cut, Stochastic programming, Stochastic convex programming

1. Introduction

(Birge, J. R. & Louveaux, F. V.,1997)L-shaped algorithm for stochastic programming problems with recourse generally generate a single cut at each major iteration. While(Ruszczynski, A. & Shapiro, A.,2004) the multicut version of the algorithm allows for cuts up to the number of outcomes to be placed at once. So the L-shaped algorithm tends to have more major iterations than the multicut algorithm, however the multicut algorithm have more optimality cuts, the size of master problem relatively big. To settle the disadvantage of L-shaped algorithm and multicut algorithm, Svyatoslav Trukhanov, Lewis Ntaimo and Andrew Schaefer (Trukhanov, S.,Ntaimo, L., & Schaefer, A.,2007) have proposed the adaptive multicut aggregation algorithm for solving two stage stochastic linear programming with recourse. The computational results of the algorithm shows that the algorithm is more effective than L-shaped algorithm and multicut algorithm.

Two-stage problems of stochastic convex programming are difficult for solving. For solving they are transformed into problems of linear programming by linearization, but the size of the problems is greatly increased, the problems are difficult to solve. In this paper we extend directly adaptive multicut aggregation method for solving two-stage stochastic linear programming problems to two-stage stochastic convex programming with recourse. The method is simple and has certain convergence.

2. Two-Stage Stochastic Convex Programming

A two-stage stochastic convex programming with fixed recourse in the extensive form can be given as follow:

$$\min_{x\in X}\left\{ f(x) := f_1(x) + \sum_{s=1}^{S} p_s Q^s(x)\right\} \tag{1}$$

Where

$$Q^s(x) = \min_{y\in Y^s} f_2^s(x) \tag{2}$$

$$\text{s.t. } T^s x + Wy = h^s$$

$$y \in Y^s$$

Where s is the scenario(outcome). $f_1(x): R^{n_1} \to R$ and $f_2^s(x): R^{n_2} \to R, s = 1,2,3\cdots S$,are convex functions. X and Y^s are bounded convex sets. $T^s = T(s)$ is $m_2 \times n_1$ matrix, W is $m_2 \times n_2$ matrix, $h^s = h(s), h^s$ is m_2 vector.

3. Adaptive Multicut Aggregation Method

The adaptive multicut aggregation method (Trukhanov, S.,Ntaimo, L., & Schaefer, A.,2007) has point out that this method has two advantages comparing L-shaped algorithm and multicut algorithm. First, it use more information from subproblems, which assumes adding more than one cut at each major iteration avoiding 'information loss'; Second ,it can keep the size of master problem relatively small, which requires to limit the number of cuts added to master problem. The adaptive multicut aggregation method is required to partition the sample space S into D aggregates $\{S_d\}_{d=1}^{D}$, such that $S = S_1 \bigcup S_2 \bigcup \cdots \bigcup S_D$, $\forall i \neq j, S_i \bigcap S_j = \varnothing$. The sample space S can be partitioned into some subsets based on some aggregation rules. So each subset can generate a optimality cut, and it introduce D different optimality variables θ_d.

At the k-th iteration, let the scenario set partition be $S(k) = \{S_1, S_2, \cdots S_{L_k}\}$,where the set $S_i, i = 1,2,\cdots L_k$, are disjoint, that is $\forall i \neq j, S_i \bigcap S_j = \varnothing$ and $\bigcup_{i=1}^{L_k} S_i = S$. Let $F(k)$ denote the set of iteration numbers up to k where all subproblems are feasible and optimality cuts are generated .The optimality cut at k-th iteration has following form:

$$\bar{\alpha}_d^t + \left(\bar{g}_d^t\right)^T x \le \theta_d, t \in F(k), d \in S(k) \tag{3}$$

Where $\bar{\alpha}_d^t, \bar{g}_d^t$ is defined in (14). Then the method generated $|S(k)|$(the number of element in $S(k)$) different optimality cuts. If for every $d \in S(k)$, the following formula hold:

$$\bar{\alpha}_d^t + \left(\bar{g}_d^t\right)^T x^k \ge \theta_d, t \in F(k), d \in S(k) \tag{4}$$

the algorithm stop, x^k is optimal, otherwise the algorithm add optimality cut like (3) to the master problem.

At each iteration, the number of aggregation D must satisfy $1 < D < |S(k)|$. The master problem will have 'adaptive' optimality variables θ_d, that is ,the number of optimality variables will change during the course of the algorithm. The goal is to let the algorithm use more information and then settle for a level of aggregation that tends to faster convergence to the optimal solution. Svyatoslav Trukhanov, Lewis Ntaimo and Andrew Schaefer (Trukhanov, S., Ntaimo, L., & Schaefer, A.,2007) has proposed the redundancy threshold $\delta\ (0 < \delta < 1)$to be a aggregation rule. In the master problem, if the optimality cuts contain 'little' information about the optimal solution, then these cuts are inactive. These inactive optimality cuts can be aggregated into one cut without information loss. Conside some iteration k after solving the master problem for some aggregate $d \in S(k)$, let f_d be the number of iterations when optimality cuts corresponding to d are redundant. If $\frac{f_d}{|F(k)|} > \delta$, then all d are combined to form one aggregate, and there is a new optimality cut generated in the next iteration. As a supplement to the redundancy threshold, a bound on the minimum and maximum number of aggregation $|S(k)|$ should be imposed. This prevents the algorithm leading to the L-shaped algorithm (highest level of cut aggregation) and multicut algorithm(no cut aggregation).

4. description of the algorithm

4.1 the master problem

For $S_i \in S(k) = \{S_1, S_2, \cdots S_{L_k}\}$, the aggregation probability of S_i is defined as $p_{S_i} = \sum_{s\in S_i} p_s$ with $\sum_{i=1}^{L_k} p_{S_i} = \sum_{s\in S} p_s = 1$. Then the master problem has the following form:

$$\min \sum_{d \in S(k)} \theta_d \tag{5a}$$

$$\text{s.t.} \quad \overline{\alpha}_d^j + \left(\overline{\beta}_d^j\right)^T x \le \theta_d, j \in F(k), d \in S(k) \tag{5b}$$

$$\beta^{j,s} + \left(\gamma^{j,s}\right)^T x \le 0, j \in \{1, \cdots k\} \setminus F(k), s \in S \tag{5c}$$

$$x \in X \tag{5d}$$

Where (5b) is the optimality cut, (5c) is the feasibility cut.

4.2 feasibility cut

The method of getting feasibility cut is the same as one for stochastic linear programming(Ruszczynski, A., & Shapiro, A.,2004).

Solving following programming:

$$\min_{y,z} \|z\| \tag{6}$$

$$\text{s.t.} \quad Wy + z = h^s - T^s x$$

$$y \in Y^s$$

Where z is the artificial variable, $\|\cdot\|$ is a norm on the space R^{m_2}.Let $U^s(x)$ be the optimal of problem (6).If $U^s(x^k) = 0$, $\forall s \in S$,then x^k is the feasible point of problem (2),otherwise feasibility cut like (5c) is generated $\beta^{k,s} + \left(\gamma^{k,s}\right)^T x \le 0$,

$$\text{where} \quad \begin{cases} \gamma^{k,s} \in \partial U^s(x^k) \\ \beta^{k,s} = U^s(x^k) - (\gamma^{k,s})^T x^k \end{cases} \tag{7}$$

$$\text{and} \quad U^s(x) \ge U^s(x^k) + (\gamma^{k,s})^T (x - x^k) = \beta^{k,s} + \left(\gamma^{k,s}\right)^T x \tag{8}$$

4.3 optimality cut

Solving the subproblem (2), let π_s^k be the dual multipliers associated with an optimal solution of problem (2).then calculate:

$$\begin{cases} g^{k,s} = -\left(T^s\right)^T \pi_s^k \\ \alpha^{k,s} = \left(h^s\right)^T \pi_s^k \end{cases} \tag{9}$$

For $f_1(x)$ the optimality cut at x^k is

$$f_1(x) \ge \alpha^{k,0} + \left(g^{k,0}\right)^T x \tag{10}$$

$$\text{where} \quad \begin{cases} g^{k,0} \in \partial f_1(x^k) \\ \alpha^{k,0} = f_1(x^k) - \left(g^{k,0}\right)^T x^k \end{cases} \tag{11}$$

So for $f(x)$ the optimality cut at x^k is:

$$f^s(x) \ge \overline{\alpha}^{k,s} + \left(\overline{g}^{k,s}\right)^T x \tag{12}$$

$$\text{where} \quad \begin{cases} \overline{g}^{k,s} = g^{k,0} + g^{k,s} \\ \overline{\alpha}^{k,s} = \alpha^{k,0} + \alpha^{k,s} \end{cases} \tag{13}$$

4.4 Update Cut Aggregation Level

Generate aggregation $S(k)$ using $S(k-1)$ based on some aggregation rules, each element of $S(k)$ is a union of some elements from $S(k-1)$.For example , $d_1, d_2, \cdots d_j \in S(k-1)$ are aggregated into $\overline{d}$, $d \in S(k)$,then $d = \bigcup_{i=1}^{j} d_j$

and $p_d = \sum_{i=1}^{j} p_{d_j}$,Master problem will be modified by removing variables $\theta_{d_1} \cdots \theta_{d_j}$ and introducing the new one θ_d .For each major iteration ,the optimality cut is updated as following:

$$\begin{cases} \overline{g}_d^t = p_d \sum_{i=1}^{j} \left(1/p_{d_i}\right) \overline{g}_{d_i}^t, \forall d \in S(k), t \in F(k) \\ \overline{\alpha}_d^t = p_d \sum_{i=1}^{j} \left(1/p_{d_i}\right) \overline{\alpha}_{d_i}^t, \forall d \in S(k), t \in F(k) \end{cases} \tag{14}$$

where

$$\begin{cases} \overline{g}_{d_i}^t = \sum_{s \in S_{d_i}} p_s \overline{g}^{t,s} \\ \overline{\alpha}_{d_i}^t = \sum_{s \in S_{d_i}} p_s \overline{\alpha}^{t,s} \end{cases} \tag{15}$$

With above formula, a new aggregation optimality cut is generated:

$$\overline{\alpha}_d^t + \left(\overline{g}_d^t\right)^T x \le \theta_d, t \in F(k), d \in S(k) \tag{16}$$

5. Algorithm

Step0: Let $k = 0, F(0) = \phi$, initialize $S(0), \theta_i = -\infty, i \in S(0)$;

Step1: For every $s \in S$, solve subproblem (6) at $x = x^k$:

(a) if $U^s(x^k) = 0$,construct the optimality cut (12.);

(b) if $U^s(x^k) > 0$, construct the feasibility cut (8);

Step2: Generate $S(k)$ using $S(k-1)$ based on some aggregation rules, construct aggregation optimality cut (16) ;

Step3: if $f(x^k) = \sum_{d=1}^{|S(k)|} p_d \theta_d$, $\sum_{d=1}^{|S(k)|} p_d \theta_d = \theta^k$ stop, otherwise $F(k) = F(k-1) \bigcup \{k\}$, continue;

Step4: Solve the master problem (5),if it is infeasible, stop, otherwise denote by $\left(x^{k+1}, \theta^{k+1}\right)$ it's solution, $k = k+1$,and go to step1;

6. convergence of the algorithm

Assumption: There exists a constant C such that $\left\|\overline{g}_d^k\right\| \le C$, for all $k = 1, 2, \cdots$ and $d \in S(k)$.

Lemma 1(Ruszczynski, A., & Shapiro, A.,2004): For every $s \in S$, the number of iterations for which $U^s(x^k) > 0$ is finite.

Theorem 1: If problem (1) has no feasible solutions the algorithm will stop at step4 after finitely many iterations; If problem (2) has feasible solutions then the method either stops at stop3 at an optimal solution or generates a sequence of point $\left\{x^k\right\}$,such that $\lim_{k \to +\infty} f(x^k) = f^*$ (f^* is the optimal of problem (1)).

Proof: Since the master problem is a relaxation of (1), if the method stops at step4, the original problem is infeasible. Also, It always have $\theta^k \le f^*$, so the method can stop at step3 only if x^k is optimal. It remains to analyze the case of infinitely many steps.

The construction and the use of feasibility cuts is the same as in the linear case. By lemma1 It is true that if the problem has no feasible solutions, the method will discover this after finitely many iterations. Moreover, if feasible points exist and the method does not stop at an optimal solution, It must have $f(x^k) < +\infty$ for all sufficiently large k .

For $\varepsilon > 0$ define $K_\varepsilon = \left\{k : f^* + \varepsilon < f(x^k) < +\infty\right\}$ .Let $k_1, k_2 \in K_\varepsilon$ with $k_1 < k_2$.

Since $f(x^{k_1}) > f^* + \varepsilon$ and $f^* \ge \theta^{k_1}$ there will be many new optimality cuts at x^{k_1} . It will be in the master from k_1 on, so it has to be satisfied at x^{k_2} :

$$f(x^{k_1}) + \left(\sum_{d \in S(k_1)} \overline{g}_d^{k_1}\right)^T (x^{k_2} - x^{k_1}) \le \theta^{k_2} \le f^* \tag{17}$$

On the other hand $\varepsilon < f(x^{k_2}) - f^*$ (18)

By (17) and (18), It must have the following formula :

$$\varepsilon < f(x^{k_2}) - f(x^{k_1}) - \left(\sum_{d \in S(k_1)} \bar{g}_d^{k_1} \right)^T (x^{k_2} - x^{k_1}) \tag{19}$$

The function $f(x)$ is subdifferentiable in its domain and X is compact, so there is a constant C such that $f(x_1) - f(x_2) \le C\|x_1 - x_2\|$, for all $x_1, x_2 \in domf(x) \cap X$ .By assumption, a C big enough can be chose so that $\left\|\bar{g}_d^k\right\| \le C$ for all k . It follows that

$$\varepsilon < \left(|S(k_1)| + 1\right) C \left\|x^{k_1} - x^{k_2}\right\| \quad \text{for all } k_1, k_2 \in K_\varepsilon \tag{21}$$

Since the set X is compact, (21) implies that the set K_ε is finite for each $\varepsilon > 0$, then $\lim_{k \to +\infty} f(x^k) = f^*$.

7. Summary

This paper extend directly adaptive multicut aggregation method for solving two-stage stochastic linear programming with recourse to solving two stage problems of stochastic convex programming with recourse. The algorithm of the method is exactly described and its convergence proof is given. In the future, more work should be done to find the effective aggregation rules and apply for multi-stage stochastic programming.

References

Birge,J.R.,&Louveaux,F.V.(1997). Introduction to Stochastic Programming. Springe-Verlag, (chapter2).

Ruszczynski, A. & Shapiro, A.(2004). Stochastic programming. Handbooks in operations research and management science 10. Elsevier Science, (chapter3).

Trukhanov, S.,Ntaimo, L., & Schaefer, A.(2007). On Adaptive Multicut Aggregation for Two-Stage Stochastic Linear Programs with Recourse.[online] Available: http://www.optimization-online.org/ DB_HTML/2007/11/1849.html (Novenmber, 2007).

Van Slyke, R., & Wets, R. B. (1969). L-shaped linear programs with application to optimal control and stochastic programming. SIAM Journal on Applied Mathematics, 17, 638–663.

Higle, J., & Zhao, L.(2007). Adaptive and nonadaptive samples in solving stochastic linear programs Computational investigation, Submitted to Computational Optimization and Applications.

Higle, J., & Sen, S.(1991). Stochastic decomposition: An algorithm for two-stage stochastic linear programs with recourse. Mathematics of Operational Research, 16, 650–669.

Birge, J.(1985). Aggregation bounds in stochastic linear programming. Mathematical Programming, 31, 25–41.

Modern Applied Science

www.ccsenet.org/journal.html

Vol. 2, No. 5

September 2008

Research Progress in Prevention and Cure of Fibrosis by Traditional Chinese Medicine

Yiwen Ma

Hospital of Qingdao Technological University

Qingdao 266033, China

Ruixia Kang

Department of Stomatology

Qingdao Eighth People's Hospital

Qingdao 266100, China

Xiaoli Liu

308 National Road Community Health Service Station in Fushan Road of Licang-District

Qingdao 266100, China

Abstract

The development of study on traditional Chinese medicine has seen considerable progress in the prevention and cure of fibrosis by Chinese herbs. Further elucidation on the pathogenesis of fibrosis will be helpful for the study on anti-fibrosis traditional Chinese medicine and medicine selection. Traditional Chinese medicine has the advantage of achieving multiple targets with one dose. And the multiplicity can be enhanced by finding among natural materials activated monomer that has specific pharmacological effect, by elucidating the mechanism of different monomers and effective target positions, and by treating fibrosis according to its multi-facetedness. This paper is a review of major literature produced in the past ten years concerning the anti-fibrosis mechanism of traditional Chinese medicine.

Keywords: Traditional Chinese medicine, Fibrosis, Review

Fibrosis is a slow but dynamic process involving the mutual interaction and mutual regulation of cells, extracellular matrix, cellular factors, and vasoactive substances. Fibrosis may happen in several organs or tissues. The main pathological process of fibrosis includes two aspects: (1) the migration and proliferation of fibroblast in the injury, (2) the accumulation of extracellular matrix. The study on prevention and cure of fibrosis by traditional Chinese medicine in recent ten years is reviewed as follows.

1. The pathological mechanism of visceral fibrosis

1.1 Myocardial fibrosis

Myocardial fibrosis is inevitable when the heart disease comes to its end stage. It symbolizes a crucial change of heart function from compensatory stage to decompensatory stage. Its symptoms often include the proliferation of cardiac fibroblasts, the increase of extracellular matrix, the remarkably increased concentration of extracellular collagen, and the abnormally high level of collagen volume fraction. Myocardial fibrosis is the structural basis for the cirrhosis of injured tissue; it will lead to the decrease of ventricular compliance and influence the systolic and diastolic function of heart. Usually, the accumulation of extracellular matrix will lead to the weakening of electrical coupling between cardiac muscle and the abnormality of E-C coupling of cardiac muscle, and then induce cardiac arrhythmia. The accumulation and reshaping of collagen fiber have close relationship with the diastolic function of heart; It has been widely accepted that myocardial fibrosis and cardiac diastolic dysfunction are among the reasons for heart failure.

1.2 Liver fibrosis

When the hepatic cells putrefy or inflame, connective tissue growth factor will aberrantly increase, which will lead to

proliferation of fibroblasts and the accumulation of extracellular matrix. The imbalance of fibril hyperplasia and fibril decomposition will lead to the connective tissue hyperplasia and deposition in the liver. Liver fibrosis precedes liver cirrhosis pathologically. And the prevention of liver fibrosis is of great significance for the prevention and cure of live cirrhosis. In recent years, drugs for activating blood circulation and removing stasis are used to treat liver cirrhosis, and great achievement has been made in the study on prevention and cure of liver fibrosis by traditional Chinese medicine.

1.3 Pulmonary fibrosis

Pulmonary fibrosis is the short name of diffuse pulmonary fibrosis. There are two kinds of pathogeny-based pulmonary fibrosis: idiopathic pulmonary fibrosis and secondary pulmonary fibrosis, both of which are caused by alveolus inflammation and alveolus structure turbulence. Firstly the pathogenic factors injure the blood vessel endodermis cells and alveolus epithelia, and induce inflammation reaction and immunoreaction. Secondly, various inflammatory cells release cellular factors and inflammatory mediators, expand the tissue injury and induce stroma hyperplasia. Thirdly, fibroblasts, endothelial cells migrate and proliferate, and the metabolism of collagen and extracellular matrix is disturbed, which worsens the injury and hyperplasia, eventually leads to injury of alveolus wall and the dysfunction of capillary vessel.

1.4 Renal fibrosis

Various renal diseases develop to their end stage through renal fibrosis, which is the major pathologic symptom of the diseases turning chronic. Modern medical science has focused on the molecules mechanism of renal interstitial fibrosis and found that the balance between two kinds of molecules plays an important role in the progress of renal interstitial fibrosis. One kind of molecules is the factors that can promote the renal interstitial fibrosis, including transforming growth factor β, connective tissue growth factor, angiotensin Ⅱ, endothelin (ET), platelet-derived growth factors, platelet-derived endothelial growth factor, tissue inhibitor of matrix metal proteinase, plasminogen activator inhibitor, monocyte chemo-attractant protein, etc. The other kind of molecules is the factors that can counteract the renal interstitial fibrosis, including γ-interferon, hepatocyte growth factor (HGF), matrix metal proteinase, relaxin, and so on. The study on renal fibrosis has gone deep into molecular and protein level. The development of modern medical science has enabled traditional Chinese pharmacists to explore more efficacious anti-fibrosis medicines. It is of great significance to combine Chinese traditional medicine and modern medical sciences in the development of anti-fibrosis medicines.

2. Study on the single traditional Chinese medicine and its effective ingredient in anti-fibrosis

2.1 Total saponins of Panax notognseng (PNS)

2.1.1 Prevention and cure of liver fibrosis

To observe the effects of Panax notoginseng saponins (PNS) on liver fibrosis, Yu et al (2005) established a mice liver fibrosis model induced by CCl_4. Yu's research show that PNS could improve liver fibrosis and decrease the level of TNFα, TGF-β, IL-1, and IL-6 in serum. The research indicates that PNS had the effect of anti-liver fibrosis, which might be relevant with the decrease of TNFα, TGF-β, IL-1, and IL-6 level in the serum.

2.1.2 Prevention and cure of pulmonary fibrosis

Quan et al (2005) established a pulmonary rat fibrosis model by bleomycin. Quan's morphological observation shows that PNS and dexamethasone could obviously alleviate inflammation and fibrosis induced by bleomycin. The research also shows that the content of hydroxyproline and expression of TGF-β1 in the lung tissue decrease ($P < 0.01$ and $P < 0.05$ after the use of PNS). Quan et al conclude that that PNS could obviously delay the development of pulmonary fibrosis induced by bleomycin in rats.

2.1.3 Prevention and cure of renal fibrosis

Using the methods of flow cytometry (FCM) and immunofluorescence, Zhang et al (2005) studied the effect of PNS on α-SMA expression of HK-2 cell induced by TGF-β1. Semi-quantitative reverse transcriptase polymerase chain reaction (RT-PCR) was used to detect the expression of α-SMA. And decreased expression of α-SMA was observed when HK-2 cells were induced by TGF-β1 in 200-800 mg/L PNS groups. The research of Zhang et al shows that PNS could relieve renal interstitial fibrosis by inhibiting trans-differentiation of renal tubular epithelial cells.

2.2 Salviae miltiorrhizae

Song et al (1998) revealed that salviae miltiorrhizae of certain concentration could effectively inhibit the collagen synthesis and the proliferation of fibroblasts.

2.2.1 Prevention and cure of myocardial fibrosis

Sun et al (2003) observed the effect of salviae miltiorrhizae on left ventricular hypertrophy and myocardial fibrosis prevention in spontaneous hypertensive rats.

2.2.2 Prevention and cure of liver fibrosis

Jiang et al (2002) studied the anti-lipid peroxidation effect of salviae miltiorrhizae on mitochondria of hepatic fibrosis in rats. Their results show that salviae miltiorrhizae could effectively inhibit the production of malondialdehyde, a product of peroxidation, and enhance the activity of superoxide dismutase (SOD) in the liver. Zheng et al (2003) found that Tanshensu could inhibit the proliferation of hepatic stellate cells. Their study indicates that salviae miltiorrhizae could reduce the production of extracellular matrix and inhibit the stellate cells from becoming myogenic fibroblasts.

2.2.3 Prevention and cure of pulmonary fibrosis

Wang et al (1994) revealed that sodium tanshionone ⅡA sulfonate could prevent the pulmonary fibrosis by eradicating oxygen free radicals.

2.2.4 Antagonizing renal fibrosis

Zhang et al (1997) showed that salviae miltiorrhizae could inhibit the proliferation of fibroblast and promote the programmed cell death through raising c-myc protein expression in human renal fibroblasts.

2.3 Astragalus and Astragaloside

2.3.1 Prevention and cure of myocardial fibrosis

Zhang et al (2003) treated the murine myocarditis model with 9% astragaloside. Their results showed that 9% astragaloside could improve survival rate, reduce collagen synthesis and cardiac myocytes apoptosis effectively. According to Zhang et al, the anti-apoptotic effect of astragaloside could play an important role in alleviating and reversing myocardial fibrosis.

2.3.2 Prevention and cure of liver fibrosis

Zhou et al (2005) revealed that astragalus had an inhibitive effect on hepatic fibrogenesis and that the mechanism might be associated with its antioxidant activity, decrease of laminin and its inhibition of hepatic stellate cell proliferation. Mou et al (2002) found that astragalus could increase the level of hepatic cell growth factor (HGF), which could reduce the expression of TGF-β1, and accelerate the decomposition of extracellular matrix and counteract fibrosis.

2.4 Matrine

2.4.1 Counteract myocardial fibrosis

Wu et al (2004) found that Matrine could inhibit myocardial fibrosis and collagen synthesis stimulated by angiotensin Ⅱ. They also found that Matrine could counteract myocardial fibrosis by reducing the angiotensin Ⅰ and TGFβ1 expression and increasing the level of MMP13 mRNA expression.

2.4.2 Counteract liver fibrosis

Matrine can inhibit liver inflammation and inhibit the activation of hepatic stellate cells and the proliferation of fibroblasts, so it could counteract the liver fibrosis (Wang and Zhao, 2005).

2.5 Ligustrazine

2.5.1 Counteract myocardial fibrosis

Song et al (1998) found that ligustrazine could effectively inhibit the collagen synthesis and proliferation of fibroblasts. Ren et al (2003) studied the effect of ligustrazine on myocardial fibrosis in rats with pressure overload. Their results showed that collagen volume fraction and myocardial fibrosis decreased significantly. It was indicated that ligustrazine could inhibit the TGF-β/Smads signal pathway, which might be one of the mechanisms to counteract fibrosis. Zhao et al (2006) found that ligustrazine could influence the production of endothelin and nitric oxide (NO) and the balance of both factors. Therefore, ligustrazine plays a role in inhibiting cardiac fibrosis.

2.5.2 Counteract liver fibrosis

Ligustrazine could inhibit the proliferation and activation of hepatic stellate cells in hepatic fibrosis rats induced by CCL_4 (Ji, et al 2003). Dai et al (1999) revealed that therapeutic effect of Ligustrazine on fibrosis might lie in its suppression on pre-collagen Ⅰ mRNA.

2.5.3 Counteract pulmonary fibrosis

Li et al (2007) found that ligustrazine could interfere with the collagen Ⅲ and laminin.

2.5.4 Counteract renal fibrosis

Wang Yaping et al (2004) revealed that ligustrazine could inhibit the transformation of fibroblasts when the kidney was injured, reduce the expression of myofibroblast, and therefore inhibit the process of the formation and development of renal interstitial fibrosis. Sun et al (1995) indicated that ligustrazine could reduce the secretion of IL-6 in mesangial cells, and inhibit the proliferation of mesangial cell and the production of extracellular matrix.

2.6 Cordyceps sinesis Sacc

2.6.1 Counteract liver fibrosis

Cordyceps sinesis Sacc could influence various phases of liver fibrosis, it could prevent hepatitis virus, inhibit the activation of hepatic stellate cells, and inhibit the collagen synthesis and promote collagen decomposition (Wu and Liu, 2001).

2.6.2 Counteract renal fibrosis

Liu et al (1995) treated rats with resection of greater part of kidney and found that the glomerulus cirrhosis, renal tubule shrinking and renal interstitial fibrosis were much less than those of renal failure rats.

2.7 Emodin

2.7.1 Counteract liver fibrosis

Emodin could significantly inhibit the synthesis of hepatic stellate cell collagen, hyaloplasm and laminin, so it could counteract the liver fibrosis (Zhan, et al, 2006)

2.7.2 Counteract renal fibrosis

Wang et al (2002) found that emodin could inhibit the proliferation of human renal fibroblasts and the production of IL-6.

2.8 Ginkgo Biloba leaf

2.8.1 Counteract liver fibrosis

The extract of Ginkgo Biloba leaves has obvious antioxidant and anti-lipid peroxidation effect according to the findings of Liu et al. The researchers asserted that those leaves could markedly improve the activity of SOD and GSH-Px, reduce the content of MDA and counteract the liver fibrosis (Liu et al., 2003)

2.8.2 Counteract pulmonary fibrosis

Ginkgo Biloba leaf preparation has definite effect in treating pulmonary fibrosis, the mechanism might be through inhibiting the activity of NF-kB, decreasing TGF-β mRNA expression and protein, so as to ameliorate the inflammation and fibrosis (Chen et al., 2000).

2.8.3 Counteract renal fibrosis

Tang et al (1998) found that Ginkgo Biloba leaf could ameliorate glomerulus sclerosis and renal tubule-interstitial damage but might not completely prevent the occurrence of this damage.

2.9 Genistein

Gao et al (2001) revealed that genistein could inhibit the proliferation of cardiac fibroblasts and arrest the myocardiac cell progression at G2/M phase and accelerate the cell apoptosis.

2.10 Tetrandrine.

Xu et al (1996) revealed that the proliferation and collagen synthesis in cardiac fibroblast induced by angiotensin Ⅱ might be mediated by angiotensin Ⅱ receptor, and these stimulatory effects could be inhibited by the calcium channel blocker tetrandrine.

2.11 Total flavone of Metasequoia Glyptostroboides

Tian et al (2006) found that flavone of Metasequoia Glyptostroboides could inhibit the proliferation and collagen synthesis of cultured myocardial fibroblast of neonatal mouse induced by insulin-like growth factor 1.

2.12 Salidroside

Wang and Liu (2004) found that salidroside could significantly inhibit HSC proliferation, and inhibit Type Ⅲ collagen, hyaluronic acid and laminin secretion in different degree.

2.13 Rhizome sparganii and radices zedoariae

Luan and Li (2004) revealed that rhizome sparganii and radices zedoariae had immunological regulation function and could counteract hepatic fibrosis.

2.14 Tetrandrine

Tian et al (1997) indicated that tetrandrine could directly inhibit cell proliferation, reduce collagen synthesis and counteract fibrosis. He et al (1995) found that tetrandrine could inhibit directly or indirectly the transcription of collagen gene and thus reduce synthesis of collagen protein. The research teams agreed with each other on tetrandrine's ability to prevent and cure pulmonary fibrosis.

3. Problems and future research

Prevention and cure of fibrosis with traditional Chinese medicine is a valuable and applicable research field. There are many kinds of fibroblasts with different characteristics, but all the fibroblasts have the function of collagen and extracellular matrix synthesis, collagen decomposition, and connective tissue contraction. Fibroblasts are the main places of collagen synthesis, so the study on fibrosis pays much attention to fibroblasts. The influence of drugs, especially the traditional Chinese medicine, on the fibroblast is an important research field. Studies have shown that many traditional Chinese medicines could influence the proliferation, collagen synthesis and DNA synthesis of fibroblasts, but the mechanism is complex. Current studies mainly focus on the function of single traditional Chinese medicine, and drugs for activating blood circulation and removing stasis could significantly inhibit the proliferation and collagen synthesis of fibroblasts. The clinical symptoms of patients are different, so it is inappropriate to treat various kinds of diseases with one medicine. The western medicine has strong side effect, and is expensive, so it is difficult to be popularized. The advantage of traditional Chinese medicine should be thoroughly brought into play, compound medicine should be used to influence the function of fibroblasts and achieve overall regulation and treatment. At present, traditional Chinese medicine has exhibited sound clinical effect in treating fibrosis, but its mechanism is still unclear. Few studies have been devoted to the understanding of the influence of compound traditional Chinese medicine and the combination of traditional Chinese medicine and western medicine on fibroblasts. It is the author's belief that further research will help to clarify how (compound) traditional Chinese medicine can influence fibroblast and that new drugs will be developed. It is also the author's hope that breakthroughs in the prevention of cure of fibrosis can be achieved by combining advantages of traditional Chinese medicine and Western medicine.

References

Chen, Jian. He, Bing. Liu, Xinmin et al. (2000). Experimental study on the effect of folium Ginkgo Biloba in treating pulmonary interstitial fibrosis in rats [J]. *Chinese Journal Of Integrated Traditional And Western Medicine*. 20 (6): 441-443.

Dai, Lingjuan. Hou, Jie. Cai, Hourong et al. (1999). The mechanism of treating pulmonary fibrosis with ligustrazin [J]. *Journal of Postgraduates of Medicin*e. 22 (11): 24-25.

Gao, Zhan. Zhu, Miaozhang. Zhou, Shisheng et al. (2001). Effects of genistein on the proliferation of cardiac fibroblasts [J]. *Chinese Journal of Pharmacology and Toxicology*. 15 (2). 159-160.

He, Yuxian. Liu, Bingci. Miu, Qing et al. (1995). Inhibition of mRNA expression of silicotic collagen gene by tetrandrine [J]. *Chinese Journal of Preventive Medicine*. 29 (1): 18.

Ji, Chengwei. Liu, Jinmin. Li, Liangcheng et al. (2003). Effects of tetramethylpyrazine on prohibiting hepatic fibrosis in rats [J]. *Journal of Shanxi Medical University*. 34 (4): 293-295.

Jiang, Shulin. Yao, Xixian and Lv, Tao. (2002). Inhibitory effect of Danshen on lipid peroxidation in mitochondria of hepatic fibrosis in rats [J]. *World Chinese Journal of Digestology*. 10 (11): 1253-1256.

Li, Jiang. Wu, Fang. Huang, Mao et al. (2007). Interference role of Ligustrazine to Collagen-Ⅲ and Laminin in pulmonary fibrosis rats [J]. *Journal of Applied Clinical Pediatrics*. 22 (4): 290-291.

Liu, Qiang. Hou, Jishou. Ma, Jiming et al. (1995). Experimental study on the effects of Cordyceps sinesis Sacc on chronic renal function failure. *Chinese Journal of Nephrology*. 11 (2): 81-82.

Liu, Shiquan. Yu, Jieping and Ran, Zongxue. (2003). Experimental study on Ginkgo Biloba extract against carbon tetrachloride-induced chronic liver damage in rats [J]. *Journal of China Pharmaceutical University*. 34 (1): 61-64.

Luan, Xiying and Li, Keke. (2004). The effects of rhizome sparganii and radices zedoariae on IL21, IL26, TNF2α of hepatic fibrosis rat [J]. *Chinese Journal of Immunology*. 20 (12): 834-837.

Mou Na. Zhang, Qingyi. Ni, Zhaohui et al. (2002). Effect of astragalus membranaceus on HGF by renal interstitial fibroblasts in the high glucose [J]. *Chinese Journal of Integrated Traditional and Western Nephrology*. 3 (1): 7.

Quan, Yan. Xia, Qianming. Li, Fuxiang et al. (2005). Effect of Panax Notoginsenosides on pulmonary fibrosis induced by bleomycin in rats. *Medicial Journal of National Defending Forces in Southwest China.* 15(3): 235-238.

Ren, Hailing. Jiang, Shisen. Xie, Dujiang et al. (2003). Effect of ligustrazine on myocardial fibrosis in rats with pressure overload [J]. *Chinese Journal of Clinical Rehabilitation*. 7 (12): 1748-1749.

Song, Deming. Su, Hai. Wu, Meihua et al. (1998). Effects of Tetramethylpyrazine and Radix Salviae Miltiorrhizae on collagen synthesis and proliferation of cardiac fibroblasts [J]. *Chinese Journal of Integrated Traditional and Western Medicine*. 18 (7): 423-425.

Sun, Lianping. (2003). Effect of Radix Salviae Miltiorrhizae on left ventricular hypertrophy and the synthesis of collagen Ⅰ and Ⅲ of myocardial cells in spontaneous hypertensive rats [J]. *Journal of Tongji University (Medical*

Science). 4 (6): 481-483.

Sun, Lin. Yi, Zhuwen and Yu, Peilan. (1995). Effect of tetramethylhyrazine on proliferation of human fetal mesangial cells [J]. *Chinese Journal of Integrated Traditional And Western Medicine*. 15 (3): 134-136.

Tang, Jinhui. Xu, Qinru. Liu, Tonglin et al. (1998). Experimental research of folium ginkgo in preventing glomerulosclerosis and tubulointerstitial damage in rats [J]. *Chinese Journal of Nephrology*. 14 (3): 174.

Tian, Wei. Zhao, Yongqing. Peng, Haiping et al. (2006). Effects of total flavone of metasequoia glyptostroboides on the proliferation of rat cardiac myocardial cell [J]. *Chinese Journal of Experimental Traditional Medical Formulae*. 12 (4): 286-288.

Tian, Zibin. Liu, Siliang. Li, Dingguo et al. (1997). Blocking action of tetrandrine on the cell proliferation induced by PDGF in human lung fibroblasts and liver Ito cell of rats [J]. *National Medical Journal of Chin*a. 77: 50-53.

Wang, Changming. He, Qingzhong and Zhang, Ruixiang. (1994). Effects of tanshionone to bleomycin induced pulmonary fibrosis of rats on histological changes and production of lipid peroxides and hydroproline [J]. *Chinese Journal of Tuberculosis And Respiratory Diseases*. 17 (5): 308.

Wang, Lichun and Zhao, Liansan. (2005). A review of the experimental study on antagonizing the liver fibrosis with traditional Chinese medicine [J]. *Journal of Traditional Chinese Medicine*. 3: 228-230.

Wang, Xiaodong and Liu, Yongzhong. (2004). Experimental study of salidroside against hepatic fibrosis in Vitro [J]. *Lishizhen Medicine and Maieria Medical Research*. 15 (2) 138-139.

Wang, Xiaoling. Wang, Jianqian. Xia, Yanling et al. (2002). Inhibition effect of emodin on human kidney fibroblaot in vitro [J]. *Chinese Journal of Integrated Traditional and Western Nephrolog*y. 3 (11): 629-630.

Wang, Yaping and Li, Boxiang. (2004). Experimental study regarding to protective and therapeutic effects of Ligustrazine on renal interstitial fibrosis [J]. *Chinese Journal of Integrated Traditional and Western Nephrology*. 3 (2): 77.

Wu, Jianliang and Liu, Chenghai. (2001). Effects of Cordyceps sinesis Sacc on liver fibrosis [J]. *Chinese Journal of Integrated Traditional and Western Medicine on Liver Diseases*. 13 (6): 324-326.

Wu, Ke. Ouyang, Jingping. Wang, Baohua et al. (2004). Influence of matrine on the proliferation and collagen synthesis of cultured neonatal rat cardic fibroblast stimulated by angiotensinⅡ[J]. *Journal of Hubei Medical University*. 25 (3): 235-238.

Xu, Yi. Zhou, Chengyu and Li, Yunxia. (1996). The inhibitory effect of tetrandrine on angiotensin Ⅱ-stimulated proliferation in cultured neonatal rat cardiac fibroblasts [J]. *Chinese Journal of Applied Physiology*. 12 (3): 198-202.

Yu, Wangui and Zhang, Hengwen. (2005). Effects of Panax notoginseng saponins on TNFα and IL26 in serum of mice with liver fibrosis [J]. *Pharmacology and Clinics of Chinese Materia Medica*. 21(4): 31-33.

Zhao, Zhiming. Cai, Hui and Guo, Junhao. (2006). Effects of tetramethylpyrazine on the production of ET and NO in cardiac fibroblasts in neonate rat [J]. *Acta Academiae Medicinae Neimongol*. 28 (3): 202-203.

Zhan, Yutao. Li, Dingguo. Shen, Liyong et al. (2006). Mechanism of emodin for anti-fibrosis of liver [J]. *Chinese Journal of Hepatology*. 22 (1): 43-44.

Zhang, Guoqiang. Ye, Rengao. Kong, Qingyu et al. (1997). Effects of Radix Salivae Miltiorrhizae on proliferation apoptosis and c-myc protein expression of fibroblast in culture of kidney with lupus nephritis [J]. *Chinese Journal of Integrated Traditional and Western Medicine*. 17 (8): 473.

Zhang, Yi. Chen, Xiaowen. Liu, Haiyan et al. (2005). Effects of Panax Notoginsenosides on transdifferentiation of renal tubular epithelial cells induced by TGF-β1 [J]. *Chinese Journal of Integrated Traditional and Western Nephrology*. 6 (6): 317-321.

Zhang, Zhaocai. Yang, Yingzhen. Li, Shuangjie et al. (2003). Effect of astragaloside on myocardial fibrosis in viral myocarditic mice [J]. *Chinese Journal of New Drugs and Clinical Remedies*. 22 (9): 515-519.

Zheng, Yuanyi. Dai, Lili. Wang, Wenbing et al. (2003). Effect and mechanism of Tanshensu on fibrotic rats [J]. *Chinese Journal of Hepatology*. 11(5): 288-290.

Zhou, Xian. Dai, Lili. Jia, Liping et al. (2005). Study on the inhibitive effect of Astragalus injection solution on hepatic fibrosis in rats [J]. *Chinese Journal of Hepatology*. 13 (8): 575-578.

Modern Applied Science

www.ccsenet.org/journal.html

Vol. 2, No. 5

September 2008

Study on Sirospunning System to Reduce the Hairiness of Yarn

Liang Huo

College of Textile

Tianjin Polytechnic University

Tianjin 300160, China

Abstract

The twisting process of Sirospunning and Ringspunning was compared and analyzed as to the phenomenon that Sirospunning decreases yarn hairiness. It can be obtained from the analysis of geometrical model that more hairiness is twisted into the yarns and the amount of apparent hairiness is reduced through its special twisting. It can be calculated that when the count is equal Sirospunning can reduce the hairiness more than 22% compared with Ringspunning. The key factor the effect of tassel spacing of Sirospunning was studied using geometrical model, and the reason why the increase of tassel spacing could decrease the amount of hairiness was obtained. At last, the result of theoretical analysis was validated through series of experiment.

Keywords: Sirospunning, Hairiness, Tassel spacing, Geometrical Model

Sirospunning was studied by CSIRO and IWS together in 70s of 20th century. Sirospunning improves conventional Ringspunning technology, decreases the amount of apparent hairiness effectively, makes the surface of yarns smoothy, and improves the resistance of yarns to abrasion and the quality of yarns. Till now, a lot of research has been focused on Sirospunning abroad, however, the question that how to decrease the hairiness has not been resolved; In the research of the factors of Sirospun yarns, researchers got the agreement that the tassel spacing was the vital factor influencing the structure and the properties of yarns [1], and that the larger the tassel spacing the better of the rigidity, hairiness, the resistance to abrasion and amplexus [2]. The theoretical evidence of the way tassel spacing influencing the yarn hairiness is yet to be known. Consequently, the purpose of this paper was to analyze the above questions by establishing geometrical model, and to validate the results through experiment to get the conclusion.

1. The comparison of triangle region between Ringspunning and Sirospunning

The twists of Ringspunning and Sirospunning are produced by the motion of the steel traveler. The produced twist is transferred upwards to the converging point.

When Ringspunning twisting, the tassel of the jaw circumgyrates around the axis, the width of the tassel shrinks gradually, and the two sides are folded into the yarns center gradually to form the twisting triangle region, as shown in Figure. 1(left). In the twisting triangle region, the width and section of the tassel are changed, and the yarns are formed from compressed to columniform [3].

When Sirospunning twisting, firstly, two branches of tassel are combined after exported with the same pace from the front roller; before combined, there is a segment of single-yarn twisting region and the tassel form the single-yarn structure in this region, as shown in Figure. 1(right). Fibre basically array in a fastigiate screwy line. Then two branches converge to be twisted, belonging to lang lay. The combined twist increases rapidly on the basis of single twist, making the single yarn and fibre screwy line more obvious, increasing the slope degree of fibre, and making the section of branches become round structure [4].

In Figure. 1 the twist is obtained when tassel is added at section A; section B shows the distribution shapes of fibre before yarns produced; section C shows the shapes of the produced yarns.

In Sirospunning, due to the shortened single branch yarn twisting region, the obtained twist decreases, the assembly of fibre becomes relatively supple; the opportunity of the fibre ends coming out reduces, leading to the decrease of the hairiness. In addition, during the following combination of yarns, parts of the hairiness of the single yarn are twisted into the yarns, the hairiness decrease. Consequently, the hairiness of Sirospun yarn is less than that of Ringspun yarn.

2. The hairiness comparison of Ringspunning and Sirospunning

In order to study the hairiness difference between Ringspunning and Sirospunning, an ideal Sirospunning model (Figure.

3) was established on the basis of the practical observation on Sirospunning (Figure.2). It can be found from the analysis of referenced literatures [4-6] that the section shape of Sirospun yarn is round the same to the ordinary Ringspun yarn. In addition, the two single yarns separate the Sirospun yarn equally, and do not affect each other, there exists an obvious boundary. Therefore, in the model shown in Figure.3, it is assumed that the shapes of the two branches of single yarn are standard circle at section B before Sirospun yarn formed. They are represented by O1 O2, with the same size, semidiameter r; After Sirospun yarn formed, the section shapes of Sirospun yarn and Ringspun yarn are standard circle, semidiameter R, the same shape of the produced yarn at section C; the boundary is a straight line BC, as shown in Figure.3.

Ideally speaking, due to the same count of produced yarns at section B, the areas of Sirospun yarn and Ringspun yarn are equal.

$\pi R^2 = 2\pi r^2$

$$R = \sqrt{2}r \quad (1)$$

After twisted, two branches of single yarn are combined towards to the center. A part of the single-yarn hairiness are twisted into the yarns, as represented as the hairiness on part of arc of O1 O2 in Figure.3 twisted into the inside line BC of yarns. The rest hairiness of the arc would exist on the yarn surface, to form the hairiness of Sirospun yarns. It is assumed that the distribution of yarn hairiness on the yarn surface is even, the length of the section arc could represent the relative amount of yarn hairiness.

$$L_{BC} = 2R \quad (2)$$

According to the circle perimeter equation, the perimeter of O1 obtained:

$$L_{01} = 2\pi r \quad (3)$$

The outside length of single yarn untwisted:

$$L_{single} = L_{01} - L_{BC} \quad (4)$$

From (1), (2), (3), (4):$L_{single} = 3.452r$ (5)

In the model, the sizes of two branches spun yarns are same, and known as total symmetry. Then, the representative outside length of Sirospun yarn LS

$$L_S = 2L_{single} = 6.904r \quad (6)$$

The perimeter of Ringspun yarn cross section LH

$$L_H = 2\pi R = 8.880r \quad (7)$$

Consequently, the ratio of the apparent Sirospun yarn hairiness Ns to that of Ringspun yarn NH, τ:

$$\tau = \frac{N_S}{N_H} = \frac{L_S}{L_H} = 0.78 \quad (8)$$

In this situation, from the above model calculation, it can be found that the Sirospun yarn hairiness could be decreased up to 22% compared with that of Ringspun yarn. Actually, the boundary BC of the two single yarns does not must be straight line. The research demonstrated that the single yarn section inside the twisted Sirospun yarn basically belonged to circle or ellipse, and the boundary could exist as curve, which was also proved by microscope image of the cross section (Figure.3). Therefore, the calculated result that taking BC as the straight line is the minimum. That is to say, Sirospunning can decrease hairiness more than 22% compared with conventional Ringspunning.

3. The effect of spacing on Sirospun yarn hairiness

In order to study the influence of tassel spacing on Sirospun yarn hairiness, the further geometrical model was established based on the previous theoretical analysis, shown as below.

In the previous analysis, it was assumed that the fibre section on the converging point was round. But actually due to the certain spacing between Sirospun yarn tassels, so there exists an angle on the converging point, in addition, the fibre on the converging point could squeeze to each other; these reasons result in that the fibre shape at section B is not standard circle, shown in Figure. 4.

In Figure. 4, the two columns represent the formed two branches thin yarns. At section A, d represents the tassel spacing; a represents the angle between tassel and the central axis; ellipses O'1 O'2 represent the projection shape of the two thin yarns O1 O2 at section B, as the real shape yarn when it goes through section B, major diameter r, minor diameter r', shown as Figure.5.

Obtained from the according relationship in Figure.4:

$$r' = r\cos\alpha \quad (9)$$

The perimeter equation of ellipse:

$L01'=2\pi r'+4(r-r')$ (10)

Obtained from (1) (2) (4) (9) (10):

$Lsingle'=1.172r+2.28r\cos\alpha$ (11)

Obtained from (6) (7) (8) (11), the apparent hairiness ratio of Sirospun yarns to Ringspun yarns:

$\tau'=0.264+0.514\cos\alpha$ (12)

From the experimental observation, it could be obtained that the value of$\alpha$is at the range of 0~45. So$\tau'$is the decay function ofα. αincreases andτ'decreases with the rise of d. That is to say, the decreased percentage of Sirospun yarn hairiness increases with the rise of tassel spacing. When$\alpha=0$, the model is equal to the ideal condition, and$\tau'=0.78$, agree with the previous conclusion.

4. Validating experiment

On the electric small sample Sirospunning machine, using double bugles addition, Sirospun yarns with different tassel spacing were produced through modifying the central distance between the two bugles. The hairiness indexes of Sirospunning and Ringspunning with same count were compared using equipment.

Roving raw: cashmere 50%\1.5D viscose 50%

Twist: 30 twisting/m; ingot weight: 7.5g/10m

Spun yarn size: 76tex; Spun yarn twist: 420 twisting/m

Testing equipment: YG172 Spun yarn hairiness tester

Experiment time: 5 times, length of segment: 10cm

The experimental data are shown in Table 1. Compared Sirospunning with Ringspunning, it could be found that Sirospunning hairiness indexes of all kinds of length are smaller than those of Ringspunning obviously. The decreased percentage of Sirospunning hairiness with the length 3mm is at the range of 22%-48% compared with that of Ringspunning hairiness. From the table, it could be found that all the hairiness indexes of different lengths are in the decreasing trend and the decreased percentage of hairiness increases with the rise of Sirospun yarn tassel width, which validates the results from the model.

5. Conclusions

Due to the special twisting of Sirospunning, more hairiness is twisted into the yarns, then the apparent tassels decreasing; it was assumed that the tassel spacing of the perimeter in the longitudinal section and cross section was even. And the section of Sirospun yarn could be represented by geometrical model. The arc length of the hairiness distributed section could represent the hairiness condition of the whole yarn, using this method, Sirospunning with the same count could decrease the hairiness up to 22% compared with that of Ringspunning; The tassel spacing is one of the factors influencing Sirospun yarns. Theoretical analysis and experimental results show that the angulation of triangle region increases with the rise of the tassel spacing, and more hairiness would be twisted into the yarns, leading to the increase of the decreased percentage of Sirospunning.

References

Cheng ,K.P.S & Sun ,M.N. (1998). Effect of Spacing and Twist Multiplier on Cotton Sirospun Yarn. *Journal of Textile Research*, 7, 520-527.

Cheng,Longdi, Fu ,Peihua & Yu ,Xiuye. (2004). Relationship Between Hairiness and The Twisting Principles of Solospun and Ring Spun Yarns. *Journal of Textile Research*, 9, 763-766.

Li,Weiru.(2003).The research on the mechanism of Sirospunning. Shanghai: Donghua University.

Sun,M.N, Cheng ,K.P.S.(2000). Structure and ProPerties of Cotton Sirospun Yarn. *Journal of Textile Research*, 3, 261-268.

Zhang,Jinwu.(2006). Analyses of Twist Structure of Siro Spinning Yarn. *Cotton Textile Technology*, 34, 16-19.

Zhang,Tonghua, Han,Guangting & Wang,Chengjun.(2003). Discussion on twist of Siro-spun yarn. *Journal of Qingdao University*, 18, 14-16.

Table 1. The yarn hairiness of Sirospunning and Ringspunning

Hairiness length	2mm	3mm	4mm	5mm	6mm
Hairiness index of Ringspun yarn (branch/m)	44.96	15.12	5.98	2.62	1.24
d=0mm Hairiness index of Sirospun yarn (branch/m)	37.02	11.14	4.24	1.92	0.8
Decreased hairiness compared with Ringspuning (%)	18	26	29	27	35
d=3mm Hairiness index of Sirospun yarn (branch/m)	37.34	11.82	5.12	2.34	1.2
Decreased hairiness compared with Ringspuning (%)	17	22	14	11	3
d=6mm Hairiness index of Sirospun yarn (branch/m)	33.42	10.40	5.04	2.02	1.12
Decreased hairiness compared with Ringspuning (%)	26	31	16	23	10
d=11mm Hairiness index of Sirospun yarn (branch/m)	33.90	9.14	3.66	1.42	0.76
Decreased hairiness compared with Ringspuning (%)	25	40	39	46	39
d=13mm Hairiness index of Sirospun yarn (branch/m)	32.24	8.82	3.32	1.48	0.68
Decreased hairiness compared with Ringspuning (%)	28	42	44	44	45
d=15mm Hairiness index of Sirospun yarn (branch/m)	30.88	7.98	3.16	1.00	0.44
Decreased hairiness compared with Ringspuning (%)	31	47	47	62	65
d=17mm Hairiness index of Sirospun yarn (branch/m)	29.50	7.80	2.76	1.06	0.40
Decreased hairiness compared with Ringspuning (%)	34	48	54	60	68

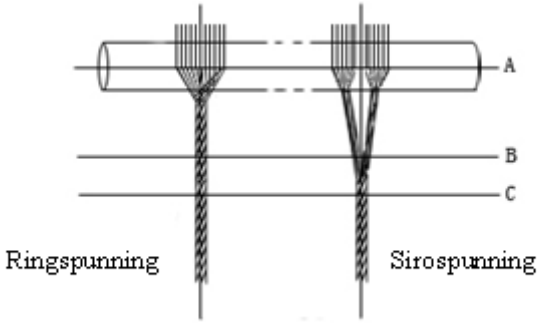

Figure 1. The twisting structures of Ringspunning and Sirospunning

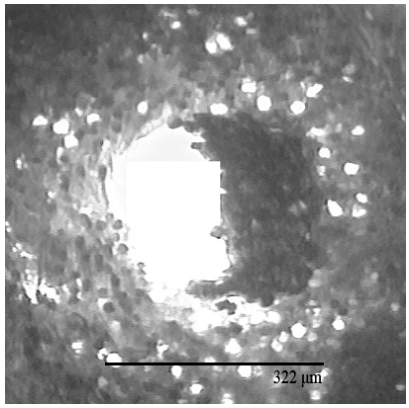

Figure 2. The cross section diagraph of Sirospun yarn

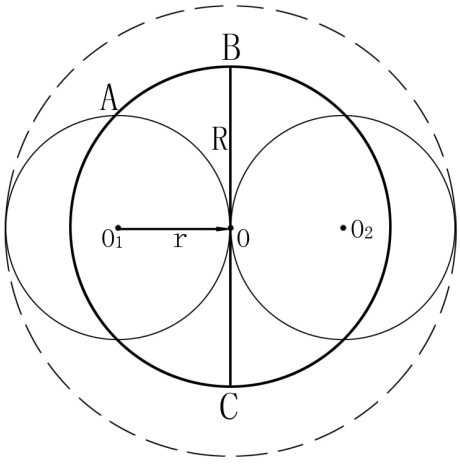

Figure 3. The Sirospun yarn structure diagraph in ideal state

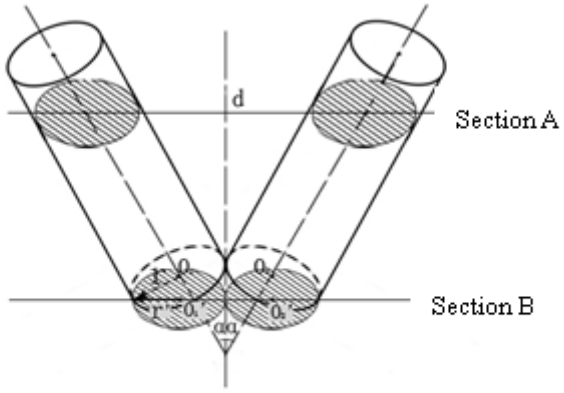

Figure 4. The analysis diagraph of Sirospun yarn triangle region

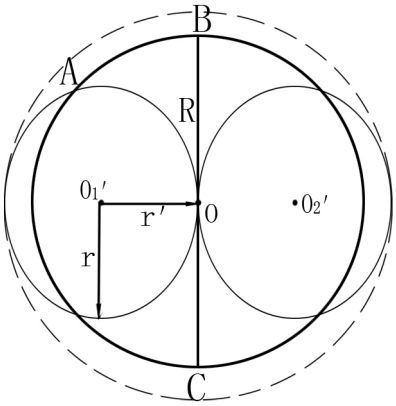

Figure 5. The structure diagraph of Sirospun yarn

Modern Applied Science

www.ccsenet.org/journal.html

Vol. 2, No. 5

September 2008

Image Denoising through Self-Organizing Feature Map Based on Wavelet-Domain HMMs

Jianxin Dai & Yaqin Jiang

School of Mathematics and Physics

Nanjing University of Posts and Telecommunications

Nanjing 210046, China

E-mail: daijx_js@126.com

Abstract

Although the Wavelet-domain hidden Markov Models (HMMs) can powerfully preserve the image edge information, it lacks local dependency information. According to the deficiency, a novel image denoising method based HMMs through the self-organizing feature map(SOFM) which exploits spatial local correlation among image neighbouring wavelet coefficients is proposed in this paper. SOFM algorithms is popular for unsupervised learning and data clustering and can capture persistence properties of wavelet coefficients. Experimental results show that the performance of the proposed method is more practicable and more effective to suppress additive white Gaussian noise and preserve the details of the image.

Keywords: Self-organizing feature maps, Image denoising, Hidden markov models

1. Introduction

Images are easy to be contaminated with noise, either because of the data acquisition process, or because of naturally occurring phenomena. Therefore, image denoising is an important processing task, both as a process itself and as a component in other processes before received images can be used in applications. Denoising images corrupted by additive white Gaussian noise (AWGN) is a classical problem to the image processing community. The aim of image denoising is to remove the noise while keeping the signal features as much as possible.

A lot of work has been done on wavelet for denoising in both the signal processing and statistics communities. However, existing methods implicitly treat each wavelet coefficient as though it is independent of all others. These models are unrealistic for many real world signals.

Recently, the wavelet-domain hidden Markov tree (HMT) model is proposed based on the following three statistical properties of the wavelet coefficients:

(1)Non-Gaussian distribution: The marginal distribution of the magnitude of the complex wavelet coefficients can be well modeled by using a mixture of two-state Rayleigh distributions. The choice for using the Rayleigh mixture model instead of the Gaussian mixture model was based upon the fact that the real and imaginary parts of the complex wavelet coefficients may be slightly correlated, and therefore only the magnitudes of the complex wavelet coefficients will present a nearly shift-invariant property, but not the phase.

(2)Persistency: Large/small wavelet coefficients related to pixels in the image tend to propagate through scales of the quad trees. Therefore, a state variable is defined for each wavelet coefficients that associates the coefficients with one of the two Rayleigh marginal distributions [one with small (S) and the other with large (L) variance]. The HMT model is then constructed by connecting the state variables (L and S) across scales using the Expectation-Maximization (EM) algorithm.

(3)Clustering: Adjacent wavelet coefficients of a particular large/small coefficient are very likely to share the same state (large/small).

The superior results of HMT model denoising have demonstrated that significant performance gains can be achieved by exploiting dependencies among coefficients. The whole parameters of HMT model can be estimated by Expectation Maximization (EM) algorithm. EM algorithm is a kind of Max-Likelihood Estimation (MLE) algorithm whose target is to find a set of hidden states to maximize the probability of observations. If the initial values for parameters of HMM

are known, EM iterates between estimating the probability for the state (Expectation) and updating the model given the state probabilities (Maximization) until the HMM converges. EM algorithm is an efficient algorithm to find local optimum parameters from an initial value. However, it is difficult to gain both reliable and local estimate results of the EM algorithm in signal denoising, because reliable estimate results require that the number of samples are big enough, while local estimate result requires to consider only neighboring wavelet coefficients. The samples are a group of identically independent distribution (iid) data that are used to train the parameters of HMM. Therefore, we should attentively design a model structure to keep a suitable number of samples for training the parameter of our model. Of course, we typically have a single noisy signal observation in signal denoising. Therefore, in order to ensure reliable parameter estimation for the signal we must share statistical information among related wavelet coefficients, and the problem becomes how to share statistical information to gain both reliable and local estimate results of EM. To accomplish this problem, the standard assumption of wavelet-domain HMMs is that all wavelet coefficients and state variables within a common scale are iid. In this assumption, wavelet coefficients within a common scale can be considered as samples of the parameter estimate, then the parameter of a HMM can be trained by all wavelet coefficients within a common scale. Thus the standard assumption provides a powerful tool to ensure reliable parameter estimation for the signal, but it lacks local dependency information. The reason is parameters of HMMs within a common scale are the same that does not consider the positions of the samples. To strike a balance between enough related wavelet coefficients and spatial adaptability, we must carefully and attentively design the related relationship among wavelet coefficients.

This paper proposes a novel structure of HMMs through SOFM (SOFM-HMM) which exploits spatial local related statistical information among image neighbouring wavelet coefficients to improve the spatial adaptability of HMMs. SOFM is one of the major unsupervised artificial neural network models and often used to learn certain useful features found in their learning process. Thus ,the new framework provides a flexible conditional probability model for efficient learning and expressing the dependencies in wavelet transforms.

The remaining sections are organized as follows. Section 2 briefly reviews wavelet-domain HMMs. Section 3 studies the SOFM algorithm. Section 4 explains the proposed image denoising method and it is followed by experimental results comparing with various wavelet denoising methods in section 5 and conclusion in section 6, respectively.

2. The Wavelet Domain Hidden Markov Models Theory

The wavelet domain HMMs theory was first proposed by Crouse based on the statistical properties introduced in Section 1.In practice, the distribution of the wavelet coefficients is described as non-Gaussian with a peak centered at 0 and a heave tail. In this paper, Gaussian mixture models are adapted to approximate this non-Gaussian density property. In this model, each wavelet coefficient w is associate with a discrete value named hidden state, $S = 0,1,\cdots,M-1,$ and the coefficient's probability density function pdf $f_{W|S}\left(w|S=m\right)$ given its hidden state can be described as a Gaussian distribution with mean μ_m and variance σ_m^2.Using these assumptions, the distribution of the coefficients can be described as $f_W\left(w\right)=\sum_{m=0}^{M-1} p_s\left(m\right) f_{W|S}\left(w|S=m\right)$.In hidden markov model, the coefficients are assumed to be independent with each other given the hidden states. Because the wavelet transform have a natural quardtree structure, so, by using the across scale persistence property, the HMT established a Markov chain structure which can avoid the two dimentional lattice's uncausal feature, and the computation consumption of the parameters estimation can be efficiently reduced. The HMT is shown in figure1.From it, we can see the dependencies across scale. Based on the M state Gaussian mixture model, the parameter set θ_{HMT} of the model is gives as $\left\{ps_i\left(m\right),\varepsilon_{i,\rho(i)}^{mn},\mu_{im},\sigma_{im}^2|m=0,1,\cdots,M-1\right\}$ Where $\varepsilon_{i,\rho(i)}^{mn}$ denote the transition probability of node $\rho(i)$ in state n to its son node i in state m and $ps_i\left(m\right)$ denote the initial distribution of node i in state m .In practice, we use a two-states, zero-mean Gaussian mixture models and the low-variance Gaussian model is used to model the low-energy wavelet coefficients, the high-variance Gaussian to high-energy coefficients.

The whole parameters of HMT can be estimated by EM algorithm. In this algorithm, the following conditional likelihoods are defined:

$$\beta_i\left(m\right)=f\left(T_i|S_i=m,\theta\right). \tag{1}$$

$$\beta_{i,\rho(i)}\left(m\right)=f\left(T_i\left|S_{\rho(i)}=m,\theta\right.\right) \tag{2}$$

$$\beta_{\rho(i)\backslash i}\left(m\right)=f\left(T_{\rho(i)\backslash i}\left|S_{\rho(i)}=m,\theta\right.\right). \tag{3}$$

And the joint probability function is defined:

$$\alpha_i\left(m\right)=p\left(S_i=m,T_{1\backslash i}|\theta\right). \tag{4}$$

Then in the E step, by upward-downward scanning, (1)-(4)leads to the desired conditional probabilities

$$p(S_i = m|W,\theta) = \frac{\alpha_i(m)\beta_i(m)}{\sum_{n=1}^{M}\alpha_i(n)\beta_i(n)} \quad (5)$$

$$p(S_i = m, S_{\rho(i)} = n|W,\theta) = \frac{\alpha_{\rho(i)}(m)\beta_{\rho(i)\setminus i}(m)\beta_i(m)\varepsilon_{i,\rho(i)}^{nm}}{\sum_{n=1}^{M}\alpha_i(n)\beta_i(n)} \quad (6)$$

To maximize the parameter set θ, we perform the within trees tying to finish the M step and get the maximized parameter set

$$ps_i(m) = \frac{1}{K}\sum_{k=1}^{K} p(S_i^k = m|W^k,\theta) \quad (7)$$

$$\varepsilon_{i,\rho(i)}^{mn} = \frac{1}{Kp_{S_{\rho(i)}}(m)}\sum_{k=1}^{K} p(S_i^k = n, S_{\rho(i)}^k = m|W^k,\theta) \quad (8)$$

$$\sigma_{i,m}^2 = \frac{1}{Kp_{S_i}(m)}\sum_{k=1}^{K}(w_i^k - \mu_{i,m})^2 p(S_i^k = m|W^k,\theta) \quad (9)$$

Where K denote the numbers of the coefficients of one subband in one scale, so the M step is finished by assuming that these coefficients are in same distribution and they are independent of each other. The following section will describe our proposed model in detail.

3. SOFM Algorithm

The self-organizing feature map (SOFM) is one of the major unsupervised artificial neural network models and often used to learn certain useful features found in their learning process. It basically provides a way for cluster analysis by producing a mapping of high dimensional input vectors onto a two-dimensional output space while preserving topological relations as faithfully as possible. After appropriate training iterations, the similar input items are grouped spatially close to one another. As such, the resulting map is capable of performing the clustering task in a completely unsupervised fashion.

SOFM is a topology preserving nonlinear transformation. Each neuron, $j, 1 \le j \le l$ is connected to the input through a synaptic weight vector $M_j = [m_{j1},\cdots,m_{jm}]^T$.At each iteration, SOFM finds the best-matching (winning) neuron j by minimizing the following cost function: $V(X) = \arg\min_{j=1}^{j=l}\|X_j - M_j\|$,

Where X_j belongs to an m -dimensional input space, $\|\cdot\|$ denotes the Euclidean distance, while the update of the synaptic weight vectors follows:

$$M_j(t+1) = M_j(t) + \alpha(t)N_j(t)[X_j(t) - M_j(t)], \quad j = 1,\cdots,l. \quad (10)$$

where $\alpha(t), 0 < \alpha(t) < 1$, designates the learning rate factor; $N_j(t)$ designates the decreasing neighbourhood function centred on the winner and means the number of neuron at the t learning times in the competitive layer. Although the algorithm is simple, its convergence and accuracy depend on the selection of the neighbourhood function, the topology of the output space, a scheme for decreasing the learning rate parameter, and the total number of neuronal units.

The SOFM algorithm can be summarized in the following basic steps.

1) Randomly select a training vector X_j from corpus. Make sure the initial value $\alpha(0)$, make sure the initial value $N_j(0)$, make sure the total learning times T ..

2) Find the winning neuron j with the weight M_j which is closest to X_j by minimizing the cost function $V(X)$.

3) Adjust the weight between the competitive layer neuron and input vector which in the neighborhood $N_j(t)$ of the competitive layer by formula (10).In practice, in order to better reflect the relationship between the input patterns and the neural weight vector in competition and improve the classification accuracy, we change the weight adjusting formula as:

$$M_j(t+1) = M_j(t) + \alpha(t)N_j(t)\exp\{-\rho_{XM}\}[X_j(t) - M_j(t)], \quad j = 1,\cdots,l. \quad (11)$$

Where ρ_{XM} is correlation coefficient and reflects the correlation of X_j and M_j, it changes between [-1,1],and ρ_{XM} is designated as:

$$\rho_{XM}=\frac{E\left\{\left[X_j-E\left(X_j\right)\right]\left[M_j-E\left(M_j\right)\right]\right\}}{\sqrt{D\left(X_j\right)}\sqrt{D\left(M_j\right)}} \tag{12}$$

Where $E\left(X_j\right)=\frac{1}{n}\sum x_{ji}$, $E\left(M_j\right)=\frac{1}{n}\sum m_{ji}$,

$D\left(X_j\right)=E\left(X_j^2\right)-\left[E\left(X_j\right)\right]^2$, $D\left(M_j\right)=E\left(M_j^2\right)-\left[E\left(M_j\right)\right]^2$

4) Renew $\alpha(t)$ and $N_j(t)$

$$\alpha(t)=\alpha(0)\left(1-\frac{t}{T}\right) \tag{13}$$

$$N_j(t)=INT\left|N_j(0)\left(1-\frac{t}{T}\right)\right| \tag{14}$$

5) $t=t+1$ and return step (2),until $t=T$.

4. Image Denoising based SOFM-HMM

After doing a 2D wavelet transform, we get four frequency subbands, namely, LL, LH, HL, and HH at every decomposition level. Because most energy of noise concentrates in high frequency , only wavelet coefficients in the high frequency levels need to be thresholded. Since the correlation among image wavelet coefficients is stronger and the correlation among white-noising wavelet coefficients is much weaker, wavelet coefficients can be easily classified through application of the SOFM algorithm. Wavelet coefficients in every high frequency level (LH, HL, and HH) are trained respectively, such resolves the problem of shortage of memory, and at the same time improves the training speed. SOFM-HMM has smaller number of observations than standard HMM, such as HMT, because the observations are separated into several classes using SOFM, and the number of observations in each class is smaller than the number of observations in all the classes. For this reason, SOFM-HMM has lower computation complexity than HMT.The other factor that affects the convergent speed is the structure of HMM.As the dependency model underlying the HMMs becomes more complicated, each iteration of the EM algorithm becomes slower, and the algorithm may take longer to converge. Hence, it is important to keep the HMMs as simple as possible. Thus, SOFM-HMM yields a flexible framework for signal denoising that strikes a balance between enough samples and spatial adaptability of the training algorithm. Once a trained HMM is obtained, estimation of the true signal wavelet coefficients (denoising) is straightforward. We can get the modified wavelet coefficients using the estimate formula . The final signal estimate (denoised signal) is computed as the inverse wavelet transform of these estimates of the signal wavelet coefficients.

Briefly, the SOFM-HMM algorithm of image denoising can be described as follows:

1) Perform forward 2D wavelet decomposition on the noisy image.

2) Apply the SOFM-HMM algorithm to train wavelet coefficients in every high frequency level (LH, HL, and HH) respectively.

3) Apply EM algorithm to estimate the whole parameters of SOFM-HMM.

4) Compute the estimation of the wavelet coefficients.

5) Perform inverse 2D wavelet transform of the estimation of the wavelet coefficients.

From our experiments we find that SOFM-HMM performs better than VisuShrink and HMM.

5. Experimental Results

The 512 x 512 standard grayscale image Lena is used in experiment. For comparison, we implement SOFM- HMM, VisuShrink and HMT. The Daubechies wavelet with 8 vanishing moments is used for the wavelet decomposition. For comparison,we implement VisuShrink, HMT, SOFM- HMM. VisuShrink is the universal soft-thresholding denoising technique. For different Gaussian white noise levels, the experiental results in Peak Signal to Noise Ratio (PSNR) are shown in Table 1 for denoising images Lena. The PSNR is defined as

$$PSNR=-10\log_{10}\frac{\sum_{i,j}\left(B(i,j)-A(i,j)\right)^2}{n^2\max_{i,j}A(i,j)^2} \tag{15}$$

where $B(i,j)$ is the denoised image and $A(i,j)$ is the noise-free image. The first column in this table is the PSNR of the original noisy images, while other columns are the PSNR of the denoised images by using different denoising methods. From Table 1 we can see that SOFM- HMM outperforms VisuShrink and HMT for all cases.

By studying the denoised images in Figure 2, we see that SOFM-HMM produces smoother and clearer denoised images.

6. Conclusions and Future Work

In this paper, we propose a wavelet image denoising method based HMMs through the SOFM algorithm which exploits spatial local correlation among image neighbouring wavelet coefficients. The main contribution lies in the classification strategy based on the SOFM algorithm. Experimental results have show that SOFM-HMM gives better results when the noise variance gets larger. However, the main drawbacks of this approach is the high computational cost, which grows exponentially with the dimensions of the output space. Future work may be done by extending this idea to the multiwavelet case.

References

Achim A, Kuruoğlu E E, (2005). Image denoising using bivariate α-stable distributions in the complex wavelet domain [J]. *IEEE Signal Processing Letters*. 12(1): 17-20.

Crouse M.S., Nowak R.D.and Baraniuk R.G., (1998). Wavelet-based statistical signal processing using hidden Markov models. *IEEE Trans. Signal Processing*. 46 (4), pp.886-902,.

D.L.Donoho, (1995).Denoising by soft-thresholding. *IEEE Trans.on Information Theory.* vol. 41, pp. 613–627.

Donoho D L, Johnstone I M, (1994). Ideal spatial adaptation via wavelet shrinkage [J]. *Biometrika*. 81(3): 425-455.

Ferrari Ricardo J, Winsor R ,(2005). Digital radiographic image denoising via wavelet-ased hidden Markov model estimation [J]. *Journal of Digital Imaging.* 18(2): 154-167.

Romberg J K, Choi H, Baraniuk R G, (2001). Bayesian tree-structured image modeling using wavelet-

domain hidden Markov models [J]. *IEEE Transactions on Image Processing.* 10(7): 1056-1068.

T. T. Cai , B. W. Silverman, (2001). Incorporating information on neighbouring coefficients into wavelet estimation. *Sankhya: The Indian Journal of Statistics*.Vol. 63, Series B, Pt. 2, pp. 127-148.

Table 1. The PSNR (dB) of the noisy images of Lena and the denoised images with different denoising methods.

Noisy Image	VisuShrink	HMT	SOFM-HMM
25.28	25.19	27.12	27.65
21.20	24.03	25.38	25.93
17.32	22.31	24.89	25.34
15.12	21.16	22.09	23.83

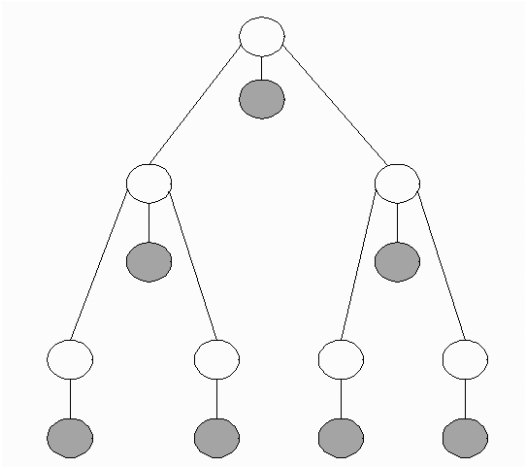

Figure 1. HMT where white nodes represent hidden states and dark nodes represent wavelet coefficients.

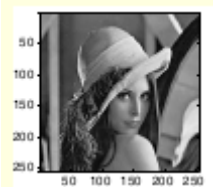

Noise free image

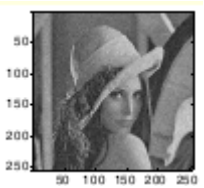

Noisy image

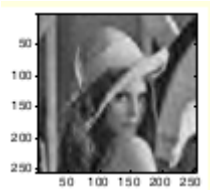

VisuShrink

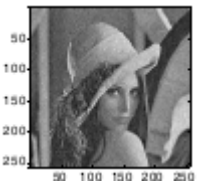

HMT

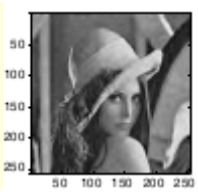

SOFM-HMM

Figure 2. Image denoising by using different methods on anoisy image with PSNR = 21dB.

Modern Applied Science

www.ccsenet.org/journal.html

Vol. 2, No. 5

September 2008

Study on the Service Quality Evaluation and Improvement for Medium and Small Sized Hotels

Fan Chen

Commercial College

Tianjin University of Commerce

Tianjin 300134, China

E-mail: pzhcf117@126.com

Abstract

The tourism industry is in the important state in the national economy, and the hotel industry is the important part of the tourism industry, and the medium and small sized hotels occupy certain market share because of the numerous quantity. Because the service qualities of medium and small sized hotels are different, so the service quality of the hotel is the nuclear content of hotel management. At present, the supply exceeds the demand in the global hotel market, and the competitions among hotels are very intense, and who can supply excellent service for customers, who can obtain predominance in the market and attract more customers and get good benefits, and so the service quality is the life of hotel. In China hotel industry, especially for medium and small sized hotels, their management methods are draggled and there service qualities are relatively low, so many problems exist in this industry. As viewed from customers, this article discusses the satisfactory degree measurement about medium and small sized hotels based on the SERVQUAL method put forward by Parsuraman and the domestic scholars' opinions about hotel service research, and analyzes the service quality problem of medium and small sized hotels and puts forward the project of improvement.

Keywords: Medium and small sized hotels, Service quality evaluation, SERQUAL

1. The research meaning and definition of service quality

The service quality is the core of service management, and the early researches about service quality mainly are focused in the domain of service marketing. After that, the researches are gradually extended to the service operation, human resource management and other relative domains. The service quality presents the character across many subjects. And according to one literature search made by US scholar, Raymand Fisk, the service quality is the most centralized problem in the research of service management so far.

2. The model of service quality evaluation: SERVQUAL

2.1 The theoretic basis of SERVQUAL scale

In 1985, US scholars Parasuraman, Zeithaml and Berry established a sort of new service quality evaluation scale, SERVQUAL, and constructed the five-points difference theory based on Gronroos's research, i.e. manager service quality perception difference, service quality rule standard difference, service process difference, market communication difference and customer service quality perception difference. Whether the difference exists in the expectation of customer service quality and the actual perception of service quality is the important part to implement the service quality evaluation and advance the improvement of service quality. The service quality comes from the difference that customers compare their actual perception of service quality with the expectation of service quality offered by the service providers. If customers' actual service perception equals to or exceeds the expectation, they will think the service quality is high. And if customers' actual service perception is under the expectation, they will think the service quality is unsatisfactory.

2.2 The structure system of SERVQUAL scale

The SERVQUAL scale is established based on the fifth point difference in the difference theory, i.e. the perception difference of customer service quality. In 1988, Parasuraman and other scholars reestablished this evaluation system, and they centralized and reduced 10 evaluation dimensions to 5 dimensions, i.e. reliability, assurance, tangibility, empathy and responsiveness. In order to effectively evaluate these 5 dimensions, they designed a questionnaire table

including 22 problems in 1988, which was called as the SERVQUAL scale afterward. The questionnaire includes the customer expectation for service quality and the customer actual perception for service quality. In these 22 problems containing 5 dimensions, every dimension contains 4-5 problems, and the answer of every problem is denoted by the method of 7 point Likert scale, where 1 represents very disaccording and 7 represents very according. The questionnaire must implement two times investigation to same one informant, and require him answer two parts of problems in the questionnaire in order to respectively measure the expectation and the actual perception of customer service quality, and the result of two times evaluations will decide whether the difference exists in the service quality.

3. The actual application of SERQUAL in medium and small sized hotels

The SERVQUAL method put forward by Parsuraman can be applied in China medium and small sized hotels, but it should be implemented some adjustments according to Chinese actuality, for example, the national current investigation scale is 7 point scale and the medium value is 4, but in China, most groups have not clear recognitions to these concepts, and the 7 point scale is difficult to be differentiated clearly, which will influence the reality of the investigation, so the reasonable investigation scale is 5 point scale in China, which is easily differentiated and accepted by the public and which result will more reflect actual situation. The investigation showed that in five attributes of service quality in SERVQUAL scale for China hotels, the customers' satisfactory degree of materiality (including dish taste, disposal of guest room, staff dress, menu print, establishment and restaurant position) is lowest. After evaluating the hotel service quality through SERQUAL scale, we should implement the equal index analysis of SERVQUAL evaluation through the weighted formula

$$SQ = \sum_{k=1}^{5} W_k \sum_{i=1}^{R} (\overline{P_i} - \overline{E_i})$$

Where, SQ denotes the total perception quality in the SERVQUAL scale, Wk denotes the weight of every attribute, R denotes the problem amount of every attribute, Pi denotes the mark of customer's perception to the i'th problem, Ei denotes the mark of customer's expectation to the i'th problem.

This method can quantify the effects of various attribute levels to the customer evaluation service quality through evaluating mutual influences and functions among main attributes of product or service.

4. The limitation of SERVQUAL in the application in medium and small sized hotels

For the industry management, following problems exist in the application of SERVQUAL quality evaluation system, and they will influence the veracity and reliability of service quality evaluation.

4.1 The structure limitation of SERVQUAL questionnaire

In the questionnaire of "difference" theory of SERVQUAL, every dimension is composed by 4-5 questions, and all dimensions form the evaluation questionnaire composed by 22 questions. However, 4-5 questions can not completely contain all connotations of one dimension. So when we design the questionnaire, we can not copy the structure of the former questionnaire, we should add, delete or modify the content of the questionnaire according to the specific characters of tourism industry, restaurant industry and catering industry.

Because the inquirer needs evaluating the expectation and actual perception of service quality, so two questionnaires are needed, and one checks the expectation and the other checks the actual perception. After the customer completes the first questionnaire, because the second one is very similar with the first one in the aspects of structure, sentence form and diction, so it will make customer usually confuse these two questionnaires, and he would think two questionnaires are same and reject filling in the second questionnaire or fill in part of the questionnaire, which will induce the reduction of reliability and creditability of questionnaires.

4.2 The SERVQUAL system can not fully consider the weights of 5 dimensions which compose the service quality of the hotel industry

Wong pointed out that the hotel service quality evaluation should emphasize the differences of 3 dimensions including employee, creditability and materiality, not the differences of 5 dimensions. Domestic scholars had pointed out that the materiality was the dimension which was urgently solved to improve and enhance the hotel service quality in the comparative research of service quality in many three-star or four-star medium and small sized hotels. The difference of chain hotel service quality consists in that the perceptions of empathy and responsiveness are under the expectations, but the evaluations of creditability and materiality are good (Antony & Ghosh, 2004). Because the management characters of the hotels with different ownerships, different levels and different objectives are different, so the evaluation of the hotel service quality should consider the management character of this hotel, especially we should confirm the various weights of 5 dimensions which form the service quality aiming at the management character of medium and small sized hotels, and accordingly scientifically evaluate the service quality of medium and small sized hotels.

4.3 The characters of medium and small sized hotels influence the authenticity and creditability of SERVQUAL scale evaluation

Carman (1990) pointed that the real point in the hotel service process, the complexity and the occurrence frequency of service transfer process would influence the authenticity and creditability of SERVQUAL evaluation result. First, the hotel management possesses the character of complexity and diversity, and the customer needs experiencing the services of various departments including gatehouse, guest room and catering, and any one bad service quality of single department in the whole service process will influence customer's satisfactory degree to the service quality of this department, and accordingly influence the veracity of the service quality evaluation of the whole hotel. Second, the service occurrence frequency also will influence the validity of the SERVQUAL scale. For example, the difference exists in the expectations of service quality between familiars and the customer who first patronizes this hotel, and they will give different evaluation results for the service quality.

5. The service quality management and countermeasure analysis of medium and small sized hotels

When we complete the discussion of hotel service quality evaluation, we will put forward the service quality management and countermeasure analysis aiming at some problems possibly occurred in the evaluation in order to obtain the actual effects of finding and solving problems. This article will improve the service quality from following three aspects.

5.1 Satisfying customers' demands and enhancing customers' perceptive values

Facing customers' continually mature consumption concepts and demands, only we timely know customers' changes of demand, we can develop the service project according with the market and customer satisfaction aiming at customers' demands. For example, add network equipment in the guest room to enhance customers' convenience to the demand of information. In the hotel industry, customers' consumption habits and mentalities are different, and they require services with more individuations, so we should enhance customer's perceptive value and satisfactory degrees when satisfying customers multi-levels demands. And only the perceptive service achieves or exceeds expectative service, the customer will satisfy.

5.2 Service standardization

The variance exists in the service quality, and the main reason is that the service has not been standardized, and employee's service always bases on his will. So the effective service standard must be established. But the establishment of service standard should follow following principles including (1) fulfilling customer's expectation, (2) science, (3) quantification and concretion, and (4) the character of characteristic and times. The service standardization mainly includes three aspects, i.e. the service quality standardization, the service method standardization, and the service process proceeding. To achieve the quality standard of the service, there need not only the method to ensure the service quality, but a set of strict procedure in the service process, and these procedures must be fit for the normal services, which is the proceeding of service process. Every service work, whether the direct service or the indirect service, must be performed according to the regulatory procedure, so the service quality can be guaranteed basically. At the same time, the service standardization must combine with the service individuation.

5.3 Adopting objective management and implementing team cooperation

The essential of objective management is to emphasize that the organizational members participate the objective project themselves, realize self control and work surrounding the objective. The objective management also can make the right of process management transfer to a lower level, make employees consider nothing when they independently solve customers' problems, and make the hotel service more individuation and people-oriented under the premise keeping the whole effective control. We can utilize the team cooperation such as department work team, trans-functional work team and specially appointed work team which can quickly produce responses to customers' continually changeable demands and expectations according to the limitation of traditional class system to the decision ability, and establish effective performance objective and achieve this objective.

References

Antony, J. Ghosh. (2004). Evaluating Service Quality in a UK Hotel: a Case Study. *International Journal of Contemporary Hospitality Management.* No.16 (6). p.380-384.

Dang, Zhongcheng & Zhou, Zhili. (2002). On the Measurement and Improvement of Hotel Service Quality. *Tourism Tribune.* No.2.

Zhang, Jingtai. (1999). Analysis of the Service Quality Management Emphasis for Hotel. *Systems Engineering Theory Methodology Applications.* No.1.

Zhang, Lili. (1995). Study on the Management and Control of Hotel Service Quality. *Tourism Tribune.* No.6.

Zhuhang & Wang, Chunxiao. (1995). Study on the Management and Control of Hotel Service Quality. *Tourism Tribune.* No. 6.

Modern Applied Science

www.ccsenet.org/journal.html

Vol. 2, No. 5

September 2008

A Study of a New Shaped Mechanism of a Ring Spinning Machine Based on Eccentric Cam System Controlled by Microcomputer

Wei Wang, Jiancheng Yang & Zhe Liu

School of Mechanical & Electronic Engineering

Tianjin Polytechnic University

Tianjin 30016, China

E-mail: wangwei120911@yahoo.com.cn

Abstract

This study has for the first time developed a new shaped mechanism of the ring spinning frame based on an eccentric cam system controlled by microcomputer to solve the shortcomings of traditional shaped mechanism of a ring spinning mechanism of a ring spinning machine driven by a plate cam at a constant rotation speed. It has established a model of the shaped mechanism of the ring spinning frame and proposed an optimum control algorithm. The study has theoretically proved that the feasibility of the new shaped mechanism and made simulation experiments. The results of application show that the new shaped mechanism does not only overcome shortcomings of the traditional one, but has much generality.

Keywords: Eccentric cam system, Shaped mechanism, Ring spinning frame, Control

1. Introduction

Ring Spinning Frames are main machines which have been using in the textile industry. And study on their shaped mechanisms has been concerned by both domestic and overseas experts. At present, the shaped mechanisms of ring spinning frames, which have been used in cotton, wool, silk, and flax ring spinning machines, are controlled by constant speed plate cams. Motion regulations of the shaped mechanisms can be obtained just by designing their profile curves of cams. However, these kinds of shaped mechanisms have shortcomings such as: (1) where the profile curve of the cam changes a lot, it is easy to cause pounding or pause, and to lead to the bad reel. Therefore, the yarn quality is affected. (2) It is difficult to manufacture the profile curve of the cam by using common methods. (3) The cam is inflexible, and can satisfy only one kind of motion regulation. Therefore, it is valuable to study the shaped mechanism theoretically and practically.

In recent years, there have been two major approaches to study the shortcomings of the cams mentioned above. On the one hand, an optimum cam profile curve may be designed by some special methods(Yu Q, 1996, p.181-186 & Shen, 1991, p.12-15); on the other hand, the concept of an eccentric cam is introduced(Leslie, 1996, p.39-41), which deferent from traditional cam, it is an actuator which simulates the cam at a constant rotation speed, that is, the cam does not contact driven components, between which there is only electrical relationship. An application to robot is introduced in the paper (Hiroshi, 1999, p.39-40). In paper (Yao, 1999), kinematical and dynamic characteristics of cam driven by servo motor by changing different input functions are studied , which are under the condition of non-changing cam profile curve.

In the light of analyses of the problems existing in the traditional shaped mechanisms of ring spinning frames, a new shaped mechanism has been successfully developed firstly. In particular, an eccentric cam which is programmable is used as a kind of general executive component, by which some desired output regulations can be obtained through changing program without changing the cam profile curves. In addition, there are no needs of considering the problems such as minimum curvature radius and pressure angle and so on.

Obviously, the problems mentioned above can be solved by making use of the new shaped mechanism.

2. Control Rules of Eccentric Cam

2.1 Determining motion laws of angular displacement and angular velocity of eccentric cam

A scheme of the eccentric cam of roller follower and an identical scheme of one are given in Figure 1. (a) and (b), respectively.

Supposing Crank $l_1 = e$ (e is an eccentric distance)

Linkage $l_2 = r + r_1$ (where r is radius of cam ; r_1 is radius of roller follower)

Rock bar $l_3 = l_{\mathrm{AO_f}}$ (the length of frame)

$l_4 = l_{\mathrm{o_c o_f}}$

Given rotation angular of crank is φ ; rotation angular of rock bar is ψ (see Figure 1. (b))

Hence
$$\psi(\varphi) = \delta - \psi_0 \tag{1}$$

Where
$$\psi_0 = \cos^{-1}\frac{{l_3}^2 + {l_4}^2 - (l_2 - l_1)^2}{2 l_3 l_4}$$

$\delta = \angle \mathrm{O_c} O_f \mathrm{A_1}$

According to geometrical knowledge, the following result can be obtained
$$\delta = \mathrm{tg}^{-1}\frac{A}{B} - \sin^{-1}\frac{C}{\sqrt{A^2 + B^2}} \tag{2}$$

Where
$$A = \frac{l_4}{l_1} + \cos(\varphi_0 + \varphi)$$

$B = \sin(\varphi_0 + \varphi)$

$$C = \frac{{l_3}^2 + {l_4}^2 + {l_1}^2 - {l_2}^2 + 2 l_1 l_4 \cos(\varphi_0 + \varphi)}{2 l_1 l_3}$$

$$\varphi_0 = \sin^{-1}[\frac{l_3}{l_2 - l_1}\sin\psi_0]$$

The regulation of driven member is presented as follows:

$$\psi = \psi(t) \tag{3}$$

Angular velocity can be obtained by the first derivation of angular displacement with respect to time

$$\dot{\psi} = \frac{\mathrm{d}\psi(t)}{\mathrm{d}t} = \frac{\mathrm{d}\psi(\varphi)}{\mathrm{d}\varphi} \times \frac{\mathrm{d}\varphi}{\mathrm{d}t}$$

Rewriting the formula above leads to

$$\dot{\varphi} = \frac{\mathrm{d}\varphi}{\mathrm{d}t} = \dot{\psi} \Big/ \frac{\mathrm{d}\psi(\varphi)}{\mathrm{d}\varphi} \tag{4}$$

where $\frac{\mathrm{d}\psi(\varphi)}{\mathrm{d}\varphi}$ is hold according to Eq. (1)

Angular displacement of the eccentric cam is obtained based on Eq. (4).

$$\varphi(t) = \int_0^t \frac{\dot{\psi}}{\frac{\mathbf{d}\psi(\varphi)}{\mathbf{d}\varphi}} \mathbf{d}t \tag{5}$$

2.2 Optimum calculus of control instructions of angular displacement of the eccentric cam

It is only suitable to solve several values of some points with calculus to solve angular displacement of the eccentric cam by Eq. (5).

Considering continuous conditions, it is suitable to adopt spline function to approach function φ(t) by steps.

2.2.1 Simulation with the 5th order spline function

Two factors should be considered when proceeding curve simulation is done. Firstly, fewer inserting values in keeping simulating accuracy should be chosen under the condition of equal distribution of insert points. Secondly, when changing the distribution of insert points to meet the needs of simulation accuracy in order to obtain optimum simulation curve with third derivation, the best simulation curve can be reduced to the following optimum design.

$$\phi(x_j) = \min\left\{ \max_{j=2,3\ldots,n_{j-1}} (\Delta y(x_j) \right\} \tag{6}$$

Subject to:

$$\Delta y = y_j(x_i) - \overline{Y}_j(x_i) \le \varepsilon$$

2.2.2 Optimum design of curve simulation by steps with 5th order spline function.

We can adopt the 5th order spline function to replace Eq.(5) by steps, if cam angular displacement and angular velocity of every section of beginning and end are given

$$\sum_{i=1}^{n} [\varphi(t)_i - \hat{\varphi}(t)_i]^2 \le \varepsilon, \quad i = 2,3,\ldots,\text{n-1}$$

Note that, it should be to considered that $\sum_{i=1}^{n} [\varphi(t)_i - \hat{\varphi}(t)_i]^2 \le \varepsilon$,($i$ =2,3,…,n-1) is among the middle value of section the control law $\hat{\varphi}$（KT）（K=1,2,….)of angular displacement of eccentric cam can be obtained according to adoptive sample T. Control rules $\hat{\varphi}$（KT）（K=1, 2…) of eccentric cam can be obtained according to adoptive sample T after spline $\hat{\varphi}(t)$ of every section function is given.

That is

$$\hat{\varphi}(t) = \sum_{k=0}^{5} a_k (t - t_1)^k \tag{7}$$

Boundary conditions:

$$\varphi(t_1) = \varphi_1, \quad \varphi(t_n) = \varphi_n; \dot{\varphi}(t_1) = \omega_1 \ , \dot{\varphi}(t_n) = \omega_n; \ddot{\varphi}(t_1) = \varepsilon_1 \ , \ddot{\varphi}(t_n) = \varepsilon_n . \tag{8}$$

where φ_1 and φ_n —— Angular displacement of beginning and end points, respectively

ω_1 and ω_n ——Angular velocity of beginning and end points, respectively

ε_1 and ε_n ——Angular acceleration of beginning and end points, respectively

t_1 and t_n ——time of beginning and end points, respectively

3. Design of Control System

3.1 System model of variable frequency and adjusting speed

The block figure of control system of changing frequency and adjusting speed is shown in Figure 2.

$V(t)$ —— Changing frequency sign which is sent into frequency converter; $\omega(t)$ —— Regular velocity of motor spindle on the basis of frequency; $V_D(t)$——Sign which is sent by computer; $V(t)$——Simulation sign which comes from D/A converter; $M(t)$—— Motor torque.

Transfer function is expressed as follows:

$$\frac{\omega(s)}{M(s)} = \frac{1}{Js + c} \tag{9}$$

Where J—— The moment of inertia

c—— The damping coefficient

If frequency converge is taken as inertia system, its transfer function is $\frac{k_1}{\tau_1 s + 1}$;

Where k_1 —— Defined as increasing rate of frequency controller (v/s)

If D/A controller is taken as keeper of 0 order, its transfer function is taken as $\frac{1-e^{Ts}}{s}$. Therefore, transfer function of the system based on D/A controller is shown in Figure 3.

Considering sign delay, the transfer function of the cam system is

$$HGp(z)=\frac{K(b_1z^{-(d+1)}+b_2z^{-(d+2)})}{1-a_1z^{-1}-a_2z^{-2}} \tag{10}$$

Where

$a_1=e^{-\frac{T}{\tau_1}}+e^{-\frac{T}{\tau_2}}$

$a_2=e^{-\frac{T}{\tau_1}-\frac{T}{\tau_2}}$

$b_1=1+\frac{\tau_1e^{-\frac{T}{\tau_1}}-\tau_2e^{-\frac{T}{\tau_2}}}{\tau_2-\tau_1}$

$d=\tau_d\big/T$

$b_2=e^{\frac{-T}{\tau_1}-\frac{T}{\tau_2}}+\frac{\tau_1e^{\frac{-T}{\tau_2}}-\tau_2e^{\frac{-T}{\tau_1}}}{\tau_2-\tau_1}$

(d and b_2 are whole numbers, and τ_d is delay time)

$k=\frac{k_1k_D}{c}$, $\tau_2=\frac{J}{c}$

3.2 Design of control approach

Here, the control method of increment may be chosen, which consists of the front feedback and the hind feedback, that is, combinations of open loop and closed loop as shown in Figure 4, because the cam may pursue after any position sign without error in theory.

3.2.1 Design of front feedback and hind feedback

The block figure on the basis of Figure 4. is expressed in Figure 5, in which the part depicted as dotted line is composition controller realized by computer program.

Where $\Delta X(z)$ —— Theoretic angular displacement increment of the eccentric cam in theory

$\Delta Y(z)$ ——Actual angular displacement increment

$\Delta E(z)=\Delta X(z)-\Delta Y(z)$ ——Error value

$M_1(z)$ and $M_2(z)$ —— Feedback positive number and front feedback positive number

$M(z)=M_1(z)+M_2(z)$ —— The total correct value

In the light of Figure 5, transfer function scheme is expressed as follows:

$$\frac{\Delta Y(z)}{\Delta X(z)}=\frac{G_F(z)HG_P(z)+G_C(z)HG_P(z)}{1+G_C(z)HG_P(z)} \tag{11}$$

If $G_F(z)HG_P(Z)=1, \Delta Y(z)/\Delta X(z)=1$, the theoretic transfer function of pursuing input sign without output sign is obtained.

So transfer function of front feedback control may be written as:

$$G_p(z)=\frac{M_2(z)}{\Delta X(z)}=\frac{1}{HG_p(z)}=\frac{1-az^{-1}}{bz^{-d-1}} \tag{12}$$

Front feedback positive number is

$$M_2(z)=\frac{1-aZ^{-1}}{bZ^{-d-1}}\Delta X(z)=\frac{1}{b}[Z^{d+1}\Delta X(z)-aZ^d\Delta X(z)] \tag{13}$$

Thus, the recurrence formula of front feedback is expressed as follows:

$$M_2(k)=K_F[\Delta x(k+d)-a\Delta x(k+d)] \tag{14}$$

In order to decrease the calculation time of practical control program, this paper calculates the front feedback error value in advanced, and produce a table of front feedback for testing. The controller $G_c(z)$ of closed feedback can adapt the simple PID controller. Considering the dynamic characteristic of frequency converter, it is suitable to choose PI controller, and its error value is defined as

$$m_1(t) = K_P \Delta e(t) + K_I \int_0^1 \Delta e(t)dt \tag{15}$$

The formula of feedback error value can be obtained by discrediting Eq.15.

$$M_1(k) = K_P \Delta E(k) + K_I E(k) \tag{16}$$

3.2.2 Design of PI controller parameters

In order to obtain K_p of PI controller and K_I of PID controller, calculate K_p and k_I on the basis of experiential formulas. After an initial result is obtained, modify it by experiential method.

According to PID formulas, several formulates are obtained as follows:

$$K_P = 0.45K_{PU} \tag{17}$$

$$K_I = K_P /(0.83T_U) \tag{18}$$

Where K_{PU} ——PI controller increment

T_U ——Oscillation period

To obtain K_{PU} and T_U, make pulse transfer function HGP(Z) restore continuous transfer function, and it can be expressed as follows:

$$G_P(s) = \frac{Ke^{-\tau_d s}}{\tau s + 1} \tag{19}$$

where K = 1.274, τ =0.068, τ_d =0.11

According to Nyquist criterion, and considering function GK(jω), several results, which are obtained by solving equation (19), can be obtained as follows:

ω_ψ =19.2921

K_{PU} =0.7851

So $$T_U = 2\pi / \omega_U = 0.3257$$

Substituting K_{PU} and T_U to Eqs. (17) and (18), the initial numerical value can be obtained as follows:

K_{PU} =0.3533

T_U =1.3158

Choosing PI controller parameters depends on the formulas, which is applied to experiment and modified. Considering that the total error amount consists of front feedback error and feedback error, it is suitable to adopt front feedback error and to pursue the slope wave input. A diagram with slope wave $x(k)$ =20, 10 (responsibility to 600r/min and 300r/min.) and $K_p = K_I$ =0.34 is depicted in Figure 7.

From Figure 6, we can come to the conclusions that stable errors are zero, without surpass, but transition time is too long. When rotation speed is 600r/min. adjustment time is 0.94s; when 300r.p.m, 0.49s. If K_p and K_I are increased, there are surpass or saturation.

On the basis of analyses mentioned above, it is reasonable to choose K_p =0.3533, K_I =1.3138.

4. Experiment of Cam Mechanism

On the basis of theoretical study and simulation mentioned above, a new shaped mechanism of ring spinning frame based on eccentric cam system controlled by microcomputer is developed firstly as shown in Figure 7. This system consists of single chip computer, frequency converter, A.C. motor, gear reducer, shift encoder and mechanism of eccentric cam with roller follower and so on, which is illustrated in Figure 8. in broken line.

The ring spinning frame may be selected as an experimental device (see Figure 7.). The prototype is shown in Figure 7. Here, choosing. a =15(mm); b =93(mm); c =400(mm) (see Figure 8.).

Solving Eqs. (1) ~ (15) leads to the law of movement, just as shown in Figure 9.

As shown above, some results are obtained. Firstly, the time is about the same with the two kinds of cam. Secondly, the shock is about the same by two kinds of cam. Thirdly, the curves between two cams drivers are about the same.

There, however, is a little pause when curve is in changing direction, whose main causes are the response speed of motor is lower at the corner of changing speed, so that the ring board moves behind.

Output motion regulations can be obtained illustrated in Figure 10. When constant speed law is input.

The new shaped mechanism is characteristic by the eccentric cam that is simple contracture and easily manufacturing and every output law of roller follower can be obtained by changing program. The experimental results show that it is obvious that the new shaped cam mechanisms can overcome the disadvantages of the traditional ones. Therefore, this kind of shaped mechanism has more practical effect.

5. Conclusions

(1)A new shaped mechanism is put forward, and it proves theoretically and practically that this mechanism works effectively.

(2) The optimum control instructions can be obtained by Optimum design of curve simulation by steps with 5th order spline function.

(3) Errors can be decreased by using the front feedback and the hind feedback.

(4) The old shaped mechanisms of ring spinning frames, which have been used in cotton, wool, silk, and flax ring spinning machines, may be replaced by the new shaped mechanism developed by this study.

References

Gu, Ningxi & Wang, Shuigen. (1991). Analyzing and Improvement of Building cam shock in spinning Frame. *Journal of Textile Research*, 12(7), 13-13.

Hiroshi, Makino. (1999). Smart cam application to robot Control. *Assembly Automation*, 19(1), 39-40.

Jan, van Gerwen. (1999). Electronic cam and gear. *Assembly Automation*, 19(1), 35-38.

Leslie, Langnau. (1996). Using electronic cams for motion control. Power Transmission Design, 2(6), 39-41.

Shen, Shide & Lv, Shiyuan. (1991). New Method for Designing Textile Cam. *Journal of Textile Research*, 12(1), 12-15.

Yu, Q. (1996). Optimum design of cam mechanisms with oscillating flat-face followers. *Mechanics Research Communications*, 23(2), 181-186.

Yao, Yan'an. (1999). Active Control for Cam Mechanism. Ph. D thesis, Tianjin University, Tianjin, China.

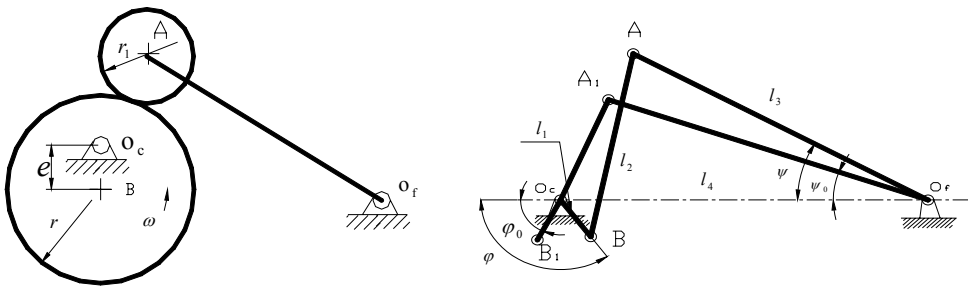

(a) (b)

Figure 1. Scheme and identical scheme of an eccentric cam of roller follower

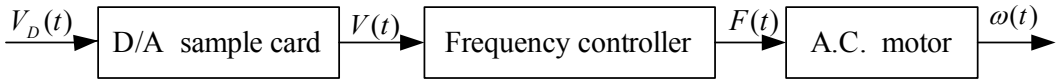

Figure 2. Scheme of changing frequency and adjusting speed

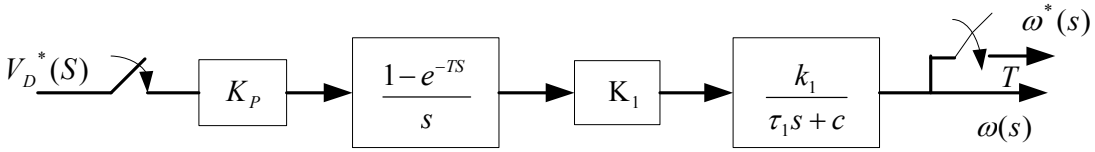

Figure 3. Block figure of transfer function of controlled system

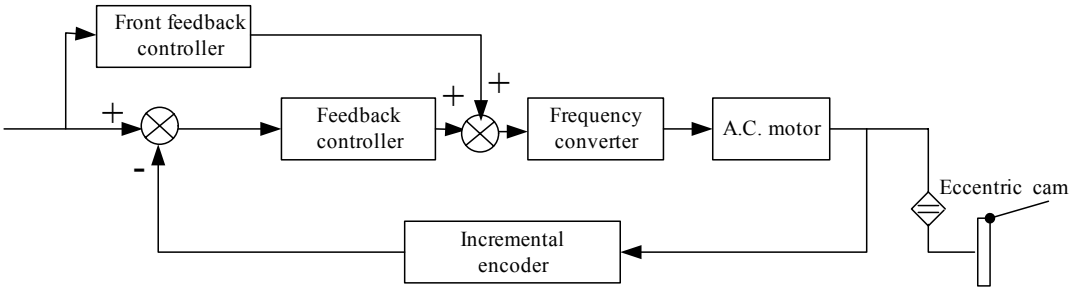

Figure 4. Scheme of control system

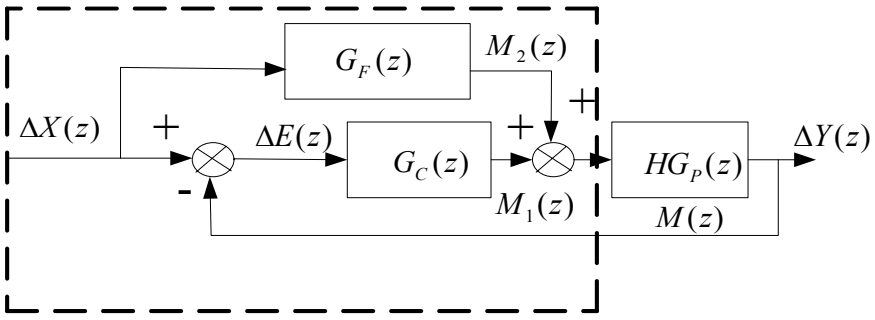

Figure 5. Transfer function figure of control system

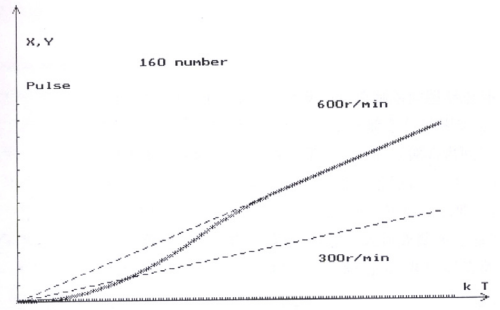

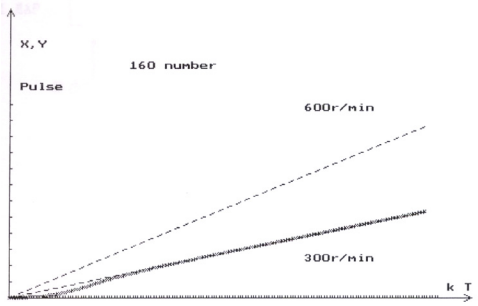

(a) $x(k)$ =20 slope wave input (b) $x(k)$ =10 slope wave input

Figure 6. Output scheme of slope wave input

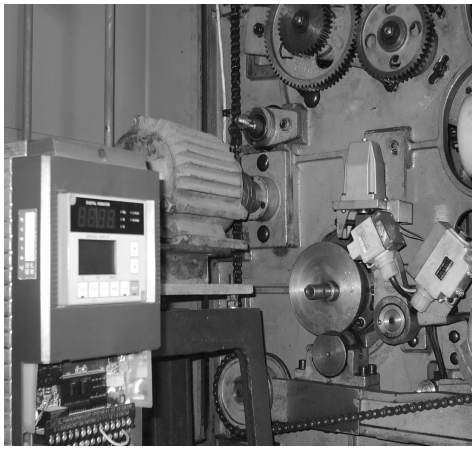

Figure 7. A prototype of the eccentric cam system

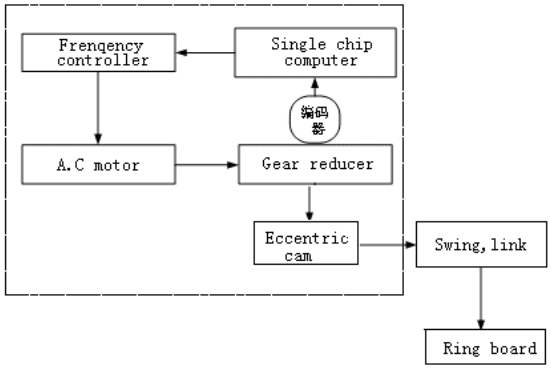

Figure 8. Schematic diagram of the eccentric cam system

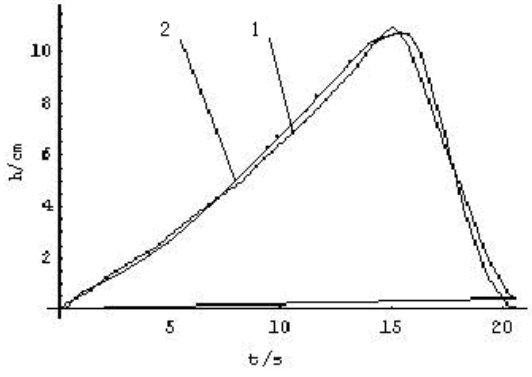

Figure 9. Displacement curve of ring board

1. The law of the old plate cam
2. The law of eccentric cam

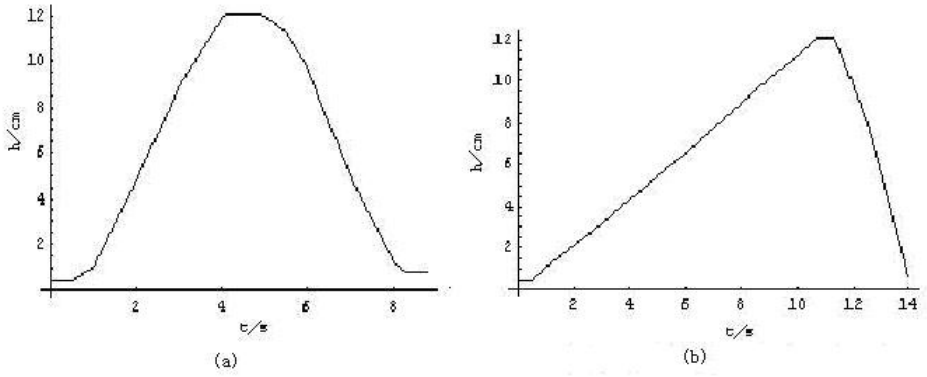

Figure 10. Output motion law scheme of input constant rotation

(a) Input constant rotation at the same rotation

(b) Input constant rotation at the different rotation

Modern Applied Science

www.ccsenet.org/journal.html

Vol. 2, No. 5

September 2008

Steady-state Analysis of the GI/M/1 Queue with Multiple Vacations and Set-up Time

Guohui Zhao
College of Science, Yanshan University
Qinhuangdao 066004, China
E-mail: zhaoguohui821@163.com
Xinxin Du
College of Science, Yanshan University
Qinhuangdao 066004, China
Naishuo Tian
College of Science, Yanshan University
Qinhuangdao 066004, China
Xiaohua Zhao
College of Science, Yanshan University
Qinhuangdao 066004, China
Dongmei Zhao
College of Science, Yanshan University
Qinhuangdao 066004, China

Abstract

In this paper, we consider a GI/M/1 queueing model with multiple vacations and set-up time. We derive the distribution and the stochastic decomposition of the steady-state queue length, meanwhile, we get the waiting time distributions.

Keywords: Multiple vacations, Set-up time, Stochastic decomposition

Introduction

Vacation queues servers to stop the customers' service at some periods, and the time during which the service is interrupted is called the vacation time. Vacation queue research originated from Levy and Yechial, then many researchers on queuing theory deal with this fields. So far, the theory frame whose core is the stochastic decomposition is developed and vacation queues have been applied successfully to many fields, such as computer systems, communication networking, electronic and call centers. Details can be seen in the surveys of Doshi and the monographs of Tian. For GI/M/1 type queues with server vacations, Tian used the matrix geometric solution method to analyze and obtained the expressions of the rate matrix and proved the stochastic decomposition properties for queue length and waiting time in a GI/M/1 vacation model with multiple exponential vacations.

1. Description of the model

Consider a classical GI/M/1 queue, inter-arrival times are i.i.d.r.vs. Let $A(x)$ and $a^*(s)$ be the distribution function and L.S transform of the inter-arrival time A of customers. The mean inter-arrival time is $E(A) = -a^{*'}(0) = \lambda^{-1}$,Service times during service period, vacation times and set-up times are assumed to be exponentially distributed with rate μ, θ, β, respectively. We assume that the service discipline is FCFS.

Suppose τ_n be the arrival epoch of nth customers with τ_0=0. Let $L_n = L_v(\tau_n^-)$ be the number of the customers before the nth arrival. Define

$$J_n = J(\tau_n) = \begin{cases} 0, \text{the nth arrival occurs during a service period,} \\ 1, \text{the nth arrival occurs during a set - up period,} \\ 2, \text{the nth arrival occurs during a vacation period.} \end{cases}$$

The process $\{(L_n, J_n), n \geq 1\}$ is a Markov chain with the state space

$$\Omega = \{(0,2) \bigcup (k, j), k \geq 1, j = 0,1,2\}.$$

We introduce the expressions below

$$a_k = \int_0^\infty \frac{(\mu t)^k}{k!} e^{-\mu t} dA(t), k \geq 0, \quad b_k = \int_0^\infty \int_0^t \beta e^{-\beta x} \frac{[\mu(t-x)]^k}{k!} e^{-\mu(t-x)} dx dA(t), k \geq 0,$$

$$c_k = \int_0^\infty \int_0^t \int_0^{t-y} \theta e^{-\theta x} \beta e^{-\beta y} \frac{[\mu(t-x-y)]^k}{k!} e^{-\mu(t-x-y)} dx dy dA(t), k \geq 0.$$

First, the transition from $(i,0)$ to $(j,0)$ occur if $i+1-j$ services complete during an inter-arrival time. Therefore, we have

$$p_{(i,0)(j,0)} = a_{i+1-j}, i \geq 1, j = 1, \cdots, i+1.$$

Similarly,

$$p_{(i,1)(j,0)} = b_{i+1-j}, i \geq 1, j = 1, \cdots, i+1. \qquad p_{(i,1)(i+1,1)} = \int_0^\infty e^{-\beta t} dA(t) = a^*(\beta) = \gamma_2 \cdot$$

$$p_{(i,2)(i+1,2)} = \int_0^\infty e^{-\theta t} dA(t) = a^*(\theta) = \gamma_3 \cdot \qquad p_{(i,2)(j,0)} = c_{i+1-j}, i \geq 0, j = 1, \cdots, i+1.$$

$$p_{(i,2)(i+1,1)} = \int_0^\infty \int_0^t \theta e^{-\theta x} e^{-\beta(t-x)} dA(t) = \theta(a^*(\beta) - a^*(\theta)) \big/ (\theta - \beta) = \alpha(\gamma_2 - \gamma_3) \cdot$$

The transition matrix of (L_n, J_n) can be written as the Block-Jacobi matrix

$$\widetilde{P} = \begin{bmatrix} B_{00} & A_{01} & & & & \\ B_1 & A_1 & A_0 & & & \\ B_2 & A_2 & A_1 & A_0 & & \\ B_3 & A_3 & A_2 & A_1 & A_0 & \\ \vdots & \vdots & \vdots & \vdots & \vdots & \ddots \end{bmatrix}$$

where $B_{00} = 1 - c_0 - \alpha(\gamma_2 - \gamma_3) - \gamma_3, \quad A_{01} = (c_0, \alpha(\gamma_2 - \gamma_3), \gamma_3),$

$$A_0 = \begin{pmatrix} a_0 & 0 & 0 \\ b_0 & \gamma_2 & 0 \\ c_0 & \alpha(\gamma_2 - \gamma_3) & \gamma_3 \end{pmatrix}, \qquad A_k = \begin{pmatrix} a_k & 0 & 0 \\ b_k & 0 & 0 \\ c_k & 0 & 0 \end{pmatrix}, k \geq 1 \qquad B_k = \begin{pmatrix} 1 - \sum_{i=0}^{k} a_i \\ 1 - \sum_{i=0}^{k} b_i - \gamma_2 \\ 1 - \sum_{i=0}^{k} c_i - \alpha(\gamma_2 - \gamma_3) - \gamma_3 \end{pmatrix}, k \geq 1,$$

The matrix $\widetilde{P}$ is a GI/M/1 type matrix.

2. Steady-state queue length distribution

Lemma1. If $\rho = \lambda \mu^{-1} < 1$, $\theta, \beta > 0$, then $\delta > 0$, $\frac{\theta\beta}{\theta - \beta}(\delta - \Delta) > 0.$

where $\delta = \frac{\gamma_1 - a^*(\beta)}{\beta - \mu(1 - a^*(\beta))} = \frac{\gamma_1 - \gamma_2}{\beta - \mu(1 - \gamma_2)}$, $\Delta = \frac{\gamma_1 - a^*(\theta)}{\theta - \mu[1 - a^*(\theta)]} = \frac{\gamma_1 - \gamma_3}{\theta - \mu(1 - \gamma_3)}$. (1)

Theorem 1. If $\rho < 1$, $\theta, \beta > 0$, then the matrix equation $R = \sum_{k=0}^{\infty} R^k A_k$ has the minimal non-negative solution

$$R=\begin{pmatrix} \gamma_1 & 0 & 0 \\ \beta\delta & \gamma_2 & 0 \\ \alpha\beta(\delta-\Delta) & \alpha(\gamma_2-\gamma_3) & \gamma_3 \end{pmatrix}$$

where γ_1 is the unique roots in the range $0<z<1$ of the equation $z=a^*(\mu(1-z))$.

$\alpha=\theta/(\theta-\beta)$, δ and Δ are defined as in (1).

Proof. Because all $A_k, k\geq 0$ are lower triangular, we assume that R has the same structure as

$$R=\begin{pmatrix} r_{11} & 0 & 0 \\ r_{21} & r_{22} & 0 \\ r_{31} & r_{32} & r_{33} \end{pmatrix}$$

we obtain

$$\begin{cases} r_{11}=\sum_{k=0}^{\infty} r_{11}^k a_k = a^*(\mu(1-r_{11})), \quad r_{22}=\gamma_2, \quad r_{33}=\gamma_3 \\ r_{21}=\sum_{k=1}^{\infty} r_{21}\left(\sum_{i=0}^{k-1} r_{11}^i r_{22}^{k-1-i}\right)a_k+\sum_{k=0}^{\infty} r_{22}^k b_k, \quad r_{32}=\alpha(\gamma_2-\gamma_3) \\ r_{31}=\sum_{k=1}^{\infty} r_{31}\left(\sum_{i=0}^{k-1} r_{11}^i r_{33}^{k-1-i}\right)a_k+\sum_{k=2}^{\infty} r_{32}r_{21}\left(\sum_{i=0}^{k-2} r_{11}^i \sum_{j=0}^{k-2-i} r_{22}^j r_{33}^{k-2-i-j}\right)a_k \\ \qquad +\sum_{k=1}^{\infty} r_{32}\left(\sum_{i=0}^{k-1} r_{22}^i r_{33}^{k-1-i}\right)b_k+\sum_{k=0}^{\infty} r_{33}^k c_k \end{cases} \tag{2}$$

As we known, if $\rho<1, \theta>0$, the first equation has the unique root $r_{11}=\gamma_1$ in the range $0<r_{11}<1$. We can compute

$$\sum_{k=0}^{\infty} r_{22}^k b_k=\frac{\beta[a^*(\mu(1-r_{22}))-r_{22}]}{\beta-\mu(1-r_{22})}=\frac{\beta[a^*(\mu(1-\gamma_2))-\gamma_2]}{\beta-\mu(1-\gamma_2)}, \qquad 1-\sum_{k=1}^{\infty}\left(\sum_{i=0}^{k-1} r_{11}^i r_{22}^{k-1-i}\right)a_k=1-\sum_{k=1}^{\infty}\frac{\gamma_1^k-\gamma_2^k}{\gamma_1-\gamma_2}a_k=1-\frac{\gamma_1-a^*(\mu(1-\gamma_2))}{\gamma_1-\gamma_2}$$

$$=\frac{a^*(\mu(1-\gamma_2))-\gamma_2}{\gamma_1-\gamma_2},$$

Finally, we obtain $r_{21}=\beta\delta$, $r_{31}=\alpha\beta(\delta-\Delta)$ and the expression for R.

Theorem 2. The Markov chain (L_n, J_n) is positive recurrent if and only if $\rho<1$, $\theta, \beta>0$.

Proof. Based on Neuts, the Markov chain (L_n, J_n) is positive recurrent if and only if the spectral radius SP(R)=max $\{\gamma_1, \gamma_2, \gamma_3\}$ of R is less than 1, and the matrix

$$B[R]=\begin{pmatrix} B_{00} & A_{01} \\ \sum_{k=1}^{+\infty} R^{k-1}B_k & \sum_{k=1}^{+\infty} R^{k-1}A_k \end{pmatrix}$$

has a positive left invariant vector. Evidently, SP(R)=max $\{\gamma_1, \gamma_2, \gamma_3\}$<1. Substituting the expressions for R, A_k and B_k in $B[R]$,we obtain

$$B[R]=\begin{pmatrix} 1-c_0 & c_0 & 0 & 0 \\ \frac{a_0}{\gamma_1} & 1-\frac{a_0}{\gamma_1} & 0 & 0 \\ 1-\frac{\beta\delta a_0}{\gamma_1\gamma_2}+\frac{b_0}{\gamma_2} & \frac{\beta\delta a_0}{\gamma_1\gamma_2}-\frac{b_0}{\gamma_2} & 0 & 0 \\ A & B & \alpha\frac{\gamma_2-\gamma_3}{\gamma_3} & 1 \end{pmatrix}$$

Where

$$A=-\alpha\beta\left(\frac{\delta-\Delta}{\gamma_1\gamma_3}+\frac{\delta(\gamma_2-\gamma_3)}{\gamma_1\gamma_2\gamma_3}\right)a_0-\alpha\frac{\gamma_2-\gamma_3}{\gamma_2\gamma_3}+\frac{c_0}{\gamma_3}-\alpha\frac{\gamma_2-\gamma_3}{\gamma_3}$$

$$B=\alpha\beta\left(\frac{\delta-\Delta}{\gamma_1\gamma_3}+\frac{\delta(\gamma_2-\gamma_3)}{\gamma_1\gamma_2\gamma_3}\right)a_0+\alpha\frac{\gamma_2-\gamma_3}{\gamma_2\gamma_3}-\frac{c_0}{\gamma_3}\cdot$$

It can be verify that $B[R]$has the left invariant vector

$$\pi_0=K(1,\alpha\beta(\delta-\Delta),\alpha(\gamma_2-\gamma_3),\gamma_3)\cdot \tag{3}$$

Thus, if $\rho<1$, $\theta,\beta>0$, the Markov chain (L_n,J_n) is positive recurrent.

If $\rho<1,\theta,\beta>0$, let (L_v,J) be the stationary limit of the process (L_n,J_n).Let

$$\pi_0=\pi_{02};\quad \pi_k=(\pi_{k0},\pi_{k1},\pi_{k2}),k\geq 1,$$

$$\pi_{kj}=P\{L=k,J=j\}=\lim_{n\to\infty}P\{L_n=k,J_n=j\},(k,j)\in\Omega.$$

Theorem 3. If $\rho<1$, the stationary probability distribution of (L_v,J) is

$$\begin{cases}\pi_{k0}=K\alpha\beta\left(\dfrac{\gamma_1^k-\gamma_2^k}{\gamma_1-\gamma_2}\delta-\dfrac{\gamma_1^k-\gamma_3^k}{\gamma_1-\gamma_3}\Delta\right),k\geq 1,\\ \pi_{k1}=K\alpha(\gamma_2^k-\gamma_3^k),k\geq 1,\\ \pi_{k2}=K\gamma_3^k,k\geq 0,\end{cases}$$

where $K=\dfrac{(1-\gamma_1)(1-\gamma_2)(1-\gamma_3)}{\alpha\beta\left[(1-\gamma_3)\delta-(1-\gamma_2)\Delta\right]+\alpha(\gamma_2-\gamma_3)(1-\gamma_1)+(1-\gamma_1)(1-\gamma_2)}$

Proof. $(\pi_{02},\pi_{10},\pi_{11},\pi_{12})$ is given by the positive left invariant vector (3) and satisfies the normalizing condition

$$\pi_{02}+(\pi_{k0},\pi_{k1},\pi_{k2})(I-R)^{-1}e=1$$

Then, we get

$$K=\frac{(1-\gamma_1)(1-\gamma_2)(1-\gamma_3)}{\alpha\beta\left[(1-\gamma_3)\delta-(1-\gamma_2)\Delta\right]+\alpha(\gamma_2-\gamma_3)(1-\gamma_1)+(1-\gamma_1)(1-\gamma_2)}\cdot$$

We obtain

$$\pi_{02}=K,\quad (\pi_{10},\pi_{11},\pi_{12})=K(\alpha\beta(\delta-\Delta),\alpha(\gamma_2-\gamma_3),\gamma_3)\cdot$$

We have

$$\pi_k=(\pi_{k0},\pi_{k1},\pi_{k2})=(\pi_{10},\pi_{11},\pi_{12})R^{k-1},\quad k\geq 1,$$

Finally, we obtain the theorem.

Theorem 4. If $\rho<1$, the stationary queue length L_v can be decomposed into the sum of two independent random variables: $L_v=L+L_d$, where L is the stationary queue length of a classical GI/M/1queue without vacation, follows a geometric distribution with parameter γ_1; L_d follows the discrete PH distributions (φ,T) of order 2,where

$$\varphi=\frac{K}{1-\gamma_1}\left(\alpha\frac{\gamma_2-\gamma_1+\beta\delta}{1-\gamma_2}\quad -\frac{(\alpha-1)(\gamma_3-\gamma_1)+\alpha\beta\Delta}{1-\gamma_3}\right),\varphi_3=\frac{K}{1-\gamma_1},$$

$$T=\begin{pmatrix}\gamma_2 & \\ & \gamma_3\end{pmatrix},T^0=\begin{pmatrix}1-\gamma_2\\ 1-\gamma_3\end{pmatrix}$$

Proof. The PGF of L_v is as follows:

$$L_v(z)=\sum_{k=0}^{\infty}z^kP(L_v=k)$$

$$= K\alpha\left[\frac{z^k\gamma_3^k}{\alpha}+\left(\gamma_2^k-\gamma_3^k\right)z^k+\frac{\beta\delta\left(\gamma_1^k-\gamma_2^k\right)}{\gamma_1-\gamma_2}z^k-\frac{\beta\Delta\left(\gamma_1^k-\gamma_3^k\right)}{\gamma_1-\gamma_3}z^k\right]$$

$$= \frac{1-\gamma_1}{1-z\gamma_1}\frac{K}{1-\gamma_1}\left(\alpha\frac{1-z\gamma_1+z\beta\delta}{1-z\gamma_2}-\frac{(\alpha-1)(1-z\gamma_1)+z\alpha\beta\Delta}{1-z\gamma_3}\right)=L(z)L_d(z)$$

Where $L(z)$ is the PGF of L of a classical GI/M/1queue without vacation.

$$L_d(z)=\frac{K}{1-\gamma_1}\left(\alpha\frac{1-z\gamma_1+z\beta\delta}{1-z\gamma_2}-\frac{(\alpha-1)(1-z\gamma_1)+z\alpha\beta\Delta}{1-z\gamma_3}\right) \tag{4}$$

$$\frac{1-z\gamma_1+z\beta\delta}{1-z\gamma_2}=\left(1-z\gamma_1+z\beta\delta\right)\sum_{k=0}^{\infty}\gamma_2^k z^k \quad =1+\left(\gamma_2+\beta\delta-\gamma_1\right)\sum_{k=1}^{\infty}\gamma_2^{k-1}z^k\,.$$

Substituting the above equation into (4),we obtain the distribution of L_d.

We can get means

$$E(L_v)=\frac{\gamma_1}{1-\gamma_1}+\frac{K}{1-\gamma_1}\left[\alpha\frac{\gamma_2-\gamma_1+\beta\delta}{(1-\gamma_2)^2}-\frac{(\alpha-1)(\gamma_3-\gamma_1)+\alpha\beta\Delta}{(1-\gamma_3)^2}\right].$$

3. Waiting time distribution

Let W and $\tilde{W}(s)$ be the steady-state waiting time and its LST, respectively. Firstly, let H_0, H_1, H_2 be the probability that the server is in the service(set-up, vacation) period when a new customer arrives. We can compute

$$H_0=\frac{\alpha\beta\left[\left(1-\gamma_3\right)\delta-\left(1-\gamma_2\right)\Delta\right]}{\alpha\beta\left[\left(1-\gamma_3\right)\delta-\left(1-\gamma_2\right)\Delta\right]+\alpha\left(\gamma_2-\gamma_3\right)\left(1-\gamma_1\right)+\left(1-\gamma_1\right)\left(1-\gamma_2\right)},$$

$$H_1=\frac{\alpha\left(\gamma_2-\gamma_3\right)\left(1-\gamma_1\right)}{\alpha\beta\left[\left(1-\gamma_3\right)\delta-\left(1-\gamma_2\right)\Delta\right]+\alpha\left(\gamma_2-\gamma_3\right)\left(1-\gamma_1\right)+\left(1-\gamma_1\right)\left(1-\gamma_2\right)},$$

$$H_2=\frac{\left(1-\gamma_1\right)\left(1-\gamma_2\right)}{\alpha\beta\left[\left(1-\gamma_3\right)\delta-\left(1-\gamma_2\right)\Delta\right]+\alpha\left(\gamma_2-\gamma_3\right)\left(1-\gamma_1\right)+\left(1-\gamma_1\right)\left(1-\gamma_2\right)}.$$

Theorem 5. If $\rho<1$, $\theta,\beta>0$, the LST of stationary waiting time W is

$$\tilde{W}(s)=H_1\frac{\beta}{\beta+s}\frac{(\mu+s)(1-\gamma_2)}{\mu(1-\gamma_2)+s}\frac{\mu(1-\gamma_3)}{\mu(1-\gamma_3)+s}+H_2\frac{\theta}{\theta+s}\frac{\mu(1-\gamma_3)}{\mu(1-\gamma_3)+s}\frac{\beta}{\beta+s}$$

$$+H_0\left[\mu+\frac{(\delta-\Delta)s}{\delta(1-\gamma_3)-\Delta(1-\gamma_2)}\right]\frac{(\mu+s)(1-\gamma_1)}{\mu(1-\gamma_1)+s}\frac{(1-\gamma_2)}{\mu(1-\gamma_2)+s}\frac{\mu(1-\gamma_3)}{\mu(1-\gamma_3)+s}$$

Proof. When a customer arrives, if there are k customers and the server is in the service period, the waiting time equals k service times by the rate μ. Then, we have

$$\sum_{k=1}^{\infty}\pi_{k0}\tilde{W}_{k0}(s)=K\alpha\beta\sum_{k=1}^{\infty}\left(\frac{\gamma_1^k-\gamma_2^k}{\gamma_1-\gamma_2}\delta-\frac{\gamma_1^k-\gamma_3^k}{\gamma_1-\gamma_3}\Delta\right)\left(\frac{\mu}{\mu+s}\right)^k$$

$$=H_0\left[\mu+\frac{(\delta-\Delta)s}{\delta(1-\gamma_3)-\Delta(1-\gamma_2)}\right]\frac{(\mu+s)(1-\gamma_1)}{\mu(1-\gamma_1)+s}\frac{(1-\gamma_2)}{\mu(1-\gamma_2)+s}\frac{\mu(1-\gamma_3)}{\mu(1-\gamma_3)+s} \tag{5}$$

When a customer arrives, if there are k customers and the server is in the set-up period, the waiting time is the sum of the residual set-up time and k service times by the rate μ. Then, we have

$$\sum_{k=1}^{\infty}\pi_{k1}\tilde{W}_{k1}(s)=K\alpha\frac{\beta}{\beta+s}\sum_{k=1}^{\infty}(\gamma_2^k-\gamma_3^k)\left(\frac{\mu}{\mu+s}\right)^k$$

$$= H_1 \frac{\beta}{\beta+s} \frac{(\mu+s)(1-\gamma_2)}{\mu(1-\gamma_2)+s} \frac{\mu(1-\gamma_3)}{\mu(1-\gamma_3)+s}. \tag{6}$$

Similarly,

$$\sum_{k=1}^{\infty} \pi_{k2} \tilde{W}_{k2}(s) = K \sum_{k=1}^{\infty} \left(\frac{\mu\gamma_3}{\mu+s} \right)^k \frac{\beta}{\beta+s} \frac{\theta}{\theta+s} = H_2 \frac{\theta}{\theta+s} \frac{\mu(1-\gamma_3)}{\mu(1-\gamma_3)+s} \frac{\beta}{\beta+s}. \tag{7}$$

From (5)-(7), we have the result in Theorem 4.

With the structure in Theorem 4, we can get the expected waiting time

$$E(W) = H_2 \left[\frac{1}{\theta} + \frac{1}{\mu(1-\gamma_3)} + \frac{1}{\beta} \right] + H_1 \left[\frac{\gamma_2}{\mu(1-\gamma_2)} + \frac{1}{\mu(1-\gamma_3)} + \frac{1}{\beta} \right]$$

$$+ H_0 \left[\frac{\gamma_1}{\mu(1-\gamma_1)} - \frac{\delta-\Delta}{\mu\left[\delta(1-\gamma_3)-\Delta(1-\gamma_2)\right]} + \frac{1}{\mu(1-\gamma_2)} + \frac{1}{\mu(1-\gamma_3)} \right].$$

4. Numerical examples

In the above analysis,we obtain the expected queue length in the steady state. The difference of parameters may influence the queue length. So, we present numerical examples to explain.

References

Doshi, B.T.(1986).Queuing systems with vacations-a survey. *Queuing Syst* 1, 29-66

Neuts, M. (1981). Matrix-Geometric Solutions in Stochastic models, *Johns Hopkins University Press*, Baltimore.

Qin, X. (2006). GI/Geo/1 discrete-time queue with set-up period and multiple vacations, *Operation Research*, 15, 52-57.

Tian, N.S. (2006).Vacation Queueing Models: *Theory and Applications, Springer-Verlag, New York.*

Tian, N.S. (1989). The GI/M/1queue with exponential vacations, *Queueing Syst*. 5 331-344.

Tian, N.S.(2002). The discrete time GI/Geo/1 queue with multiple vacations. *Queueing Syst*. 40 283-294.

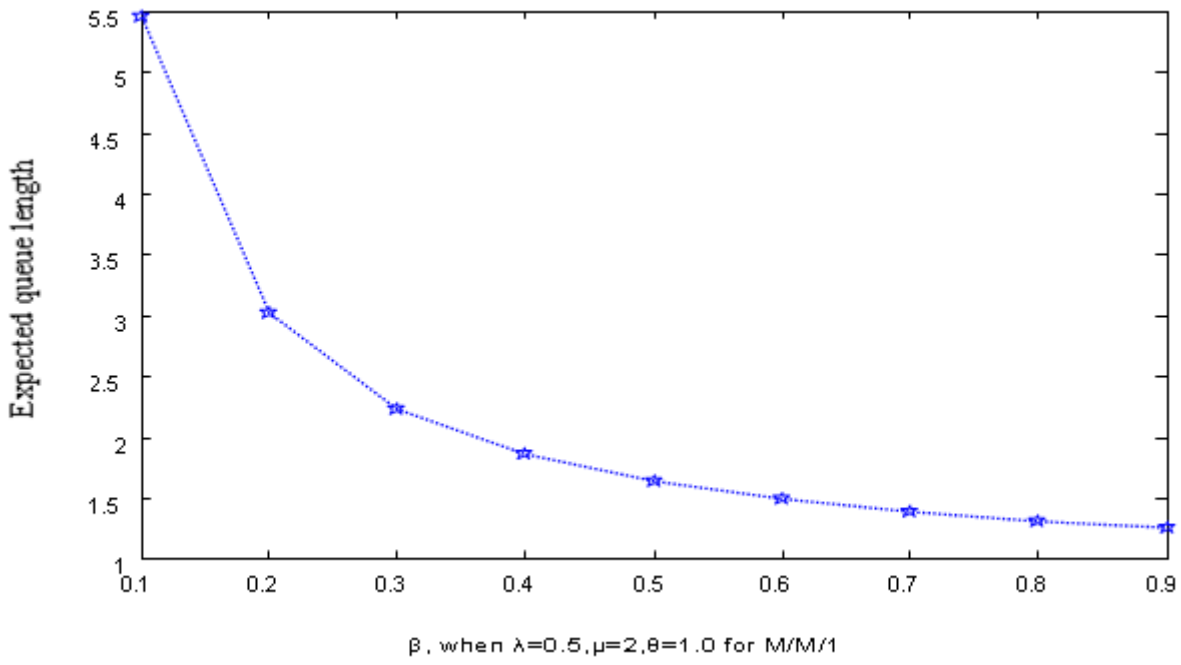

Figure 1. The relation of $E(L_v)$with β

Modern Applied Science

www.ccsenet.org/journal.html

Vol. 2, No. 5

September 2008

The Application of BP Artificial Neural Network in Fabric Warmth Retention Test

Gaoyang Zhang

Tianjin Polytechnic University

Tianjin 300160, China

E-mail: qwe2001ren@163.com

Guangli Song

Tianjin Polytechnic University

Tianjin 300160, China

E-mail: sgl2001@163.com

Abstract

The fabric warmth retention test is a complex process that is influenced by various factors, so errors often appear in the test. There lies a function relation between the fabric thickness, gram weight and warmth retention rate, CLO value. Artificial neural network BP algorithm was used to simulate the function mapping relation, and realized the automatic mapping from basic performance to warmth retention performance, and exhibited high mapping precision, it could also be used to amend the numerical value and reduce errors. It is demonstrated that the method is of high efficiency.

Keywords: Fabric warmth retention test, Artificial neural network, BP algorithm, Function mapping, Error

The data is often influenced by many errors in traditional fabric warmth retention test, especially the CLO value of fabric. CLO values of one fabric might be greatly different when it is tested with the same tool in different seasons or in different places, even the CLO values within a day might be different when it is tested in the morning, at noon or in the evening. These phenomena always confuse the people who are engaged in warmth retention test, so it is urgent to eliminate the errors and ensure the correctness of test result.

Fabric warmth retention rate and CLO value are two important indexes exhibiting the performance of fabric, while the thickness, gram weight, temperature and humidity of the environment directly influence the fabric warmth rate and CLO value.

Hence, if the data and result in the fabric warmth retention test can be simulated and quantified with computer, the influence of errors on test result will be greatly reduced. Neural network can be used to simulate the function of human brain neural cell; it has strong reserving and learning ability and can thoroughly approach to the complex nonlinear relationship. So it is necessary to study and simulate the data and result of fabric warmth retention performance by artificial neural network BP algorithm to reduce the influence of errors on test result and ensure the correctness and accuracy of test result.

1. Introduction to artificial neural network algorithm

Artificial neural network is a simulation of microcosmic physiological structure of life form and human neural system, it is a complicated computer network system comprising of interlinked simple processing units. It is indicated that neural network has the basic characteristics of human brain, i.e. learning, memorizing and concluding, it can be used to approach to any complex nonlinear system, so it is studied and applied widely in recent years.

Feed-forward neural network is one of the most important and widely used artificial neural networks. At present, many algorithms are in allusion to feed-forward neural network, EBP (error back propagation) algorithm (briefly as BP algorithm) is one that is widely used and can approach to any nonlinear function. Figure 1 shows the BP structure of feed-forward three-layered neural networks.

It can be seen from figure 1 that the neural network has three layers, input layer, hidden layer and output layer, the hidden layer can be one or more. (x_1, x_2, … x_n) are input vectors, (y_1, y_2, … y_n) are output vectors, w_1 is input layer and w_2 is output layer. The hidden layer and the output layer link with the weight value matrix, θ_1 and θ_2 are the threshold of hidden layer and output layer.

The learning process of BP algorithm comprises two parts, 1), forward propagation, the input vector, after processed by hidden layer, will be propagated to the output layer, the state of one layer only influences that of the next layer. The input layer unit is numbered by *i,* the hidden layer unit is numbered by *j*, and the output layer unit is numbered by *k,* accordingly, the output of hidden layer is $Oj = f\{\sum w_{1ji} Oi + \theta 1j\}$ (O_i is the input vector). Similarly, the output of output layer is $Ok = f\{\sum w2kjOj + \theta 2k\}$, of which *f* is activation function, usually, Sigmoid function $f(x) = 1/(1 + e^{-x})$ is used. 2) Reverse propagation of error, the error signal will be returned along the original neural network, during the returning, each weight value will be modified, so as to make the sum of squares error (*E*) between actual output of network and supposed output be the least, in light of gradient descent method, educe the adjusted value of weighting coefficient.

$$E = \frac{1}{2} \sum_{p} \sum_{k} (y_{pk} - O_{pk})^2$$

(*p*, the number of sample)

Reverse propagation of error

$$\delta_k = (y_k - O_k) f\left(\sum_j w_{1kj} O_j + \theta_{2k} \right) \Rightarrow$$

$$\delta_k = (y_k - O_k) O_k (1 - O_k)$$

(Output layer)

$$\delta_j = O_j (1 - O_j) \sum_k \delta_k w_{2kj}$$

(Hidden layer)

Weight value modification

$$\Delta w_{1,ji}(t+1) = \eta \delta_j O_i + \alpha \Delta w_{1,ji}(t)$$

$$\Delta w_{2kj}(t+1) = \eta \delta_k O_j + \alpha \Delta w_{2kj}(t)$$

Threshold value modification

$$\Delta \theta_{1j}(t+1) = \eta \delta_j + \alpha \Delta \theta_{1j}(t)$$

$$\Delta \theta_{2k}(t+1) = \eta \delta_k + \alpha \Delta \theta_{2k}(t)$$

η means learning rate, if η is larger, the change of weight value will be larger, the training process of network will be accelerated, but the result might surge. In order to increase learning rate but produce no surge, momentum item is usually added to the weight value modification and threshold value modification as follows:

$\alpha \Delta w_{1,ji}(t)$, $\alpha \Delta w_{2kj}(t)$, $\alpha \Delta \theta_{1j}(t)$, $\alpha \Delta \theta_{2k}(t)$.

α is momentum constant, it determines the influence of the past weight variation on the present weight variation. After training, when the *E* meets the need, the weight value of each node will be determined, and then the network will be able to be used in relating aspects.

2. Fabric warmth retention test based on BP algorithm

2.1 The determination of input vector and output vector in BP artificial neural network

The factors that influence the fabric warmth retention performance usually are the temperature and humidity of constant temperature room, gram weight and thickness of fabric, the structure of fabric and the thermal resistance of fiber. It is difficult to quantify the structure of fabric, so we took fabric composed of the same fiber and having the same structure as the test sample, i.e. 100% terylene double-faced polar fleece. The warmth retention rate and CLO value were used to represent the warmth keeping performance of fabric, the data and calculated results were used in BP artificial neural network.

In the BP artificial neural network, input vectors are the temperature and humidity of constant temperature room, the gram weight and thickness of fabric; while the output vectors are warmth retention rate of fabric and the CLO value.

2.2 The determination of training sample

The performance of neural network has close relationship with training sample; numerable reliable samples are of great importance. The training sample in this study came from the constant temperature room of Tianjin Polytechnic University and the test was carried out in the constant temperature room of Tianjin Knitting Technology Research

Institute. Firstly, 25 different fabric samples were tested, three tests were done to ensure the accuracy of the data, and then got the warm retention rate and CLO value through weighted average value. The gram weight, thickness, temperature and humidity of 25 samples were taken as the input of neural network, while the warmth retention rate and CLO value were taken as the output of neural network, all of them constituted the training sample of artificial neural network. 20 samples were training sample, and 5 were test sample.

The BP algorithm of neural network takes Sigmoid function as activation function, and the output of Sigmoid function is between 0 and 1, so the output vectors should be normalized. In addition, the units of input vectors are different, so the input vectors should also be normalized. The following two expressions were used to normalize the sample (*Xp*, *Yp*):

$$X(p,i) = (X_{act}(p,i) - X_{min}(i) \times 0.9) / (X_{max}(i) - X_{min}(i)) + 0.05 \quad (1)$$

$$Y(p,i) = (Y_{act}(p,i) - Y_{min}(i) \times 0.9) / (Y_{max}(i) - Y_{min}(i)) + 0.05 \quad (2)$$

Of which, $X(p, i)$, $Y(p, i)$ are the training sample value, Xact (p, i), Yact (p, i) are the actual sample value, Xmin (i), Ymin (i) are the minimum of training sample in i node, Xmax (i), Ymax (i) are the maximum of training sample in i node. After testing in the neural network, the test sample will be changed to the actual value by expression (1) and (2).

3. Experiment and result analysis

3.1 Parameters of the model

The network as shown in figure 1 was used, the node numbers of input layer and output layer were 11 and 9 respectively, and the node number of hidden layer was 10. According to the expression: $n1 = \sqrt{n + m + \omega}$ (n, node number of input layer, m, node number of output layer, ω is a constant between 0 and 10), learning rate η is 019, momentum constant α is 017, the initial value of weight value *w1* and *w2*, threshold value $\theta 1$and $\theta 2$ is a random number between [-1, 1].

3.2 Results and analysis

The results of neural network training are shown in figure 2 and figure 3.

In table 1, the tested CLO value was the expected CLO value, the temperature, humidity, gram weight and thickness were the inputs of neural network, CLO value and warmth retention rate were the output of neural network. As we can see from figure 3 that the artificial neural network basically met the actual need, the method in the experiment was feasible.

4. Conclusion

Using the artificial neural network BP algorithm model to study and simulate the objective function mapping relationship between factors influencing fabric warmth retention rate and tested results, realized the computer test of tested data and results, the unvalued data would be taken out so as to reduce the influence of errors on results and guarantee the objectiveness and accuracy of fabric warmth retention performance test. The study indicates that the method is of high efficiency and accuracy; more scientific training data can be modified by this method.

References

Cheng, L and Adam s, D. L. (1995).Yarn strength prediction using neural network. *Text. Res. J.* 65: 495-500.

Cong, Shuang. (2005). *Theory about Matlab neural network kit Hefei* [M]. University of Science and Technology of China Press.

Dong, Changhong. (2005). *Matlab neural network and its application*. Beijing, National Defence Industry Press.

Han, Liqun. (2002). *Principles, design and application of neural network*. Beijing, Chemical Industry Press.

Wang Zh. (2003). Heat and moisture transfer and clothing thermal comfort. Hong Kong Polytechnic University.

Table 1. Part of the tested results of samples

Sample number	Temperature	Humidity	Gram weight	Thickness	Tested CLO value	CLO value output	Warmth retention rate
1#	21.4℃	65.1%	198g/m^2	4.3mm	0.833	0.813	53.12%
2#	21.1℃	64.3%	203g/m^2	4.6mm	0.912	0.914	55.41%
3#	20.5℃	64.9%	188g/m^2	3.3mm	0.675	0.715	48.63%
4#	22.1℃	63.5%	267g/m^2	4.8mm	1.345	1.356	58.46%
5#	21.6℃	65.4%	253g/m^2	5.1mm	1.324	1.319	57.37%
6#	20.9℃	63.1%	389g/m^2	7.4mm	2.225	2.145	77.05%
7#	22.6℃	64.6%	413g/m^2	7.6mm	2.653	2.456	79.31%
8#	21.6℃	65.4%	311.6g/m^2	6.2mm	2.154	2.316	76.32%

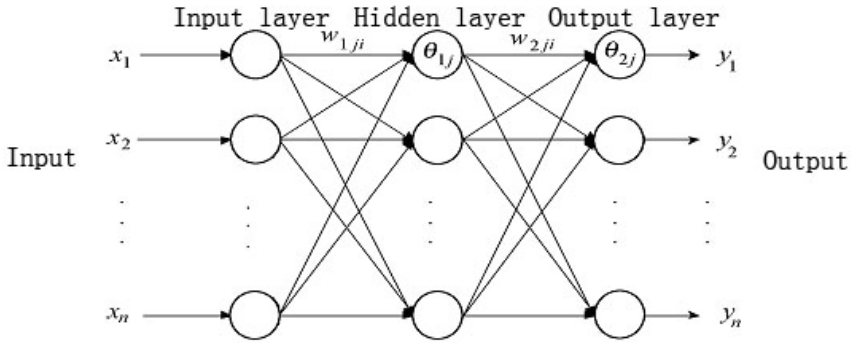

Figure 1. Structure of three layer feed forward neural network

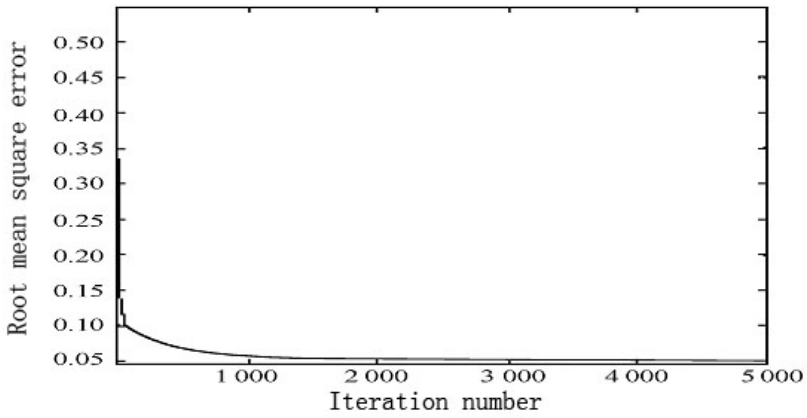

Figure 2. Error curve for network training

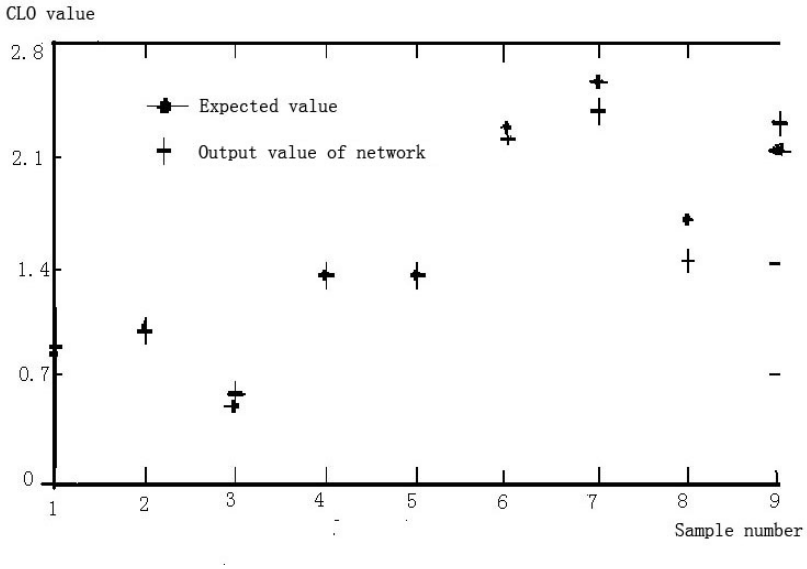

Figure 3. The compare of actual output and expected output of CLO value

A journal archived in Library and Archives Canada
A journal indexed in CANADIANA (The National Bibliography)
A journal indexed in AMICUS
A leading journal in applied science research
A journal indexed in Zentralblatt MATH

Modern Applied Science

Bimonthly
Publisher Canadian Center of Science and Education
Address 4915 Bathurst St. Unit # 209-309, Toronto, ON. M2R 1X9
Telephone 1-416-208-4027
Fax 1-416-208-4028
E-mail mas@ccsenet.org
Website www.ccsenet.org
Printer William Printing Inc.
Price CAD.$ 20.00

ISSN 1913-1844